The University of Hull

The Use of Digital Signal Processing in Adaptive HF Frequency Management

by

Mark Gallagher

B.Eng (Hons), DipEng., AMIEE, MIEEE

Being a thesis submitted to the
Department of Electronic Engineering
in
The University of Hull

in partial fulfillment of the requirements for the degree of

Doctor of Philosphy
March 1995

Declaration

None of the material contained in this thesis has been submitted in support of an application for another degree or qualification of this, or any other university or institution.

Mark Gallagher

Acknowledgments

There have been many people who have helped in the production of this thesis and the research that went into it. Of those, I must initially acknowledge the support, encouragement and direction of my supervisor–Professor Michael Darnell. In the Hull-Lancaster Communications Research Group thanks go to Nick Riley, Diane Low (for keeping me sane), the Crow's Nest Bunch (Tim Speight, Kamlesh Masrani, Dave Melton and Paul Clark), The Flatites (Mark Grayson, Tim Phipps, Prasad and Andy Carnegie) for all making the years doing research interesting and most of all enjoyable!

Not withstanding all of the above, I must also acknowledge the support of the Science and Engineering Research Council (SERC) and Roke Manor (Siemens-Plessey) Research Ltd., and in particular, Bob Goodwin, Stuart Bennett and Graham Smith, for supporting the project and providing constructive criticism.

Lastly, I wish to use this space to acknowledge the unstinting support, understanding, encouragement of Kathryn Land.

Abstract

High Frequency (HF) radio systems operate in the frequency range 2-30 MHz and utilise ionised layers in the upper atmosphere (termed the ionosphere) to reflect transmitted radio signals. The ionosphere can allow transmitted signals to be successfully received in the range several tens of kilometres to several thousands of kilometres. The use of radio signals in this frequency range has enabled long-distance communication for more than 50 years, but has traditionally required expensive equipment and trained operators to operate efficiently.

This PhD research programme addresses the problem of using modern, high speed, computer-based tools to automate selection of 3 kHz bandwidth segments, or channels, from the frequency range 2-30 MHz. Accurate and efficient selection of such HF radio channels enables the HF radio system to operate more effectively than if channels were selected randomly, since propagation relies on well-described physical constraints and may be subject to interference from other users. Furthermore, efficient use of allocated bandwidth means that spectral intrusion will be minimised. The thesis describes the systematic methods used to select a channel and then optimise performance for that particular channel. The term "frequency management" encompasses all of these ideals.

Specifically, the focus of the PhD is on the role of Digital Signal Processing (DSP) techniques in the frequency management process. The thesis will describe two key tools developed and tested during the research programme that enable automatic channel selection and automatic channel optimisation to take be undertaken. The wider implications of the use of DSP technology is also presented.

The research programme was industrially sponsored and it is anticipated that several of the solutions investigated by this research programme will be embedded in future HF radio systems.

Contents

Declaration 1

Acknowledgments 2

Abstract 3

Glossary 14

1 Introduction 18

1.1 Motivation and Previous Research 18

1.2 Key Functional Elements of a Frequency Management System 19

1.3 Outline of Thesis 22

1.4 Original Research Contributions 23

1.5 Review of Chapter 24

2 The HF Environment 25

2.1 Historical Perspective on the Use of HF Communication 25

2.2 Strengths and Weaknesses of Operating in the HF Band 26

2.3 HF Propagation 27

2.3.1 Fading Mechanisms 30

2.3.2 Less Predicatable Propagation Effects 30

2.4 Noise and Interference 30

2.4.1 Co-Channel Interference 31

2.4.2 Man-Made Noise and Intermodulation Products 32

2.5 Review of Chapter 33

3 Frequency Management Processes **34**

3.1 Philosophy of Frequency Management 34

3.2 Adaptive HF Radio 35

3.3 Channel Selection 37

3.3.1 HF Prediction Methods 37

3.3.2 Real-Time Augmentation of Prediction Models 39

3.4 Channel Optimisation 41

3.5 Real-Time Channel Evaluation (RTCE) 41

3.6 Review of Successful Frequency Management Systems 44

3.6.1 Channel Evaluation and Calling (CHEC) System 45

3.6.2 Home Defence Radio System (HDRS) 45

3.7 Review of Chapter 49

4 Philosophy of Implementation **50**

4.1 Introduction 50

4.2 DSP Device Characteristics 50

4.2.1 Common DSP Device Characteristics 50

4.2.2 Typical Applications of DSP Devices 52

4.2.3 Specific Characteristics of the DSP32C 52

4.2.4 Use of DSP with Voice Band Channels 53

4.3 System Design Philosophy 53

4.4 The Generic Architecture Concept 54

4.4.1 Host Computer (CPU) 55

4.4.2 Signal Processing Subsystem 56

4.4.3 Radio System 56

4.5 Algorithms and Processes used to Facilitate Frequency Management 57

4.5.1 Artificial Intelligence in HF Systems 58

4.5.2 Object Orientated Design of HF Frequency Management Systems . . . 59

4.5.3 Conventional Programming Methods as Applied to HF Frequency Management 59

4.6 Performance Specification 61

4.7 Review of Chapter 62

5 Elements of a Channel Selection Subsystem **63**

5.1 Chapter Introduction 63

5.2 Description of the Barry Chirpsounder System 64

5.3 Description of the Linear FM (Chirp) Waveform and Methods to Achieve Optimal Detection 67

5.3.1 The Linear FM Waveform 68

5.3.2 Detection of the Linear FM Signal 68

5.3.3 Digital Matched Filter Detection of Linear FM 70

5.4 Non-Linear FM Signals 71

5.5 Operation of the DSP-based Reception System 73

5.5.1 Implementation of the Matched Filter on a Digital Signal Processor . 73

5.5.2 Windowed Detection Schemes 74

5.5.3 Evaluation of Matched Filter Performance 75

5.5.4 Peak Detection Algorithms 76

5.5.5 System Integration 78

5.5.6 Comparative Trial between Chirpmonitor and Barry Chirpsounder Receiver 80

5.5.7 Ionogram Display 80

5.6 Operation of the DSP-based Sounding System 81

5.7 Review of Chapter 86

6 A Channel Optimisation Subsystem **89**

6.1 Chapter Introduction 89

6.2 Analysis of In-band Signals 90

6.2.1 Determination of the Channel Spectrum 90

6.2.2 Data Averaging 91

6.3 The Template Correlation Algorithm 92

6.3.1 Implementation of the Template Correlation Algorithm 92

6.3.2 Extension to the Template Correlation Algorithm 93

6.3.3 Relationship between SNR and the FDCCF 96

6.3.4 Prediction of BER 96

6.4 Tone Placement Algorithms 97

6.5 'Figure-of-Merit' Concept 98
6.5.1 The Generalised Transmission Model 98
6.5.2 Algorithms Suitable for Digital Processing 100
6.5.3 Empirical Estimation Based Upon Probabilistic Approach 103
6.5.4 Estimation of Performance in Fading Conditions 103
6.5.5 Estimation for a Non-Gaussian Channel with Memory 106
6.5.6 Figure of Merit Algorithm for MFSK Systems 106
6.6 Review of Chapter 108

7 Results from Field Trials **110**
7.1 Results achieved utilising the DSP-Based Chirp Receiver 110
7.1.1 Results from the Previous Chirpmonitor Receiver 110
7.1.2 Ionogram Construction 111
7.1.3 Example Ionograms 111
7.1.4 Comparative Trials 114
7.1.5 Statistical Analysis of the Channel Impulse Response 117
7.2 Trials of the Active Sounder 120
7.3 Trials of Template Correlation System 122
7.4 Trials of the Integrated Channel Selection and Optimisation System 125
7.5 Analysis of Results 128

8 Recommendations for Future Work and Concluding Remarks **132**
8.1 Recommendations for Future Work 132
8.1.1 Improvements to the Channel Selection System 132
8.1.2 Improvements to the Channel Optimisation System 133
8.1.3 System Integration 133
8.2 Novel Work 133
8.3 Concluding Remarks 134
8.3.1 Channel Selection Systems 134
8.3.2 Channel Optimisation System 134
8.3.3 Figure of Merit (FOM) 135
8.3.4 System Implications 135

8.3.5 Specifications 135
8.4 Final Remarks and Acknowledgements 135

References **137**

A Overview of HF Propagation **144**
A.1 Ionospheric Propagation Effects 144
A.2 Oblique Propagation 147
A.3 Oblique Propagation Parameters 150
A.4 Noise and Interference 150
A.5 Appendix Review 150

B Chirp Detection Ambiguity Functions **152**
B.1 Linear FM 152
B.2 Matched Filter Detection 153
B.3 The ambiguity function of Linear FM Signals 155
B.3.1 Rectangular Window 155
B.3.2 Unilateral Hamming Window 156
B.3.3 Bilateral Hamming Window 157

C Spectral Estimation Methods **158**
C.1 Spectral Analysis of In-Band Signals 158
C.1.1 Fourier Analysis Techniques 158
C.1.1.1 Discrete Fourier Transform 159
C.1.1.2 Fast Fourier Transform 160
C.1.2 Linear Prediction Techniques 160
C.1.2.1 Common Theory 160
C.1.2.2 Parametric Power Spectrum Estimation 164
C.1.2.3 ARMA Model for Power Spectrum Estimation 166
C.1.3 Wavelet Transform 167
C.2 Appendix Review 169

D Maximum Likelihood Detection of Signals in the Time-Frequency Domain 170
D.1 Introduction 170

D.2 Algorithm Details and Results 171
D.3 Concluding Remarks 172

E Analytical Description of the Template Correlation Algorithm **173**

F Publications **176**

List of Figures

1.1 Model of Elements in an HF Frequency Management System 21

2.1 Plot of the multipath effects of layers in the ionosphere 28
2.2 Plot of F layer MUF and LUF for diurnal variation: 29
2.3 A Plot of Typical HF Channel Capacity 31
2.4 Distribution of Block Errors 32

3.1 An example output (textual) from CCIR 894 38
3.2 An example output (graphical) from CCIR 894 39
3.3 The Format of the CHEC Probing Signal 45
3.4 The timing schedule in the HDRS system 47
3.5 Schematic of a typical HDRS Terminal 48

4.1 Typical Architecture for a DSP System. 52
4.2 Schematic Diagram of Adaptive HF Terminal Architecture. 55
4.3 Modified generic architecture with multiple DSP Sub-Systems 57
4.4 Schematic Diagram of Hierarchy of Performance. 58
4.5 A Frequency Management System using Object-Orientated Knowledge Sources. 60

5.1 Block Diagram of a Barry Receiver 65
5.2 The Mixer Products at the IF stage of a Barry Receiver 66
5.3 The Impulse Response Raster from a Barry Receiver 66
5.4 Output from a Barry Receiver 67
5.5 A matched filter detection scheme 69
5.6 Simulation of Linear FM Matched Filter System 70
5.7 Channel Simulation with No Additive Noise and Two Propagating Modes . . 76

5.8 Channel Simulation with Additive Noise and Two Propagating Modes 76
5.9 Chirp Signal Captured from Off-Air Data 77
5.10 Flow-chart showing the operation of the Chirpmonitor 79
5.11 The synchronisation process within the Chirpmonitor 79
5.12 Configuration of the Chirp Reception Systems for the Comparative Trials . . 81
5.13 A Plot of a Colour-Modulated Ionogram 82
5.14 A Plot of Colour-Coded Impulse Response Data 83
5.15 A Contour Plot of a "Waterfall" Display 84
5.16 Configuration of equipment for the Active Sounding Trial 86
5.17 Format of the SSFM Signal 87
5.18 Flow-Chart of the operation of the Active Sounder 87

6.1 A Schematic of Adaptive Overlapping Spectral Estimates 92
6.2 Spectral Estimate with Large region of Low Energy 94
6.3 Spectral Estimate With 16-Tone Modem Overlaid 94
6.4 Flow Chart Describing Operation of Template Correlation Algorithm 95
6.5 Channel Model using Tap Delays and Scattering Gain 99
6.6 Plot of Channel Scattering Function 101
6.7 Channel Transmission Model 101
6.8 Error Plot with for MFSK m $\rightarrow \infty$, ... 105
6.9 Error Plot with m = 1 105
6.10 Simulation Results from Preliminary Figure-Of-Merit Trials: 108
6.11 Simulation Results from Preliminary Figure-Of-Merit Trials: 109

7.1 Initial Plots taken on Various Paths 112
7.2 Series of Impulse Responses 113
7.3 Chirpmonitor Output: Oslo - Hull 114
7.4 Chirpmonitor Output: Oslo - Cobbett Hill 114
7.5 Proprietary Chirpsounder Output: Oslo - Cobbett Hill 116
7.6 Chirpmonitor Output: Oslo - Cobbett Hill 116
7.7 Proprietary Chirpsounder Output: Hong Kong - Cobbett Hill 117
7.8 Chirpmonitor Output: Hong Kong - Cobbett Hill 118

7.9 Averaged Chirpmonitor Output: Hong Kong - Cobbett Hill 118
7.10 An Ionogram showing Propagation Modes: 119
7.11 A Plot of the Standard Deviations of Impulse Response Data: 119
7.12 Histogram of Impulse Responses 120
7.13 Histogram of an Impulse Response when a Chirp Signal *is* Present 121
7.14 Histogram of an Impulse Response when a Chirp Signal is *not* Present 121
7.15 First Example Ionogram Generated by DSP Sounder: 122
7.16 Second Example Ionogram Generated by DSP Sounder: 123
7.17 Template Correlation Results I: Steady Co-Channel Interference 124
7.18 Interference Spectrum: Steady Co-Channel Interference 124
7.19 Template Correlation Results II: Steady Co-Channel Interference 125
7.20 Interference Spectrum: Fading Co-Channel Interference 126
7.21 Template Correlation: Fading Co-Channel Interference 126
7.22 Interference Spectrum: No Co-Channel Interference 127
7.23 Template Correlation: No Co-Channel Interference 127
7.24 Chirpmonitor Output: Akrotiri - Cobbett Hill 129
7.25 Impulse Response of the Best Channel 130
7.26 Impulse Response of One Backup Channel 130

A.1 Ionospheric Skywave Propagation 145
A.2 Ionospheric Structure: Summer's day, Mid-Latitude 146
A.3 Plot of the effects of layers in the Ionosphere 146
A.4 Relationship between Oblique and Vertical Propagation 147
A.5 Plot of F layer critical frequency for diurnal variation: 149
A.6 Noise Levels as a function of Frequency from Various Sources 151

B.1 Complex Envelope of Simple Linear FM 153
B.2 Surface Plot of Linear FM Ambiguity Function 156

D.1 Contour Plots of FSK Signal 171
D.2 Error-Curve Results from FFT-based demodulator 172

List of Tables

5.1 A table comparing the Rectangular Window and Hamming Window 75

6.1 Properties of the Discrete Fourier Transform 90

7.1 The example frequencies for the Channel Selection and Optimisation Trial . . 128

7.2 Channels sorted according to single mode propagation 129

7.3 Channels resorted according to average interference level 129

Glossary

This section details the main abbreviations and terms used in this thesis.

ACF Autocorrelation function.

ACK Acknowledge.

ADC Analogue to Digital Conversion.

Ae Antenna.

AGC Automatic Gain Control.

AI Artificial Intelligence.

ALE Automatic Link Establishment.

AR Auto-regressive.

ARMA Auto-regressive moving average.

ARQ Automatic Repeat Request—a feedback protocol.

base-band The part of the spectrum in the range 0-3000 Hertz. In a more general sense, however, this means the same bandwidth as the original signal.

BBS Blackboard system.

BER Bit error rate.

BER Bit error ratio.

CCF Cross-Correlation function.

CCIR International Radio Consultative Committee.

Chirp See Linear Frequency Modulation.

cos The cosine an angle (in radians).

CPU Central Processing Unit.

DAC Digital to analogue converter.

dB Decibel.

DFT Discrete Fourier Transform.

DSP Digital signal processing/processor.

DTFT Discrete time Fourier Transform.

EOW Engineering Order Wire.

F1B FSK transmission.

FAX Facsimile

FDCCF Frequency domain cross-correlation function.

FEC Forward Error Correction.

FEK Frequency exchange keying.

FFT Fast Fourier Transform.

FIR Finite impulse response.

FOM Figure-of-Merit.

FOT Frequency of Optimum Traffic (translation from French). This is usually at 85% of the system MUF (MOF).

FMS Frequency Management System.

FSF Frequency selective fading.

FSK Frequency Shift Keying.

H(f) The frequency domain response of a filter with an impulse response, h(t).

HDRS Home Defence Radio System.

HF High frequency.

HFM Hyperbolic FM.

h(t) The unit impulse response function of a filter.

h(n) discrete representation of the filter h(t).

HLCRG Hull-Lancaster Communications Research Group.

IDFT Inverse discrete Fourier transform.

IFFT Inverse FFT.

in-band The spectrum contained in the intended transmission bandwidth.

Ionogram This is a two dimensional graph of the macroscopic propagation conditions relating received signal time delay to frequency.

IF Intermediate frequency.

IIR Infinite impulse response.

ISI Intersymbol interference.

ITU International Telecommunication Union.

j Denotes $\sqrt{-1}$.

J3E The CCIR term to denote single sideband modulation format.

Linear Frequency Modulation (LFM) This signal format, also known as 'chirp', describes a family of signals that have a linearly increasing, or decreasing, frequency component with respect to time.

LUF Lowest usable frequency.

LQA Link Quality Assessment

LQE Link Quality Estimate.

LSB Lower sideband.

MDS Modulation derived synchronisation.

MFSK Multiple Frequency Shift Keying or M-*ary* FSK. In this type of modulation format there are M keyed tones.

MIL-STD Military Standard (US term).

MOF System Maximum Observed Frequency. This is also termed the system MUF.

MUF Maximum usable frequency. There is a difference between the system MUF (also termed MOF) and the true MUF.

NAK Not acknowledge.

NVIS Near-Vertical Incidence Skywave.

PA Power amplifier.

PC Personal computer.

PCA Polar cap absorption.

p.d.f Probability density function.

PSK Phase Shift Keying.

PSR Peak-to-sidelobe ratio.

RPC Radiated power control.

RTTY Radio tele-type.

RTCE Real-Time Channel Evaluation.

SATCOM Satellite communications.

sin The sine of an angle (in radians.

sinc(x) the mathematical relationship $sin(x)/x$.

SINAD Signal plus noise plus distortion to noise plus distortion ratio.

SMC Symbiotic Modulation Concealment.

SNR Signal to Noise Ratio.

SSB Single sideband modulation.

SSFM Segmented Swept FM; this describes time sliced narrow-band linear FM segments being transmitted on discrete frequencies across the whole or part of the HF band.

SSN Sun spot number.

STFT Short time Fourier transform.

STIFS Short-term Ionospheric Forecasting Service.

USB Upper sideband.

UT Universal Time.

Chapter 1

Introduction

This chapter provides a general introduction to the thesis. The thesis describes, in detail, the research undertaken for a project entitled "Application of Digital Signal Processing to Adaptive Frequency Management" in the period October 1989 to September 1992. Funding was from a Science and Engineering Research Council Research CASE Studentship award in conjunction with Roke Manor Research (Siemens) Limited. Assistance on radio trials was provided by Roke Manor, Hull, Warwick and Lancaster Universities, and the Defence Research Agency (DRA), Aerospace Division, Farnborough.

1.1 Motivation and Previous Research

The motivation for this research programme was to extend previous research from programmes in the area of adaptive high frequency (HF) radio systems.

HF radio systems operate in the 2-30 MHz band and typically have a number of 3 kHz bandwidth channels allocated to the operator for communication purposes. The channels are used to support voice and digital data over ranges from a few tens of kilometres and up to several thousands of kilometres. The radio channels are performance limited by (i) fading, where the signal can fluctuate over a wide amplitude range, (ii) phase instability, (iii) multipath, where several signal returns are received, (iv) dispersion, (v) noise, and (vi) interference caused by other users occupying the band. The transmission mechanism for HF signals is usually skywave propagation via the ionosphere. The ionosphere is a body of ionised gases, that extends from about 70-500 km above the earth's surface, whose properties are primarily determined by solar radiation. The ionosphere refracts (bends) propagating radiowaves; therefore, by appropriate orientation of antennas and selection of frequency, HF radio systems can communicate over large distances.

The concept of adaptive HF is intended to allow such radio systems to operate automatically, as a part of the telecommunication infrastructure, without operator involvement. Such a concept means that many of the traditional limitations on HF communication efficiency, caused by operating radio links in a variable propagation and noise/interference will have to be overcome. Extending the operating efficiency of HF radio systems requires that new algorithms and methods be applied to the problem. Specifically, the use of high-speed

digital signal processing (DSP) technology has allowed many of the analogue or simple digital processes, for example automatic gain control, to be replaced by software systems operating in real-time on a dedicated microprocessor. Digital signal processing has been applied successfully to many of the signal generation and processing elements of an HF radio system — typically the modem and some of the radio equipment elements. Currently, the available DSP technology is well matched to real-time processing the 3 kHz channels commonly allocated to an HF radio system.

The starting point of the research was an investigation by a previous researcher into the operation of HDRS (Home Defence Radio System) developed by Roke Manor Research in the early 1980s. This radio system development was sponsored by UK MOD and is a system that maintains a communication infrastructure in times of national disaster. The investigation (in the period 1985-1989) concentrated on how the application of DSP technology would improve performance. As with all conventional HF systems, the HDRS system had a designed adaptivity that was limited according to the operational role that was specified. It was concluded that, to be fully adaptive, the system would have to be redesigned to allow the benefit of DSP technology to be maximised. At this stage, the development of a series of DSP-based software tools to aid the construction of a technology demonstrator, was initiated. It was further decided that the key to operation of an adaptive HF system was to make the system controller that decided which frequency to operate at any instant, termed the "frequency management controller", fully aware of the operating environment. The focus of research effort described in this thesis has been in this key area, since correct choice of operating frequency would enable the system's digital modem to operate with increased efficiency.

It is important to acknowledge the research programme undertaken by A. P. Jowett in the period 1986-1989, since that project identified the common elements in several automatic HF radio systems (Jowett, 1989). Furthermore, the use of the 'chirp' signals and spectral estimation of the channel structure as an aid to optimising frequency usage was initiated in that period. Sub-systems were simply prototyped or simulated and, as such, enabled the work described in this thesis to start at a stage where ideas could be advanced quickly.

1.2 Key Functional Elements of a Frequency Management System

The purpose of frequency management within an HF system is to provide lists of frequencies that are suitable for communication purposes. Due to variability of the propagating medium (the ionosphere) the frequency management system must operate periodically to track propagation variations so as to keep the frequency list updated. The frequency management process was traditionally undertaken by an operator, who, guided by lists of computer generated prediction tables, specialist training and experience, maintained communication with the rest of the system. Computer technology to automate the frequency management process often attempted to emulate some of the actions of the human operator. Hence, the operator used propagation prediction tables to choose a set of frequencies - termed "candidate" frequencies. The candidate frequencies were individually examined to find a set that was relatively free of noise and interference. Then communication was attempted on the quiet channels which were predicted to be propagating. This mechanistic operation was

a task ideally suited for a computer. The accuracy of the basic predictions models and co-channel interference quantification still presented practical limitations however.

Propagation predictions are based on computer models of the ionosphere. Such models use measured ionospheric electron density data to aid their computation of signal refraction. Signal to noise estimates use simplifications of radio system parameters. The output from a prediction provides a window of frequencies that are predicted to be operational. However, at best, such models are only median estimates of the propagation conditions and do not cover anomalous ionospheric states. To improve reliability, the choice of optimum working frequency (OWF) is usually taken as 85% of the maximum predicted frequency.

Measuring whether or not a channel is propagating is straightforward. It is possible to accurately measure the received field strength using a calibrated antenna, or estimate an approximate field strength in the radio system by having complete knowledge of the parameters in the radio system. Once the field strength is estimated it is then necessary to calculate the signal to noise ratio and, hence, predict the performance of the system in terms of bit errors in a digital signal. However, deciding if a channel is usable may not be simple, because of the time variability of both the wanted and unwanted signals.

At this stage the human operator would make an estimate of the best channel by using training and experience. This may involve rejecting the prediction tables and using a frequency that had measured propagation at some earlier instant, or identifying the source of interference and attempting to co-exist with it. A simple automated system would not embody all of this experience and probably fail.

The basis of this research is that frequency management can be undertaken successfully by examining the operations of the human operator, emulating those that are suited to automation and embodying others in new algorithms. A typical frequency management system performs two processes in its choice of candidate frequencies. The first, termed "channel selection" encompasses propagation prediction methods, measurement of external sources of propagation, and operator experience of propagation, in selecting a set of candidate propagating channels and rejecting those that are not suitable. Secondly, the candidate channels are ranked by the channel optimisation process. This involves the measurement of quiet channels, identification of co-channel interference, and knowledge of traffic parameters to rank the candidate channels into an order of merit. These processes rely on real-time measurements of channel state, or RTCE (real-time channel evaluation), being undertaken to describe the state of the channel at any instant. This state model allows the system to optimise its operation and channel selection.

A simple functional model of the frequency management problem is presented in Figure 1.1. As can be seen the problem is defined by two processes, each of which can be further broken down into sub-processes. The diagram also reflects the range of parameter measurements which can be applied to frequency management. These involve jointly processing the channel selection and optimisation data to form a link quality assessment (LQA) table or to give a figure of merit (FOM) for each channel. The diagram also demonstrates that the simple operator-based frequency management example discussed above only encompasses a small part of the frequency management problem.

Effective frequency management is one of the key functional elements in an adaptive HF system, since the system needs to utilise all of its frequencies (spectral resources) efficiently.

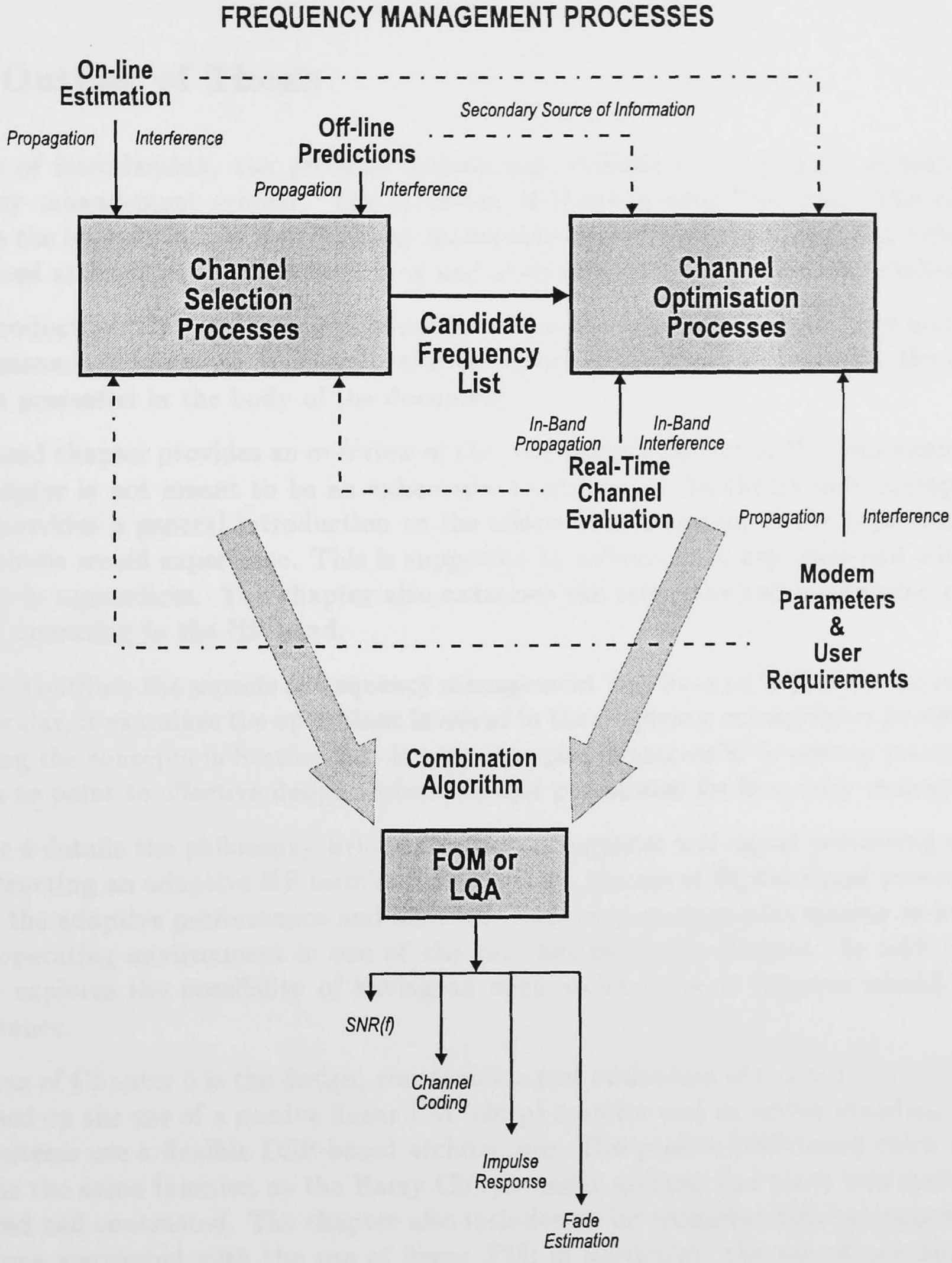

Figure 1.1: Model of Elements in an HF Frequency Management System

The use of DSP technology has enabled many individual channel selection, channel optimisation and RTCE processes to be undertaken automatically; however, the key problem is to allow the diverse data generated by each of the sub-systems to be processed and integrated so as to provide appropriate information on ionospheric state and so control the actions of the frequency management system.

1.3 Outline of Thesis

By way of introduction, the previous section has outlined the functional elements of a frequency management system. The structure of thesis is now described. The chapters describe the background to the frequency management issues and the philosophy behind the DSP-based architecture, before describing and analysing the specific solutions implemented.

The introduction, Chapter 1, is a brief outline of the fundamental concepts and motivation of the research programme. It presents the framework of the thesis and outlines the original research presented in the body of the document.

The second chapter provides an overview of the propagation aspects of HF communications. This chapter is not meant to be an exhaustive treatment of the theory and concepts, but rather provides a general introduction to the effects that a system of the type considered in this thesis would experience. This is supported by references to key texts and additional material in appendices. The chapter also examines the strengths and weaknesses of radio systems operating in the HF band.

Chapter 3 outlines the aspects of frequency management that have an impact on the research. In particular, it examines the operations involved in the frequency management process, thus extending the concepts in Section 1.2. It uses examples of successful frequency management systems to point to effective design techniques and procedures for frequency management.

Chapter 4 details the philosophy behind the use of computer and signal processing systems in constructing an adaptive HF terminal. Specifically, the use of digital signal processing to achieve the adaptive performance and allow the frequency management system to be aware of the operating environment is one of the key themes of this chapter. In addition, the chapter explores the possibility of having an open architecture to improve overall system performance.

The focus of Chapter 5 is the design, construction and evaluation of a channel selection system based on the use of a passive linear FM (chirp) monitor and an active sounding system. Both systems use a flexible DSP-based architecture. The passive DSP-based chirp receiver performs the same function as the Barry Chirpsounder system, and these two systems are compared and contrasted. The chapter also includes an investigation into propagation considerations associated with the use of linear FM; in particular, the use of non-linear FM signals to combat normal propagation anomalies, such as Doppler shifts, is considered.

Chapter 6 describes the channel optimisation system developed for the research programme. Specifically, details of both theoretical and practical aspects of the template correlation algorithm are presented. This algorithm operates in the frequency domain and directs modem energy towards regions of low interference. This algorithm improves error performance by reducing transmission energy in regions where poor signal to noise ratios (SNR) caused by

localised interference would induce errors. The final part of the chapter introduces a novel concept for HF frequency management systems — that of a joint channel selection and optimisation mechanism based upon a set of practical measurements. This technique, which involves generating a figure of merit for channel ranking, has implications for automatic link establishment (ALE) techniques, as well as for continuity of transmission. The research presented here takes the form of a theoretical investigation with some short simulation trials. The main function is to predict a bit error rate (BER) performance with respect to different types of transmission format. This data is used to predict the performance of the terminal, and 'intelligent' channel selections then can be made.

In Chapter 7, the results from several radio trials, both on and off-air, together with simulation results are analysed and presented. The results relate to all aspects of the practical investigations undertaken in the research programme.

The final chapter is devoted to presenting a set of conclusions and future directions for research. The appendices detail the additional theoretical background of specific elements of the project. The thesis concludes with a list of all the publications arising from the project.

1.4 Original Research Contributions

For the reader's convenience, the original contributions to engineering knowledge and practice arising from the research programme may be summarised as follows:

(i) for the purposes of channel selection, the implementation of in-band chirp (linear FM) monitor that allows the frequency management system to construct a model of ionospheric state utilising a commercial sounding network;

(ii) implementation of an active sounding system based upon the use of a segmented sounding scheme. This system allows the frequency management system to build its own ionospheric state estimates and allows channel selection to take place, independently of the commercial linear FM sounder network;

(iii) for the purposes of channel optimisation, spectral estimation of in-band noise/-interference energy to allow a DSP-based modem to change state so as to concentrate energy in regions of low noise/interference;

(iv) to enable joint channel selection and optimisation, a 'figure-of-merit' algorithm allows channel selection and optimisation based upon measured information. This section includes specification of a channel scattering function for frequency management purposes;

(v) development of an integrated systems architecture for DSP-based HF radio systems.

1.5 Review of Chapter

This chapter has introduced the motivation for and scope of the research programme. The next chapter discusses propagation in the HF band.

Chapter 2

The HF Environment

The purpose of this chapter is not to examine exhaustively the HF environment (2-30 MHz) but rather to provide a general introduction into the effects that a system, of the type described in this thesis, would experience when providing an ionospheric skywave(and groundwave) radio link. This chapter will concentrate on these effects and their physical basis, with more detailed material being provided in appendices.

2.1 Historical Perspective on the Use of HF Communication

Although communication using the ionosphere was only discovered in the early part of the 20th century, the need for frequency management was identified as early as 1914. The lack of frequency management was one of the factors that caused problems for British fleet communications (1917) when only a single frequency was available for all messages. The first solution to the problem was the use of tables of frequency changes for various paths and improved operator training. By 1939, the accuracy of such frequency tables had been substantially improved and communication was increasingly reliable. However, coupled with the increase in reliable communication there was an increase in the number of communicators. This accentuated to the problem of congestion in the HF band, which was increasingly being used by a number of organisations including the military, government agencies, large corporations and commercial broadcasters.

The use of HF was of strategic importance for communications in the period 1939-1945 for all major powers. Advances in HF signalling technology, predictions and information coding algorithms improved the reliability of HF communications. However, the effective use of HF resources was dependent upon the training of individual operators, their experience in choosing clear channels and their interpretation of predictions provided by propagation assessment services.

The improvement of HF services continued late into the 1960s when radio propagation provided reliable, long- distance communications. However, telecommunications technology and services provided by the new communications satellites were beginning to reduce the overall importance of HF radio systems. By the late 1970s, the use of HF had reduced substantially. This was due mainly to the performance of the latest generation of satellites

that could provide a near 100% communication coverage to anywhere in the world and support wider bandwidth services, for example television channels. In addition, the overall costs of operating an HF network were being scrutinised carefully, particularly the large costs of maintaining aging equipment and training and housing operators.

However, by the mid 1980s a new generation of HF equipment has given rise to a resurgence of the interest in strategic HF networks and systems (Gallagher *et al.*, 1994). This new interest was based on signal processing technology, improvements in frequency management and real time channel evaluation, and had a primary aim of providing a channel suitable for higher speed data modems (NATO, 1982). In addition, channel optimisation/selection and frequency changes were required to be automatic and transparent to the system user. Also, the use of computers has enabled HF networks potentially to be an effective part of a telecommunications architecture by allowing them to be incorporated into a more general communications infrastructure. The use of HF has also benefited from the realisation that communication satellites are subject to both propagation and capacity limits, high tariffs, solar interference (in particular, flares can cause a satellite to shut down), and space-borne and terrestrial jamming.

2.2 Strengths and Weaknesses of Operating in the HF Band

The use of HF (2–30 MHz) offers some substantial practical advantages to a communicator, these are:

(i) low cost of terminal equipment;

(ii) portability of terminal equipment; communication can be successfully achieved using 'manpack' sized equipment; (Darnell, 1986a)

(iii) low power requirements: this and the previous items imply that HF is very economical to use;(Hall & Barclay, 1990; Jowett, 1989)

(iv) flexibility of HF systems; they can be networked with relative ease and can offer communication in difficult terrain (Williams & Clarke, 1988);

(v) adequate available bandwidths: a typical HF user has a number of 3 kHz bandwidth SSB channels allocated across the the HF band;(Hall & Barclay, 1990; Jowett, 1989)

(vi) adequate signals strengths for data reception may be available over long distances;(Speight, 1992)

(vii) HF propagation is supported in areas of the world where signals from geostationary telecommunication satellites are strongly attenuated (latitudes greater than 70° north or south) (Davies, 1990).

The list of advantages, however, must be viewed in conjunction the disadvantages that such links exhibit when compared with 'line-of-sight' links (for example satellite communication–SATCOM). The disadvantages are:

(i) the variability of the propagation medium means that frequent frequency changes may be necessary to maintain link reliability. Links are also subject to anomalous propagation effects, such as ionospheric storms, which may affect the optimum operating frequency; (Hall & Barclay, 1990)

(ii) time dispersion (multipath) on a single link results from the multiple possible signal paths through the ionosphere, thus causing intersymbol interference (ISI); (Darnell, 1986b)

(iii) links are subject to frequency/phase and signal level fluctuations (fading); (Darnell, 1986b)

(iv) the large number of ionospheric users means that there may be a high degree of congestion and mutual interference (Wong *et al.*, 1985);

(v) wider bandwidth signals may be subject to frequency selective distortions; (Hall & Barclay, 1990)

(vi) some of the currently installed equipment is manpower-intensive in achieving optimal operation and is thus expensive to operate; (Darnell, 1986a)

(vii) some installed equipment has reliability problems due to aging effects; (Goodman, 1992)

A more detailed discussion of the HF communication environment, building on the preceding framework of strengths and weaknesses will now be presented

2.3 HF Propagation

HF radio propagation occurs in the band 2 to 30 MHz, with corresponding wavelengths in the range 150 down to 10 metres. Therefore, a 1/4 wavelength resonant antenna can have dimensions ranging from 2.5 to 37.5 metres and can be implemented using a simple suspended wire and a suitable tuning balun. The major propagation mechanisms are groundwave and skywave. Groundwave is a propagation mode that is dependent upon the shape and conductivity of the earth; skywave propagation exploits refraction of radiowaves by the ionosphere to achieve beyond line-of-sight (BLOS) communications. Groundwave propagation can be used for both line-of-sight (LOS) and BLOS links, with maximum ranges of a few hundred kilometres occuring over seawater.

It is well known that the effectiveness of HF skywave propagation depends upon the refractive properties of the ionosphere. The ionosphere is the ionised region of the upper atmosphere that lies between about 70 km and 500 km. Frequencies higher than 30 MHz tend not to be refracted by the ionosphere in normal operations, although Sporadic E propagation has been observed at frequencies up to 100 MHz (Davies, 1990). This means that propagation mechanisms, operating protocols and bandwidth limitations normally change above 30 MHz.

A radio terminal design of the type described in this thesis will predominantly be operating via oblique skywave propagation. This section focuses on the propagation effects that

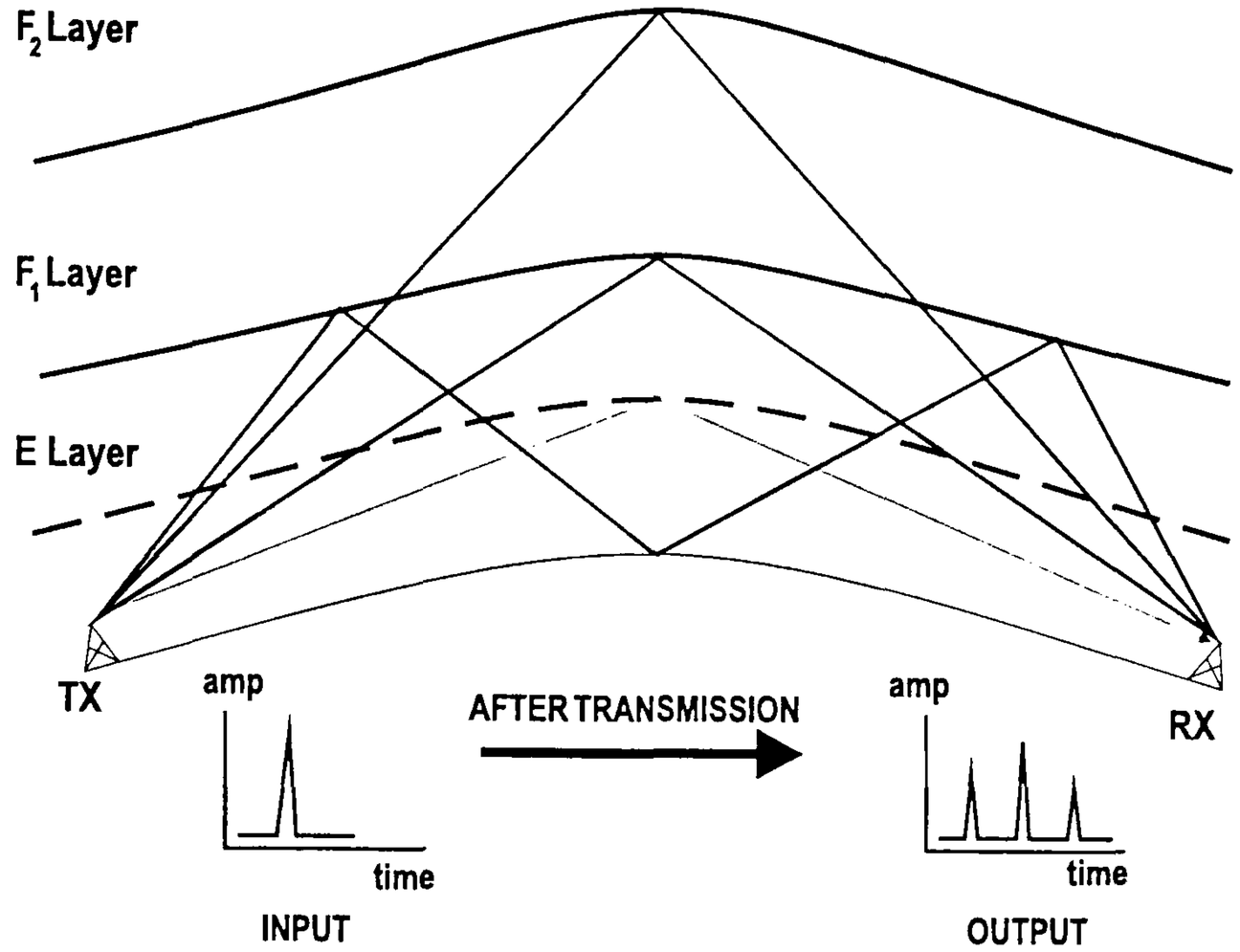

Figure 2.1: Plot of the multipath effects of layers in the ionosphere

will be observed during typical operation. The underlying concepts and some supporting mathematics for vertical and oblique incidence propagation are given in Appendix A.

A signal is refracted from the ionosphere because the ionisation is not vertically uniform and consequently has a varying refractive index with respect to height above the Earth's surface. The differing ionisation causes the ray to bend and subsequently return to the Earth, as would a light ray if transmitted through several layers of a transparent material with different refractive indices. By launching a radiowave, with a given frequency and angle of elevation, it is possible to realise a radio communication link whose range exceeds the visible horizon.

The received radiowave may exhibit multipath because solar effects, the earth's magnetic field and gravity give rise to ionospheric layers. These layers are termed, D, E and F, and have different refractive and absorptive effects on the signal; more information is given in Appendix A. Normally the F layers (F1 and F2) provide the predominant mechanisms of refraction (Davies, 1990), with additional refraction being provided by the E layer. The combined effect of the layer structure can be seen in Figure 2.1; it can be seen that a pulse transmitted towards the ionosphere may take several possible routes between the transmitter and receiver and consequently will have an impulse response, or delay profile, that illustrates the different refractive paths present. A link subject to different routes through the ionosphere is said to exhibit "multipath". This time dispersion can cause severe distortion to signals transmitted through the ionosphere. In addition, frequencies exceeding a critical frequency will not be sufficiently refracted and will therefore not return to Earth. The refractive process is dependent upon the height variation of ionisation. From atmospheric studies it has been shown that the amount of ionisation is largely dependent on the amount of solar radiation. Therefore, for a particular link there will be a diurnal cycle of available frequency range. There is also an 11-year cycle of solar radiation (Davies, 1990). The amount of solar radiation is influenced strongly by sun-spots that are cooler regions

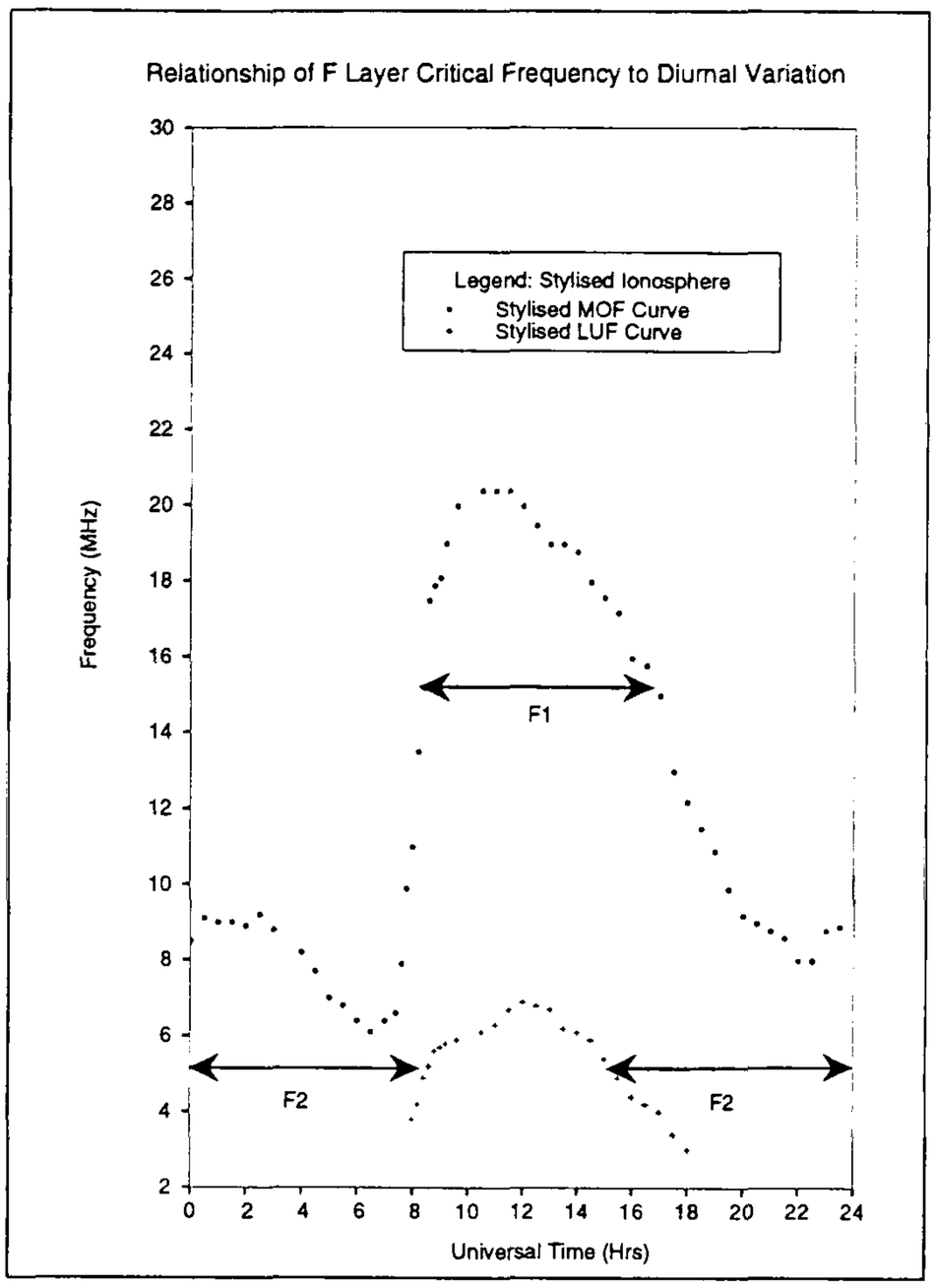

Figure 2.2: Plot of F layer MUF and LUF for diurnal variation: Stylised Ionosphere—Winter in Mid-Latitudes, Sunspot Number = 29, Path Length = 1000km, Predictions From SUP252. (Appropriate operating frequencies F1 and F2 are also shown.)

of the sun's corona and emit a large amount of harsh radiation. Finally, the link will be subject to seasonal variation, dependent on the latitude of the link. Predicting the critical frequency thus requires the path length, sun-spot number, season, and link orientation to be known (Goodman, 1992). A plot of a typical diurnal cycle of a mid-latitude path path in winter is shown in Figure 2.2. As can be seen, to maintain communication different frequencies must be used at different times during the day. The lower bound to propagation is caused by the lowest signal-to-noise ratio (SNR) at which the signal can be recovered. During the day, the D layer absorbs proportionately more of the radio energy and consequently the minimum frequency that can be used increases. The maximum propagating frequency supporting the required conditions for communication is usually termed the maximum usable frequency (MUF); similarly the minimum frequency from which the signal can be recovered is termed the lowest usable frequency (LUF). Further discussions of the MUF and LUF is given in Appendix A.

There exists a complex physical relationship between the Earth, the ionosphere and the sun. The discussions so far have concentrated on the behaviour of a radio signal as it is varied in frequency. However, the signal when set to a particular frequency will be subject to fading. Fading is an important limiting factor for an HF communication link.

2.3.1 Fading Mechanisms

In an HF radio communication system, the fading characteristics provide the main limitation on the system performance. All types of fading disrupt communication; for example slow, deep fades, which have been measured to last several minutes, can cause cessation of communications during the fade out period; transmission resumes when the signal returns. Fading in the HF band is caused by several different mechanisms. The following are typical of those that an HF system will encounter:

Frequency Selective Fading (FSF) is caused by the fact that a fixed time delay (multipath profile) includes different numbers of wavelengths at different frequencies. The resultant interaction (constructive and destructive interference), is observed as a notch (instantaneous frequency null), or notches, in the passband of the receiver. The changing frequency characteristics of FSF are caused by the movement of the ionosphere.

Flat fading is mainly caused by variations in ionisation density and absorption within the ionosphere. The fading has been found to possess log-normal characteristics in the long-term with a Rayleigh model being applicable when rapid fading occurs or in the short term (0.5-10 minutes) (Davies, 1990; Goldberg, 1966). Fading depths of greater than 20dBs have been measured with fade- outs occurring over several minutes (Davies, 1990; Hargreaves, 1979; Goldberg, 1966).

2.3.2 Less Predicatable Propagation Effects

The ionosphere can exhibit a wide range of comparatively unpredicatable effects. Typically, these conditions are (Darnell, 1983):

(i) sudden ionospheric disturbances or SIDs (Davies, 1990; Hargreaves, 1979);

(ii) polar cap absorption, or PCA This effect is usually only observed in systems operating at high latitude; (Matshushita, 1959).

(iii) ionospheric storms (Davies, 1990; Noyes, 1982);

(iv) travelling ionospheric disturbances, or TIDs (Hall & Barclay, 1990; Thrane, 1986b);

(v) geomagnetic field disturbances. (Davies, 1990; Matshushita, 1959)

The above mechanisms can have severe effects on the performance of an HF communication link and can cause the system to observe ionospheric "black-outs" where no communication is possible. The amount of time that the system cannot use the ionosphere can vary between a few minutes and several tens of hours (Hunsucker & Bates, 1969).

2.4 Noise and Interference

It has already been stated that, in a practical HF system, the lowest usable frequency (LUF) is largely dependent upon the signal-to-noise ratio (SNR) at the receiver. In a

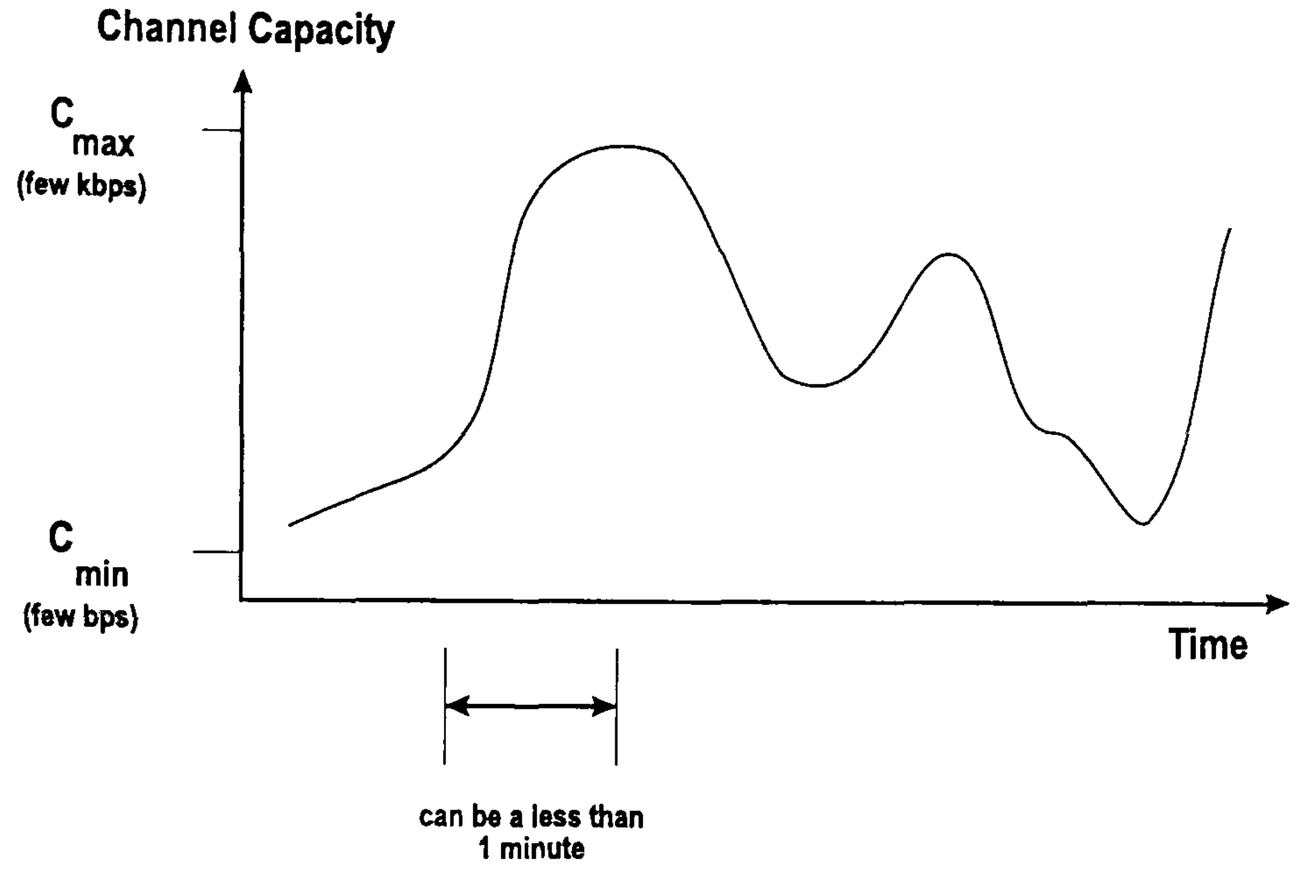

Figure 2.3: A Plot of Typical HF Channel Capacity

typical HF communication system, the SNR is determined by system considerations such as transmitter power, antenna gain and beamwidth, and ionospheric absorption and fading. The bandwidth of the channel is set by international channel assignment policy but may be further limited by the multipath spread produced by the ionosphere which will result in intersymbol interference (ISI) (Schwartz, 1981) at the receiver.

In addition, the received SNR is further degraded by interference from other users, termed co-channel interference. These combined effects make the HF channel difficult to use reliably. The temporal variations in the HF channel are well documented and a typical capacity versus time plot is shown in Figure 2.3. The conditions can change rapidly from a stable high capacity channel supporting data at a few kbps, to a state where maintaining transmission of a few tens of bps is extremely difficult. The transition time between states can be very small (Darnell, 1986a). The modelling HF channel time variability has been attempted (Tsai, 1969), but with only with limited precision. The resulting model does reflect the "bursty" nature of the communication medium where large error-free data blocks, or blocks with randomly distributed errors can be interspersed with completely corrupted data. In these cases, it is essential that the error-control capability of the transmission system can cope with this type of variability. Figure 2.4 shows a typical error variability plot from a radio trial (Darnell, 1981).

2.4.1 Co-Channel Interference

Co-channel interference is due to other spectrum users. Although parts of the HF band are allocated on a global scale by the ITU, it is the responsibility of individual countries to allocate groups of channels. Channels are allocated to users according to need and availability and may be spread across part or the whole of the HF band. Military users and broadcasters have large dedicated sections of the spectrum allocated for their purposes. This allocation process works reasonably as most channels are allocated by imposing a large reuse distance. However, at night when propagation can be restricted to lower parts of the spectrum and the absorption of the D layer is at its minimum, congestion can become a

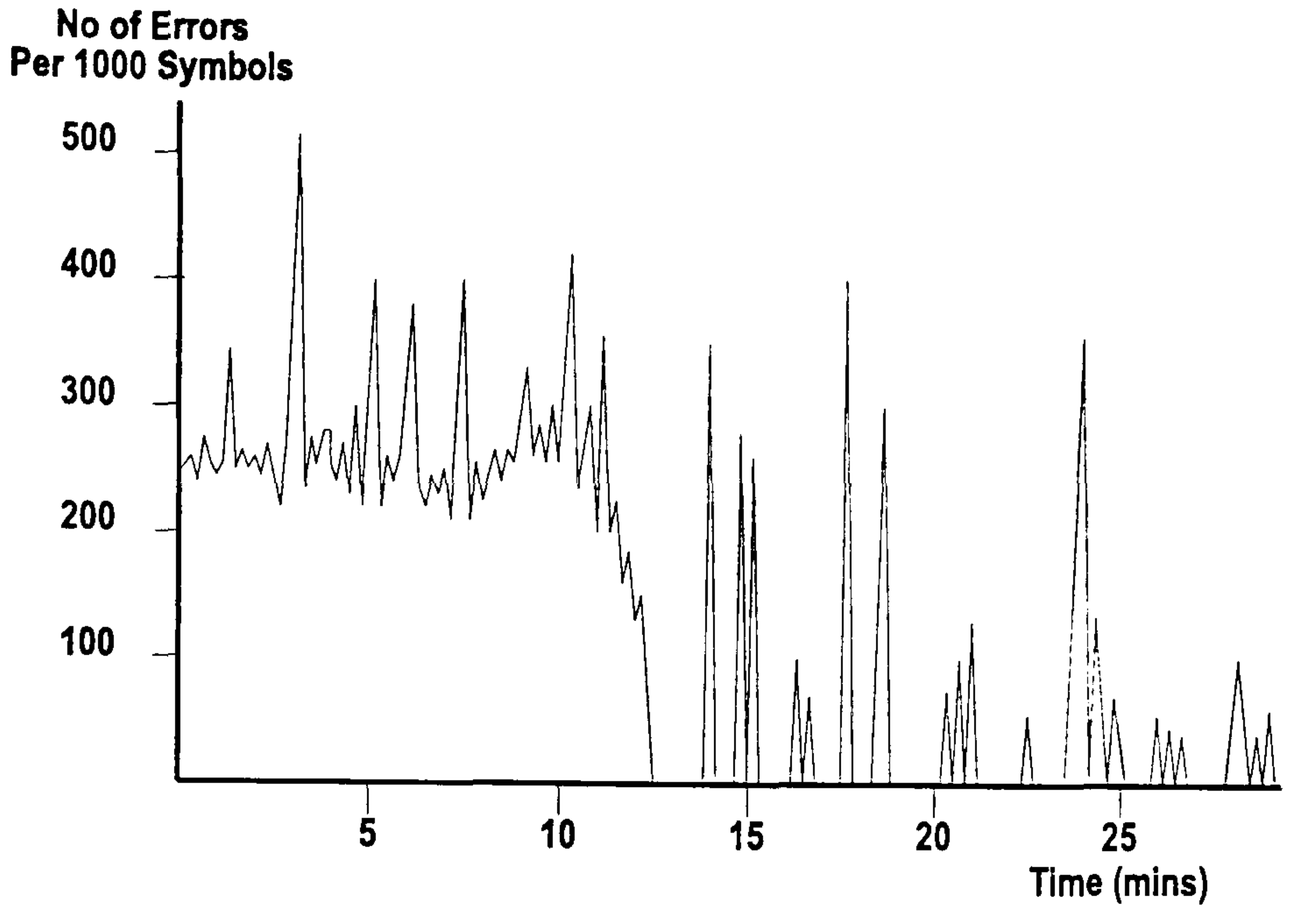

Figure 2.4: Distribution of Block Errors
Showing "Bursty" Nature of HF Transmissions (Courtesy M. Darnell)

problem and interference from other users can disrupt allocated channels. The disruption is also due, in part, to poorly designed HF equipment and emissions in excess of the normal 3 kHz SSB allocation (Hall & Barclay, 1990; Darnell, 1983).

Co-channel interference is predominantly narrow-band (Darnell, 1982) and it is very difficult to quantify. It has been shown that co-channel interference spectra tend to remain stable for several minutes (Gott & Staniforth, 1978). Statistical modelling of the interference structures present on HF communication links was undertaken in the early 1980s (Wilkinson, 1982). A systematic study of the problem was also started at UMIST (Laycock *et al.*, 1988; Gott *et al.*, 1991). The aim of this research programme is to build a comprehensive statistical model of the interference structures in Western Europe over a solar cycle. The statistics relate the probability of choosing a clear channel of given bandwidth to the phase of the diurnal cycle, seasonal cycle, solar cycle and HF system parameters (Gott *et al.*, 1994).

2.4.2 Man-Made Noise and Intermodulation Products

Statistical characteristics of man-made noise and other interference sources are reasonably well defined; thus, statistical models of average interference spectra and noise powers are used to estimate the limitations that may be placed upon the HF communication system.

Man-made noise is generally caused by electrical machinery, for example car ignition and power distribution, and the noise powers associated with man-made noise are well correlated with the type of location. The overall noise power associated with man-made noise tends to attenuate sharply with distance, so siting antennas away from urban areas can reduce interference problems considerably.

Passive intermodulation products (IPs) can cause effects similar to those of man-made noise. The generation of IPs is due to the presence of non-linearity. Such non-linearity causes some of the radiated power to be transferred from the fundamental frequencies found in a typical

electrical system to a series of harmonics and sum and difference frequency products. In a poorly designed system, these IPs can have a severe effect on the performance of the system. In addition, the products can be spread across the HF band and hence can cause interference to other users. The non-linearities found in a typical HF system occur both in the receiving and transmission equipment (antennas, feeders, couplers, etc.). Minimisation of IP generation is an EMC (electromagnetic compatibility) problem. The non-linear junctions where IPs can occur can be modelled by a finite, complex power series, i.e.

$$P_{out} = \sum_{n=0}^{N} A_n x^n \tag{2.1}$$

where

P_{out} = Output power
x = Input power
A_n = Complex coefficient characterising the power series
N = the number of terms in the series

Typically, intermodulation production can occur predominantly in the power amplifier (PA) due to poor design causing the PA to saturate; in mixers, because they are inherently non-linear; in oxidised interfaces in antennas, couplers and feeders (this is often called the "rusty bolt" effect). The "rusty bolt" mechanism is often a limiting effect in maritime mobiles. Reduction of the IPs generated at such junctions is based on special treatment at interface points between dissimilar metals or a metal and its oxide.

2.5 Review of Chapter

This chapter has presented an overview, from an engineering perspective, of the propagation, noise and interference environment encountered by HF systems. It is not meant to be exhaustive in terms of physical models, but instead to indicate the nature of the problems associated with the operation of systems in this environment.

The following chapters provide the details of the more specific aspects of the project; in particular, on the subjects of adaptive frequency management, and DSP-based approaches to the problems of HF radio terminal design, construction and operation.

Chapter 3

Frequency Management Processes

This chapter provides an introduction to HF frequency management. The development of frequency management procedures and implementing such procedures on DSP devices was one of the key aims of the research programme described in this thesis.

3.1 Philosophy of Frequency Management

The term "frequency management" describes the function of maintaining radio communication by efficient use of the frequencies allocated to the system. By using effective frequency management procedures, radio connectivity can be made more reliable and the system is able to pass traffic between radio stations with greater efficiency. In a practical system, this means that channel selection and optimisation procedures are used to select the best channel for a particular traffic type, for example voice or digital data. Conventional frequency management systems usually perform these processes during link establishment; further frequency management is only usually performed at specified times, or if communication ceases suddenly, due say to unfavourable ionospheric conditions. Conversely, an adaptive, automatic frequency management system performs the operations continuously so as to maintain optimal performance.

In a basic frequency management system, channel optimisation is usually not performed and channel selection is made using off-line predictions of ionospheric state. This does not take into account short-term channel perturbations, unusual propagation effects (for example sporadic E, E_s), or interference, and the frequency management is clearly not optimal.

The use of off-line predictions only will provide a list of frequencies which will provide the requested SNR averaged over time. Therefore, the propagation model is typically used as a system planning tool, or as an initial estimate of the channels that can be used by the system. For efficient operation the system must use more sophisticated channel selection and optimisation procedures to optimise usage of all the frequencies allocated to the system.

In a typical system terminal there are two periods when frequency management is particularly important. The first period is during the initial connection, or link establishment, phase; the second is when frequency changes are required. During both these periods, communication may be intermittent, but it is essential that periods when communication is

inhibited are kept to a minimum.

To aid understanding of the issues of frequency management, a model of the procedures incorporated in a typical frequency management system is presented. The relationship between each of the operations must be quantified in order to establish the relative of importance between and benefit of each. As detailed in the introduction this is a key aim of this thesis. This model is outlined in Figure 1.1.

The model of the frequency management task is partitioned into channel selection and channel optimisation procedures. The output of the channel selection procedure will be a set of ranked channels which will then be further processed by the channel optimisation procedures. The channel selection procedure relies on the use of off-line propagation estimates to provide an initial estimate of the conditions. These are then updated in response to on-line measured data. Once the channels are ranked, the channel optimisation procedure will further analyse the set and suggest a sub-set that will match prevailing channel conditions and traffic type chosen.

The task model is also extended to allow the possibility of combined channel selection and optimisation. In Figure 1.1, this is termed as "figure-of-merit" (FOM). The aim of such a combined procedure is to estimate the channel's fundamental model, termed a scatter function, and to relate this to the modulation scheme under consideration. Such procedures are examined in Chapter 6.

3.2 Adaptive HF Radio

In order to understand the complex concept of adaptive HF radio, the historical development of frequency management and HF systems needs to be outlined. However, adaptive HF is the most technologically advanced area of HF communications, since the demands on HF systems increasingly include being part of the normal telecommunication infrastructure. This means that an HF system may be utilised as an alternative radio telecommunication network for medium rate telegraphy (300-9600 bps) for medium to long range links. In such cases the system must be able to use data standards such as ATM (asynchronous transfer mode) as part of the protocols of the system.

In the period 1940-1960, the frequency management and operation of HF systems were performed using simple propagation models in conjunction with trained operators controlling the frequency management processes. Such HF systems had a typical link reliability of the order of 50-80% (Elvy, 1985). Such reliabilities were a direct consequence of median nature of the propagation models, the use of the FOT[1] and the ability of the human operators. These levels of link reliability were observed until the 1960s when the first "adaptive" systems were introduced. The adaptivity was limited to some simple form of channel tracking, for example in the channel evaluation and calling (CHEC) system (Stevens, 1968). This potential for adaptation pushed the reliability of communication to 70-90%. Reliability was often reduced if only limited numbers of frequencies were allocated to the system, or if there were poor training resources for HF operators.

The first use of automatic HF systems in the period 1970-1990 attempted to achieve greater

[1]Typically FOT=85% of the predicted MUF.

reliability than those using direct operator involvement (Elvy, 1985). However, it was not feasible to increase the reliability of links to much above 85% using the available technology. In the late 1980s, a solution to this problem was devised in the form of adaptive HF. It was hoped that by using such adaptive systems, communication reliability would be increased to over 90%.

"Adaptive HF" is a rather vague concept: one proposed definition is:

> "Adaptive HF requires the capability of channel trait-tracking coupled with near real-time system parameter adjustment to optimise system performance." (Goodman, 1992).

Coupled with adaptive HF systems, which encompass all aspects of system design, e.g. channel coding methods [modulation, demodulation, error-control and synchronisation] and channel tracking algorithms (RTCE), is a need for a comprehensive adaptive frequency management system to control the frequencies, or pool of frequencies, allocated to the system. The adaptive frequency management system has a focused objective:

> "Adaptive Frequency Management defines the processes involved in providing a transparent communication medium that can support requested traffic, regardless of channel or propagation state (Gallagher & Darnell, 1991)."

In order to attain fully adaptive operation, the philosophy surrounding HF system design and the concepts involved in the utilisation of HF systems needs to be re-examined and possibly redefined. From the two example definitions provided above, it can be seen that the HF system needs to be able to make rapid control decisions, not only in response to changes in propagation conditions, but also in response to complex user requirements or changes in data traffic. To facilitate this process real-time measures of channel state should be available on a continuous basis. Ideally, therefore, it can be seen that a system with this form of adaptivity would be able to operate even with the most adverse of propagation conditions and varied user requirements. This type of operation contrasts strongly with that of systems such as HDRS (Reed & Hopkinson, 1988) or CHEC (Stevens, 1968) where state measurements were only taken according to a schedule, or on a link-by-link basis at setup.

Implicit in any design is the need for appropriate forms of embedded RTCE, off-line prediction models and an on-line mathematical model of the system that would allow the effect of system changes to be estimated before committing the system to adapt. This would require a significant embedded processing capability and also the system to 'learn' from its operating environment in order to make 'knowledge-based' control decisions. An important aspect of any adaptive system would be the signal interfacing sub-systems. These would need to operate in many different modes, ranging from voice and robust data transmissions to high-speed serial data formats. In order to control such a system, a frequency management process would have to be scheduled in response to changes in either data, user requirements or environment.

In addition to adaptivity at the individual terminal level, the adaptive HF frequency management processes must also be able to cope with being integrated into adaptive networks

where environmental measurements are distributed. In such cases, the frequency management system will have more responsibility for maintaining network connectivity rather than the simpler link-based connectivity used to date (Gallagher *et al.*, 1994).

The next sections examine the conventional processes of channel selection and channel optimisation, and examples of how such procedures are undertaken.

3.3 Channel Selection

The channel selection procedure is one of the most complex elements within a frequency management system. It is essential that for successful communication the parts of the HF band that are propagating over the link of interest be identified. This can be undertaken by a variety of methods, of which a propagation prediction procedure often forms the basis. This is usually augmented by the use of an updating real-time propagation assessment procedure which measures the actual propagation conditions. Comprehensive real-time operation may not be possible if bi-directional data transfer between HF radio stations is not available; in this case the use of other methods to update the median outputs from propagation predictions, such as passive monitoring of the ionosphere, are needed (Masrani & Riley, 1991).

3.3.1 HF Prediction Methods

As indicated above, for successful frequency management, a sophisticated approach to selecting frequencies for transmission must be adopted. The use of an off-line prediction program can form the basis of initial channel selection since the output from such a system will produce an estimate of range of median propagation conditions. There are several popular ionospheric prediction programs (Thrane, 1986a; Goodman, 1992; Davies, 1990). All are based on empirical techniques; measurement databases are used in conjunction with analytical propagation models.

Examples of readily available prediction programs include:

(i) SUP252-2: The algorithms utilised in this program are based upon simple ray-tracing techniques using CCIR approved ionospheric maps (CCIR, 1970). Its approach to the problem has been superseded by more modern propagation prediction methods.

(ii) IONCAP (ICEPAC): This propagation prediction program uses calculations based upon ray-tracing and predefined parabolic equations, but employs additional statistical techniques to improve performance with anomalous ionospheric effects, for example sporadic E (Teters *et al.*, 1983).

(iii) CCIR-894: This model is based upon calculating HF signal strength according to predefined parabolic equations that describe a 'typical' ray in the ionosphere. It is primarily designed for planning of HF broadcast circuits, but its accuracy and computational speed make it very popular (CCIR, 1986a).

```
1                METHOD  6    REP894-2  VER-1.02  24.JAN.90                PAGE   1

                 OCT     1991          SSN = 174.
   HULL                    OSLO                      AZIMUTHS    SP   N. MI.      KM
   53.78 N     0.33 W    60.06 N    10.13 E      37.98  226.76      508.5    941.6
   MIN ANG  0.0 DEG, PWR   0.10 KW, XLZ  2.8 DB, XLY -4.2 DB, FTZ DIST  7000. KM
     TX-ANT  ISOTROPIC   TBEAR  0.0           RX-ANT  ISOTROPIC   RBEAR  0.0
       LUF 50       NOISE CATEGORY 2        3000 HZ RX BDWTH       REQ S/N  5 DB

   UT  MUF                                                                LUF   FOT OPMUF

    1  6.6   3.0   5.0   5.7   6.0   7.0   8.0  12.0  15.0  18.0  21.0 FREQ  2.0   7.0   8.2
       1F2   1F2   1F2   1F2   1F2   1F2   1F2   1E    1E    1E    1E   MODE
        39    39    39    39    39    39    39    10    10    10    10  ANGL
        24    21    23    24    24    24    18   -51   -50   -49   -49  DBU
        18    12    16    17    18    18    14   -53   -51   -50   -50  S/N
       .92   .78   .87   .90   .91   .91   .85   .01   .01   .01   .01  FS/N

    2  6.2   3.0   5.0   5.7   6.0   7.0   8.0  12.0  15.0  18.0  21.0 FREQ  2.0   6.6   7.7
       1F2   1F2   1F2   1F2   1F2   1F2   1F2   1E    1E    1E    1E   MODE
        39    39    39    39    39    39    39    10    10    10    10  ANGL
        24    21    23    24    24    22    13   -51   -50   -49   -49  DBU
        18    13    17    18    18    16     8   -53   -51   -50   -50  S/N
       .91   .79   .88   .90   .90   .88   .69   .01   .01   .01   .01  FS/N
```

Figure 3.1: An example output (textual) from CCIR 894 propagation prediction package

(iv) MINIMUF: This is another prediction package using a curve-fitting method for calculation of the MUF. The curve shape is parameter-based with the current sun-spot number being the predominant factor that affects computation (Sailors *et al.*, 1986).

(v) ASAPS. This prediction program also employs ray-tracing algorithms but augments the CCIR ionospheric maps with further estimates based the use of daily solar activity parameters e.g. sun-spot number and 10.7cm flux (IPS, 1991).

These prediction programs have been assessed by the CCIR and the results published (CCIR, 1982). It has been found that the 'ray-tracing, methods produce the most accurate results, but the signal-to-noise predictions can be very inaccurate (Peres & Finkelberg, 1981). The empirical predictions suffer from the most inaccurate results and MINIMUF can produce outputs that are several MHz below the actual MUF (Sailors *et al.*, 1986).

Example formats from the offline prediction program CCIR 894 are shown in Figures 3.1 and 3.2.

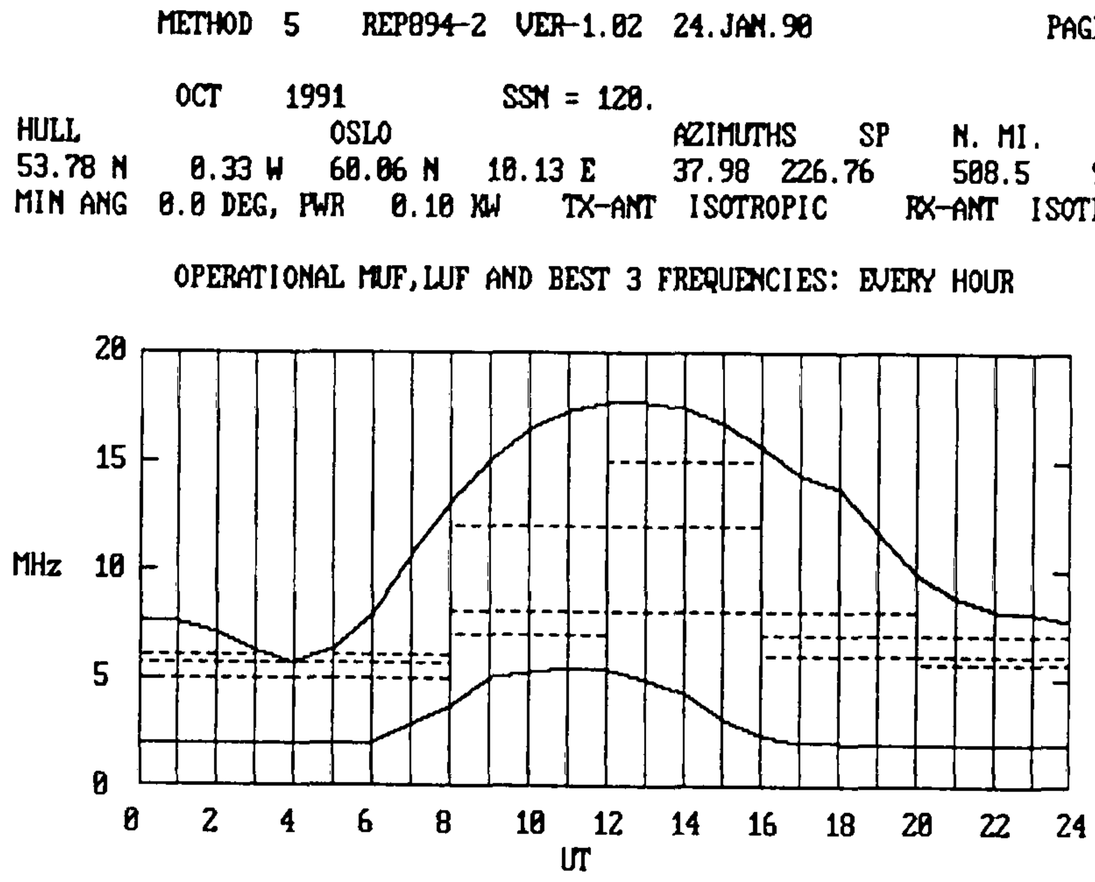

Figure 3.2: An example output (graphical) from CCIR 894 propagation prediction package

3.3.2 Real-Time Augmentation of Prediction Models

The inherent inaccuracy of off-line predictions compared to real-time propagation conditions means that, in a practical HF system, the results usually need to be augmented by real-time propagation measurements. Of the several possible ways of implementing this procedure, the most popular include: actual link propagation data, the use of results from passive propagation assessment, the use of vertical ionosonde data, and active sounding of the ionosphere over the path of interest. In many cases, measured results may have to be interpolated from diverse sources to estimate the ionospheric conditions on the path of interest.

Vertical ionosonde data is available from collection centres (for example Slough, UK) and that data is then used to update off-line predictions (Milsom, 1987). The data can be correlated over a period of several days to facilitate short-term prediction of future ionospheric trends (for periods of several hours). This has been used to provide the Short-Term Ionospheric Forecasting Service (STIFS—Marconi Communications).

One of the problems with using data from a remote ionosonde is that the correlation of ionospheric parameters between remote vertical ionosonde and the actual communication link may be low (Goodman & Daehler, 1988). Therefore, any improvements to the results produced by the off-line prediction programs will be modest (Hunsucker, 1990).

Further improvement may be obtained if ionospheric data is gathered passively at the communication terminal. This may be achieved by monitoring signals of opportunity, for example chirp signals, utility signals (RTTY, FAX), time signals and broadcast signals. This data can be built into a database of ionospheric conditions; some of the signals close to the path of interest will be particularly useful (Masrani & Riley, 1991) since interpolation routines will not have to be sophisticated.

The best method of updating the outputs from an off-line prediction program is to sound the path of interest. This may be achieved by chirp (linear FM) sounding, coded-sequence sounding or by simple pulse sounding (Daehler, 1984). The coded-sequence and chirp sounding methods are essentially spread spectrum operations and rely on processing the received signal by a pulse compression algorithm at the receiver. No extra processing of the data is necessary in pulse sounding, apart from accurate synchronisation to track the signal as it sweeps across the band. Pulse sounding needs specialised RF equipment since the processed sounding signal must be of an effective duration much less than the multipath spread that it is intended to quantify. In coded pulse schemes, synchronisation may be taken from the coded pulse structure as the signal duration can be substantially longer than the minimum multipath structure; for example, a chirp signal of length 30ms and sweep rate 100 kHz s^{-1} can detect multipath spreads of 0.3ms or greater in a normal 3 kHz channel. In coded-pulse schemes, the limiting factor tends to be the bandwidth allocated for signal transmission. Multipath analysis may be performed by post-detection processing of the received signal in complex matched filters.

Sounding the path (of interest) may be performed when required, or periodically. This type of sounding can produce precise assessment of 'all-band' conditions; for example, the LUF and the MUF can be accurately measured. In addition, the impulse responses near, or on, frequency allocations can be measured. This allows the channel selection procedure to produce results that can also be exploited in the channel optimisation procedure.

The channel selection procedure is ultimately designed to indicate a set of channels that are propagating. If accurate measurements of the propagation conditions are possible, the procedure can be refined. This may mean that the channels can be sorted into a set that offers the best chance of not being blocked by interference, or that can support the chosen modulation scheme. This is best illustrated by considering sporadic E as the mechanism supporting communication: if sporadic E can be identified, it offers the option of transmitting at a frequency greater than the normal predicted MUF. A system using just off-line predictions will be limited to transmitting on frequencies less than the predicted median MUF. Since the FOT is typically taken as 0.85× MUF, many systems will attempt communication in the same part of the HF band. Initiating transmission away from the crowded parts of the spectrum, and transmitting above the normal MUF, means that the initial link establishment procedure has a greater probability of success. Error rates caused by co-channel interferers will also be reduced.

When determining the set of channels that are propagating it is possible, for example, to rank the channels according to the number of modes propagating. This is because signal error rates tend to be limited by intersymbol interference (ISI), which is a function of multipath spread and transmission rates; choosing channels that have minimum dispersion will allow maximum data rates to be achieved. This does not take into account the effects of processing at the receiver, where an equaliser can counteract the effects of ISI. Low rate transmission, for example using the PICCOLO modem (Bayley & Ralphs, 1972), can tolerate large multipath spreads because the symbol intervals are so long; a serial modem, however, is sensitive to changes in the multipath structure since the equaliser must adapt to the changes.

3.4 Channel Optimisation

Once the channels that are propagating have been identified, and have been sorted into a set that offers the best overall chance of allowing communication, the next stage is further analysis to provide a sub-set that can support the type of traffic desired. The ability of a channel to support a given transmission format is ultimately based on constraints such as the signal-to-noise ratio (SNR) of the received signal and ionospheric distortion — for example, multipath, frequency dispersion and fading.

The simplest form of channel optimisation procedure is to assess the amount of interference in the channel (Darnell, 1975a) and hence provide an indication of the average SNR. Channels with a low average SNR would be rejected since they would give rise to a large number of errors in the received signal. This assessment can be achieved by using frequency domain analysis of the channel bandwidth or by using the output of the AGC (automatic gain control) circuits. If the results are time averaged, channels that exhibit high average levels of interference can be rejected.

This type of channel optimisation procedure can be effective when coupled with a channel selection scheme that ranks channels according to their multipath structure. This has been demonstrated by several workers (Darnell, 1975b; Barry & Fenwick, 1975; Gallagher & Darnell, 1991) and is the basis of several commercial frequency management systems, for example CHIRPCOM. Such a channel selection and optimisation procedure is, however, not an optimal solution. It suffers from several deficiencies: in particular, the channel ranking procedure, when searching for frequencies exhibiting single mode propagation, does not take the stability of the mode into account; frequently it rejects channels that have a high average interference but which could still could support narrowband communication in spectral "gaps" within the channel bandwidth. In addition, ranking channels simply according to their mode structure without taking into account the effects of the time spread and frequency dispersion upon the modulated signals (in terms of ISI and Doppler offsets) means that channels that are adequate for communication may be rejected.

Clearly, channel optimisation would be more effective if the "in-band" interference structure could be characterised accurately and the interference spectrum compared with that of the desired modulation scheme. A combination of channel optimisation and channel selection effectively specifies a comprehensive channel model in the form of a scatter function (Bello, 1963). Estimating the channel scatter function allows its effects on different modulation schemes to be assessed by using a convolution process; hence the corresponding error rates can be estimated.

3.5 Real-Time Channel Evaluation (RTCE)

The need for real-time channel evaluation is based on the limitations os prediction models in assessing the impact of man-made interference, transient propagation effects and mode structures on specific transmission schemes. Although a channel may be propagating, communication could be severely limited by unfavourable propagation effects, such as deep fading or the presence of a strong co-channel interferer. Real-time channel evaluation attempts to extract this more precise channel state information and use it to improve communication

efficiency. In contrast to long-term and short-term prediction (forecasting), the processes of real-time channel evaluation (RTCE) may be termed "nowcasting" (Goodman, 1992). The use of RTCE techniques has developed to a point where they are of critical importance in effective frequency management of automatic and adaptive HF systems.

Real-time channel evaluation is essential in the frequency management process and is required in both the channel selection and optimisation phases. One of the recognised definitions of RTCE (adopted by the CCIR) is given below:

> "Real-Time Channel Evaluation is the term used to describe the processes of measuring appropriate parameters of a set of communication channels in real time and employing the data thus obtained to describe quantitatively the states of those channels and hence the capabilities for passing a given class, or classes, of communication traffic." (Darnell, 1978; CCIR, 1986b).

The above definition implies that (Darnell, 1986b):

(i) the processes involved in RTCE are used to derive a mathematical model of the conditions on each of the propagating channels, that can then be used for system control and performance prediction purposes; the RTCE algorithm must be designed to match the data or signal traffic being transmitted;

(ii) "real-time" operation means that channel parameters are measured and updated more frequently than the response time of communication system to control inputs— measurements taken too frequently will be redundant;

(iii) the output of the RTCE algorithms must be in a form that is meaningful for system control; for example, the estimated BER when transmitting data, and intelligibility for speech;

(iv) RTCE is used to measure not only the effects of propagation on system performance, but also other limiting factors such as interference from other users, or man-made noise;

(v) RTCE can be used to indicate effective transmission "time" windows;

(vi) RTCE enables relatively transient propagation modes, other than the normal modes predicted, to be used for communication; for example, sporadic E and tropospheric propagation.

Implementations of RTCE algorithms fall into three basic classes (CCIR, 1986b):

Class I: **Remote Transmitted Signal Preprocessing.** In this class of RTCE, information is extracted by processing signals at the remote site. The signals chosen are often probing transmissions from the base station, for example this method is used in the Channel Evaluation and Calling System (CHEC) and chirpsounder receivers. Similarly, signals of opportunity, for example broadcast and time signals, can also be used to obtain information about the channel state.

Class II: **Base Station Signal Preprocessing.** This class of RTCE obtains channel state information by processing signals at the base station. Although propagation information can be obtained passively by monitoring signals of opportunity, channel state information may also be obtained by actively probing the ionosphere, for example using vertical-incidence sounders and backscatter sounding systems.

Class III: **Remote Received Signal Processing.** This class of RTCE describes methods of extracting channel state information by processing information embedded in the transmitted signal. It processes signals transmitted normally as traffic, although specific components may be necessary for RTCE purposes. Examples of Class III RTCE systems include error-counting systems and pilot tone systems.

Although the CCIR has defined the three types of RTCE above, RTCE can also be classified in other ways, including in-band (current channel) and out-of-band (alternative channel) RTCE, or active and passive RTCE (Darnell & Honary, 1991). Specifically, in active RTCE systems signals are used to probe the in-band and out-of-band channel states, whereas for passive RTCE systems, a terminal assesses the radio environment by 'in-band' and 'out-of-band' received signal analysis alone. Passive RTCE techniques, dependent upon data traffic analysis, are also termed *embedded* RTCE, since relevant channel state information is extracted after processing the normal communications traffic. In this thesis, a classification of RTCE techniques in terms of "in-band" and "out-of-band" types is most appropriate. Some of the in-band methods considered can also be viewed as "embedded" techniques.

Examples of metrics that have been used in successful RTCE systems include (Darnell, 1983; Darnell, 1986b):

(i) signal amplitude;

(ii) signal frequency;

(iii) signal phase (absolute, relative or differential);

(iv) propagation time (absolute or relative);

(v) noise or interference level;

(vi) channel impulse response function;

(vii) SNR, signal plus noise plus distortion to noise plus distortion ratio (SINAD), or signal-to-interference ratio (SIR) level;

(viii) automatic repeat request (ARQ) rates;

(ix) error control decoder metrics;

(x) received bit error rate (BER);

(xi) speech intelligibility; etc.

In general, it can be assumed that most RTCE techniques attempt to extract the instantaneous SNR estimate for each frequency, or each sub-channel, in order to relate it to Shannon's channel capacity, C, given by:

$$C = B \log_2 \left(1 + \frac{S}{N}\right) \qquad \text{bits s}^{-1} \tag{3.1}$$

where

B = Channel Bandwidth (Hz);
S = Signal power in bandwidth;
N = Noise power in bandwidth.

Alternatively, the SNR can be used to estimate statistically the BER that the system will experience.

Although estimation of the instantaneous or average SNR forms a valuable component of the RTCE procedure for predicting channel capacity or BER, the effects of fading, multipath delay spread and frequency (Doppler) offsets should also be incorporated into the algorithms. As mentioned previously, some of these effects are can be characterised by estimating the channel's scattering function, $S(\nu, \xi)$, which is a function of multipath delay spread and frequency dispersion. The significance of incorporating these factors is that channel ranking will differ from that obtained from simply estimating the SNR (Aarons & Grossi, 1986). It is more difficult to estimate the multipath dispersion and measure the frequency offset/spread in any given channel, since additional processing must be used over and above that used to estimate the instantaneous SNR. The final metric from the RTCE system should be a composite of all factors that perturb signal transmissions. Therefore, it is proposed that a joint channel selection and optimisation measure, or 'figure- of-merit' be derived which can be used to rank dissimilar channels. The process of developing this metric is described in Chapter 6.

3.6 Review of Successful Frequency Management Systems

Two successful frequency management systems that have been utilised in commercial and military communications are now described. The descriptions highlight elements of the system designs that exploit effective RTCE or forecasting techniques.

The channel evaluation and calling system (CHEC) was implemented in the 1960s; this was later developed into the RACE (radiotelephone with automatic channel evaluation) system. In the 1980s, development began on the HDRS (Home Defence Radio System) by UK MOD-sponsored contractors. This research into a strategic HF network has been a stimulus for UK research into modern, adaptive frequency management systems. Several other frequency management schemes have been developed (Beamish, 1994). However, the two presented here are considered to be reasonably representative of the technology and, or, algorithms involved in such systems.

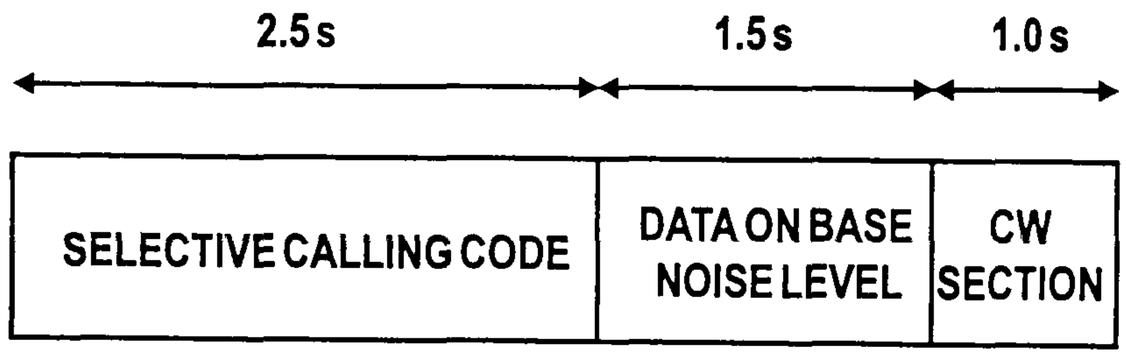

Figure 3.3: The Format of the CHEC Probing Signal

3.6.1 Channel Evaluation and Calling (CHEC) System

The channel evaluation and calling (CHEC) system was designed in the early 1960's to improve air-ground communication for the Canadian Armed Forces. Its particular aim was to improve communication throughput from a number of mobiles to a single base station (Stevens, 1968).

The system was assigned m channels, where typically $5 \leq m \leq 22$. The base station radiated a probing signal that cycled through each assigned channel frequency. The format of the probing sequence is shown in Figure 3.3. It contains three distinct elements: the first is a coded selective calling sequence which is intended to uniquely alert the mobile; next is a set of data conveying information about the interference state at the base station; finally a CW portion is transmitted to enable the mobile to estimate the SNR on the channel. Each of the remote mobiles listens for its address, contained in the calling code; once it identifies its call sign it steps through each of the assigned channels, decoding the relevant probing sequences. The CW signal is analysed to allow to estimation of the SNR from the mobile to the base-station, assuming a reciprocal channel.

The calculation is performed by using the transmitted average noise statistic for the base station $\overline{n(t)}$, for each of the open channels, coupled with the computed received signal levels $\overline{A(t)}$, from processing the CW portion of the probes. The final part of the calculation is to weight each of the results with a factor to compensate for differences in base and mobile transmitter configurations and antenna efficiencies, G. The calculation of SNR, $S_{mb}(t)$, for the mobile to base-station was then calculated for each open channel, f_j:

$$S_{mb}(t)\Big|_{f_j} = \left(\frac{G\,\overline{A(t)}}{\overline{n(t)}}\right)\Bigg|_{f_j} \qquad 1 \leq j \leq m \tag{3.2}$$

The channel selected for communication is that for which the calculated SNR is a maximum. CHEC was shown to provide significant improvements in channel availability and reliability during radio trials and was developed to form the basis of the RACE (Radiotelephone with Automatic Channel Evaluation) system where the algorithms were embedded in a specialised processing unit (McLarnon, 1982).

3.6.2 Home Defence Radio System (HDRS)

The rationale for this radio system is to provide a fall-back HF radio network in times of national disaster, thus enabling the maintenance of communication between government

agencies, the military and local authorities. Such a network would be needed if telecommunication resources were limited, or could not be operated successfully. In addition, in emergency situations, it could offer the possibility of reliable communication with remote areas. Such a network must be very robust and offer reliable data throughput. The use of an HF network allows relay stations to pass data to sites that are experiencing interference on normal traffic channels.

Any frequency management system operating in such an environment with very complex user requirements needs to exhibit adaptivity but, at the same time, the system must operate reliably. Therefore, a compromise between the adaptivity, system performance and reliability of connections needs to be reached.

In HDRS, the frequency management processes are constrained to a cyclic period of setup, data and frequency management. This traditional approach to the frequency management problem is complemented by novel ideas contained in the channel selection and data optimisation procedures. The features of the system are:

(i) fully automatic system control;

(ii) embedded propagation and noise models;

(iii) noise/interference assessment via passive monitoring of frequency allocations;

(iv) active probing of the ionosphere to determine propagating channels;

(v) frequency exchange keying (FEK) modulation scheme with optional in-band diversity or multiplexed operation;

(vi) data rates of 75, 150 and 300 baud;

(vii) embedded RTCE via error-counting;

(viii) system control via the use of ARQ.

Initial channel selection, during the start up period, is achieved by estimating the MUF using the embedded propagation model—based on miniMUF (Sailors *et al.*, 1986). The channels below the predicted MUF are then examined to assess the interference levels and their effects on the available modem types. Channels exhibiting poor interference characteristics are noted and rejected.

In addition, system probes the ionosphere to provide a real-time estimate of the MUF, that updates the predicted MUF, and to determine the frequency range(s) propagating. Once some form of transmission is established, the system then moves into fully automatic operation. The operation schedule is shown in Figure 3.4. To allow effective frequency management, 40% of the system allocated channels are dedicated to network frequency management control. During part of the cycle, frequency management channels are activated with a small burst of traffic, used as a probing signal. The probes are transmitted in the frequency management channels between frequency management terminals. This enables the MUF and propagating frequency range to be established and also determines whether any of the terminals can propagate using groundwave or via sporadic E. The results are weighted and stored in a database for subsequent use by the system.

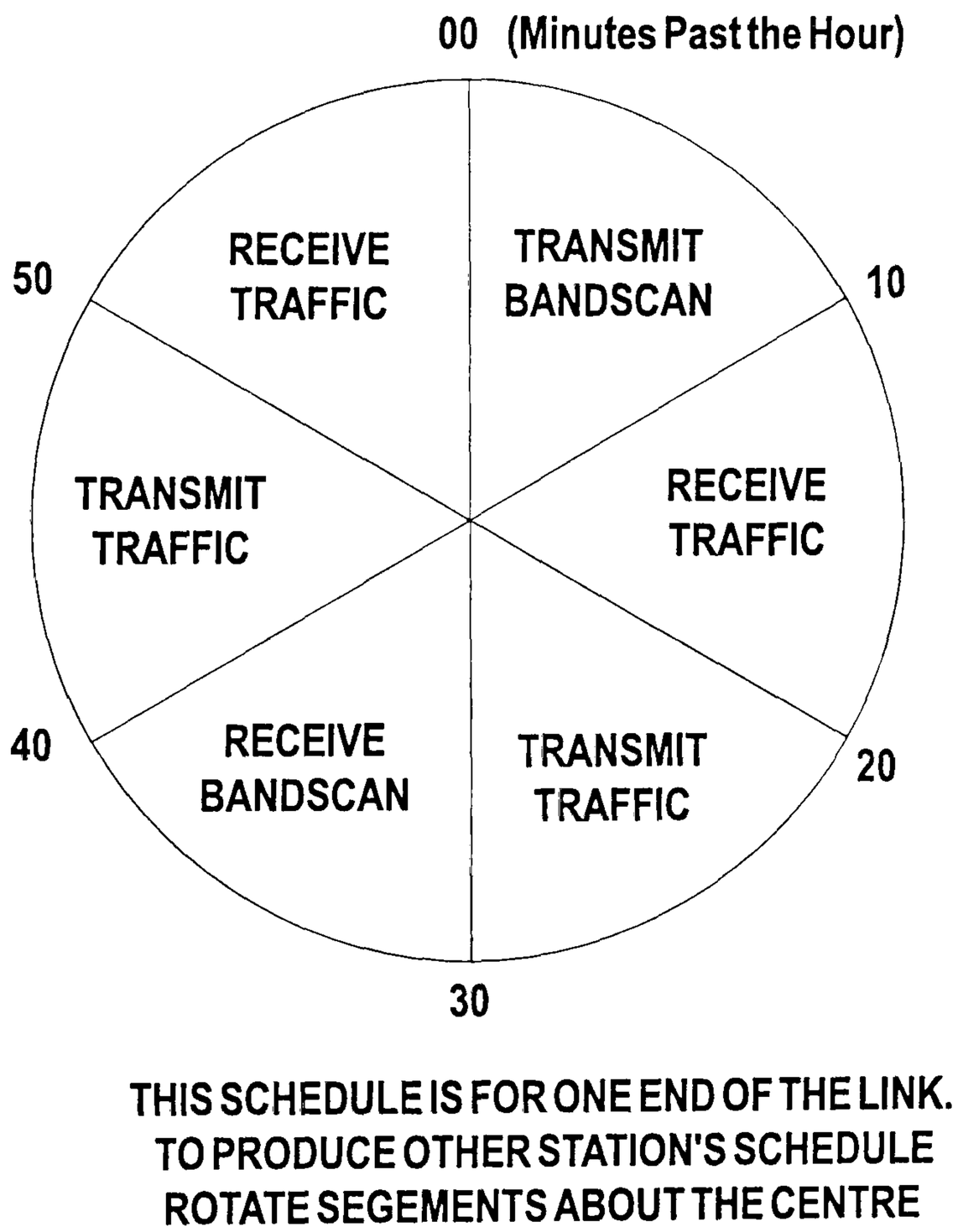

Figure 3.4: The timing schedule in the HDRS system

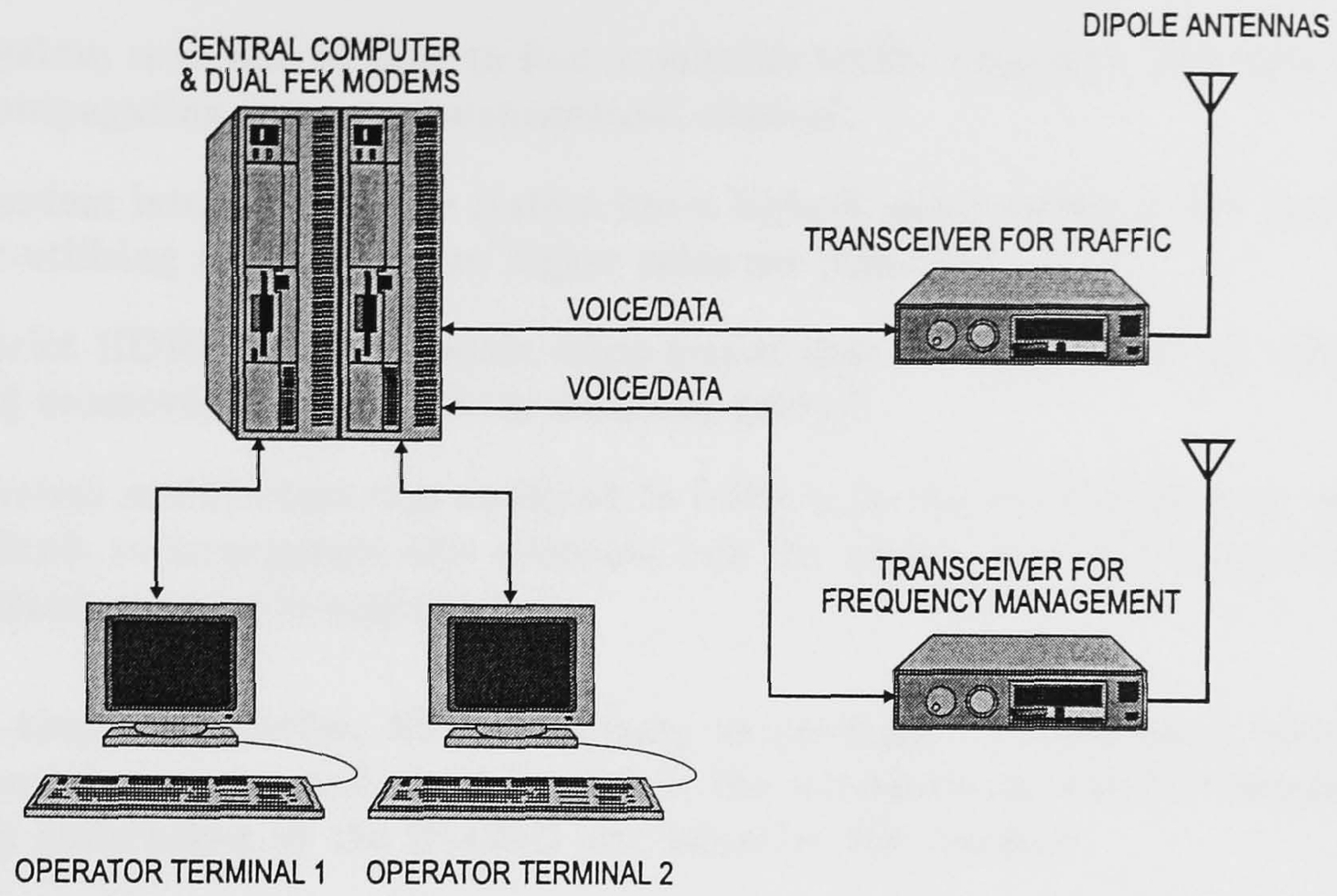

Figure 3.5: Schematic of a typical HDRS Terminal

In addition to the frequency management phase, the terminals can independently use their traffic statistics to assist passing data. Using the premise that a successful previous transmission may allow the link setup time to be reduced, terminals always attempt transmission on the same channel used previously before going through the link set-up procedure again.

The terminal configuration is shown in Figure 3.5. Each terminal has a traffic or scanning capability. In addition, the system designers recognised that a limiting influence on transmission could be narrowband interference. The call rotation system and the 'in-call' RTCE (Reed & Hopkinson, 1988) is designed to overcome this limitation. This allows the interference to be assessed on a probing call before transmission begins. If serious errors in the probe signal are encountered, then full transmission is attempted at a lower data rate, before trying an alternative channel.

The performance of the system is excellent, within a framework of rigid time scheduling. In published traffic details, the system had successful initial link establishment >80% of the time and can transfer a large amount of text-based data (Reed & Hopkinson, 1988).

However, the deficiencies of the HDRS system stem from:

(i) initial channel selection being made using propagation analysis tools which only provide broad-based median results; even though the system is augmented by RTCE to improve channel selection, the RTCE is largely directed by the results from the propagation prediction system;

(ii) although co-channel interference is accepted as one of the possible limitations on the system, the use of a non-adaptive modem and poor interference assessment techniques could not be fully compensated for by the use of the 'in-call' RTCE technique;

(iii) the use of so many channels for frequency management purposes means that approximately 40% of the allocated frequencies are unavailable for traffic;

(iv) the system may not be able to find a suitable traffic frequency allocation near to a propagating frequency management channel;

(v) the modem integrated in the system has a highest speed rating of 300 bps, thus under-utilising channels where higher rates are possible;

(vi) the strict HDRS timing schedule often meant that messages could be curtailed during crossover from a traffic to scanning period;

(vii) the system architecture was designed to fulfill a particular requirement; thus it is difficult to incorporate new elements into the system and test them without undertaking major re-engineering.

In spite of these deficiencies, HDRS operates successfully. It provides a benchmark for future automatic systems and, as indicated in the introduction, was the starting point of the research undertaken by the HLCRG into adaptive HF systems.

3.7 Review of Chapter

This chapter has provided an overview of the philosophy of HF frequency management systems. The focus of the discussion has been the use of channel selection and channel optimisation processes that enable the chosen channel to be matched to the traffic type for example, voice or digital telegraphy. The chapter has also attempted to show that the frequency management process cannot be made upon decisions from a single source of channel state information, but requires data from multiple channel state sources. The chapter briefly introduces the area of adaptive HF which was one of the considerations of this research programme.

The chapter concluded by discussing the role of real-time channel evaluation and providing a top-level overview of two successful, commercially produced, frequency management systems.

The framework of the research programme is presented in the next chapter. This details the scope of the problems to be addressed and outlines specifications for the frequency management system. The discussion also focuses on the use of digital signal processing techniques, since such methods are essential for the next generation of frequency management systems. Later chapters detail the channel selection, channel optimisation and joint selection and optimisation processes implemented for this research programme.

Chapter 4

Philosophy of Implementation

4.1 Introduction

The aim of this chapter is to focus on the implementation philosophy used in the research programme and to develop the 'generic' architecture concept. The brief description in Chapter 1 highlighted the fact that the DSP-based algorithms developed during the research programme were facilitated by adopting a 'generic' integrated architecture. This 'generic' architecture was based upon the integration of the DSP elements into a standard computer terminal. However, the benefits of using such an architecture can only be realised if the philosophy adopted for developing and constructing HF systems is changed accordingly. This chapter will highlight such benefits and philosophical changes by describing the use of digital signal processing (DSP) and the development of the 'generic' architecture. Finally, a performance specification for the terminal is presented.

4.2 DSP Device Characteristics

All of the algorithms developed for the channel selection and channel optimisation procedures, described in Chapters 5 and 6, were designed to operate in real-time on a DSP device. Specifically, the Chirpsounder transmitter and receiver, and the template correlation routines were configured for a particular DSP device, the AT&T DSP32C. Before detailing the characteristics of this device it is important to outline common characteristics of most DSP devices.

4.2.1 Common DSP Device Characteristics

Digital signal processing devices are special-purpose microprocessors designed to optimise the implementation os signal processing algorithms. In order to achieve this, most digital signal processing devices have a set of common characteristics (Proakis & Manolakis, 1992):

(i) a RISC (reduced instruction set computer) -based assembly language. The DSP device has a limited set of instructions but can execute a substantial majority

of these instructions in a single cycle. This feature benefits applications and algorithms, since they can be completed extremely quickly;

(ii) a 'fetch-execute-store' process. Most DSP devices have this process pipelined so that the next instruction is fetched into the processor whilst the current statement is executing and the previous statement's outcome is being stored. In the most advanced processors the pipeline can extend over 7 or more stages, allowing the instruction to be loaded with two memory accesses whilst the CPU core is executing and saving two of the most recent values;

(iii) a separate integer and floating point unit. This allows the partitioning of floating point and integer operations since, in general, floating point operations take much longer to complete;

(iv) an integer unit containing barrel-shifters and numerous registers. In a DSP device the barrel-shifter can be used to multiply or divide by 2N in a single instruction. The use of multiple registers allows temporary values to be stored and accessed in a single instruction and multiple register indexed addressing of memory to take place;

(v) a separate multiply and adder in the mathematical processing unit. This allows multiply-and-add functions to take place concurrently. The multiply-and-add function is the core function in most digital signal processing operations. When this capability is combined with the flexibility of the pipelined CPU and the separate integer processing unit, it is seen that the integer unit can control the access to memory whilst the mathematical processing unit undertakes the mathematical operations at the core of the signal processing algorithm;

(vi) subsidiary DSP device functions include the ability to operate circular buffers in memory that are temporary storage whilst undertaking digital filtering; in-place bit reversing for fast Fourier transform operations and zero-overhead looping to enable repetitive operations to take place without the need to stop processing to check counters;

(vii) memory organisation and system architecture. To enable the multiple memory accesses per cycle, a Harvard architecture is usually adopted. This separates the program and data memory into different areas, often on different buses. This type of organisation is also reflected in any on-chip memory. On-chip memory is usually provided as an immediate cache for small programs and a data store for variables that are used repeatedly by the algorithm. The latest generation of DSP devices contain greater than 1 Mbyte of on-chip zero wait-state memory.

This list is not exhaustive but provides an overview of the specialised nature of DSP devices. The latest generation of DSPs also incorporate inter-processor link adapters to allow multiple processors to be used to tackle the most demanding algorithms.

DSP devices, in common with general purpose microprocessors, possess flexible links to interface with other components. Typically these interfaces include serial and parallel ports that enable analogue interface devices and external memory to be connected. To enable algorithms to operate at the fastest possible speed, the processor's serial and parallel ports

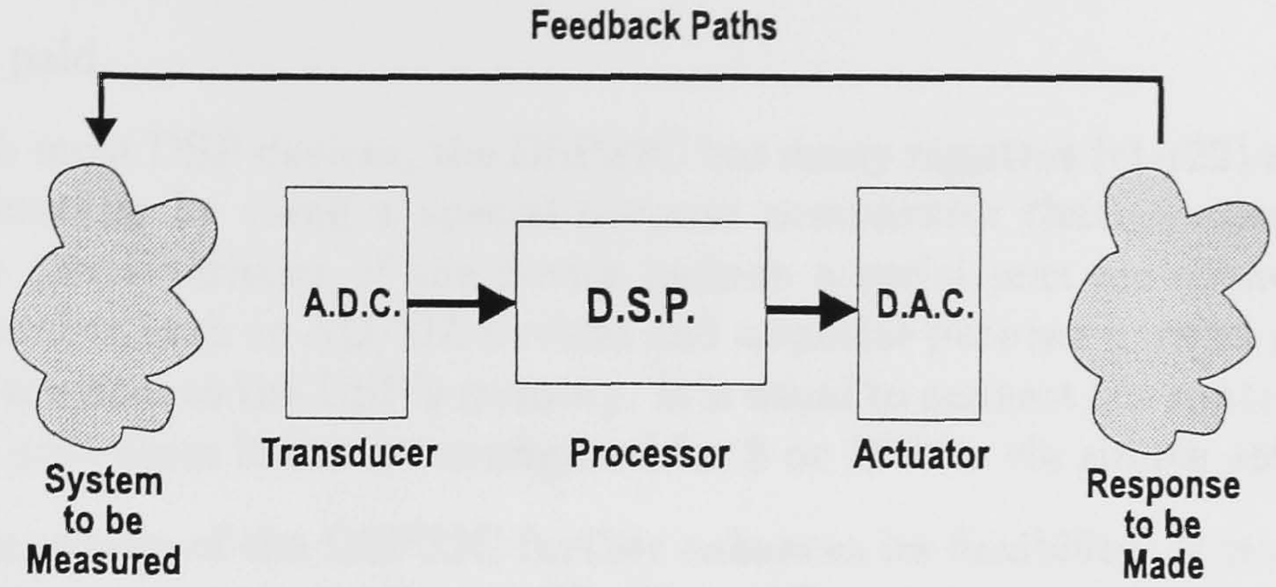

Figure 4.1: Typical Architecture for a DSP System.

are configured to allow direct memory accesses (DMA). It is, however, usual to attach zero-wait state static RAM to DSP devices to allow programs to execute and data to be fetched and stored with no time penalty.

4.2.2 Typical Applications of DSP Devices

DSP devices are able to perform signal processing functions such as convolution, spectral conversion, digital filtering and special mathematical operations in real-time using software (Proakis & Manolakis, 1992). The software is usually organised according to meet special timing considerations, but, by configuring application libraries in sequence special functions, for example a modem operation, can be achieved.

To undertake such a special function, the DSP needs to be configured as shown in Figure 4.1, to interface with the environment. The analogue interface components (transducers) convert voltage, current etc. into digital equivalents for processing. Once processed, these digital signals are converted back to analogue form by actuators.

A typical DSP device will be provided with a minimal set of application software. This will include functions such as fast Fourier transforms (FFTs) for conversion of digital samples to spectral estimates and routines for both recursive and non-recursive (IIR and FIR) digital filters.

4.2.3 Specific Characteristics of the DSP32C

The DSP32C is a floating point device that was originally developed for AT&T telephone exchanges (ATT, 1988). When configured for floating point operations then 25-40 Million floating-point operations per second (MFLOPs) are possible. The DSP32C is a 32-bit RISC processor that differs from most other DSP devices in that it uses a linear memory map, rather than the standard Harvard architecture. In order to maximise performance with the linearly addressed data space, the on-chip address decoders can access the memory in 4 pipelined stages allowing two external memory accesses per instruction.

To ensure that maximum speed is available for small loops or memory-efficient algorithms, the device has 1.5kwords of on-chip memory organised into three banks of 512 words. For most algorithms, it is desirable that these memory areas are utilised, since no penalty in

performance is paid.

In common with most DSP devices, the DSP32C has many registers (r1-r22) and can perform zero-overhead looping by using a special-purpose comparator that monitors the program counter. Other characteristics of the device include a serial port for connecting analogue interface components such as AD/DA devices and a special-purpose parallel port that allows direct-memory accesses to the DSP's memory. It is usual to connect the controlling computer to this parallel port since it can be configured for 8 or 16 bits via simple software routines. The assembly language of the DSP32C further enhances its flexibility. It is algorithmic and symbolic having a structure similar to 'C'. Since 'C' is the major development language for research software, due to its flexibility, then it is possible to convert algorithms to DSP32C assembly language by following similar software structures and conventions. The assembly language flow is simple to learn and facilitates rapid code development when used in conjunction with the large library of common DSP applications; these support a large range of typical applications, including FFTs and special mathematical operations, for example square-root.

4.2.4 Use of DSP with Voice Band Channels

Digital signal processing is particularly suited for voice band (300-3000 Hz) channels because, at Nyquist sampling rates, several thousand instructions can be undertaken between samples. This allows most functions, for example modems, spectral analysis, and channel impulse response identification to be undertaken in real-time. Furthermore, the analogue interface technology is well matched to low bandwidth channels because of previous applications such as digital telephony and compact-disc (CD) music recordings. Since HF channels usually possess bandwidths of up to 3000 Hz, then direct application of such analogue interface technology in conjunction with DSP is possible.

4.3 System Design Philosophy

In conventional HF systems, each terminal is designed to meet the required specification by overcoming the limitations of the propagating environment. In the past, systems have not been designed to facilitate evolution as system and user requirements develop, meaning that improvements or modifications may require significant re-engineering of the architecture. In addition, signal interfacing, say for example a modem, is usually undertaken by distinct subsystems, connected to the central processor using a low-speed standard interface technology, for example RS-232C. This design methodology, although widely accepted, cannot cope with the complex interactions between system elements and each solution tends to be of a unique nature with the individual elements of the terminal being different functional elements. This approach simplifies system integration since overall configuration is achieved by utilising distinct subsystems and interconnecting them via standard interfaces. The final system is a compromise between the limitations of the interfacing technology and the modes possible with each subsystem.

An alternative design methodology, based upon the use of integrated digital signal processing (DSP) elements, has been employed in this research programme. This terminal architecture

has been designed specifically to exploit commercially available system components and to interface with proprietary RF equipment (see Figure 4.2). The use of commercial RF equipment can minimise the cost of a terminal, since RF equipment is often the major cost element in a typical system. In addition, the use of an architecture based upon DSP subsystems allows the application of modern digital algorithms. These algorithms can be used to mitigate any deficiencies in the RF equipment. Furthermore, the use of integrated signal processing elements means that high speed interconnection between the central processor and the DSP subsystems is possible, thus facilitating adaptivity in response to channel conditions.

4.4 The Generic Architecture Concept

In order to meet the complex user and system requirements inherent in an adaptive HF system, it is necessary to examine the terminal architecture required to achieve the objectives of the system. An adaptive HF system (Goodman, 1992) will require the following characteristics to operate successfully:

(i) a system architecture that enables the signal generation and processing, for a example a modem function, to respond to changes in the environment, specifically co-channel interference, multipath, frequency dispersion and fading;

(ii) the adaptive system must monitor terminal characteristics, operational performance and outages in the environment to compile a database that allows the system to sense the environment and thus facilitate adaptation;

(iii) the adaptive system will use the database to schedule and optimise control functions such as frequency management and network and link management to maintain performance for a wide range of HF conditions, system and link configurations,

(iv) finally, the adaptive system must have an 'open' architecture to allow the same configuration to be used in different roles.

The architecture of Figure 4.2, used in the research, is based upon reducing the adaptive system to two elements. The first element is the radio (RF) component. This would typically be in the form of a transceiver under computer control. The second element, or control unit, comprises the integrated host CPU and DSP subsystem. The control unit is the 'intelligent' element of the terminal since its software will facilitate the adaptive operation of the terminal. The DSP subsystem is primarily dedicated to the task of real-time signal generation and processing.

The particular architecture was chosen since it provided the following benefits: (i) cost, (ii) flexibility and (iii) availability of DSP devices. The configuration in Figure 4.2, reflects the partitioning of the individual elements to maximise individual benefits and overall terminal flexibility.

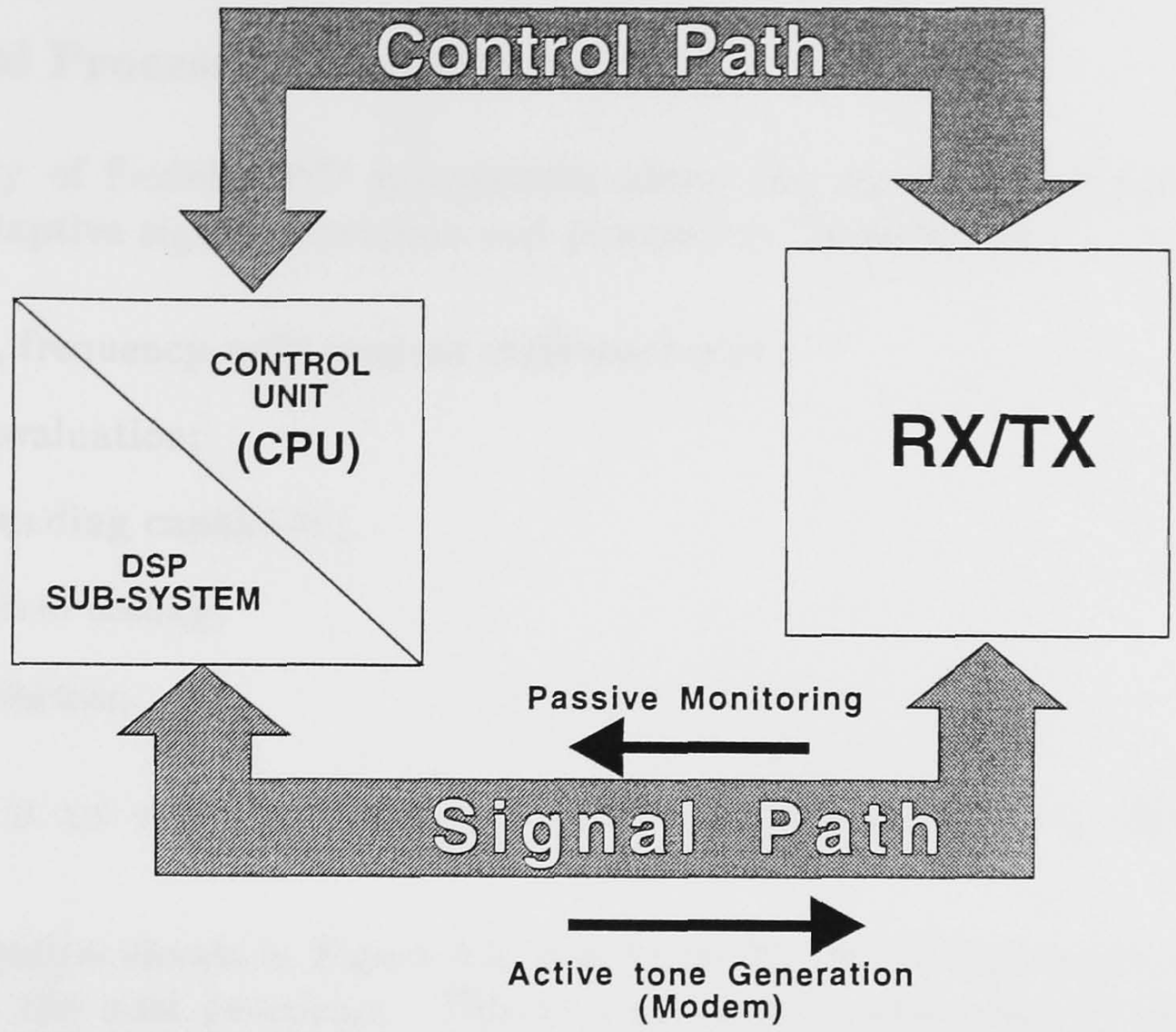

Figure 4.2: Schematic Diagram of Adaptive HF Terminal Architecture.

4.4.1 Host Computer (CPU)

The host computer element of the control unit can be realised by a personal computer (PC) although, for the most complex operations, a workstation would be more suitable. This element of the system performs all of the higher level control functions. These include, amongst others:

(i) remote control of the radio system;

(ii) host for the DSP-based subsystem;

(iii) user interface;

(iv) system scheduling;

(v) control of DSP subsystem;

(vi) off-line predictions;

(vii) mathematical modelling;

(viii) operational database;

(ix) any knowledge-based operations, e.g. frequency management.

The operations in the above list could take place sequentially or concurrently. The design of the software controlling the terminal must be able to use all the resources present on the particular host computer. For example, in a simple terminal based upon a PC, operations are scheduled sequentially. Using a more powerful computer with a multi-tasking operating system, concurrent operation would be possible.

4.4.2 Signal Processing Subsystem

The availability of flexible DSP sub-systems allows the use of digital algorithms for the provision of adaptive signal generation and processing. These include:

(i) adaptive, frequency-agile modem implementation;

(ii) channel evaluation;

(iii) active sounding capability;

(iv) error control coding;

(v) synchronisation.

The above list is not exhaustive; many of the items listed are extensive topics in their own right.

In the configuration shown in Figure 4.2, it is usual for the DSP elements to operate concurrently with the host computer. This is a substantial advantage because some signal processing operations, for example the modem function, are computationally intensive or must be available for a long period of time. If a single DSP device is available to the system, then operations must be configured serially since no concurrent DSP operations are possible. In this case, the limiting factor on the adaptivity of the terminal is the speed of response to changes in the channel state, programmed schedule changes, or user requirements.

With a single DSP device, communication may be interrupted during frequency changes because system adaptations in response to the new channel conditions will take a finite amount of time. Thus, ideally, more than one DSP device and transceiver should be used in any future adaptive terminals. The second DSP device would be used to search for alternative channels under degrading conditions. This would allow communication to be maintained because the system would be able to exchange functionality between DSP sub-systems in adverse conditions.

During favourable channel conditions, the second DSP device could be used to provide passive channel state estimates which could be used to adapt the transmitted signal to optimise the use of the available bandwidth.

These recommendations would require a modified architecture of the form shown in Figure 4.3.

4.4.3 Radio System

For efficient operation of the above system architecture, the RF elements must be remotely controllable and there should be a suitable signal interface between the DSP sub-systems and the baseband transceiver input/output. Modern transceivers provide all these functions, in addition to a synthesized frequency standard that allows tuning accurate to within a few Hertz, or better.

The use of such a 'generic' architecture allows the terminal to be enhanced by future possible improvements in RF equipment, for example through digital signal interfaces available from

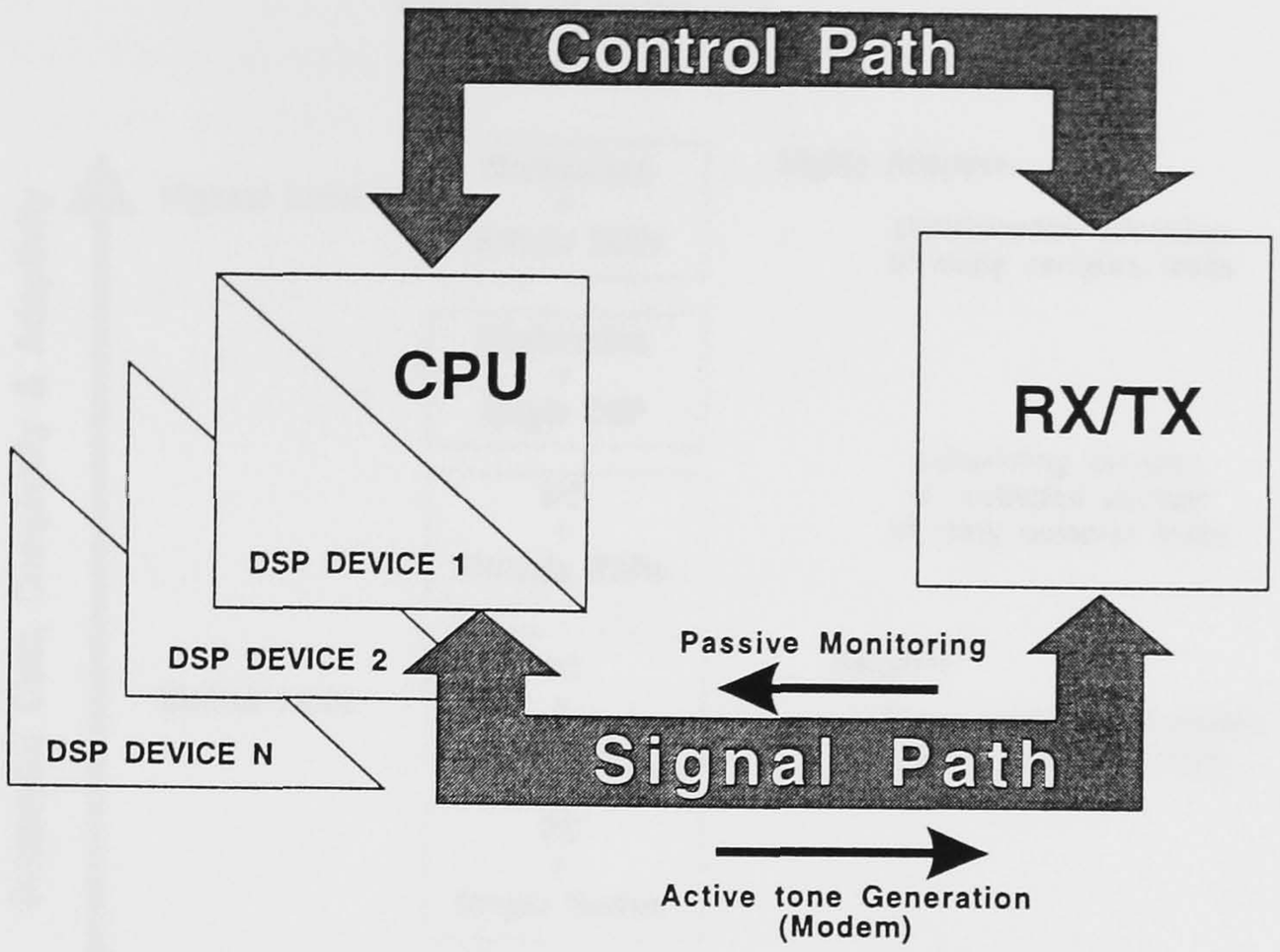

Figure 4.3: Modified generic architecture with multiple DSP Sub-Systems

the IF stages. In these cases, the RF stages will provide the signal interfacing to the environment with all signal processing provided by DSP-based sub-systems.

For each architectural configuration, there is a limit on the adaptivity that the terminal. The adaptivity indicated in Figure 4.4 is referenced to a terminal that possesses limited or no adaptivity; this schematic shows a 'hierarchy of performance'. The hierarchy of performance diagram is open-ended; this allows future systems to be added. It is independent of equipment and operational requirements.

4.5 Algorithms and Processes used to Facilitate Frequency Management

The aim of this section is to examine the procedures and processes that can be used in the frequency management system and to consider implementation issues. The procedures for automatic frequency management systems have been largely based on successful schemes devised by human operators. The rationale for such development is that a computer system could emulate human skills but operate much faster, more reliably and at much reduced cost. This methodology is well accepted and has been demonstrated to be valid for many different types of automatic frequency management systems. Essentially, it makes use of the methods of artificial intelligence (AI) and "fuzzy logic", where the input data on which a decision is to be based can only be specified in statistical terms.

A human operator can undertake the complex frequency management procedures by manipulating the available information (both current and historical) using a set of heuristics, or "rules-of-thumb", to obtain a set of reasoned decisions. These decisions are based upon learned reasoning and understanding of the problems involved in coming to a decision. It is desirable, therefore, to emulate these processes via software, as it is the skill of a human operator that makes frequency management systems adaptive in response to new environmental

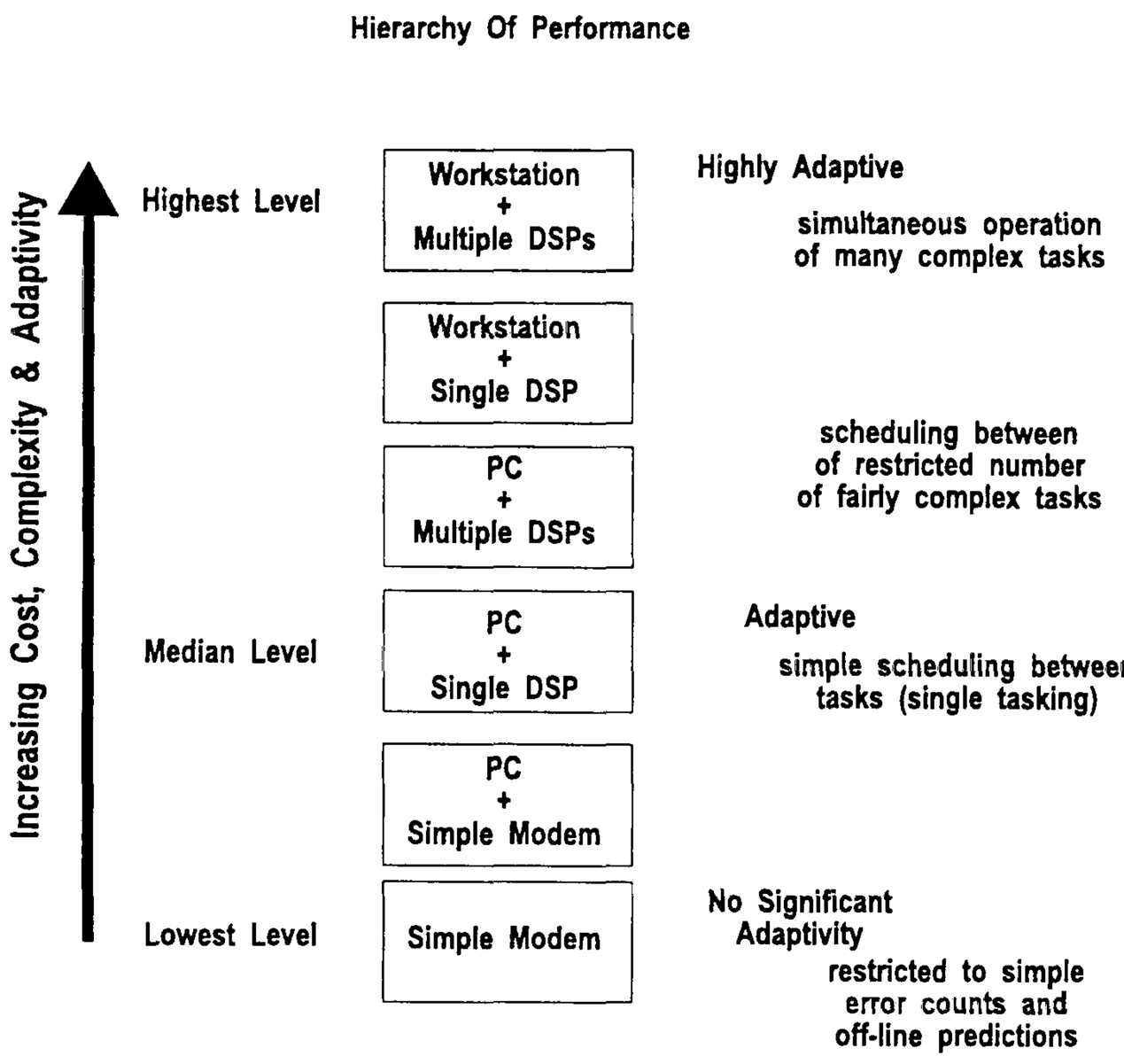

Figure 4.4: Schematic Diagram of Hierarchy of Performance.

conditions and user requirements.

Even if variables on which decisions can be based arrive a rate faster than can be assimilated, a human operator can intelligently assess the information, noting trends and then act accordingly. The operator is prepared to accept performance degradation in the short-term, whilst achieving better performance once all the dimensions of the particular problem have been learnt.

4.5.1 Artificial Intelligence in HF Systems

To achieve better performance in HF frequency management systems, a possible solution is to emulate the operator learning and reasoning processes by the use of artificial intelligence. The use of artificial intelligence (AI) techniques as a solution to frequency management has been proposed by several research workers (Jowett, 1987; Jowett, 1989; Chesmore, 1991; Scholz, 1988). Proposed solutions concentrate on two commonly available techniques: expert systems and black-board based inference systems. The expert system solution (Chesmore, 1991) attempts to simplify the problem to a set of rules, based upon learned reasoning, and "hard-wired" programs. In contrast, the black-board system uses distinct knowledge sources, in conjunction with a scheduling system which combines the knowledge available to the system. The scheduler is programmed with a set of rules to enable the information contained in the data from the knowledge sources to be extracted and used to make frequency management decisions.

The two techniques merited some extensive investigation into their relative benefits and possible implementations. The complexity of the problem means that a complete domain

solution based on either method would be cumbersome and slow. The conclusions drawn from the investigation are that AI techniques would be suitable for individual facets of the problem but it would be difficult, and probably not possible, for a real-time system to be constructed that encompasses every part of the domain. However, since computer capability is increasing rapidly, AI techniques will become increasingly important because their inherent flexibility and learning capability is well matched to the requirements of future frequency management systems.

4.5.2 Object Orientated Design of HF Frequency Management Systems

Object-orientated design is a standard programming method that complements black-board systems. It encompasses some AI methods, but in a well-defined and structured format. In an object-orientated system, each of the decision variables or modules is defined by a set of individual structured elements or 'objects'. These elements can operate independently of each other and allow subsets of the problems to be tackled and solved.

The advantage of the object orientated design method is that, once a set of such sub-systems has been designed, they can be structured to be aware of each other. Information transfer is accomplished via well defined routines—for example a data record, that contains raw data, processed data and requests for further processing. The information recipient takes the structured data, further processes it, and can return it to the originator or pass it on for further processing or storage for later usage.

Information transfer can be synchronous or completely asynchronous - this feature is crucial when using DSP subsystems since data is compiled and available in response to the operational environment. This feature allows the system to be highly adaptive in that it can respond to data changes, environmental variations or scheduled commands. The other advantage of object orientated design methods is that further elements can be added to the system as operational requirements evolve. This would allow an adaptive system to be constructed with different objects designed for the different system elements. The frequency management task diagram, Figure 1.1, is complex, but an object orientated system could approximate the individual elements and the complex inter-relations. The move to object orientated frequency management systems will be increasingly important as the computers controlling automatic HF radio systems have to allocate their power between node, network, link, traffic and frequency management. Such operation will require a multi-tasking capability and object orientation is a fundamental core of a modern multi-tasking operating system.

The concept of a frequency management system using the object orientated design method is illustrated in Figure 4.5.

4.5.3 Conventional Programming Methods as Applied to HF Frequency Management

Systems that have hard-wired frequency management will still be required. Therefore, conventionally designed frequency management systems will be applicable in small, simple radio networks. Similarly, upgrading installed HF systems will require the building of a HF frequency management system with core features only, although some of the methods used

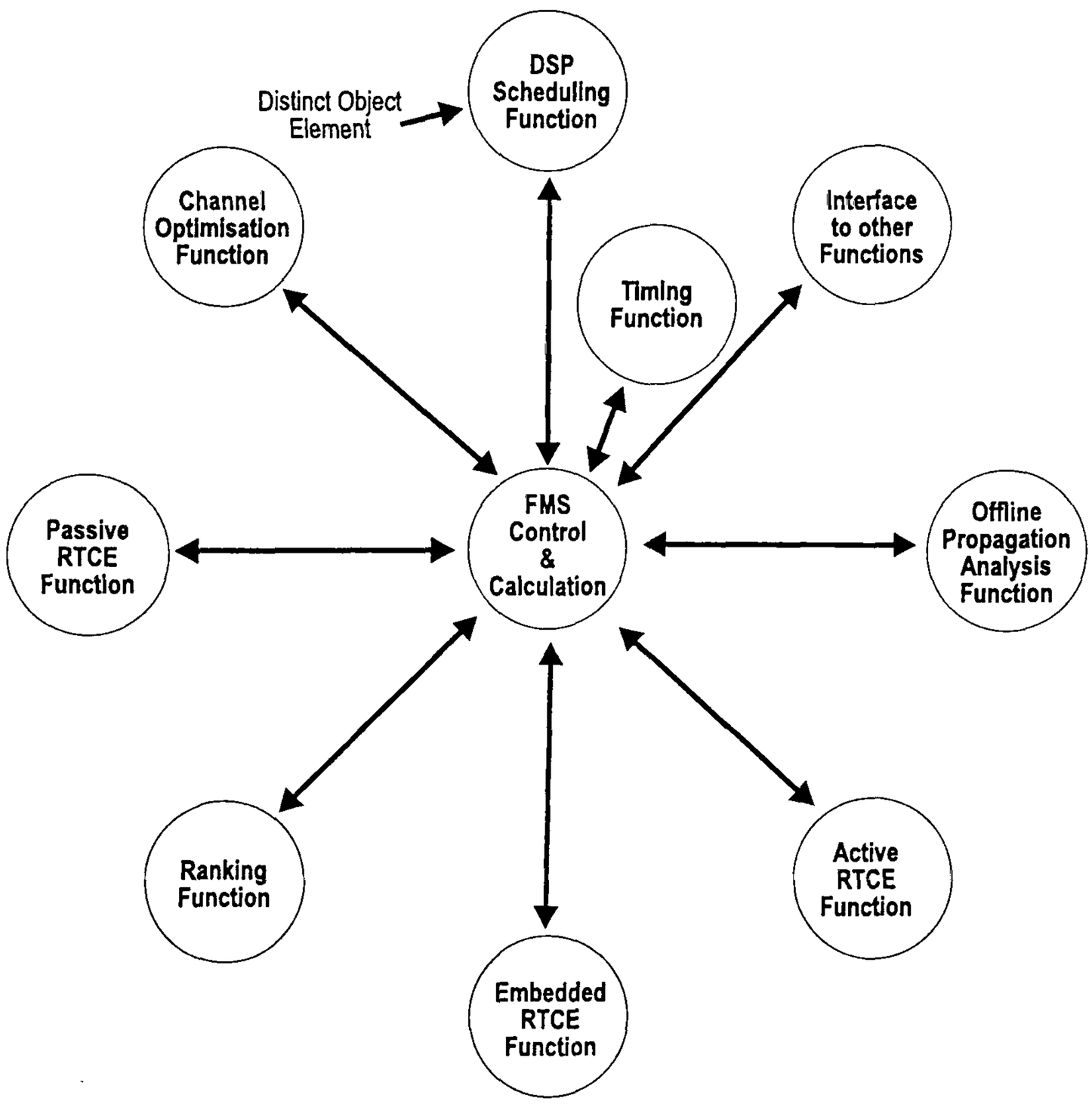

Figure 4.5: A Frequency Management System using Object-Orientated Knowledge Sources.

to implement these features may also be updatable.

Such HF systems will require that the problems associated with building a frequency management system are resolved. In these cases, the system and problem analysis should allow the solution to be reduced to a number of "if-then" statements describing information flow in the frequency management controller. Specific additional measures, such as embedded RTCE techniques, should be minimised.

4.6 Performance Specification

At the beginning of the research programme a formal specification for the terminal and its performance was not available. However, it was decided, after a literature survey, that in order to achieve some measurable objectives the project should concentrate on the area of adaptive HF frequency management by enhancing the concepts from the previous project (Jowett, 1989) and developing the channel selection and optimisation routines to a point where they could be integrated within an HF terminal. The specification for the FMS would address items (i) and (ii) of the list outlining the characteristics of an adaptive HF system given in section 4.4. Once the tools for this part of the project had been constructed, then item (iii) could be addressed.

The specifications for these tools in context of the frequency management process were:

(i) the channel selection subsystem will identify channels where propagation exists;

(ii) the channel selection subsystem will monitor the in-band and out-of-band channels to indicate if ionospheric conditions are enhanced or depressed;

(iii) the channel selection subsystem will be able to add or delete channels from the candidate frequency list identified from off-line propagation prediction;

(iv) the channel selection subsystem will identify the impulse response of selected channels and provide an indication as to whether inter-symbol interference is a limiting factor for the modem format proposed;

(v) the channel optimisation routines will use the impulse response data to suggest new symbol rates if inter-symbol interference is found to be a limiting factor;

(vi) the channel optimisation routines will measure the co-channel interference for the channel set and reject those channels where such interference is limiting;

(vii) the channel optimisation routines will use the measurements of co-channel interference to suggest optimum energy distribution for the modem, for example tone placement for MFSK modems;

(viii) the frequency management system will use the outputs from the channel selection and channel optimisation subsystems to rank channels according to the criterion of suitability for specified forms of traffic.

The project has addressed all of the issues in the list. Any subsequent project could extend the specification to include, say, performance bounds for the frequency management system and error rates that should be achieved.

One aspect of the list, item (viii), means that to use the data efficiently, techniques such as knowledge-based systems, black-board systems (Nii, 1986) and expert systems (Sell, 1985) should be evaluated (Jowett, 1987; Scholz, 1988; Chesmore, 1991) (section 4.5). This investigation demonstrated that such techniques may be applicable, but the time penalty would make data interpretation extremely slow. Furthermore, their implementation would reduce the effort available to implement the channel selection and optimisation subsystems. Consequently, it was decided to use a simple rule-base of "if-then" statements, together with simple computations using the database of channel measurements, in a traditional programming environment as a basis of the FMS.

4.7 Review of Chapter

The concepts introduced in this chapter have been associated primarily with implementational issues. The research programme has been based on implementing systems that could be used in an adaptive HF system. A new terminal architecture and design philosophy is proposed. This is intended to offer an alternative to current architectures such that the system designer is able to use disparate technologies, for example RF and DSP, in a modular, but integrated manner. This type of flexible architecture has the advantage that system adaptivity is only limited by computational efficiency, speed of the DSP subsystems and/or host computer and the ingenuity of the software designer. Typical terminal schematics are shown in Figures 4.2 and 4.3.

The work described in following chapters exploit the flexible architecture concept and the frequency management model in the context of adaptive HF system design. Chapters 5 and 6 respectively present the channel selection and optimisation subsystems that are the core aspects of HF frequency management.

Chapter 5

Elements of a Channel Selection Subsystem

5.1 Chapter Introduction

The initial stage of the frequency management process is the selection of a set of candidate channels that are assessed as suitable for traffic. The primary source for this list of channels is off-line propagation prediction. However, relying on such a list suffers from the disadvantage that calculations for each candidate frequency are based on long-term, median data and consequently may not reflect accurately the current state of the ionosphere. In order to relate the off-line measurements to the actual state of the ionosphere, it is desirable to update the list by adding channels that are propagating and/or deleting channels that have no measured propagation.

The aim of this chapter is to describe two subsystems that were developed to meet the requirements of adding or deleting channels from the initial list of candidate frequencies produced by the off-line prediction. The first of these sub-systems is the linear FM (chirp) sounder receiver. This system replicates the function of the Barry receiver (Barry, 1966), in that it can construct oblique ionograms from the linear FM signals received passively from the network of chirp sounders. By using this ionogram data and noting the range of frequencies over which propagation was measured, channels can be added to or deleted from the list provided by the off-line propagation prediction system.

It had been previously demonstrated that the Barry Chirpsounders[1] transmissions could be processed to provide a suitable, real-time display of propagation conditions (Jowett, 1989; Masrani & Riley, 1990). This project extended that previous research, to allow the synthesis of usable ionograms. The operation of the DSP-based chirpmonitor is completely different from that of the chirp detection system implemented in the previous project. The propagation assessment system constructed previously (Jowett *et al.*, 1989) operated by detecting chirp signals in a two stage process: the first stage eliminated channels exhibiting high levels of co-channel interference; the second stage used a detector matched to the phase of the chirp signal to give a chirp present/absent indication. This detection method limited

[1]It is acknowledged for the rest of the section that the term 'Chirpsounder' is a registered trademark of the Barry Research Corporation. Furthermore, the term 'Barry' refers to this company.

the decision to a pass/fail for each channel. The propagation display comprised a series of solid or open bars indicating the choice made. No attempt was made to synthesis an ionogram or to use the Barry transmissions as a timing source.

The second tool developed to perform real-time propagation monitoring was an active sounding system. This system allows the ionosphere to be sounded between flexible HF terminals of the type described in this thesis and an ionogram characterising the link constructed. The active sounder is an important development, in that it is not limited to simply transmitting linear FM signals. Other sounding waveforms can potentially be used and the advantages of say a hyperbolic FM waveform over linear FM identified. Several of the techniques used in this part of the project are modifications of implementations that have been successfully used in radar systems where linear FM signals are employed extensively in target tracking.

5.2 Description of the Barry Chirpsounder System

The Barry Research Corporation Chirpsounder receiver is one of the most common stand-alone HF support systems which is used to assist HF link establishment and management by a number of large organisations. It produces an ionogram by demodulating a received linear FM signal transmitted from a proprietary Barry transmitter. The linear FM, or chirp, waveform is produced by sweeping a CW tone from 2 to 30 MHz at a fixed rate, typically 100 kHz per second. Currently, there are c.50 Barry transmitters deployed to form a world-wide sounding network, with c.150 Barry receivers.

The Barry receiver is essentially an extremely high quality spectrum analyser that scans the HF band at a specified sweep rate and resolves the transmitted linear FM signal by using a super-heterodyne demodulation process. The basic block diagram of the system is shown in Figure 5.1. The IF (intermediate frequency) bandwidth of the system is 100kHz and its time resolution is 0.01 ms; this accuracy is sufficient to support most HF communications applications. The result of using this demodulation scheme is that the chirp compression algorithm produces a set of delayed sweeps at the IF stage. It is the amplitude and delay of these frequency components that, when converted to base-band, is used to produce the ionogram. The most important factors in Barry receiver performance are:

(i) the mixer and sweep generator use a high stability reference (that is stable to $< 1.0 \times 10^{-7}$s) to generate their frequencies;

(ii) all of the receiver components are of a high quality;

(iii) the dynamic range of the receiver is limited to 40dB;

(iv) the simple demodulation process (super-heterodyne) means that much of the complexity of the system is at the transmitter.

A schematic display of the mixer-products at the IF stage as a function of sweep time is shown in Figure 5.2. A typical impulse response raster is shown in Figure 5.3. The impulse response is computed as a function of frequency and this information is then displayed on the VDU in 100 kHz steps. The display process is relatively simple; it needs no peak-detection routines and it is ideally suited to analogue demodulation methods. In addition

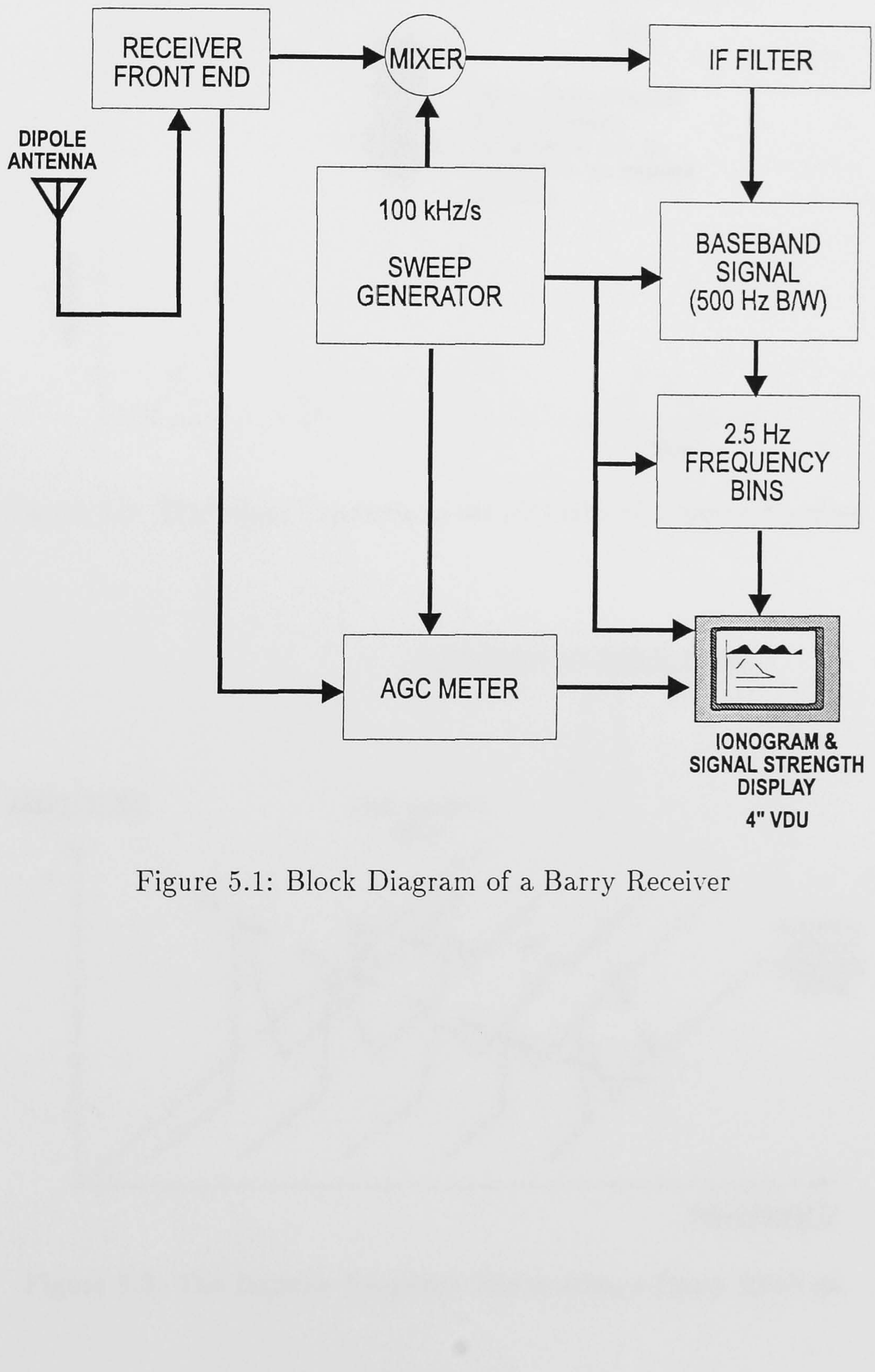

Figure 5.1: Block Diagram of a Barry Receiver

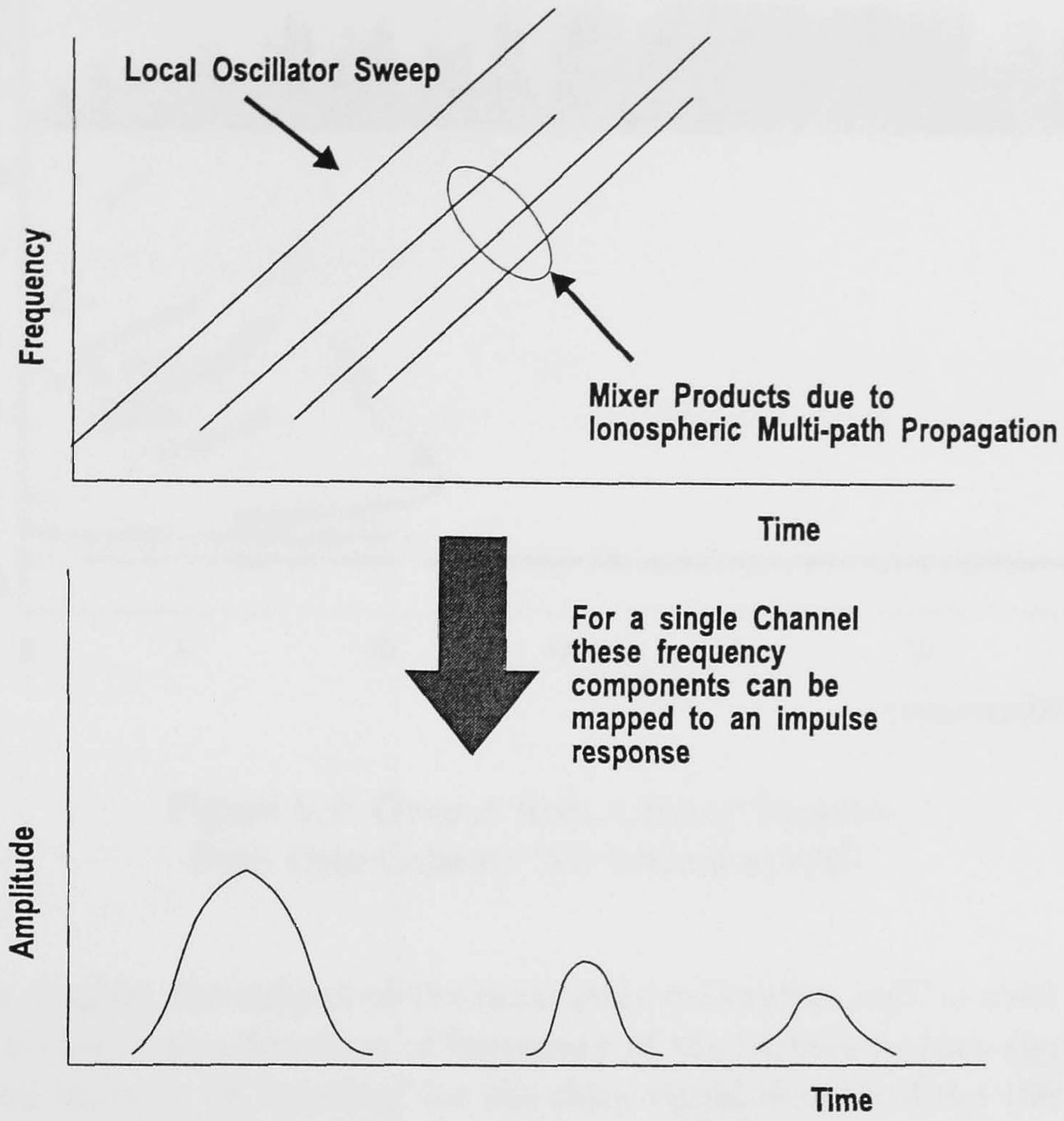

Figure 5.2: The Mixer Products at the IF stage of a Barry Receiver

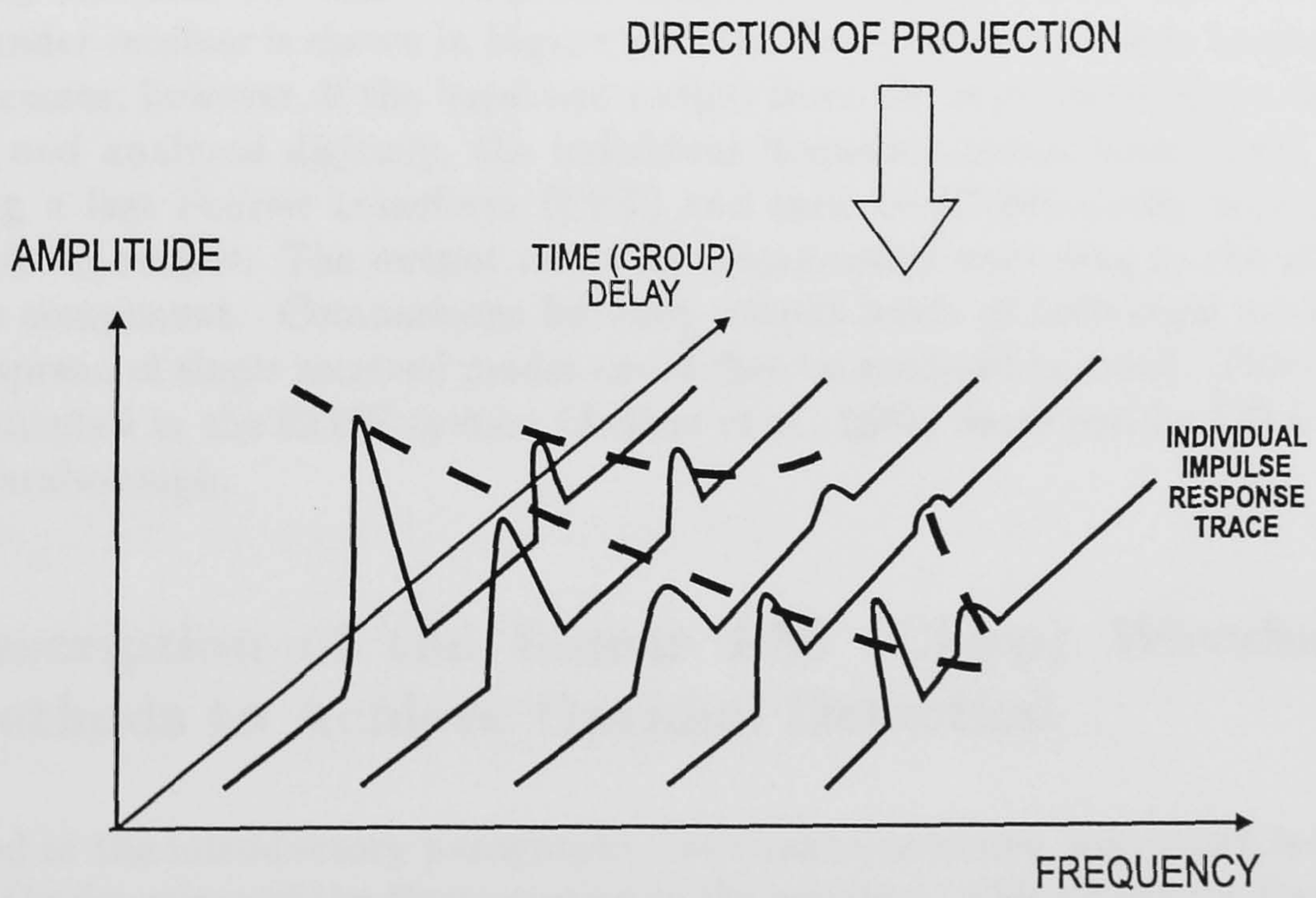

Figure 5.3: The Impulse Response Raster from a Barry Receiver

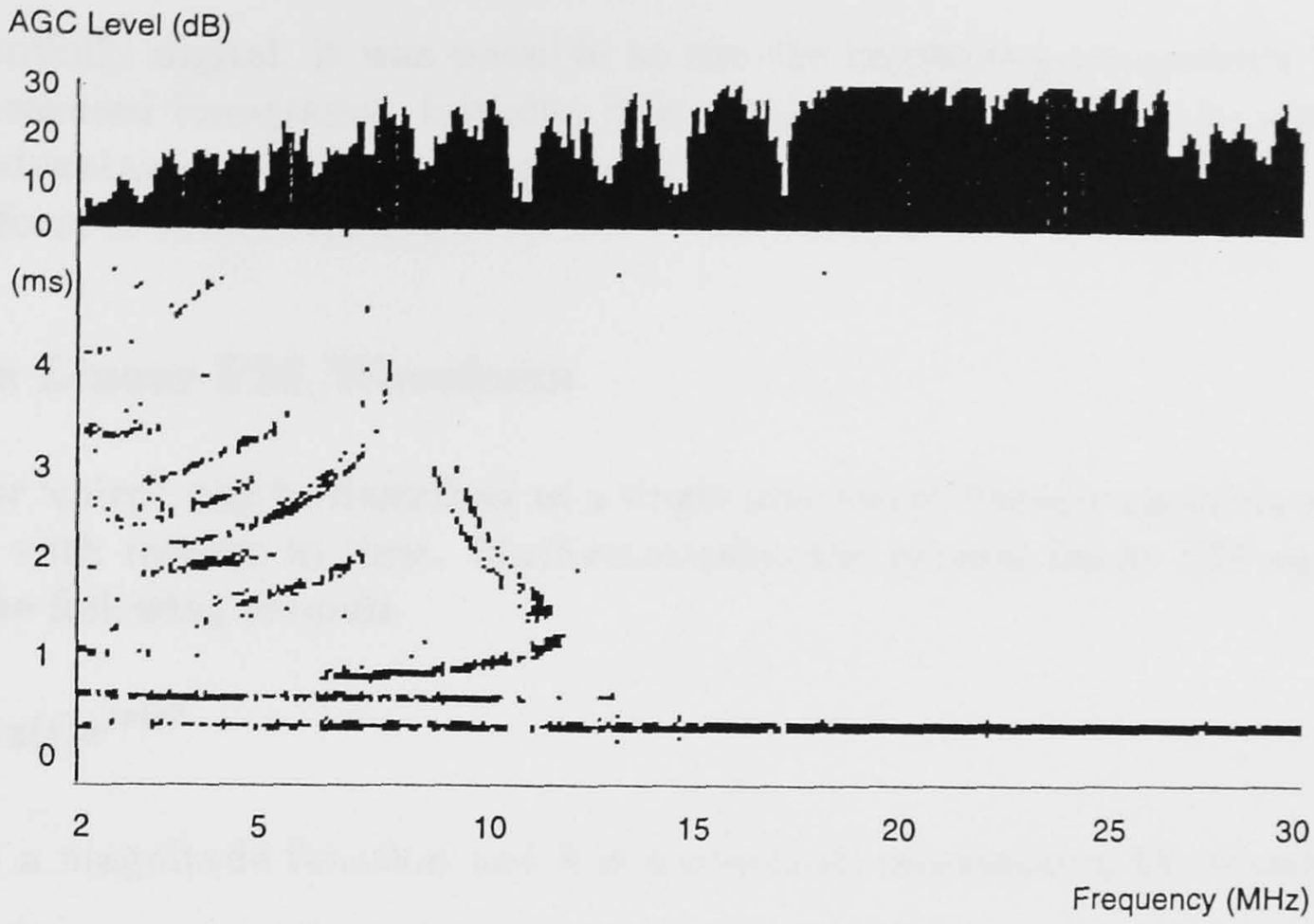

Figure 5.4: Output from a Barry Receiver
Path Oslo-Cobbett Hill 2.41am 9/8/90

to the ionogram display, the output of the accurately calibrated AGC is used to indicate the received signal strength as a function of frequency of the incoming chirp signal. Synchronisation is achieved initially by 'hunting' for the chirp signal at each of the 100 kHz steps. An approximate estimate of time is required and the sounder receiver sweeps up in frequency, following the transmitter. Once it achieves synchronisation, it stores the relative offset time of the received signal against its internal reference. This figure is then used to maintain synchronisation against any sounder. The operating organisations tend to calibrate their systems daily and drift between sounders is normally negligible. An example ionogram from a Barry sounder receiver is shown in Figure 5.4. The Barry receiver utilises analogue demodulation processes; however, if the baseband output from the super-heterodyne demodulator is sampled and analysed digitally, the individual frequency components could also be resolved using a fast Fourier transform (FFT) and then amplitude-scaled according to the calibrated AGC output. The output could be colour-coded according to the amplitude of the various component. Comparisons between output levels of individual modes and the amplitude spread of single received modes could then be analysed in detail. This method has been implemented in the ROSE system (Arthur *et al.*, 1991) developed by DRA, Aerospace Division, Farnborough.

5.3 Description of the Linear FM (Chirp) Waveform and Methods to Achieve Optimal Detection

As described in the introductory paragraphs, the channel selection subsystem is based upon replicating the functions of the Barry system in the terminal. This allows the Barry network to be used as a source of oblique sounding data, thus enabling the construction of ionograms for paths being monitored. Furthermore, since the terminal architecture described in this

thesis is essentially digital, it was possible to use the controlling computer's hard disk for storage of measured ionograms. Initially, it is required to understand the nature of linear FM and its advantages and disadvantages in sounding applications. The design of a detector for the waveform is then considered.

5.3.1 The Linear FM Waveform

Linear FM, or 'chirp', can be described as a single tone swept linearly upwards or downwards in frequency with respect to time. Mathematically, the general linear FM signal, $\mu(t)$, is defined by the following formula

$$\mu(t) = a(t)e^{j\pi kt^2} \tag{5.1}$$

where $a(t)$ is a magnitude function and k is a constant, representing the sweep rate.

The general chirp equation (5.1) defines a continuous waveform, whereas for normal, optimal detection the waveform would be confined to a short window of interest; for example when a rectangular window is overlaid on linear FM, a pulse-type envelope results. This pulse-like waveform, S(t), is described by (El-Shennawy *et al.*, 1987)

$$S(t) = a(t)e^{\left(j2\pi\left(f_0 t \pm \frac{B}{2T}t^2\right)\right)} \tag{5.2}$$

where $a(t)$, which expresses the magnitude of the linear FM signal, is defined by

$$a(t) \quad = \quad \begin{cases} 1, & |t| < \frac{T}{2} \\ \\ 0, & |t| > \frac{T}{2} \end{cases} \tag{5.3}$$

here

f_0 = start frequency of chirp signal;
B = bandwidth of chirp signal;
T = duration of the chirp signal.

5.3.2 Detection of the Linear FM Signal

The analogue detection methods used in the Barry receiver are not appropriate in the DSP-based chirp detector terminal. The SSB radio equipment is designed to demodulate a 3 kHz channel to baseband; therefore detection was undertaken at baseband.

The digital detection scheme chosen was matched filtering (Turin, 1960). This process is a maximum-likelihood energy detection scheme which is optimal (Stremler, 1992). Furthermore, since the matched-filter detection of linear FM signals, termed chirp compression, is essentially correlation detection of an analogue spread-spectrum signal, the output from the detector will be an impulse response estimate of the channel. The rectangular windowed

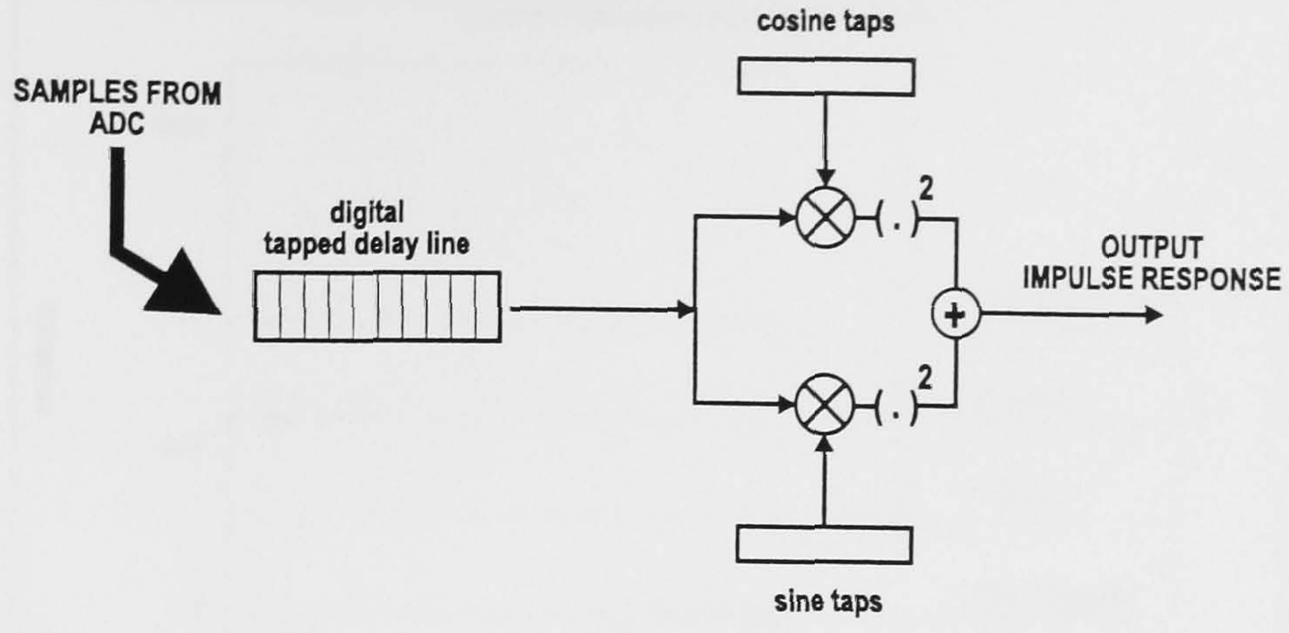

Figure 5.5: A matched filter detection scheme

linear FM pulse, defined by equation (5.2), has the real and imaginary components defined by

$$\mathrm{Re}\{S(t)\} = a(t)\cos\left[2\pi\left(f_0 t \pm \frac{B}{2T}t^2\right)\right] \tag{5.4}$$

$$\mathrm{Im}\{S(t)\} = a(t)\sin\left[2\pi\left(f_0 t \pm \frac{B}{2T}t^2\right)\right] \tag{5.5}$$

These two components are commonly termed the in-phase and quadrature (I and Q) components of the signal. They can be detected and extracted by the use of a Hilbert filter (Proakis & Manolakis, 1992), but this process is complicated. A more practical realisation is that of a non-coherent matched filter shown in Figure 5.5, which incorporates a mixer and an integrator. To construct the matched filter detector, we consider a generalisation of the detection process: if the input linear FM signal waveform, $s(t)$, and the impulse response of the filter, $h(t) = ks(-t)$, then the matched filter output is defined by

$$g(t) = k\int_{-\infty}^{\infty} s(\tau)s(t-\tau)d\tau \tag{5.6}$$

where k is a constant, normalising the gain to unity at ω_0 when defined by

$$k = \sqrt{\frac{2\mu}{\pi}} \tag{5.7}$$

with μ being the sweep rate.

Considering real signals only, s(t) and h(t) can be simplified to

$$s(t) = \cos\left[\omega_0 t + \frac{\mu t^2}{2}\right]; \qquad -\frac{T}{2} < t < \frac{T}{2} \tag{5.8}$$

$$h(t) = \cos\left[\omega_0 t - \frac{\mu t^2}{2}\right]; \qquad -\frac{T}{2} < t < \frac{T}{2} \tag{5.9}$$

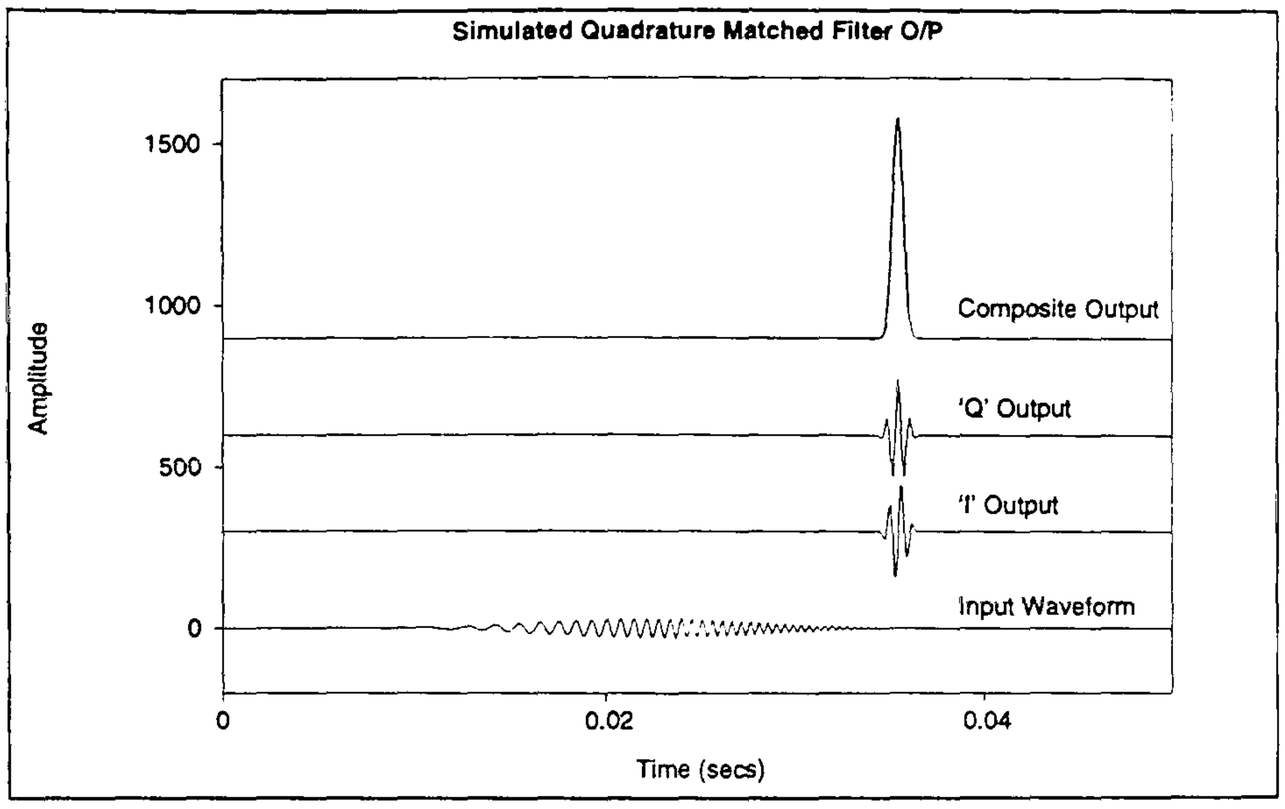

Figure 5.6: Simulation of Linear FM Matched Filter System

where

ω_0 = start frequency of the linear FM sweep;
T = length of the rectangular window.

After substitution in (5.6), it is seen that the matched filter output can be defined by

$$g(t) = \sqrt{\frac{2\mu}{\pi}} \int_{-T/2}^{T/2} \cos\left[\omega_0\tau + \frac{\mu\tau^2}{2}\right] \cos\left[\omega_0(t-\tau) - \frac{\mu(t-\tau)^2}{2}\right] d\tau \tag{5.10}$$

This reduces to (Cook & Bernfeld, 1967)

$$g(t) = \sqrt{\frac{2\mu}{\pi}} \frac{\sin\frac{\mu t}{2}(T-|t|)}{\mu t} cos\omega_0 t, \qquad -T < t < T \tag{5.11}$$

which is proportional to the linear FM matched filter autocorrelation function. A simulation of this detection procedure is shown in Figure 5.6.

5.3.3 Digital Matched Filter Detection of Linear FM

In the terminal of the type described in this thesis, the embedded DSP device can implement a digital matched filter in real time. If the useful SSB channel bandwidth is 290-3050 Hz (2760 Hz) then the Barry transmitter using a 100 kHz sweep rate will produce a chirp signal that exists in the channel passbandfor $(2760/100 \times 10^3)$s, or 27.6 ms. To enable the DSP device to detect this signal, it must be sampled at a rate greater than the minimum Nyquist rate. For example, if the sampling rate is set to 10 kHz then the waveform can be characterised by 276 samples

The main criterion for implementation on the DSP32C was optimal usage of the on-chip high-speed memory. Three sections of 256 floating point values can be accommodated in one section of this special internal memory. Allocating two of these memory sections to the I and Q components of the signal, with the remaining section for the sample history buffer, represents an efficient method of device programming. Reducing from the required 276 coefficients to 256 values means that 200 Hz of the signal spectrum is not exploited. The theoretical maximum gain in detecting a linear FM signal is defined by the time-bandwidth product (Rihaczek, 1969)

$$\text{Gain} = TB \tag{5.12}$$

A 276 coefficient-based detector would have a gain of 76.2, (37.6 dB), whereas in the 256 coefficient-based detector the gain is reduced to 65.5 (36.3 dB). This 1.2 dB loss has implications for the detection of weaker modes in the impulse response. In contrast, in the Barry system the signal is detected in 100 kHz steps, giving a gain of 100 dB which greatly exceeds the value that can be obtained using the DSP-based Chirpsounder receiver. However, the Barry system has far more complex RF equipment.

One issue of matched filtering a linear FM signal that has not been discussed is that of signal ambiguity. When matched filtering is used as the detection process, the signal mismatch characteristics (ambiguity function) must be considered (Turin, 1960). For this project, a short investigation of the ambiguity response of the chirp signal used in the chirp monitor was undertaken; this is presented in Appendix B. This investigation shows that the linear FM signal does not have an optimal impulsive response and any time mismatch will appear as a frequency offset; conversely a frequency offset will be translated to a time offset. These are important issues since the channel may be subject to Doppler shifts and frequency offsets in the equipment, hence producing a time offset in the impulse response. Since the equipment configuration did not use a highly accurate time reference, these frequency offsets could occur causing a distortion in the channel impulse response, determined by the form of the ambiguity function.

5.4 Non-Linear FM Signals

The limitation of linear FM signals indicated above means that a chirp signal will not be suitable for every HF channel condition. For example, large Doppler shifts are possible during SIDs (Sudden Ionospheric Disturbances) and at ionospheric sunrise or sunset; also mobile transmitters can induce significant Doppler shifts. The linear FM signal has a non-optimal ambiguity function that makes it relatively intolerant of such Doppler offsets.

Doppler-induced loss, when applied to pulsed linear FM detection, has been noticed by many workers in the radar field. The solution to this problem was adapted from the behaviour of hunting bats where Doppler offsets would cause the prey to be lost if the ultrasonic linear FM emission was used (Altes, 1990). Such research complemented the attempts optimise the frequency modulation of pulse compression signals by Kroszczynski (Kroszczyński, 1969) further developing the work of Fowle (Fowle, 1964). The received linear FM signal, $\mu'_R(t)$,

when subject to a Doppler (frequency) offset, is given by

$$\mu'_R(t) = a(\alpha t)\sin\left[2\pi\left(\alpha f_0 t + \frac{\alpha^2 k}{t}t^2\right)\right] \tag{5.13}$$

where α, the factor encompassing the velocity change at the point of reflection, is defined by

$$\alpha = 1 + \nu \approx 1 + (2\frac{v}{c}) \tag{5.14}$$

and

f_0 = start frequency of chirp signal;
v = velocity change at the reflection point (Doppler offset);
c = velocity of propagation;
k = sweep rate.

This means that the instantaneous frequency of the received signal, f_d, is therefore scaled by this factor,

$$f_d(t) = \alpha f_0 + \alpha k t^2 \tag{5.15}$$

By examining equation (5.15) it can be seen that the signal at the receiver not only has a shifted initial frequency offset, but a changed frequency modulation rate. Thus, for a range of typical HF conditions, the value of $f_d(t)$ modifies the matched filter response. A 10dB matched filter output amplitude loss is possible with time bandwidth products of over 10 (Cook & Bernfeld, 1967; Kramer, 1967).

The Doppler intolerance of linear FM in radar systems can be overcome by using a hyperbolic FM signal format (Rihaczek, 1969). This hyperbolic format retains some of the advantages of linear FM, for example signal resolution. The hyperbolic FM (HFM) waveform, $u(t)$ is described in (Altes, 1967), and is given by

$$u(t) = a(t)\exp\{j2\pi k\ln(t)\} \tag{5.16}$$

Reflection from a moving HF layer gives maximum frequency shifts of a few Hz per second whereas, for a fast-moving mobile, such as an aircraft, this can extend to more than 10 Hz per second. The following theoretical results were derived by adapting previous work in the radar context.

Let t, v, $u(t)$, and α be the time delay, velocity of the reflection point, a unit step function and acceleration of the reflection point respectively. It can be shown that the reflected energy, e(t), for a general FM signal is described approximately by (Altes, 1967)

$$\begin{aligned} e(t) \approx & \left[\left(1-\frac{2\nu}{c}\right)\left(\frac{2\alpha}{c}\right)\left(1-\frac{3\nu}{c}\right)(t-\tau)\right]^{\frac{1}{2}} \\ & \times\left[\left(1-\frac{2\nu}{c}\right)(t-\tau)-\left(\frac{\alpha}{c}\right)\left(1-\frac{3\nu}{c}\right)(t-\tau)^3\right] \end{aligned} \tag{5.17}$$

For HFM signals, this becomes

$$e(t) \approx u(t-\tau)\exp\left\{2j\pi k\ln\left[\left(1-\frac{2v}{c}\right)(t-\tau) - \left(\frac{\alpha}{c}\right)\left(1-\frac{3v}{c}\right)(t-\tau)^2\right]\right\} \tag{5.18}$$

$$= u(t-\tau)\exp\left(2j\pi k\left\{\ln(t-\tau)+\ln\left[\left(1-\frac{2v}{c}\right) - \left(\frac{\alpha}{c}\right)\left(1-\frac{3v}{c}\right)(t-\tau)\right]\right\}\right) \tag{5.19}$$

Using the approximation $\ln(1+x)\approx x$ for $x \ll 1$, and substituting in equation 5.16,

$$e(t) \approx u(t-\tau)\exp\left\{-j2\pi k\left[\left(\frac{2v}{c}\right)+\left(\frac{\alpha}{c}\right)\left(1-\frac{3v}{c}\right)(t-\tau)\right]\right\} \tag{5.20}$$

$$= u(t-\tau)\exp\left[j2\pi f_\alpha(t-\tau)+\varphi_v\right] \tag{5.21}$$

The reflected signal is therefore approximated by a delayed, frequency shifted and phase shifted version of the transmitted signal. The phase shift is not manifested in the matched filter output since a quadrature detector is used. The time delay caused by different layers is common to all of the signal returns. The only important factor is the frequency shift, which causes ambiguous detection. This is given by

$$f_\alpha \approx -\frac{k\alpha}{c} \tag{5.22}$$

This frequency shift is seen to be very small for the range of HF channel propagation conditions outlined above. This means that the matched filter output will be relatively unaffected, even with a demodulation bandwidth of less than 3 kHz. Therefore, it can be seen that HFM signals offer a sounding profile that can be used in situations when normal linear FM would be degraded significantly.

These important theoretical results were not implemented due to the lack of time. However, it is one area where a future research project could extend the work presented in this thesis.

5.5 Operation of the DSP-based Reception System

The discussion above has introduced the basic concepts used in the development of the DSP-based chirp receiver and transmission system. The following section focuses on certain implementation issues for the DSP-based receiver; in particular, the need to condition the received signal using a window function to maximise the peak-to-sidelobe values. This facilitates efficient operation of the impulse response peak detection algorithms that are used to estimate and synthesis an ionogram.

5.5.1 Implementation of the Matched Filter on a Digital Signal Processor

When implemented on a DSP device, a matched filter performs a correlation based on equation 5.23 (Proakis & Manolakis, 1992). In this equation, the summation utilises a

256-coefficient representation of the baseband received linear FM signal, $x[n]$, and a 256-coefficient matrix that characterises the digitised linear FM matched filter, $h[k]$. The 256 coefficient limit was chosen to maximise the use of internal high-speed DSP memory. Hence, the sampled data output of the matched filter, $y[n]$, is given by the discrete convolution

$$y[n] = \sum_{k=0}^{255} h[k]x[n-k] \tag{5.23}$$

Equation 5.23 can be efficiently programmed on a DSP device in one instruction since it involves essentially the same operations as for a non-recursive digital filter. As described in section 5.3.2, for optimum detection of the signal energy, two quadrature matched filters are necessary. In discrete form, the output of the summer in Figure 5.5 is thus given by

$$\left(\sum_{k=0}^{255} h_{\sin}[k]x[n-k]\right)^2 + \left(\sum_{k=0}^{255} h_{\cos}[k]x[n-k]\right)^2 \tag{5.24}$$

The discrete quadrature linear FM matched filter coefficients, $h_{\cos}$ and $h_{\sin}$, were calculated from sampled values of

$$h_{\cos} = \cos(2\pi \times 320t + \pi 100 \times 10^3 t^2) \tag{5.25}$$

$$h_{\sin} = \sin(2\pi \times 320t + \pi 100 \times 10^3 t^2) \tag{5.26}$$

The sweep rate of the transmitted signal is set to 100 kHz per second and the start frequency is set at 320 Hz. This value of the start frequency was chosen to take account of the passband frequency response of the receiver. At 10 kHz sampling rate, the bandwidth of the matched filter is $0.256 \times 10^3 = 2560$Hz.

The result of a simulation of a 256-tap matched filter system is shown in Figure 5.6.

5.5.2 Windowed Detection Schemes

As shown previously, the output from the matched filter is an estimate of the channel impulse response. From computer simulation, it was apparent that the matched filter output had significant sidelobes. The peak-to-sidelobe ratio (PSR) was approximately 15dB, causing the peak-detection system to make erroneous decisions since it could not accurately differentiate between peaks caused by the detection method and low-amplitude received multipath components.

Analysis of the system showed that the lack of a windowing function gave rise to the sidelobe levels generated by the detector. In mathematical terms, the matched filter detector output is a convolution of the received linear FM signal and a reference rectangular chirp window function. To reduce the sidelobe levels, a better window function was applied to the matched filter reference signal. The window chosen was a Hamming window. This choice was strongly influenced by publications describing windows normally used by radar systems (McCue, 1979). The discrete Hamming window function, $w(n)$, is described by the following expression (Harris, 1978; Proakis & Manolakis, 1992)

$$w(n) \quad = \quad \alpha + (1-\alpha)\cos\left[\frac{2\pi}{N}n\right] \tag{5.27}$$

Window	PSR (dB)	Coherent Gain	Noise Bandwidth	-3.0 dB Bandwidth	- 6.0 dB Bandwidth
Rectangular	13	1.00	1.00	0.89	1.21
Hamming	43	0.54	1.36	1.30	1.81

Table 5.1: A table comparing the Rectangular Window and Hamming Window when pre-weighting Matched Filter Taps

$$W(f) = \alpha D(\alpha) + 0.5(1-\alpha)\left[D\left(f-\frac{2\pi}{N}\right) + D\left(f+\frac{2\pi}{N}\right)\right] \tag{5.28}$$

where

$$D(f) = \exp\left(+j\frac{f}{2}\right)\frac{\sin\left[\frac{N}{2}f\right]}{\sin\left[\frac{1}{2}f\right]} \tag{5.29}$$

and

$$\begin{aligned} W(f) &= \text{frequency domain representation of } w(n) \\ f &= \text{instantaneous frequency;} \\ N &= \text{number of samples in window;} \\ n &= \text{index.} \end{aligned}$$

The Hamming window occurs when $\alpha = 25/46$ ($\alpha \doteq 0.543478$). This value of α is chosen so that perfect cancellation of the sidelobes occurs when $f = 2.5[2\pi/N]$. At this value of α, the window is described by

$$w(n) = \begin{cases} 0.54 + 0.46\cos\left[\frac{2\pi}{N}n\right], & n = -\frac{N}{2}, \cdots, -1, 0, 1, \cdots, \frac{N}{2} \\ \\ 0.54 - 0.46\cos\left[\frac{2\pi}{N}n\right], & n = 0, 1, 2, \cdots, N-1 \end{cases} \tag{5.30}$$

For the Hamming window, the first sidelobe is -43dB down on the main peak (Harris, 1978). This window is suitable for differentiating between sidelobe noise and peaks caused by multipath conditions. The window does have deficiencies; these are evident when its characteristics are compared with those of a rectangular window in Table 5.1. It can be seen from this table that a trade-off exists between the time-resolution of the windowing function and the detection peak-sidelobe ratio (PSR). A computer search for improved windowing functions is a task that any future project could usefully undertake.

5.5.3 Evaluation of Matched Filter Performance

To evaluate the performance of the matched filter detection system, a series of simulations were undertaken. These simulations produced an estimate of the impulse response for two known input conditions. The first was a noise-free simulation with two equal magnitude modes separated by about 5 ms. The second incorporated simple additive Gaussian noise

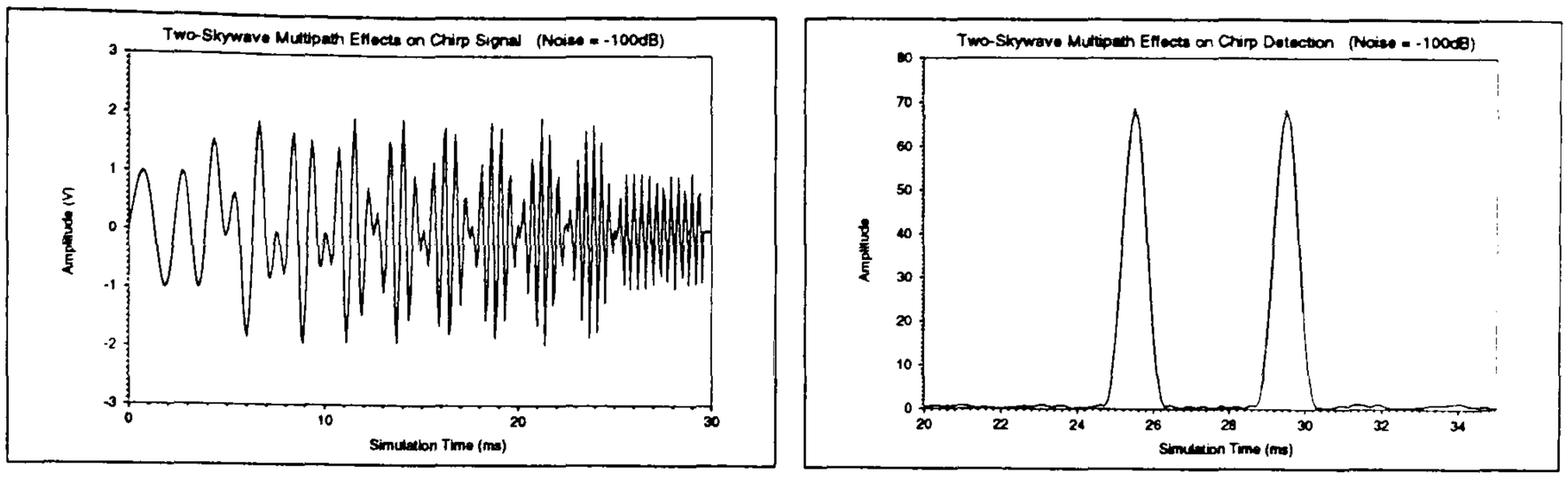

(a) (b)

Figure 5.7: Channel Simulation with No Additive Noise and Two Propagating Modes

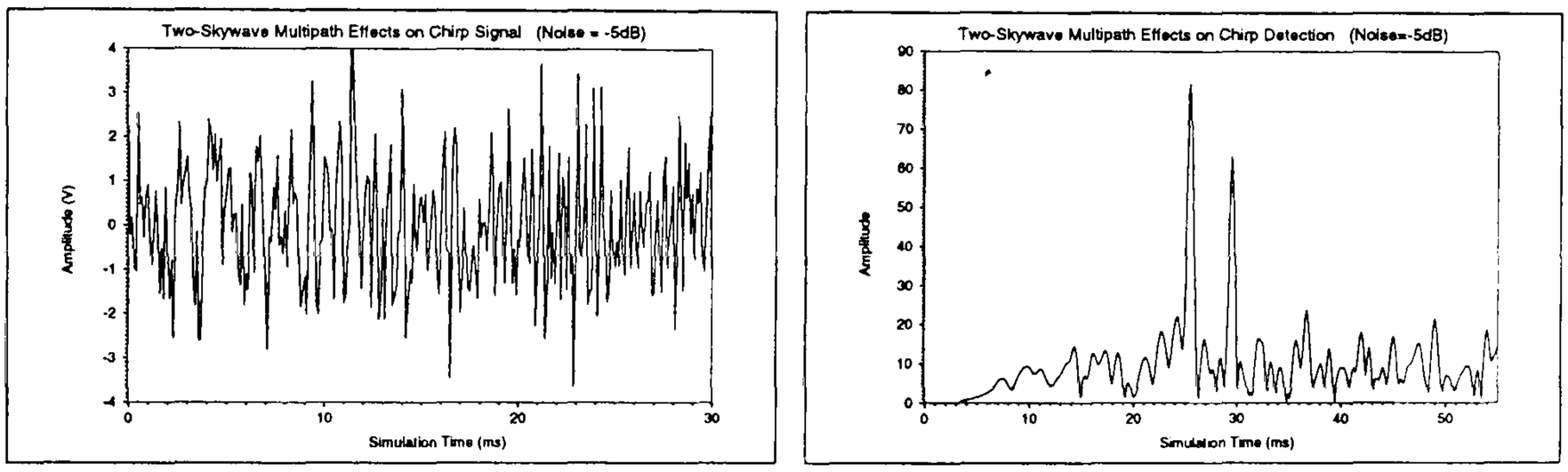

(a) (b)

Figure 5.8: Channel Simulation with Additive Noise and Two Propagating Modes

with the same mode structure. Figure 5.7 and Figure 5.8 respectively present the results from these simulations. As can be seen, the system accurately resolves the two modes. The system can reliably detect signals with additive noise up to 0 dB SNR. Real HF link situations are often non-Gaussian; an example of a real chirp signal exhibiting a frequency selective fade due to multipath is presented in Figure 5.9—this was sampled off-air using the ADC on the DSP development system using a Skanti TRP 8255 receiver. The FSF will causes the matched filter output to be distorted; it can be seen that the received signal differs greatly from the ideal chirp signal. The matched filter is effective in rejecting strong single tone interferers, but can give an incorrect estimate when multi-tone interference corrupts zero-crossings and amplitude information. In addition, the chirp signal will be affected by variations of group delay with frequency across the radio receiver's passband. This effect is normally negligible when compared with any propagation effects.

5.5.4 Peak Detection Algorithms

The final stage in the construction of the chirpmonitor system was the incorporation of an impulse response, peak-detection system. This is required to post-process the impulse response to identify the modal structure for display as an ionogram. Complex algorithms for

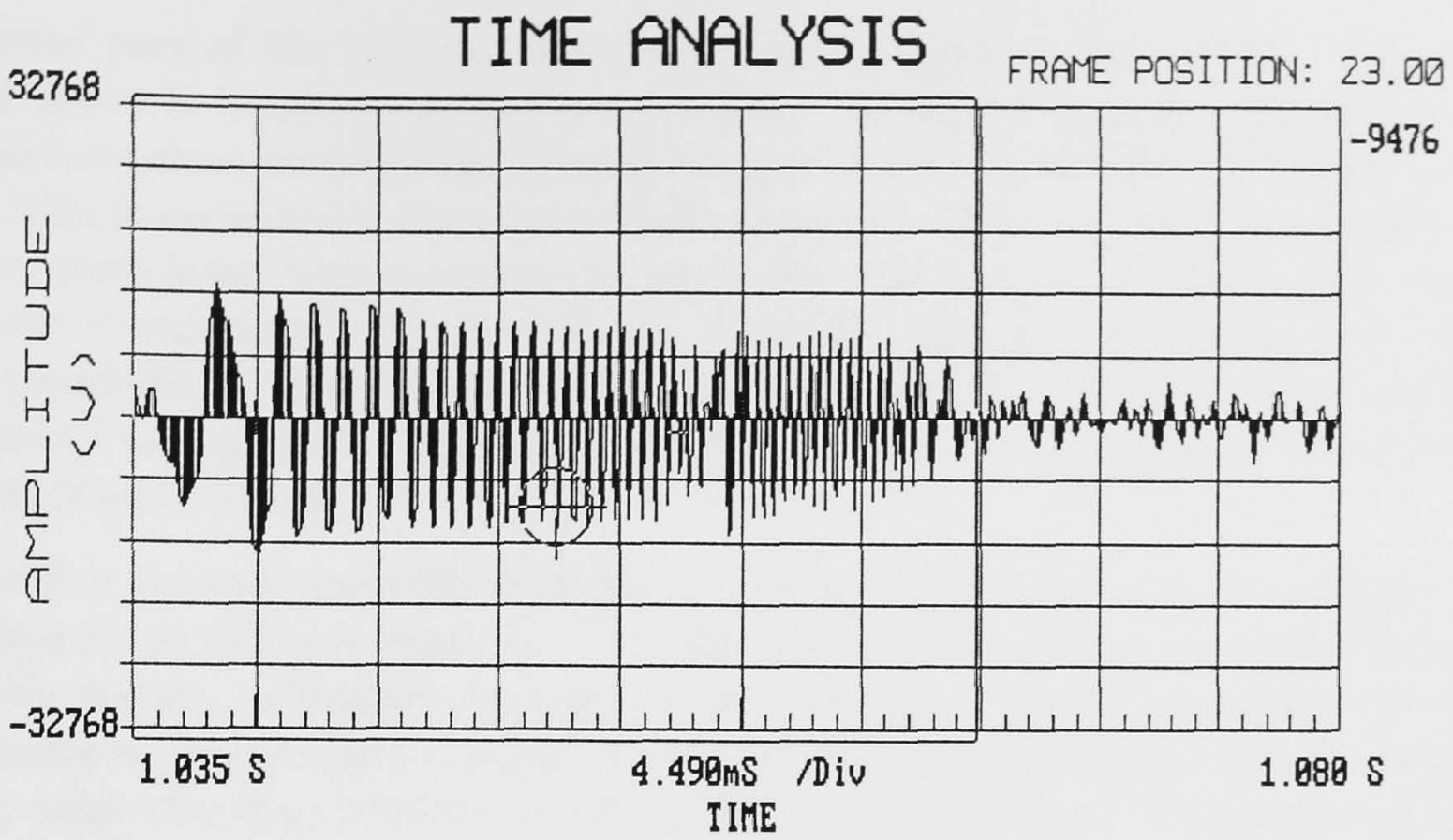

Figure 5.9: Chirp Signal Captured from Off-Air Data (Milltown Sounder); Channel at Frequency 8.0 MHz

peak detection are necessary in the DSP-based chirp receiver since a high stability timing source was not utilised; all timing was relative to the Barry transmission schedule. The final ionogram was constructed by creating a raster of peak-detected impulse responses from successive channels.

The main process is the basic peak-detection algorithm. This algorithm is used to identify maxima in the impulse response and note their positions. These are then sorted by comparing amplitudes at the maxima positions and eliminating those points that are ambiguous or clearly result from matched filter noise. In addition, the set of peak positions can be further reduced if a 'window of probability' is utilised. This time window can exclude those responses that fall outside the range where a valid matched filter response would be expected. This window relative to the initial timing reference point and would be specified after the DSP system achieved synchronisation with the Barry chirp transmission.

Once synchronisation is achieved, the first impulse response forms the reference from which all other responses are measured. It was found from trials taken over several days that a window with the parameters listed below was best suited to maximising the probability of detecting a peak in the channel impulse response and displaying the result as an ionogram correctly in the centre of the screen:

(i) Window time span of 100 matched filter samples; assuming a 10 kHz sampling rate, this equates to a 10ms window;

(ii) The leading edge of the display filter should be 25 samples before the synchronised peak; this equates to 2.5ms;

(iii) The trailing edge of the display filter should be 75 samples after the peak; this equates to 7.5ms.

(iv) Peak display will occur if the value exceeds a predefined threshold, computed from simulation and weighted by an equipment-specific calibration factor.

In the latter part of the project, the peak-detection process was revised. The algorithm described above is based upon the use of a 'hard' threshold in stage (iv); however, it was discovered from close examination of received impulse responses that weak signals were often ignored. This is undesirable since useful information is often contained in such components. To recover these lower level propagation modes from the matched filter output information, an improved detection system was devised. This new algorithm was based upon deriving a variable threshold from the information in the matched filter output. Since the threshold is calculated from the information generated in real-time, this method is essentially a 'soft' decision-directed process.

The algorithm is based upon the analysis of matched filter output levels outside the region where relevant outputs are expected. The algorithm averages all the matched filter returns outside this region, noting the maximum received signal. If the maximum value is more than 3dB above the averaged matched filter level, then the threshold is set to be 2dB above this level; otherwise the threshold is 3dB above the average level. This empirical method is effective and, if coupled with the information on the performance of the Hamming window (43dB peak-to-sidelobe ratio with a bandwidth spread of 1.3 at -6dB RMS point relative to the peak), can provide an appropriate detection system. The system can reliably detect valid matched filter output components 15-20 dB below the peak signal.

5.5.5 System Integration

With all component elements complete, the final stage in building a Chirpsounder receiver (Chirpmonitor) was integration of the individual algorithms to display the ionograms.

Figure 5.10 presents a flow chart of the system. The PC requires an accurate clock (to the nearest second); for the current system, a stable digital reference was used (1×10^{-6} TCXO). During initialisation, system uses its database to determine the start time of the chosen transmitter; it then tunes to 2 MHz to await the start of the signal. After the desired start time, the receiver tunes in 150 kHz steps 'tracking' the expected chirp signal. The matched filter dwells on a channel for 1.5 seconds if the signal is not detected before a new channel is selected. Once a signal is detected, the DSP reconfigures the system to place the 'window-of-acquisition' at the centre of the screen to allow a convenient display of the ionogram. The system then uses 'fly-wheel' synchronisation to follow the chirp signal in 50 kHz steps across the HF band; this process is detailed in Figure 5.11. The PC simply displays the matched filter peaks lying in the 'window-of-acquisition'. The DSP is the master time reference and adjusts the PC's internal clock in order to maintain synchronisation for the next sounder to be selected. The stored received channel information has three components: the raw input information can be stored, together with the matched filter output and the displayed image. If a transmitter is not detected, then the receiver advances the clock by 0.5 seconds and tries again. This time-slippage is useful for detecting sounders when only an approximate schedule is known. All operations are performed via a DSP32C device using a floating point arithmetic unit; thus no scaling operations are necessary.

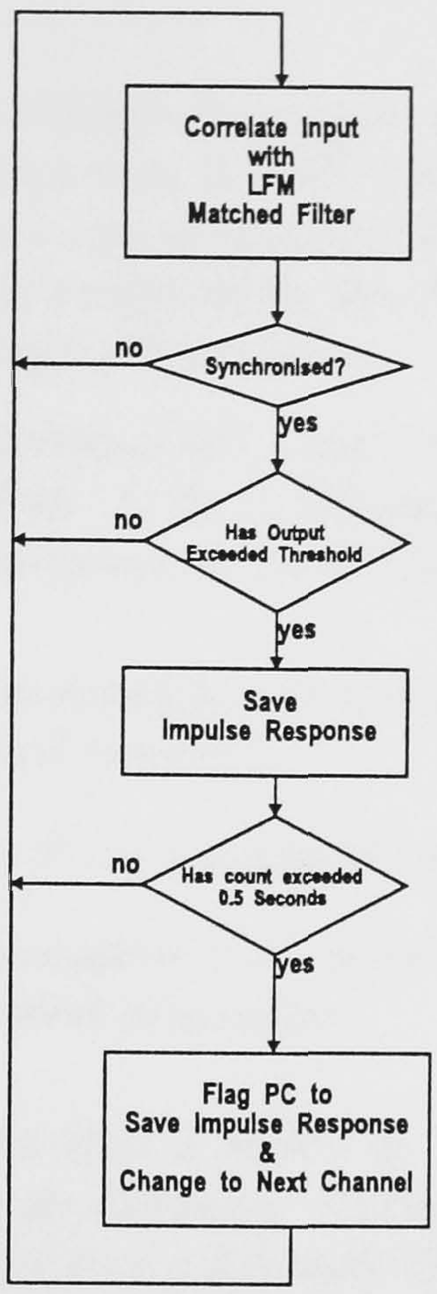

Figure 5.10: Flow-chart showing the operation of the Chirpmonitor

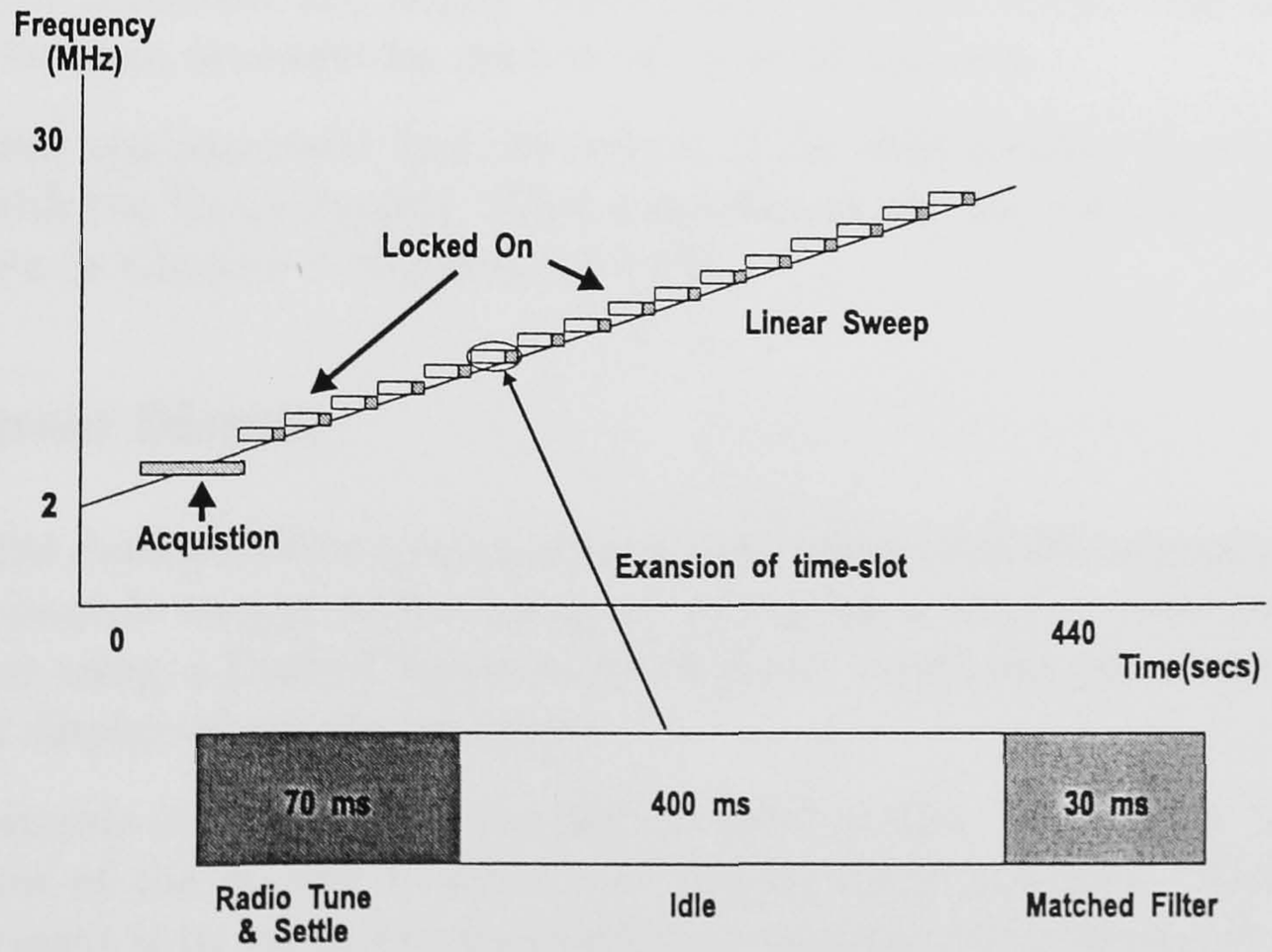

Figure 5.11: The synchronisation process within the Chirpmonitor

5.5.6 Comparative Trial between Chirpmonitor and Barry Chirpsounder Receiver

Verification of the output from the chirpmonitor receiver was an important element in the research programme. The most direct way to verify the output was to compare the ionograms produced against those from a commercial sounder receiver using the same antenna in order to show that the ionograms produced by the DSP-based sounder receiver provide a true indication of the actual propagation conditions.

Trial facilities at DRA (Aerospace Division) at Cobbett Hill were offered for a 36 hour period between the 8th and 9th August 1990. A Barry Research Chirpsounder receiver (Type 5) was available for this period for a comparative trial. The aims of the trial were:

(i) validation of the ionograms generated by the Chirpmonitor — (the term coined for the DSP-based Chirpsounder receiver);

(ii) determination of the accuracy of the ionograms from the Chirpmonitor;

(iii) extraction of any further information that would be useful in developing the software for enhanced propagation estimation.

The equipment configuration for the trial is shown in Figure 5.12. The output from the same antenna was passed through an electronic splitter in order to allow equal received signal powers to be input to both the Barry Research Chirpsounder receiver and the radio connected to the Chirpmonitor. Various sounders were monitored over the trial period; the best received signals were from Oslo, Akrotiri (Cyprus), Milltown, Chelveston, Hong Kong and Gibraltar. Several hours' reception were lost during the period of the trial since 8th August 1990 was the day that Iraq invaded Kuwait and international tension was increased! Since most of the sounders were operated by military organisations, they departed from their normal peacetime schedules and began transmitting intermittently. This made it difficult to synchronise to some sounders for periods of up to 45 minutes.

However, the trial was successful and the output of the chirpmonitor showed a high degree of correlation with the Barry output, which was taken as the benchmark. A selection of the results are shown in Chapter 7 (Figures 7.4-7.12).

5.5.7 Ionogram Display

The storage of the matched filter output information makes available several possible display formats. The simplest output is the ionogram providing a display commonly available to any HF operator using a Barry Chirpsounder receiver; amplitude information is contained in a signal level display above the ionogram.

The possible methods of displaying of the digital matched filter information are limited only by the resolution of the display monitor and display space available. The most obvious display improvement is to use colour modulation to represent the differences in received signal intensity. This substantially enhances the output clarity because resolution is enhanced since both the peak and the width of the peak, which contains additional information, are displayed. This method has been used in the ROSE system to enhance the output of the

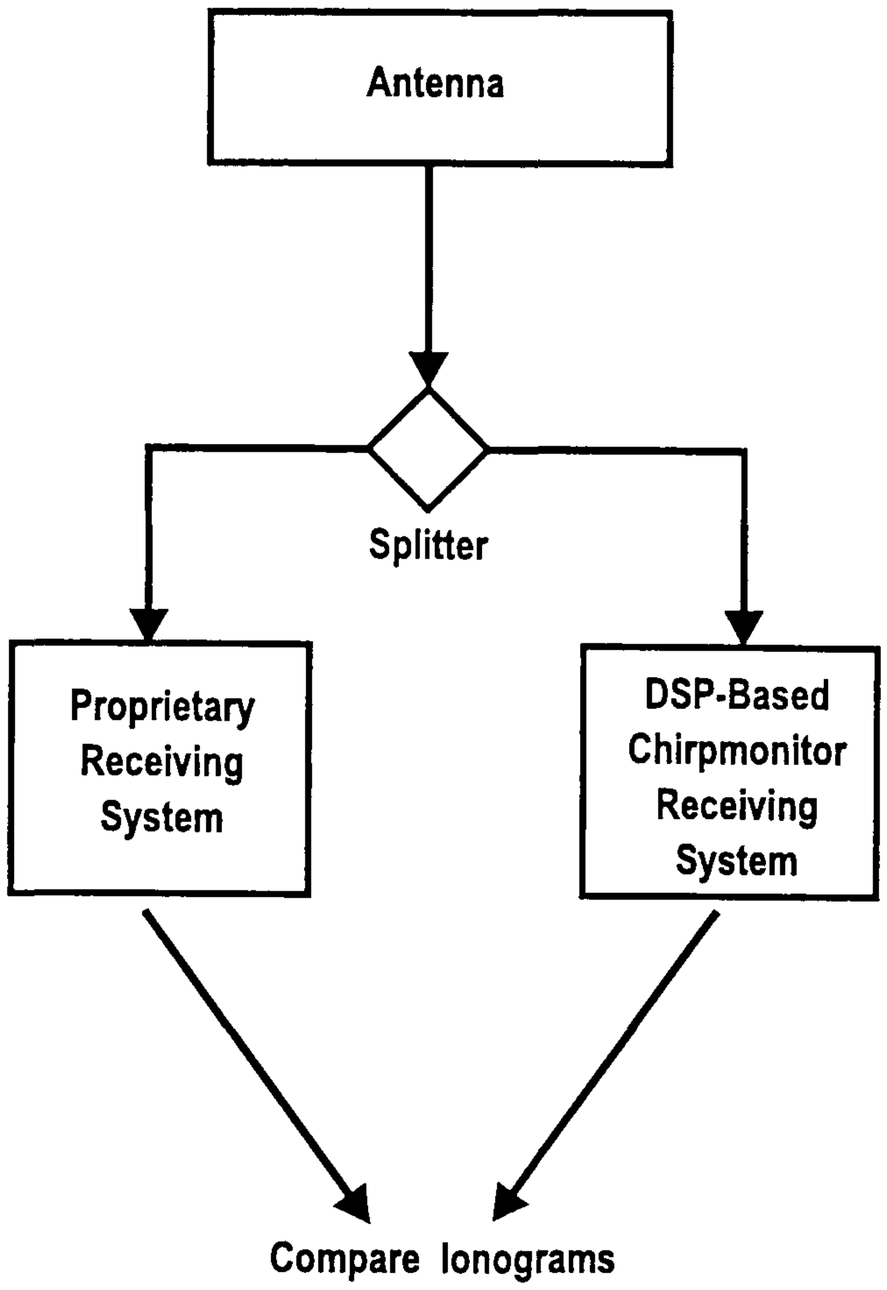

Figure 5.12: Configuration of the Chirp Reception Systems for the Comparative Trials

Barry receiver (Dickson *et al.*, 1991). An example of a simple colour modulated ionogram is shown in Figure 5.13. Colour modulation of the matched filter output waveform is another display option; such data can be sorted into a series of colour-coded ranges and displayed, as shown in Figure 5.14. Another possible output method is to use a "waterfall" display of a series of the impulse-responses. The impulse response data appears as a "mountain-range" rising above the matched filter noise. This results an effective and informative display when colour-coded. Such a format allows trends in the width of the matched filter returns to be seen. Figure 5.15 shows a colour plot taken from the computer screen of this type of display.

5.6 Operation of the DSP-based Sounding System

The construction of an active sounding system is a logical evolution from a DSP-based chirp receiving system. This allows in-band sounding of either all channels in the HF band (2-30 MHz), or just those channels allocated to an HF system. An important restriction of operating with the fixed Barry network is that it may not be possible to obtain a propagation estimate over the path of interest. With the DSP-based sounder, this restriction is removed since it can operate as controllable, independent channel sounder between two or more sites, thus providing propagation measurements that can be used directly without extrapolation or interpolation. It is envisaged that an adaptive terminal of the type described in this thesis would have an embedded sounding capability for assessing propagation conditions or link quality, say, between network nodes. An embedded channel sounding capability requires the

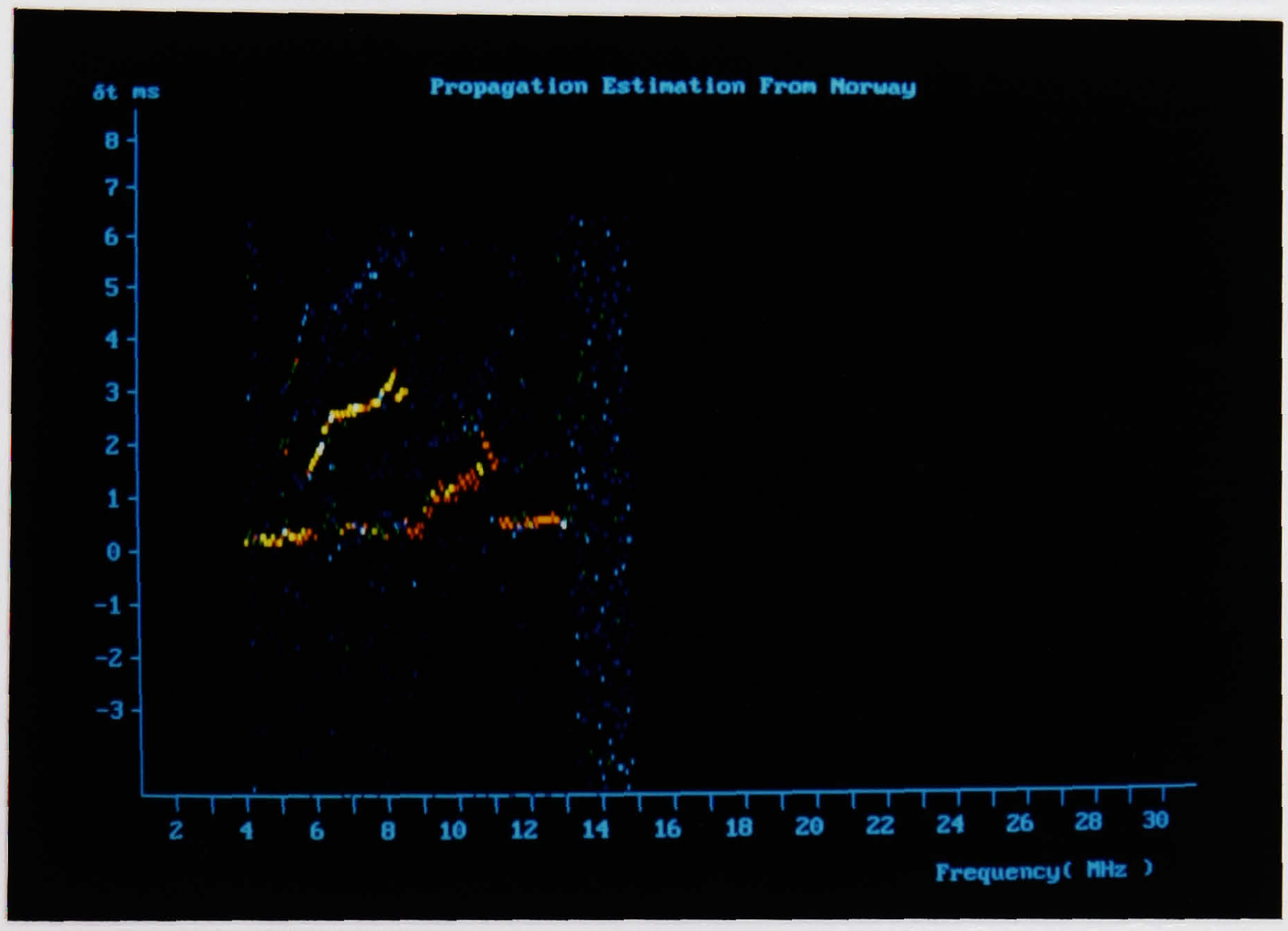

Figure 5.13: A Plot of a Colour-Modulated Ionogram

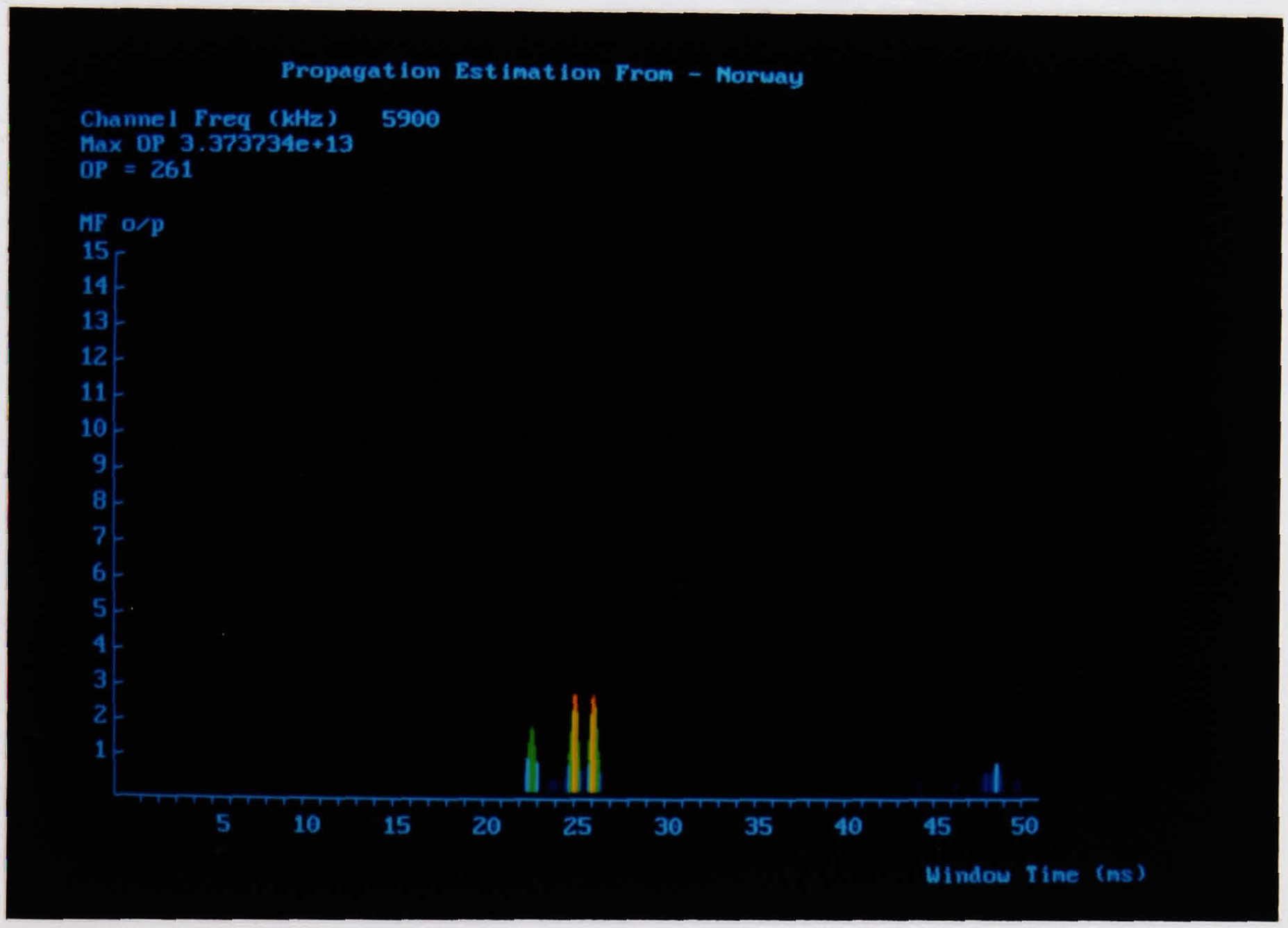

Figure 5.14: A Plot of Colour-Coded Impulse Response Data

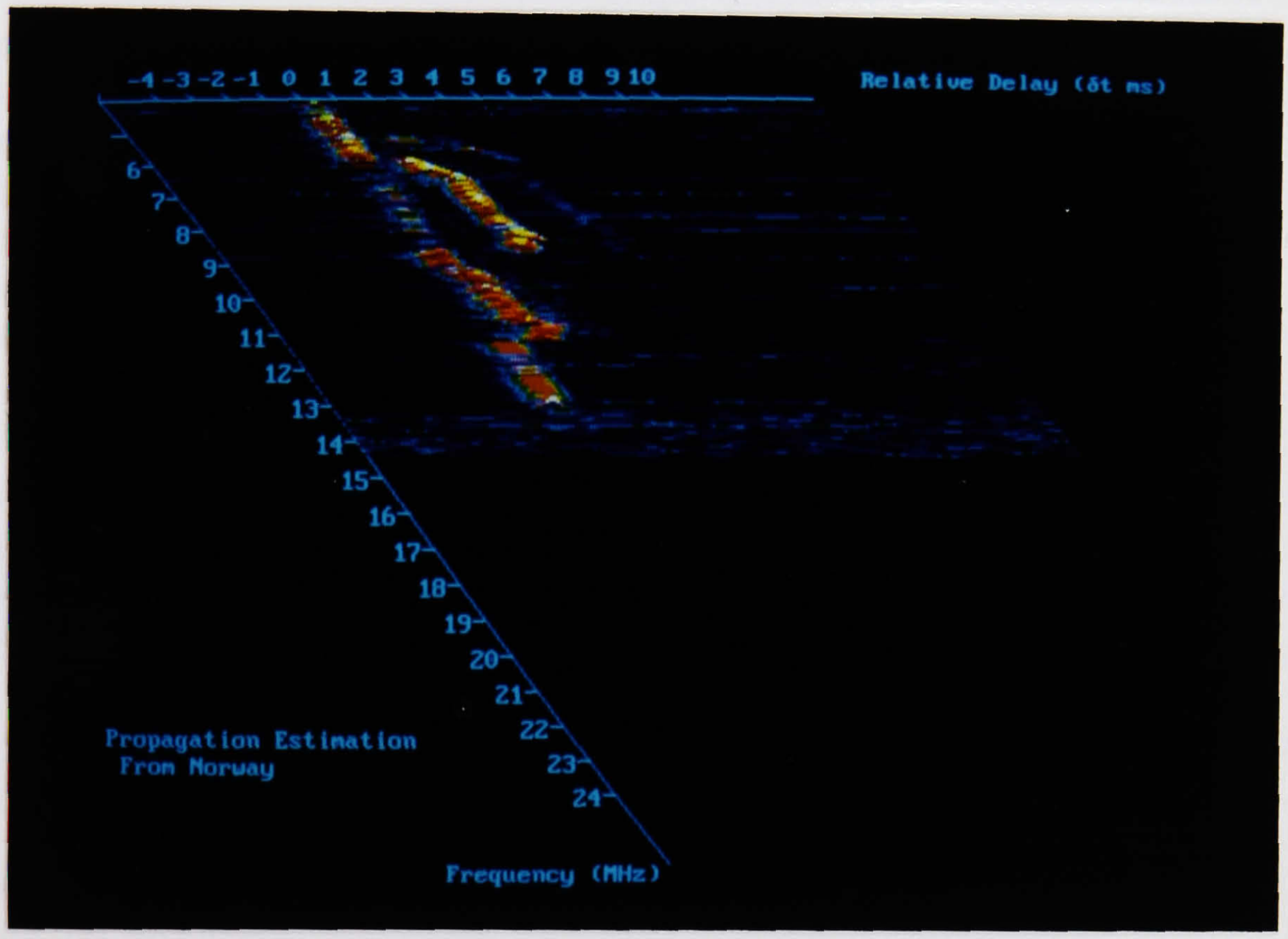

Figure 5.15: A Contour Plot of a "Waterfall" Display
of a series of Matched Filter Responses

following:

(i) time synchronisation across the whole of the HF network; this is an important criterion because if the sounding node and receiving node are not synchronised then the receiver will not be able to follow the in-band sounding schedule;

(ii) a choice of sounding profile that will enable maximum propagation information to be extracted;

(iii) a sounding profile that will not be adversely affected by normal HF traffic in the sounding channels, or by normal ionospheric effects.

Without some form of synchronisation, the system would not be able to receive and process the required signal. In a typical sounding network, the timing between nodes is maintained by accurate clocks to with $< 1.0 \times 10^{-9}$s. The system can compensate for small offsets, but it is uneconomic to have such precise synchronisation in the proposed terminal; therefore, other methods for achieving timing alignment are needed. Thus a major advantage of the sounder receiver developed is that it derives synchronisation from the transmitted signal. This 'parasitic' method of acquiring synchronisation means that only a moderately accurate timing source ($< 1.0 \times 10^{-6}$ s offset) is needed. This can be achieved using high quality standard crystals. However, a full implementation would require a higher specification timing reference to allow efficient co-ordination and networking of multiple sounders.

To enable the techniques developed for the receiver to be exploited in an active sounder, the sounding profile chosen was linear FM. Such a system offers several advantages to the research programme, i.e.:

(i) the system could directly use the available DSP-based Chirpmonitor system, thus reducing development time;

(ii) the linear FM signal energy is spread uniformly over the whole of the 3 kHz channel bandwidth the effects of co-channel users to be minimised;

(iii) the linear FM signal facilitates spreading the transmitted energy at low level over a period of time; this allows lower power radio transmitters to be used;

(iv) the DSP-based architecture allows other sounding profiles, for example HFM to be used;

(v) a "embedded" message transmission facility could be incorporated in the sounding process by using forward and reverse sweeps;

(vi) since the active sounder uses the same terminal architecture as the chirpmonitor and template correlation subsystems, this enables it to complement these other functions for frequency management purposes.

The active sounder operates on a raster scan. Channels are selected sequentially in 200 kHz steps, or in a predetermined order, and the linear FM waveform is transmitted on each. This is termed segmented swept FM (SSFM); Figure 5.16 shows the schematic configuration of the active sounding system used for practical trials.

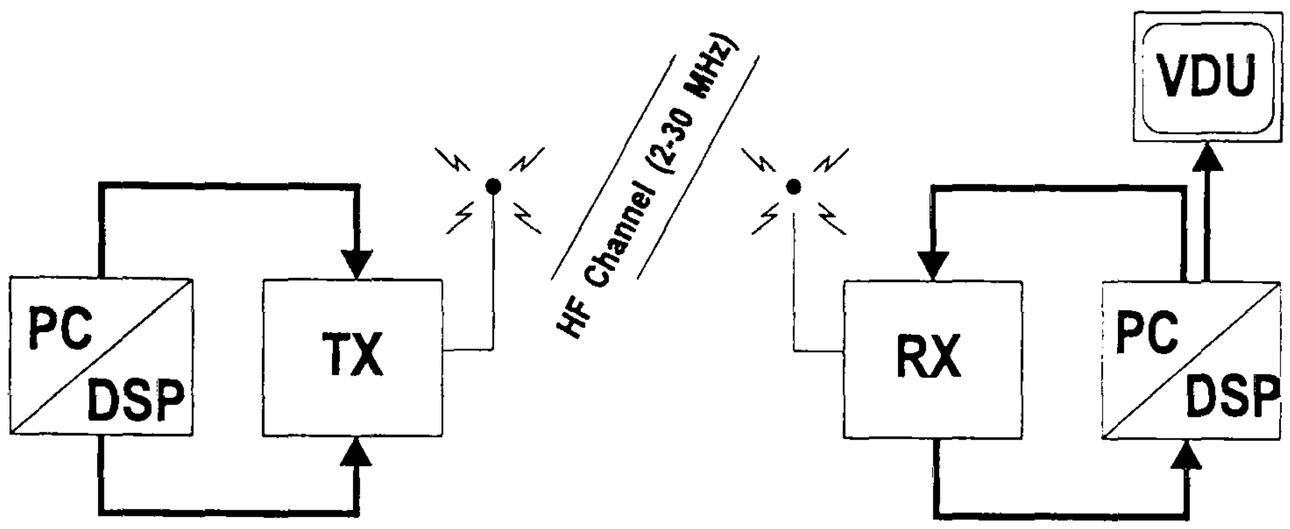

Figure 5.16: Configuration of equipment for the Active Sounding Trial

A flow chart of the operation of the sounder is shown in Figure 5.17. It can be seen that the limiting factors in the operation of the system are the tuning time for the radio and the time taken to pass information to the radio. This means that only a 'coarse' raster of 200 kHz frequency increments was possible with the radio used (Skanti Model TRP8255). A finer raster of 100 kHz steps would be possible by presetting all the frequencies and re-calling them by a single codeword, rather than by specifying a frequency group code each time. However, for the purposes of demonstrating the active sounding function, the 200 kHz raster was adequate. In back-to-back bench trials, the system worked well and all problems were resolved. A full on-air trial was held on 16th/17th July 1991. The configuration for the trial is shown in Figure 5.18. The receiver terminal was based on a TMS320C25 system and an amateur grade receiver, whereas the transmitter was based on a DSP32C and a professional grade transceiver. Incompatibility between these units caused some problems and only a limited set of useful results were obtained from this trial. However, the results demonstrated the feasibility of the system and further trials are planned in a subsequent project. A set of results is given in Chapter 7. These results demonstrate that the segmented sounding scheme is an effective alternative to continuous sweep sounding as an aid to frequency management. The development of a prototype SSFM sounder and its practical testing form an important novel element of the research described in this thesis.

5.7 Review of Chapter

This chapter has focused on the channel selection subsystem and described two DSP-based tools to measure real-time propagation effects. The first tool, the chirpmonitor, performs the same function as the Barry Chirpsounder Receiver and generates ionograms by passively processing existing signals from the Chirpsounder network. These ionograms are then used to give an overall indication of current propagation conditions and to add or delete channels from the list generated by the off-line prediction system. Further refinements to this process include analysis of the channel impulse responses to allow rejection of any channels that have inappropriate propagation characteristics. For example, channels with severe multipath dispersion that would cause severe inter-symbol interference in the transmitted signal might be rejected if the modem in use did not possess an adaptive equaliser.

The usefulness of tool is limited by the availability of Chirpsounder transmissions and the geographical location of the transmitters. If the transmitters are not close to network nodes then it may be necessary to undertake extra processing, for example interpolation of

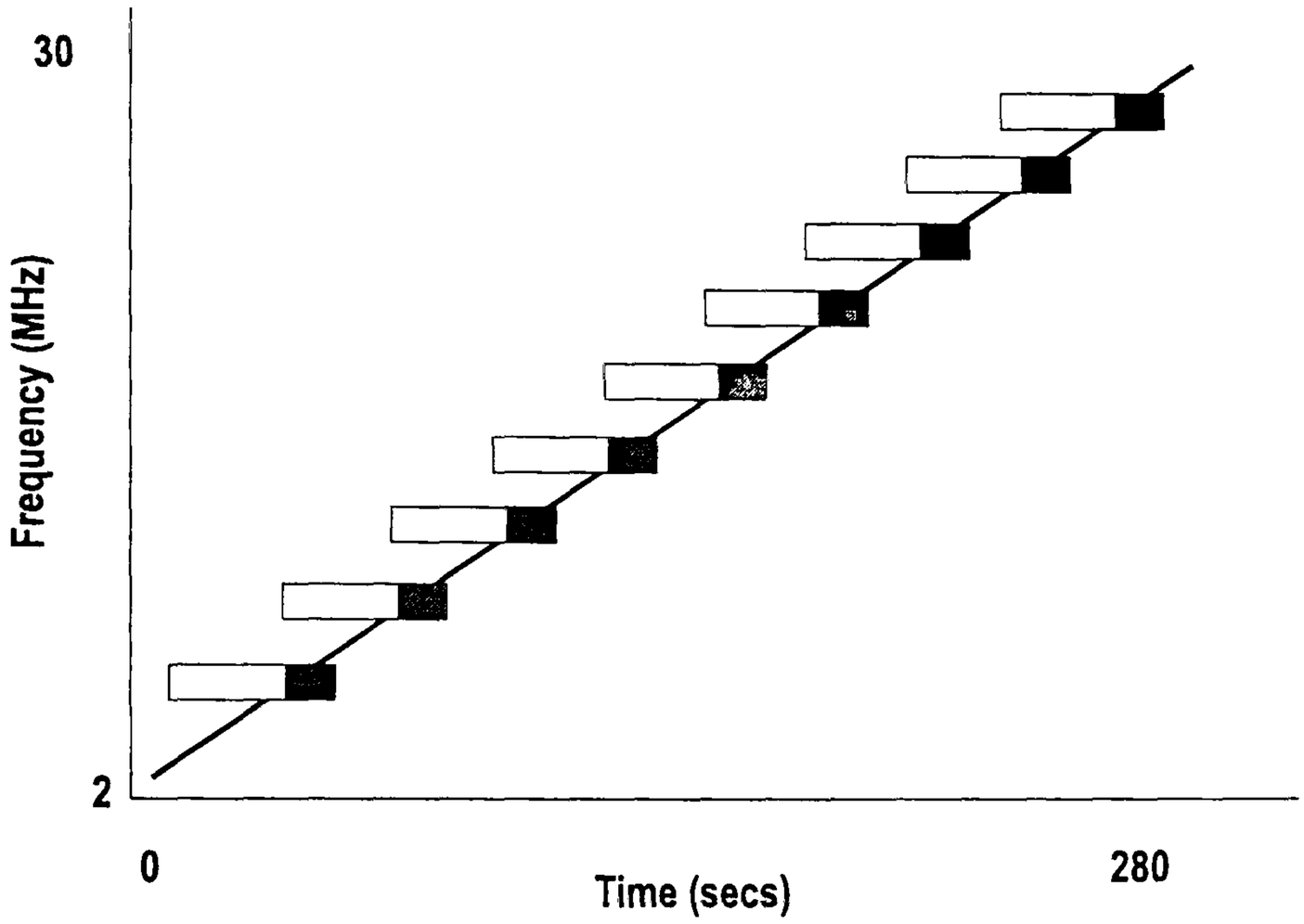

Figure 5.17: Format of the SSFM Signal

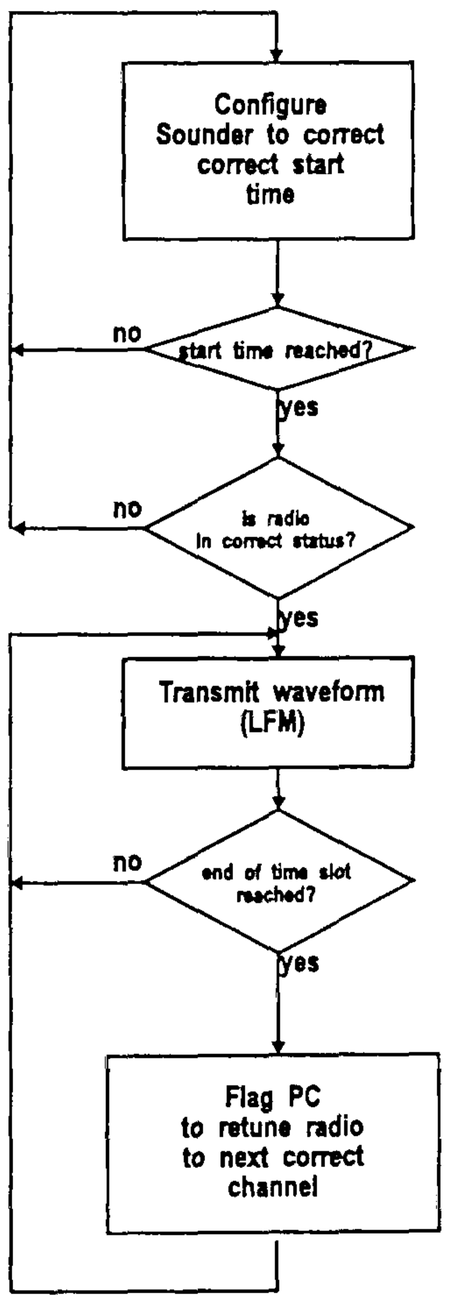

Figure 5.18: Flow-Chart of the operation of the Active Sounder

ionograms. This is a complex process in its own right and, as such, was considered to be outside the scope of the research programme. In such cases, analysis of the ionograms is restricted to identifying if the general ionospheric conditions are enhanced or depressed by comparing ionogram measurements with the off-line predictions for the available paths.

The development of an active sounding system to overcome this limitation was therefore a logical step in the research programme. This sounder employed the same terminal architecture as the DSP-based receiver but used a novel segmented linear FM transmission format. The active sounder is not restricted to the transmission of linear FM pulses but could also transmit any signal profile in order to reduce the effects of, say, Doppler shifts. The channel measurements from active sounding would be incorporated directly into the frequency management channel selection procedures since they represent the actual conditions between terminals of the communication system being supported.

The following chapter describes the next stage in the frequency management process - that of channel optimisation. This process ranks channels into an order of preference for particular modem types; it also rejects channels that have high levels of co-channel interference.

Chapter 6

A Channel Optimisation Subsystem

6.1 Chapter Introduction

The focus of this chapter is a description of the optimisation processes that occur after the first stage of the frequency management procedure has selected a channel. It should be noted, that in this and the previous chapter, the work focuses on one applicable technique; for effective frequency management in future adaptive HF systems, terminal configuration would require several techniques encompassing channel selection and channel optimisation.

In a conventional HF system, optimisation is usually restricted to checking if the channel has low noise/interference; such a simple approach has been improved by using signal processing algorithms to analyse the signals occurring on selected channels and to adjust modem parameters to achieve optimum performance. Specifically, spectral analysis of the basband signals can provide information about the noise/interference structures on the channels. Wanted signal energy is directed to low energy regions of in the observed spectrum as classified by the template correlation algorithm. This allows the channel optimisation algorithm to estimate the performance of a particular demodulation process in response to real channel characteristics, as observed by the system, and identify if a specified modulation format can be accommodated on that channel. Particular attention is focused on the benefits of the template correlation algorithm and analysis of the performance gains that can be achieved when the algorithm is applied to real "on-air" channels. The use of template correlation allows optimal tone placement procedures to be developed, and algorithms suitable for implementation on a DSP device to be defined.

The approach outlined above determines the channel's suitability for operation with any given modem. The channel optimisation process should not cease when a suitable channel has been identified but continue to select alternative usable channels. In this way, optimisation can be extended to provide a generalised channel ranking process. The process of developing a channel ranking scheme based upon correct identification of channel parameters has been extended by utilising measurements from the channel selection procedure. When combined, the measurements can give an approximate estimate of the channel scattering function (Bello, 1963). This scattering function can then be used to estimate the

Advantages	Disadvantages
linear; convert from time to frequency domain; convert from frequency to time domain;	computationally intensive; frequency/time resolution inversely proportional; frequency accuracy dependent on windowing.

Table 6.1: Properties of the Discrete Fourier Transform

performance of all transmission elements (synchronisation, demodulation and decoding). The results of a feasibility study into such estimation techniques and ranking procedures are presented in the concluding part of this chapter. This study identifies relevant theory and presents results and algorithms aimed at allowing an HF system terminal, of the type described in this thesis, to rank channels and adapt to differing channel characteristics.

Relevant results from simulations based on data from an off-air trials are presented in Chapter 7.

6.2 Analysis of In-band Signals

The channel optimisation process relies on accurate characterisation of the signals that occur in a channel. Channel characterisation can be undertaken in the time or frequency domain. Frequency domain analysis, normally requires that time-domain samples are converted to spectra for subsequent processing.

For frequency management purposes, the flexibility inherent in frequency domain processing is important, since spectral estimates can be used a variety of ways, for example estimating the channel transfer function or identifying regions of low co-channel interference. As already described, DSP devices are optimised to convert digital samples to spectral estimates.

6.2.1 Determination of the Channel Spectrum

A description of the analytical background to spectral estimation is presented in Appendix C; this section provides a brief overview of the techniques.

There are a number ways of performing the mathematical transform from the discrete time domain to the frequency domain. The most popular technique is the discrete Fourier transform (Proakis & Manolakis, 1992). The advantages and disadvantages of using this algorithm are shown in Table 6.1.

A filtering process can also be used to provide spectral estimates from time domain samples (Proakis & Manolakis, 1992). Such filters need to be trained to convert with the minimum error but, once the training period is over, they can be more efficient than a com-

parable Fourier transform. Additionally, 'wavelet' transforms offer computationally efficient conversions to the frequency domain (Hlawatsch & Boudreaux-Bartels, 1992).

The disadvantage of using transforms other than the Fourier transform is the complexity of the conversion from frequency domain to time domain, involving the relatively complex mathematical process of deconvolution. This is a computationally intensive process and can be aided by a series of look-up matrices (Rhoads & Elastrom, 1968).

6.2.2 Data Averaging

Data averaging reduces the adverse effects of a time-varying propagation environment (noise, fading and transient interference) on the computed spectrum. The data averaging process averages the spectral plots over a number of estimates and channel observation periods; for example, an average spectrum can be processed from 100 individual spectra taken over a period of several seconds. The process of data averaging reduces the statistical variability of the digitised spectral estimate.

In the frequency domain, transient interference, for example a lightning strike, manifests itself as broad-band noise which can be at a substantially higher level than the normal signals on that channel. The burst noise, observed as a broad spectrum of input energy, would give rise to an inaccurate spectral estimate in the absence of averaging.

Apart from burst noise, data averaging can be used to correct for channel fading effects. These can be both frequency-selective fading (FSF) and flat fading (Brookner, 1969). The number of spectral estimates needed to effectively measure the frequency selective fading within a channel depends on the multipath modal structure and stability. With propagation conditions involving multiple propagation paths separated by several milliseconds delay spread, data averaging over a periods of 0.5s will allow determination of the nature of the frequency selective fading. FSF will cause nulls to appear in the received spectrum of a modem. The number of samples needed to counter the effects of flat fading is a function of the fade rate and the depth of fading; for example, the effects of rapid fading will be diminished by the use of averages over several fade intervals.

The algorithms employed to compute the spectral components of the in-band signals need to be sophisticated and flexible to counter the instantaneous effects of a wide-range of channel conditions. The obvious method of sampling a few seconds of 'off-air' data and then splitting it into small segments for spectral estimation may not be directly suitable, since the spectral measurement needs to be dynamic in order to cope with situations where it is possible to estimate signal components, and to reject situations when fading causes the measured signals to be in a region where results would be unreliable. The spectral conversion takes only a fraction of the time needed to gather the required time domain samples; for example a typical DSP processor can carry out a 1024-point FFT in $\approx$2 ms, whereas when sampling at 8 kHz it will take 125ms to gather the necessary input data. Therefore, it is logical to perform the data gathering tasks at the same time as converting the data into its spectral components.

The implementation of the spectral analysis procedures used in this research programme gathers and processes data statistics serially; thus an average of 100 FFTs takes 12500ms, or 12.5s. This serial processing means that channels exhibiting fades rates in the range 2.0

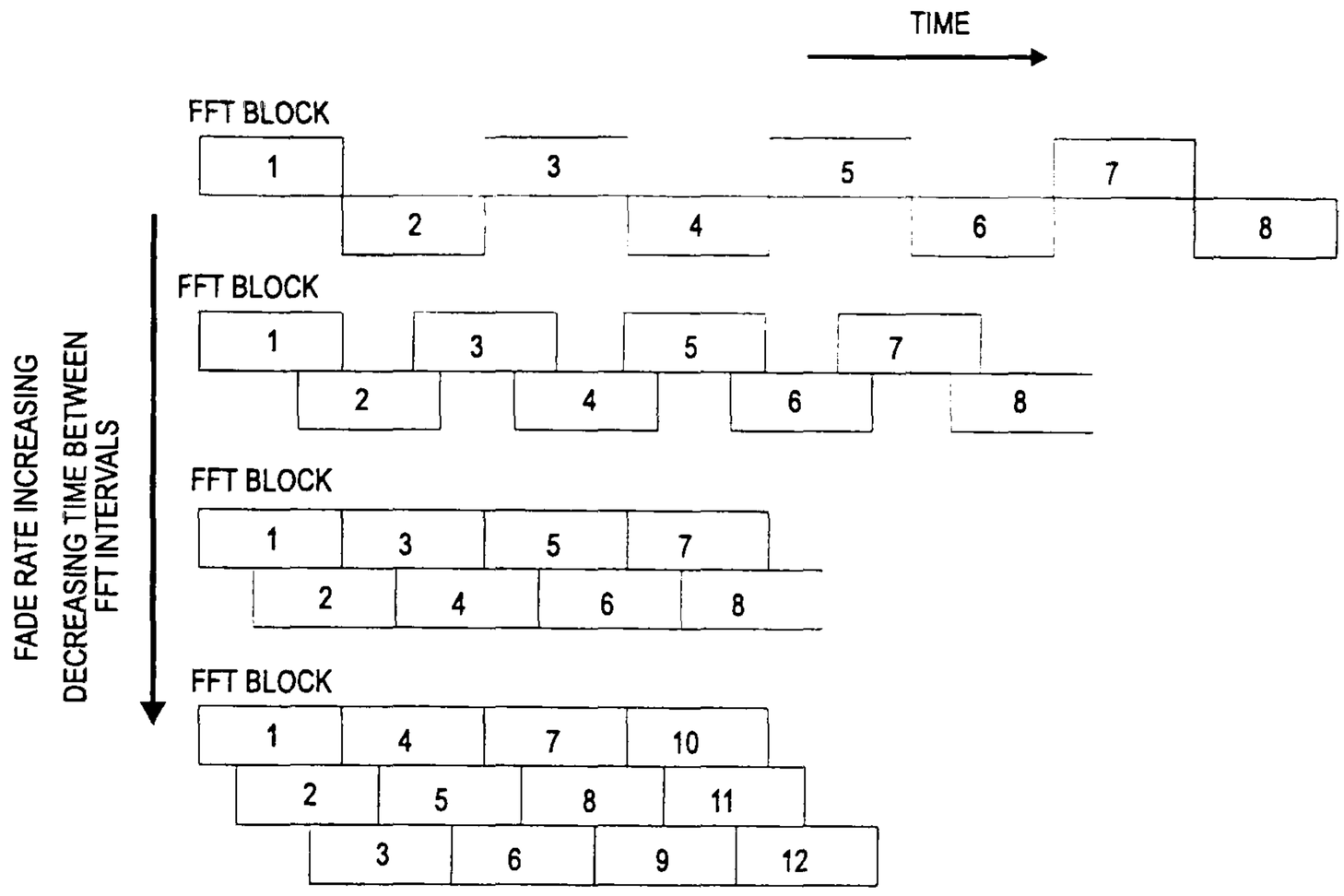

Figure 6.1: A Schematic of Adaptive Overlapping Spectral Estimates

- 0.2 Hz, can be described accurately. In the current system, the fade rate is not tracked; consequently the 100 FFT is less efficient than if overlapping windows were to be used. In this latter scheme, the FFT processing is envisaged as a 'concertina'. When there is little or no fading, then the overlap will be considerable; when long intervals between fades occur, the overlap would be reduced and the sampling period increased. In the limit, this would allow the sampling windows to be non-contiguous. This process offers advantages over a non-adaptive sampling method, but the spacing between frames would have to be characterised more precisely and related to fade rates in a more rigorous manner than that presented here. A schematic of the 'concertina' spectral sampling is shown in Figure 6.1.

6.3 The Template Correlation Algorithm

Template correlation is a frequency domain algorithm for optimising use of the in-band spectrum in terms of optimal placing of wanted signal energy to avoid co-channel interference, i.e. signal energy is steered towards regions of low interfering signal energy. This algorithm is based upon the "water-filling" concept (Goldman, 1953). Information theory shows that the maximum channel capacity is achieved when the sum of the wanted signal energy and unwanted noise components is constant wherever possible in the channel. This process is completely independent of frequency and provides a method for achieving maximum utilisation efficiency of the available spectrum. A summary of the theory is given in Appendix E.

6.3.1 Implementation of the Template Correlation Algorithm

Implementation of the algorithm was achieved using a single DSP device using the algorithm detailed below; it can be seen that the stages involved, using an example of M-ary orthogonal

FSK transmission format, are:

(i) sample the channel to be measured;

(ii) employ a Fourier transformation technique, for example an FFT, to convert the sampled data into a spectral estimate, thus providing the background noise/-interference profile;

(iii) correlate with the wanted signal spectral template with the background noise profile; the output of this process is called a frequency domain cross-correlation function (FDCCF);

(iv) identify the minima in the FDCCF and use this information to place the wanted signal template in the optimum position, i.e. at the frequency corresponding to the lowest FDCCF value.

For effective placement to be made, an averaged noise/interference profile is essential. As indicated previously, the number of spectral plots needed to form the set for averaging is based upon the variance of the channel in terms of the fade rate and characteristics of the co-channel interference present in the channel.

In mathematical terms, the template correlation algorithm is described by the following equation:

$$\Phi(f) = \int_B N(u)S(u+f)du \tag{6.1}$$

where

B = bandwidth (Hz);
u = dummy variable for frequency (Hz);
f = frequency offset;
$\Phi(f)$ = the FDCCF;
$N(u)$ = the noise spectral profile;
$S(u)$ = the spectral profile of the wanted signal energy, or template.

The wanted signal energy is placed where the noise term, $N(u)$, and signal template, $S(u)$, have maximum dissimilarity.

6.3.2 Extension to the Template Correlation Algorithm

In the initial algorithm, it was assumed that a full template of the signalling set would be used. This would then generate an FDCCF that would be centered on the optimum placement point for the whole raster. This procedure was based upon the use of statistical smoothing of the spectral data.

Considering the spectral estimate shown in Figure 6.2: the available area in the noise spectrum can just accommodate the whole of the wanted transmission raster (in this case a

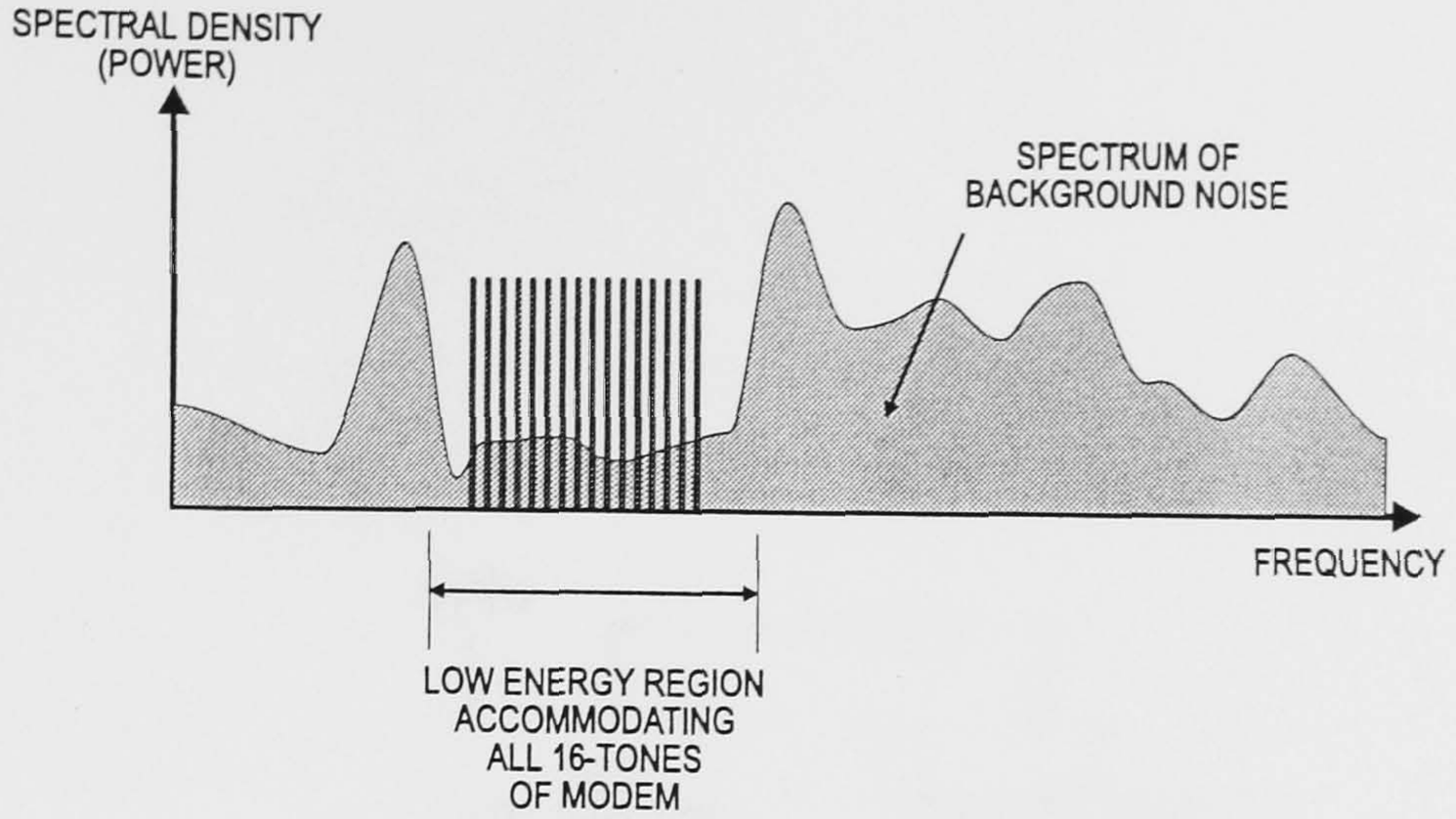

Figure 6.2: Spectral Estimate with Large region of Low Energy

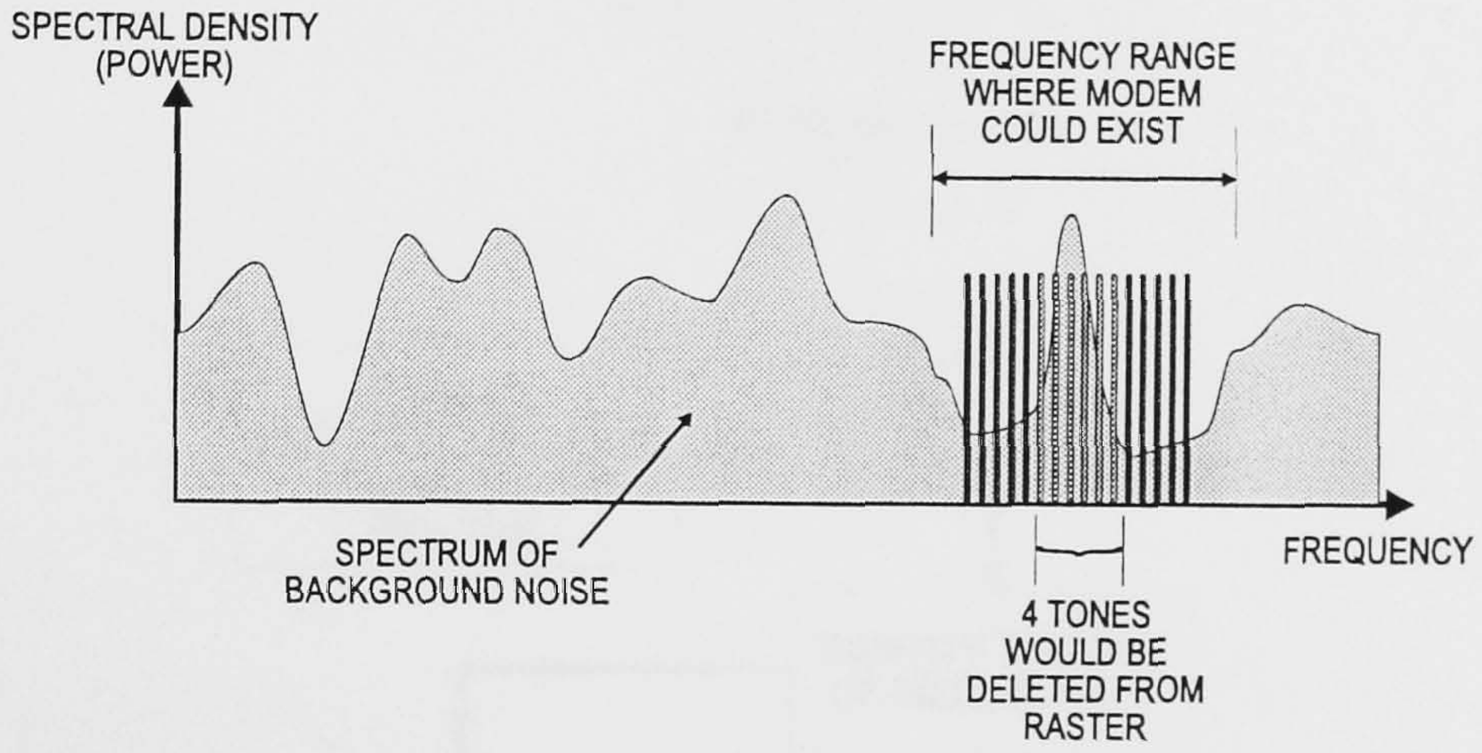

Figure 6.3: Spectral Estimate With 16-Tone Modem Overlaid
in narrow region of low energy

16-tone parallel tone modem). The second example is more complicated. In this case, Figure 6.3, the whole of the raster cannot fit within a low noise region since there are a series of interferers that stretch across the band. In this case, the traditional template correlation algorithm would reject the channel as being unsuitable. However, the 16-tone parallel modem could fit with the loss of four tones (Figure 6.3). Alternatively the raster could be split and put into a number of low energy regions. Modem optimisation is discussed in the following section. In second example, the tone placement procedure requires an extension of the template correlation algorithm based on elements of the raster rather than the whole raster. This simple extension is based upon the fact that the probability of finding a spectral gap that can accommodate the whole spectrum is less than the probability of finding a number of gaps that can independently house sub-groups of the tone elements that comprise a raster.

The extension is based upon a simple statistical relationship which was not calculated in the original algorithm.

$$\prod_{n=1}^{M} p_{spec}(n) > p_{spec}(R) \tag{6.2}$$

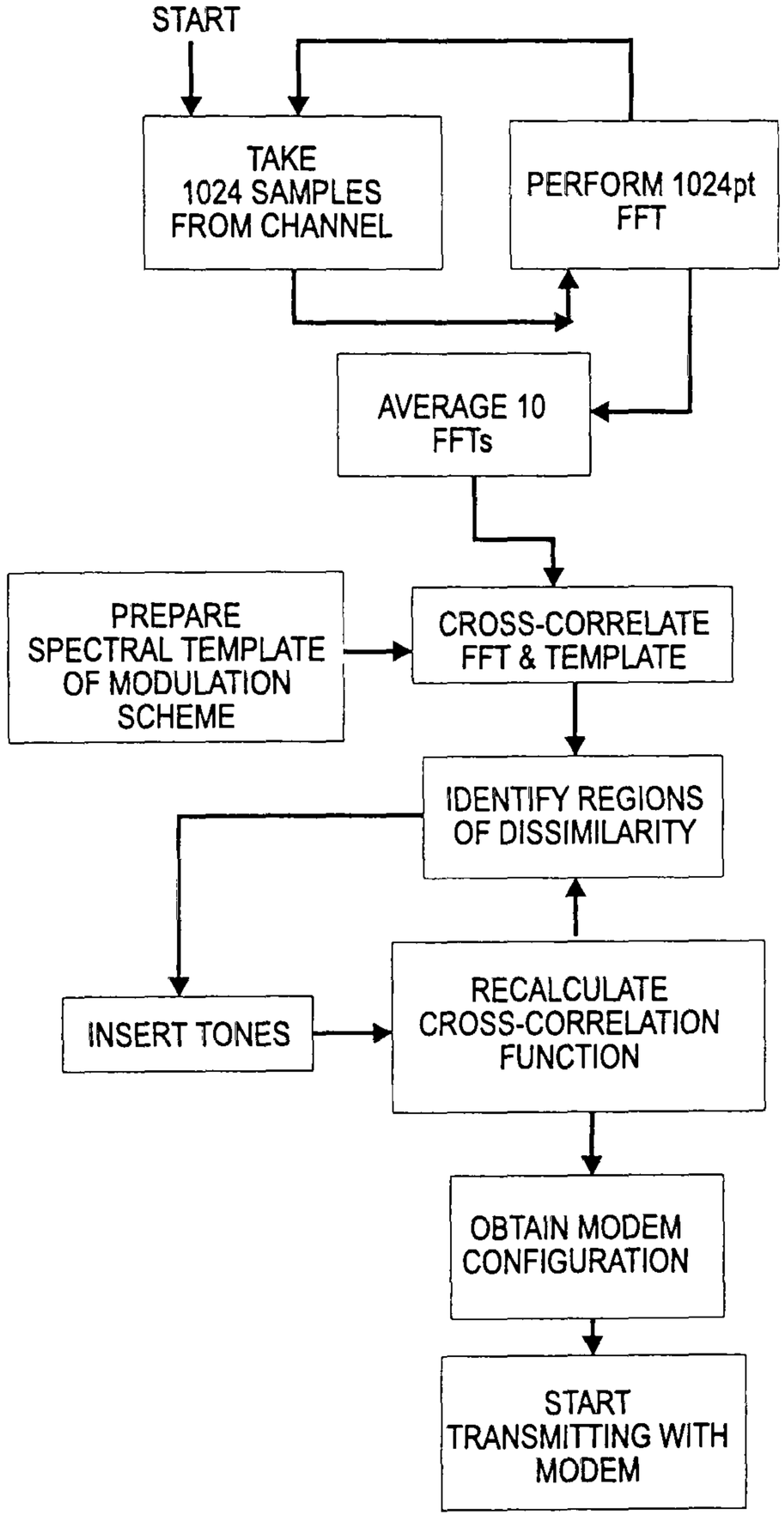

Figure 6.4: Flow Chart Describing Operation of Template Correlation Algorithm

where

n = spectral gap index;
M = number of tones;
$p_{spec}()$ = probability of finding a spectral gap;
$p_{spec}(n)$ = probability of finding a spectral gap for n^{th} raster element;
$p_{spec}(R)$ = probability of finding a spectral gap for complete raster.

Both equations (6.1) and (6.2) have been validated both by simulation (Jowett & Darnell, 1987) and experimentation (Gallagher & Darnell, 1990). If equation (6.2) is used, the BER reduces as the overall average SNR reduces, thus agreeing with observed results presented in Chapter 7.

6.3.3 Relationship between SNR and the FDCCF

The relationship between the received SNR and the output from the FDCCF is complex. The FDCCF produces an output between 0 and 1, indicating respectively low and high correlation. The FDCCF is effectively an averaged sum of the background spectral energy under the template which is then compared with the template's average energy. This means that factors determining SNR are related to the accuracy of the template. If the template is an accurate representation of the received signal, then the correlation factor is directly related to the SNR (Schwartz, 1981).

The received SNR is therefore given by:

$$\text{SNR} = -10\log_{10}(\text{FDCCF})\ \text{dB} \tag{6.3}$$

The 'minus' in equation (6.3) yields positive SNR values when the FDCCF produces an output that is less than 1. The level of the wanted signal is related to the noise template by assuming that, in the worst case, such a signal will take the same value as the smallest noise peak. This would allow the system to operate with a small SNR with respect to the background noise.

6.3.4 Prediction of BER

The bit error probability when using a non-coherent FSK (frequency shift keyed) signal is related to SNR by (Stremler, 1992):

$$P_e = \frac{1}{2}e^{-\frac{\gamma}{2}} \tag{6.4}$$

where

P_e = Probability of error;
γ = Signal-to-Noise Ratio.

Using this equation and equation (6.3), it can be seen that a direct prediction of probability of error can be deduced from the FDCCF. Therefore, a plot of predicted BER versus baseband frequency is possible (Massaro, 1975) by assessing the signal-to-noise/interference ratio across the channel bandwidth. This is shown in Figure 6.10, as part of the 'figure of merit' simulation results.

The provision of a statistical metric estimating the BER from a spectral plot for a given channel encoding scheme is one of major benefits of the template correlation algorithm. It is equivalent to the scattering function in that it allows the estimate of the effects of background noise/interference to be related to fading, frequency spread and multipath dispersion. Correct identification and utilisation of the channel scattering function is the fundamental premise of the 'figure-of-merit' concept discussed in section 6.5.

6.4 Tone Placement Algorithms

Once a baseband spectral estimate or FDCCF is available, a set of tone placement algorithms can be applied to the data. As indicated previously, the most obvious method is to place the signal energy in any regions of low noise/interference. This process may produce a sub-optimal modulation format since the modulation components may not be fully orthogonal. Furthermore, it is important that such regions nulls are reasonably static and the averaging scheme should be adjusted to reduce the effects of transient interferers and fading.

The tone placement algorithms can be categorised according to the required modulation formats. The following specific algorithms, relate to an MFSK (Ralphs, 1985; Bayley & Ralphs, 1972) signal format.

1. First algorithm for use with a fixed tone raster modem: In this case, the lowest noise/interference region is identified and an initial tone placed in this position. The subsequent tones are added one at a time until the SNR deteriorates to a point where a system performance criterion is no longer met. If the raster encompasses a region of interference, the tones within that region are eliminated. It is evident that this method may not offer advantages in all cases.

2. Second algorithm for use with a fixed tone raster modem: instead of using the template correlation algorithm to suggest tone placements and deletions, the averaged noise background is used to provide a method of specifying a non-uniform probability density function for the whole raster. This has the effect of weighting out the tones that would be subject to high levels of noise/interference. The weighting functions would be used by a channel encoding scheme to map the ideal input data stream to the measured spectrum. In this way, the channel coding scheme is controlled by channel conditions. This alternative approach could be undertaken by a frequency management controller.

3. A third algorithm suitable for an adaptive modem: an adaptive modem could easily use the previously described tone placement algorithms, but this would under-utilise its inherent flexibility. Optimal tone placement is undertaken by placing the tones individually anywhere within the channel. The tones must be

placed orthogonally, but need not be grouped to form a distinct raster. Furthermore, the order of placement could be used as an additional source of information to a soft-decision decoder, thus adding an SNR metric to the decoding algorithms.

4. A fourth algorithm offering greater adaptivity for an adaptive modem. the previous procedure is an extension of the waterfilling algorithm, whereas this algorithm requires further analysis of the channel spectrum. Regions of high predicted SNR would indicate a potential for utilising the available SNR more effectively. This could involve phase-encoding symbols and/or increasing the symbol rate, thus, matching the channel encoding scheme to the available SNR, as well as optimally distributing energy within the spectrum.

From the above description, it can be seen that the template correlation algorithm has application to both current fixed raster systems and future adaptive modems.

6.5 'Figure-of-Merit' Concept

The concept of the 'figure-of-merit' (FOM) is to enable choice of an optimum channel from a range of channels where a set of suitable (channel metric) information is available. In addition, it is assumed that a specified modulation scheme will be utilised for data transmission and this will be incorporated into the database for the FOM algorithm. This analysis complements and is developed from the preceding investigations into the basic error probability for different channel states, particularly those for (M-ary) FSK-type systems (Brookner, 1969; Salz, 1970). This research is presented as a feasibility study into the area of optimum channel selection when channel knowledge can be obtained from measurements. The following discussion initially concentrates on building a generalised channel transmission model for a continuous system prior to the synthesis of a similar model for a discrete system where digital signal processing techniques would be applicable. The discrete model is complex and the section concludes with an approximation to the final system

6.5.1 The Generalised Transmission Model

Before attempting to derive an equation that characterises the individual effects of the different elements within a channel model, it is important to examine relevant background information.

Deterministic, mathematical models for communication over dispersive media (random, linear channels) have been presented in key texts (Bello, 1963; Jourdain & Tziritas, 1984). In this case, the channels are assumed bandpass with centre frequency, ν_0 . In the following model, the deterministic signal $f(t)$, with symbol energy, E_s, and duration, T_s, is transmitted over the channel. The model is:

$$\tilde{s}(t) = \int_B \tilde{f}(t-\xi)\tilde{H}(t,\xi)d\xi \tag{6.5}$$

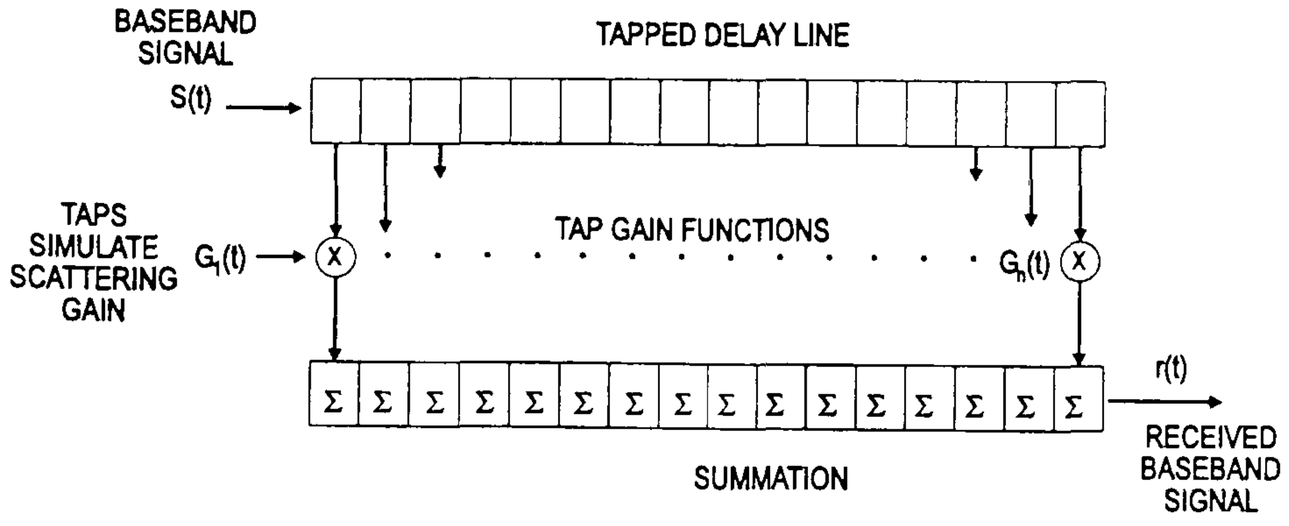

Figure 6.5: Channel Model using Tap Delays and Scattering Gain

where

$$\begin{aligned} \tilde{s}(t) &= \text{the complex output signal,} \\ \tilde{f}(t) &= \text{the complex input signal,} \\ \tilde{H}(t,\xi) &= \text{the complex channel response,} \\ B &= \text{the bandwidth of the channel,} \\ \xi &= \text{the time delay between scatter positions.} \end{aligned}$$

In addition, if

$$f(t) = \sqrt{2}\ \mathrm{Re}\left\{\tilde{f}(t)e^{j2\pi\nu_0 t}\right\} \tag{6.6}$$

$$s(t) = \sqrt{2}\ \mathrm{Re}\left\{\tilde{s}(t)e^{j2\pi\nu_0 t}\right\} \tag{6.7}$$

then the energy can be calculated according to

$$E_s = \int_0^{T_s} |f(t)|^2\, dt = \int_0^{T_s} \left|\tilde{f}(t)\right|^2 dt \tag{6.8}$$

It is assumed that $\tilde{H}(t,\xi)$ is a zero mean random function that produces delay in the range $(\xi, \xi + d\xi)$ and that the covariance function, Γ_H, is stationary with respect to 't' and uncorrelated with respect to 'ξ'. The function describes a complex modulation effect caused by multiple scatterers. This can be modelled by a discrete set of densely tapped delay lines where the input signal is initially delayed and then multiplied by a differential scattering gain; this is shown in Figure 6.5. In this diagram the 'H' values describing the continuous channel are replaced by 'G' values which represent the channel in the discrete time (sampled) domain. This has been termed the "wide sense stationary uncorrelated scattering" (WSSUS) channel model (Bello, 1963). The effect of the scattering gain and its relationship with the covariance function, Γ_H, is described by

$$E_H\left\{\tilde{H}(t,\xi)\tilde{H}_*(t',\xi')\right\} = \Gamma_H(t-t',\xi)\delta(\xi-\xi') \tag{6.9}$$

The above equation can be verified in practical cases (Watterson *et al.*, 1970) but is usually characterised statistically by its scattering function, $\tilde{S}(\nu,\xi)$, which is the Fourier transform

of Γ_H with respect to $t - t'$, i.e.

$$\tilde{S}(\nu, \xi) \overset{t-t'}{\underset{\nu}{\rightleftharpoons}} \Gamma_H(t - t', \xi) \tag{6.10}$$

Using this relationship, the covariance of the complex received signal, $\tilde{\Gamma}_s$, can also be shown to be (Bello, 1963):

$$\tilde{\Gamma}_s = \int\int \tilde{f}(t - \xi)\tilde{f}^*(u - \xi)\tilde{S}(\nu, \xi)e^{j2\pi\nu(t-u)}d\nu\, d\xi \tag{6.11}$$

The above analysis can be extended to show that the instantaneous power depends on the transmitted power and the scattering function

$$E\left\{|\tilde{s}(t)|^2\right\} \triangleq \tilde{\Gamma}_{\tilde{s}}(t, t) = \int\int \tilde{S}(\nu, \xi)\left|\tilde{f}(t - \xi)\right|^2 d\nu\, d\xi \tag{6.12}$$

Equation 6.12 illustrates the effect of transmitted power dispersion within the channel. The instantaneous complex scattering function, $\hat{S}(\nu, \xi)$, when both Doppler spread and multipath conditions exist, is therefore defined as

$$\hat{S}(\nu, \xi) = \sum_{i=1}^{N} \hat{S}_{di}(\nu)\delta\xi - \xi_i \tag{6.13}$$

As an example, when two scattering paths exist, delayed by time L, and each having a frequency spread, ν, then the scattering function is described by

$$\hat{S}(\nu, \xi) = \hat{S}_1(\nu)\delta(\xi) + \hat{S}_2\delta(\xi - L) \tag{6.14}$$

This example is illustrated in Figure 6.6. The transmission model is shown in Figure 6.7. As can be seen, the output is subject to additive noise, $\tilde{n}(t)$. The noise is usually assumed to be Gaussian with a power spectral density of N_0. The final channel model is therefore

$$\tilde{r}(t) = \tilde{s}(t) + \tilde{n}(t) \tag{6.15}$$

6.5.2 Algorithms Suitable for Digital Processing

The previous discussion has shown that the output from the channel is complex. The information contained in the algorithm is non-specific. Therefore, in order to use the algorithm for HF links using a terminal of the type described in this thesis, the elements of the algorithm need to be translated into a representation compatible with DSP implementation.

From equations (6.13) and (6.15) that the following transform can be constructed:

$$v'_K(t) = \sum_{n=1}^{N} G_n(\omega_n, t)\delta(t - \tau_n)u'(t) + N_o(t) \tag{6.16}$$

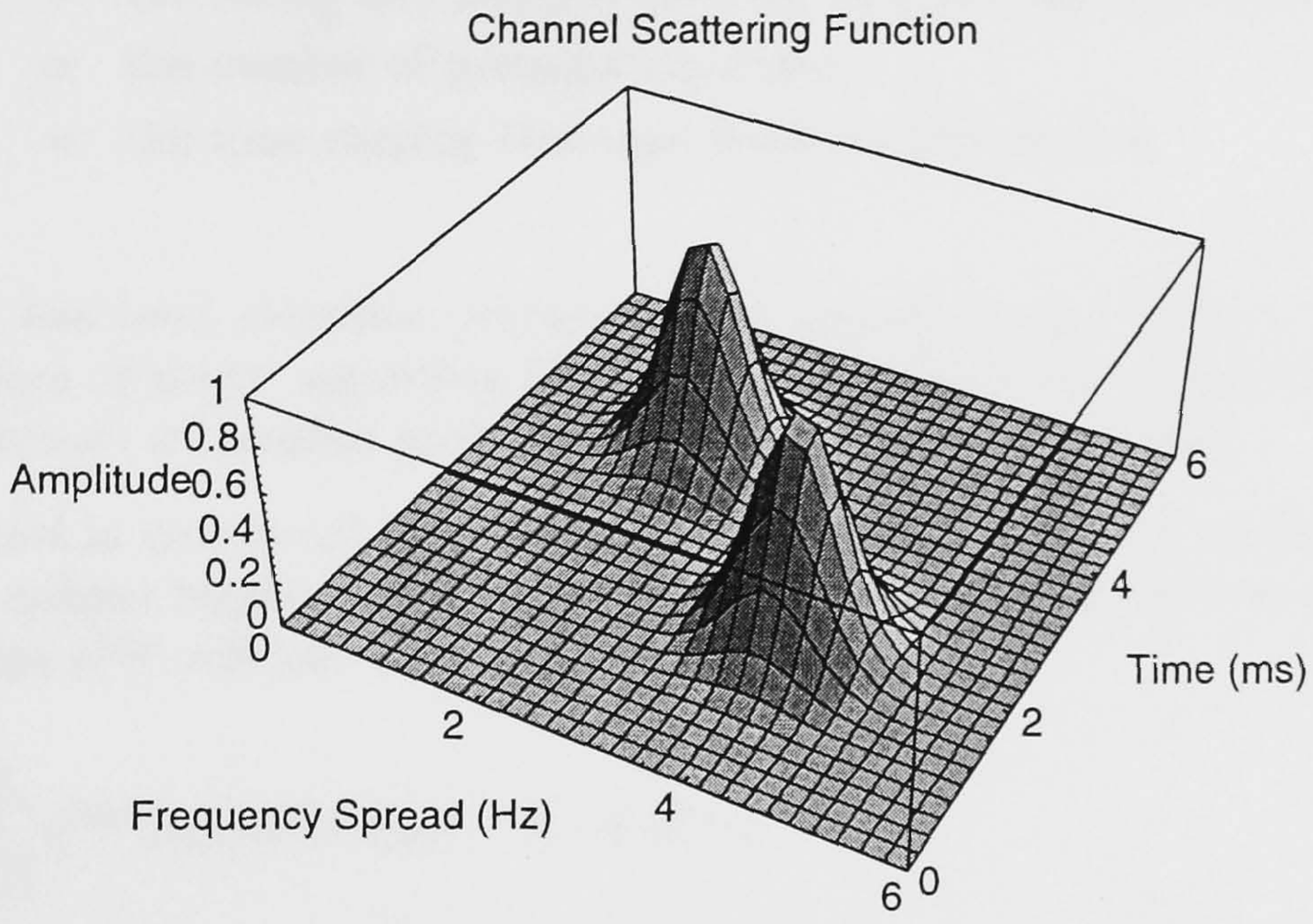

Figure 6.6: Plot of Channel Scattering Function

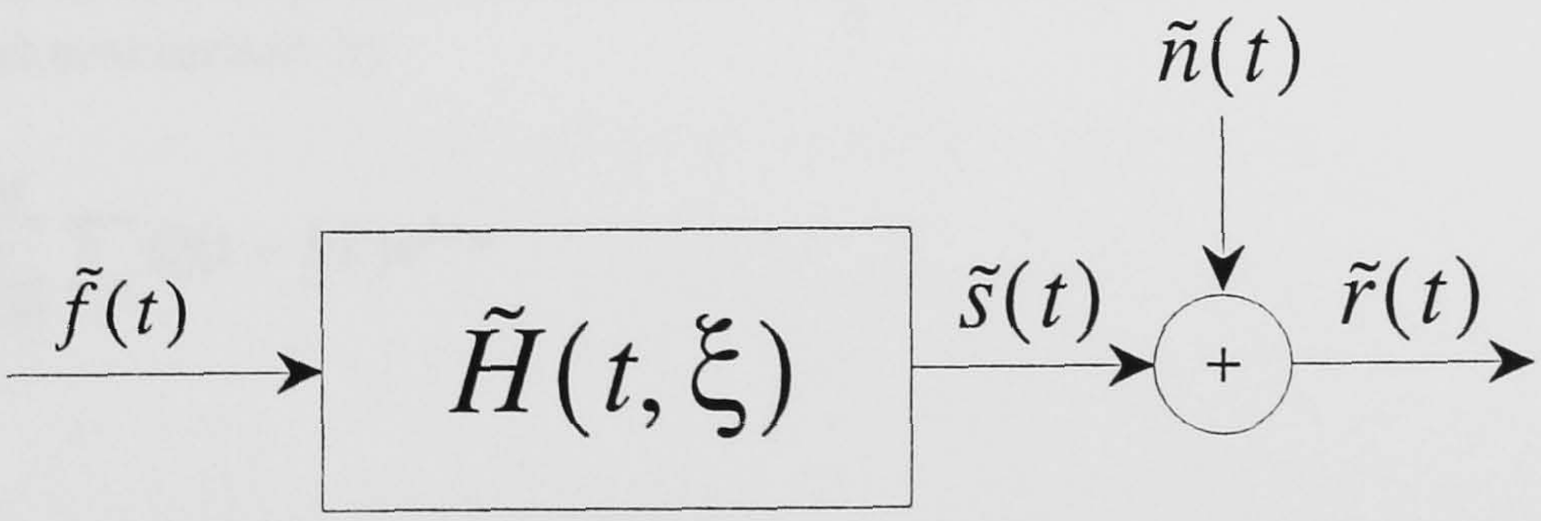

Figure 6.7: Channel Transmission Model

where

$v'_K(t)$ = the generalised, sampled output from the channel when subject to:
$u'(t)$ = a general modulation scheme,
$G_n(\omega_n, t)$ = the fading and Doppler shift on each propagating mode,
N = the number of propagating modes,
$N_o(t)$ = the time varying Gaussian Noise on the channel.

This transform has been identified previously and applied to the WSSUS channel (Bello, 1963). The 'figure of merit' algorithm builds upon the use of this channel, but uses other methods to construct a bounded probability that can be directly ranked.

If the HF channel is considered as a time-variant, dispersive channel subject to Gaussian noise, then the output response $v_k(t)$ from the k^{th} channel when subject to a single tone of complex envelope $e^{j\omega_k t}$ will be:

$$v_k(t) = \sum_{n=1}^{N} e^{j\omega_k t} A(n) G(\omega, t) \delta(t - \tau_n) + N_o(t) \tag{6.17}$$

where

ω_k = frequency of the tone,
τ_n = the time delay of the n^{th} received mode,
$G(\omega, t)$ = the complex doppler and fading response of the channel,
$A(n)$ = the attenuation of the mode,
N = the maximum number of dispersive modes received,
$N_o(t)$ = additive Gaussian white noise.

To simplify the equation combining the $A(n)$ and $G(\omega, t)$ into a composite term $G_n(\omega, t)$ allows each of the modal responses to be characterised individually. For an MFSK modulation scheme, $u(t)$, characterised by

$$u(t) = \sum_{m=1}^{M} \sum_{k} Q(t - kT) e^{j\omega_m} \tag{6.18}$$

where

M = number of tones in the FSK signal raster,
T = the duration of a symbol,
$1/T$ = the signalling rate, or baud rate,
$Q(t)$ = a rectangular pulse of duration T and height $1/T$.

Using equation 6.18 substituted into equation 6.17, the output from the channel is given by

$$v(t) = \sum_{n=1}^{N} \sum_{m=1}^{M} \sum_{k} Q(t - kT) e^{j\omega_m t} G_n(\omega_n, t) \delta(t - \tau_n) + N_o(t) \tag{6.19}$$

In principle, it is possible to estimate the probability of error caused by the channel after convolving the scatter function (which describes the channel) with the chosen modulation scheme. Practically, this may be infeasible since the modulation scheme would have to be mapped to the same Cartesian system as the scatter function.

Alternatively, the scattering function can be estimated by combination of FFT analysis and channel impulse response determination, providing data on the Doppler spread and number of multipath modes (Bello, 1965). The FFT analysis also provides the average noise/interference background on the channel. The measurements are then assimilated into a simulation of the complete system where the channel model is provided by real data. A large number of symbols are transmitted over the simulated system and the overall error performance calculated. The channels are ranked according to estimated BER performance. This method is computationally intensive and any time advantages gained by using current DSP technology would be offset by the complexity of implementation. However, with the advent of higher speed computation, greater than 1000 MFLOPS, a full implementation of the estimation technique becomes feasible. In this case, estimation errors would be determined by the accuracy of the channel measurements and the implementation efficiency.

6.5.3 Empirical Estimation Based Upon Probabilistic Approach

The previous algorithm (equation 6.19) requires significant computational power to estimate the effects of the channel upon the modulated signal. Estimation of the BER would require accurate channel measurements for correct simulation. For a large number of different channels and a flexible, adaptive modem, the time taken to estimate BER would be very large. However, with knowledge of the channel conditions, it is possible to estimate the received BER by applying available theory to the actual channel measurements. The resultant would possess inaccuracies, but with a large number of BER estimations would tend to converge towards the true BER. This method has a computational advantage since calculations could be based on a combination of simple algorithms and look-up tables.

6.5.4 Estimation of Performance in Fading Conditions

In this feasibility study, the modulation scheme is restricted to MFSK as theory exists for estimating performance of orthogonal MFSK (Crepeau, 1992) on a Nakagami-m channel (Nakagami, 1960). The Nakagami-m channel has been chosen because it is a generalisation of the overall fading conditions found in normal radio communication systems. The m variable can be used to force the p.d.f to possess Gaussian, Rayleigh and non-fading statistics and, as such, encompass most of the fading effects observed on an HF link. The received MFSK signal in the interval $(0, T)$ has the form

$$r(t) = R\sqrt{2\frac{E_s}{T}}\cos(\omega_i t + \theta) + n(t) \tag{6.20}$$

where

$$\begin{aligned} E_s &= \text{average received signal energy,} \\ n(t) &= \text{AGWN,} \\ \omega_i &= \text{one of } M \text{ orthogonally spaced frequencies,} \\ R &= \text{Nakagami-m random variable.} \end{aligned}$$

The Nakagami-m random variable has a p.d.f. described by (Nakagami, 1960)

$$p(R) = \frac{2m^m R^{2m-1}}{\Gamma(m)\Omega^m} e^{-\left(\frac{m}{\Omega}R^2\right)}, \qquad R \geq 0 \tag{6.21}$$

where

$$\Omega = \overline{R^2} \tag{6.22}$$

and

$$m = \frac{\Omega}{\text{var}\,(R^2)} \geq \frac{1}{2} \tag{6.23}$$

When $m \to \infty$ the channel has no fading; this is because the p.d.f. has an impulse format. For $m = 1$, the channel possesses Rayleigh fading, and for $m = 1/2$ a one-sided Gaussian fading distribution results. Using the normalisation convention, or $\Omega = 1$, the average received energy in a fading channel is $R^2 E_s$ with an average value of $\overline{R^2} E_s$ or $\Omega E_s = E_s$. This reduces the computational complexity.

The probability of symbol error for an MFSK system in a Nakagami-m channel is (Crepeau, 1992)

$$P_s = \int_0^\infty \sum_{i=1}^{M-1} \binom{M-1}{i} \frac{-1^{(i+1)}}{i+1} e^{\frac{-i}{i+1}\frac{E_s R^2}{N_o}} p(R)dR \tag{6.24}$$

This generalises to a bit error probability of

$$P_b = \frac{M}{2(M-1)} \sum_{i=1}^{M-1} \binom{M-1}{i} \frac{(-1)^{i+1}}{i+1} \left[\frac{m}{m + \frac{i}{i+1}(\log_2 M)\frac{E_s}{N_o}}\right]^m \tag{6.25}$$

when

$$P_b = \frac{M}{2(M-1)} P_s \tag{6.26}$$

$$E_b = \frac{E_s}{\log_2 M} \tag{6.27}$$

Plots of two conditions, when $m \to \infty$ and $m = 1$, are shown in Figure 6.8 and Figure 6.9 respectively. Assuming that the fading on the channel is Rayleigh in the short term, and log-normal in the long term, Figure 6.9 can be used to estimate the probability of uncoded error performance at any time for the MFSK transmission. If no fading is exhibited on the channel, the probability of error can be derived from Figure 6.8. For the purposes of the "figure of merit" algorithm, it is proposed that the curves are stored as look-up tables.

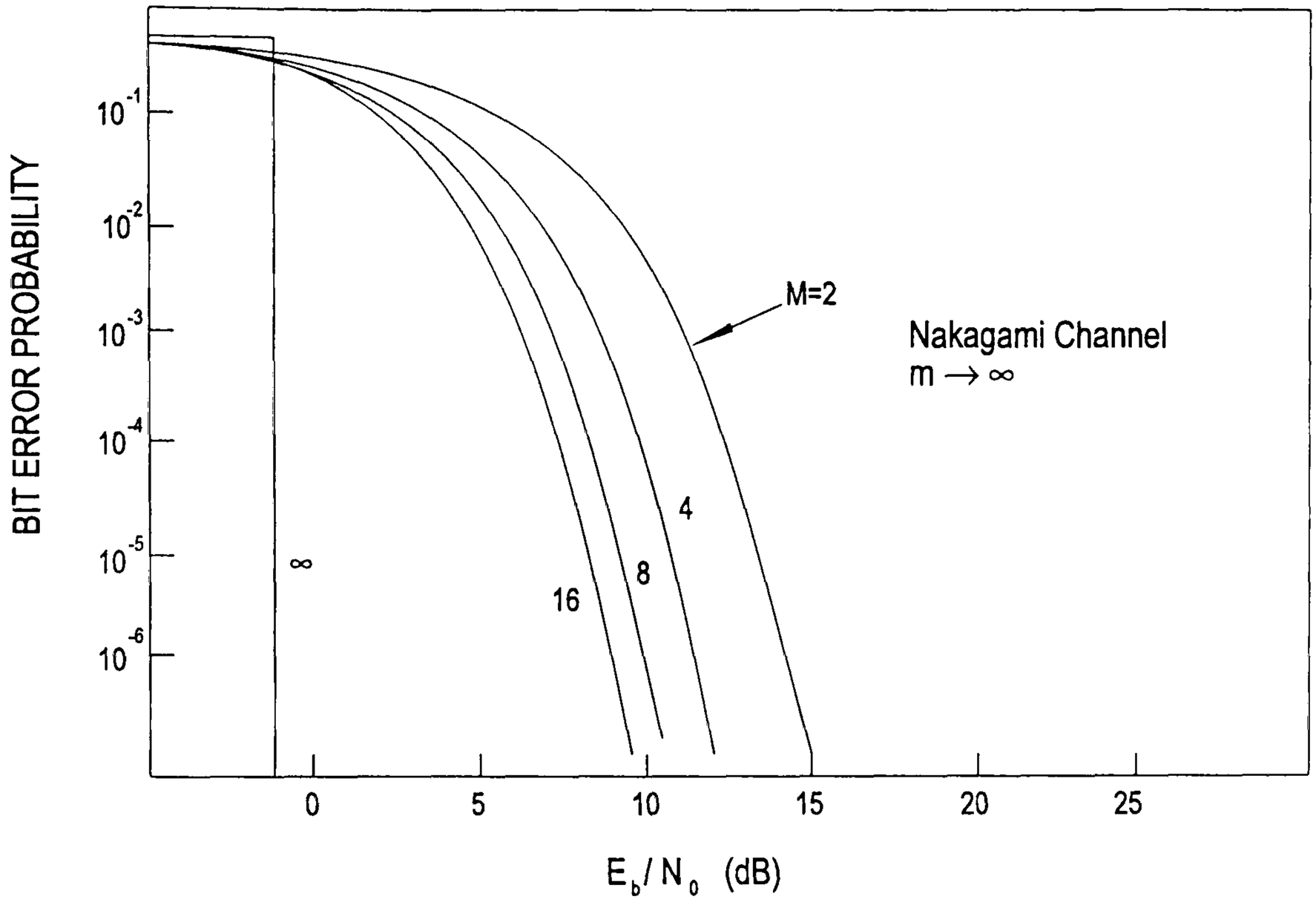

Figure 6.8: Error Plot with for MFSK m $\rightarrow \infty$,
i.e. No Fading

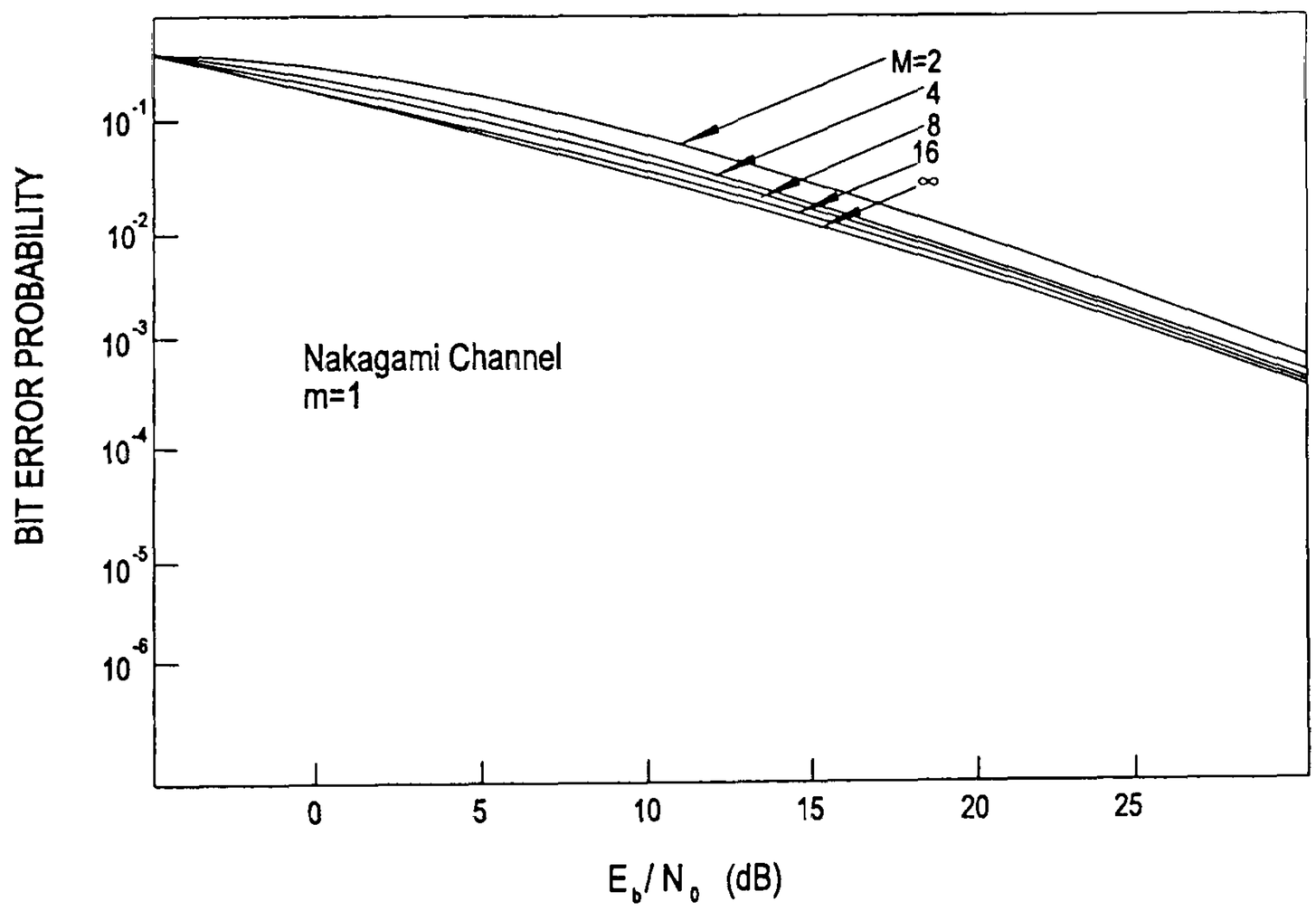

Figure 6.9: Error Plot with m = 1
i.e. Rayleigh Fading

6.5.5 Estimation for a Non-Gaussian Channel with Memory

The limitations on the probabilistic estimate characterised by equation (6.24) are due to the accuracy of measurement of E_b/N_0 and its dependence on Gaussian noise conditions. The template correlation algorithm provides a means of estimating the noise in a specified bandwidth. Consequently, by using equations (6.3) and (6.4), the instantaneous in-band frequency-dependent SNR can be estimated. By considering the effects of the noise on each tone individually, the combined error performance of the raster can be estimated in non-Gaussian conditions; consequently by combining this estimate with equation (6.24), the estimation of overall modem performance in non-Gaussian fading conditions (Trees, 1971) is possible. This forms a key term in the final "figure of merit" algorithm

This algorithm does not take into account the effects of the different multipath modes on the system. These cause inter-symbol interference on the signal. However, as long as the keying interval, T_s , is greater than the multipath time spread exhibited on the channel, the probability of error is relatively unaffected (Soliman & Scholtz, 1988)

This is important for simple data modems (Kennedy, 1969); for serial type modems where the data is subject to ISI and then equalised, then the estimation of the multipath is particularly important. The frequency stability of the modes is also neglected; for MFSK systems, the Doppler shift on the channel for each individual mode is important in estimating the frequency stability in each of the tone intervals. It has been shown that the Doppler instability can cause the greatest effect when the symbol energy is offset in frequency by half of the orthogonality constraint distance (Speight, 1991). This can be corrected in a software modem within a symbol interval and hence the Doppler distortion can be reduced considerably (Darnell *et al.*, 1992).

6.5.6 Figure of Merit Algorithm for MFSK Systems

At this stage it is important to combine all of the effects discussed in sections 6.5.3 to 6.5.5 into a single algorithm. As indicated previously, a full implementation of the WSSUS algorithm is unfeasible and a probablistic approach is applicable given the constraints of modern computer technology. This section provides the algorithm for an MFSK system.

The figure of merit (FOM) algorithm for an MFSK system, is a statistical approximation to the true BER on a channel can be described by combining: (i) the probability of error caused by the non-Gaussian noise on the channel (use section 6.5.3); (ii) the multipath induced errors; (iii) the errors induced by Doppler distortion. The composite algorithm is shown below:

$$\text{FOM} = C_b = \left(\sum_{m=0}^{M-1} \binom{M}{m} P_e(m|N_f) \right) \times P_e(m|G) \times P_e(m|D) \tag{6.28}$$

where

C_b = probabilistic combined BER performance,
B = bandwidth where the modem operates,
N_f = frequency dependent SNR level,

$$
\begin{aligned}
P_e(m|N_f) &= \text{probability of symbol error given } N_f, \\
P_e(m|G) &= \text{probability of symbol error given multipath factor } G, \\
P_e(m|D) &= \text{probability of symbol error given Doppler shift factor } D, \\
m &= \text{index to each MFSK tone}, \\
M &= \text{number of tones in the raster.}
\end{aligned}
$$

For an MFSK system, the first term in equation (6.28) is the most important factor in the estimation of BER. This is because the modem symbol rate would always be maintained below the rate at which ISI would become a problem. If the template correlation algorithm is used to determine the optimum modem tone format before using the FOM algorithm, the channel chosen would be operated with those optimal modem parameters from the start of transmission.

The figure of merit as detailed above is an empirical approximation related to the specific metrics extracted from the scattering function generated for each channel. Clearly, the algorithm requires further investigation; in particular, the time-dependent convergence of the metrics towards their true values. Equation (6.28) can be viewed as a statistical fit of the transmission parameters within the constraints provided by the measured scattering function. This statistical fit is the overlap between the p.d.f of equation (6.28) and the p.d.f. of the true probability of error p.d.f which is dependent only upon the actual channel scattering function. In addition, this statistical fit algorithm, although providing a rapid approximation to the BER that can be exhibited by the channel, becomes increasingly obsolete as the available power for computation increases and a full implementation of the "Figure-of-Merit" algorithm described in the previous section becomes possible.

The initial simulation results shown in Figure 6.10 and Figure 6.11 demonstrate that the algorithm as detailed above produces results that are reasonably accurate for uncoded MFSK modems with predetermined parameters when compared with the results obtained under fading conditions by Crepeau. These techniques now need to be generalised for different types of modem and with different channel conditions.

In addition, the algorithm does not show how the ranking procedure should be undertaken or the length of time for which the results generated would be valid. In a frequency management system, it is anticipated that during transmission a spare receiver would be used to update the FOM data. Channels would be switched after BER performance had degraded below an acceptable threshold level.

From this description, it can be seen that the estimation of the "Figure-Of-Merit" is essentially an RTCE process that determines the scattering function of the channel, instead of attempting to determine the overall SNR. This scattering function estimate is then used in collaboration with the frequency-dependent noise estimate to optimise (in this case orthogonal MFSK transmissions) in order to make most efficient use of the channel. Any future project should generalise this work further by producing results other than for simple co-channel interference and defined fading conditions.

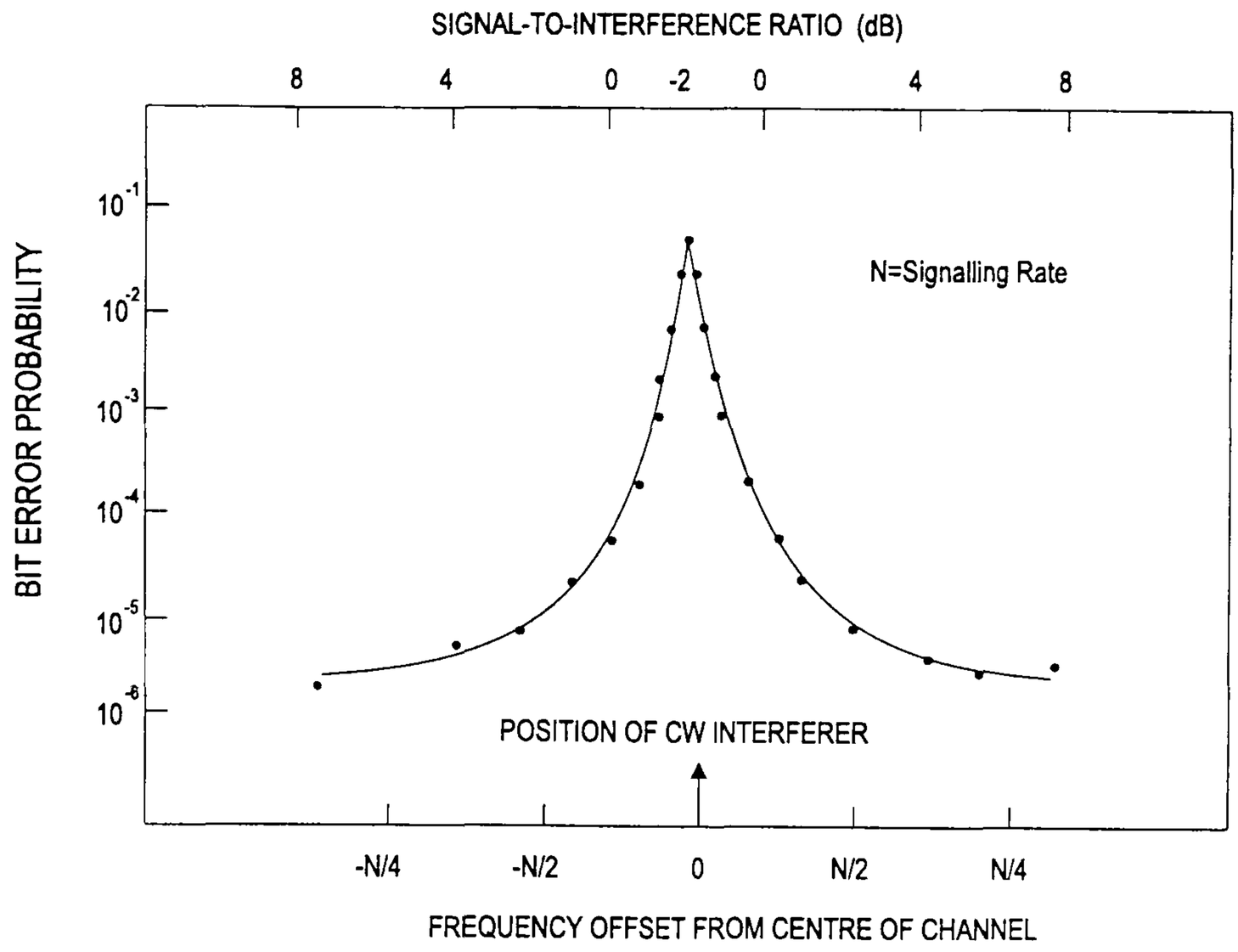

Figure 6.10: Simulation Results from Preliminary Figure-Of-Merit Trials: Performance in CW Interference, 4-FSK

6.6 Review of Chapter

In this chapter, one element of the frequency management process, channel optimisation, has been discussed with particular reference to the template correlation algorithm. This algorithm identifies regions of low noise/interference in channel spectra. Information on the position of these regions is exploited by modems to avoid co-channel interference and improve BER performance. The chapter concluded with a discussion of the fundamental concepts of channel identification and optimisation. The use of the channel scatter function allows the theoretical channel performance to be assessed for a particular modulation scheme. The computational complexity of this process is significant; consequently, a means of using simplified calculations combined with look-up tables has been developed which allows approximation to the theoretical performance.

The next chapter presents the results from 'on-air' and 'off-air trials' conducted during the research programme to evaluate channel selection and optimisation sub-systems developed.

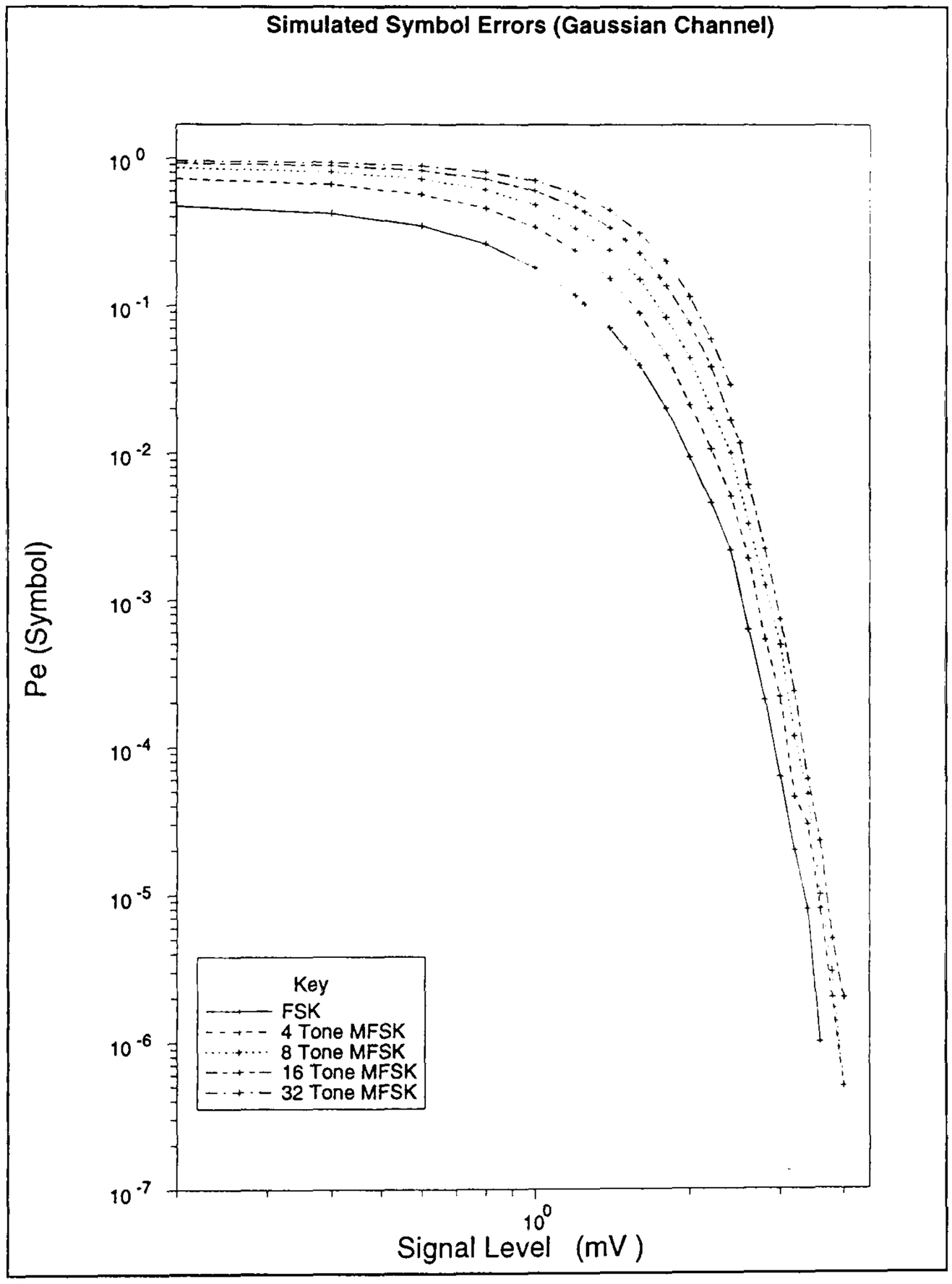

Figure 6.11: Simulation Results from Preliminary Figure-Of-Merit Trials: Performance in M-ary FSK on Gaussian Channel

Chapter 7

Results from Field Trials

This chapter initially concentrates on validating the performance from the chirp receiver as part of the channel selection procedure. The validation process includes the methods used to construct the ionograms and details statistical analyses of the impulse response data. As described in earlier chapters, the DSP-based Chirpsounder receiver performs the same function as the proprietary Chirpsounder receiver; a comparative trial was conducted to compare the outputs of the two systems under identical conditions.

The template correlation algorithm performs the channel optimisation process by analysing the baseband channel spectrum and correlating these measurements against the spectral profiles of the types of modem available to the system. The use of this algorithm has already been considered analytically in Chapter 6. In this chapter, the results of a trial using a simple FEK (frequency-exchange-keyed) modem is discussed. It is shown that in steady, narrow band, co-channel interference conditions a performance gain of approximately 6 dB, using adaptive rather than non-adaptive operation, can be achieved. This gain allows channels that would have previously been rejected to be utilised successfully.

The final part of the chapter presents the results from a further set of trials where the template correlation routines and Chirpsounder were integrated into a common tool. The channels were firstly selected by analysing the ionogram and candidate channels were then analysed spectrally and further ranked. The output from this system was selection of a channel that possessed both minimal multipath dispersion and a low measured noise/interference profile.

7.1 Results achieved utilising the DSP-Based Chirp Receiver

7.1.1 Results from the Previous Chirpmonitor Receiver

Research into deriving an ionogram from a DSP-based chirp detection system started in early 1990. The equipment available was an ICOM amateur grade transceiver and a TMS320C25 DSP device. This research concentrated on improving the output from the earlier research programme (Jowett, 1989); here, the chirp signal detector was scanned in 200 kHz increments across the HF band and the propagation was displayed as a series of bars indicating regions

where the signal had been detected.

The first technique for ionogram construction concentrated on extracting the output the matched filter signal directly from the DSP to the controlling PC device whilst the scan was taking place. The output was viewed as a pseudo-3D plot. Examples of outputs, taken in March 1990 during a radio trial at the School of Signals, Dorset, are shown in Figure 7.1. The colour plots have been reduced to a grey-scale for display purposes. It can be clearly seen that a significant matched filter response gives rise to the vertical lines. Furthermore, possible multi-path can be seen at the bases of the strongest vertical lines. Each plot shows the strength of interference, at 200 kHz intervals, combined with a plot of relative time delay (in ms) against frequency (in MHz), for the wanted chirp with uncalibrated magnitude. The magnitude is uncalibrated because the ICOM receiver could not be operated unless the AGC was enabled; this means that the plots may have different reference levels.

It was as a result of these experiments that the development of the current Chirpsounder monitoring receiver was initiated. To enable the research to proceed, a new DSP device was procured; a floating point microprocessor, the DSP32C, which enabled the implementation of more complex algorithms than the TMS320C25 device. In addition, the project had access to a professional grade HF receiver; this receiver had higher specification baseband sensitivity and full USB (Upper Sideband) passband (300-3050 Hz), rather than the reduced passband of the ICOM receiver. A 'flywheel' timebase applied to a received chirp signal enabled the first ionograms to be generated; all the more recent ionogram plots utilise this technique.

7.1.2 Ionogram Construction

Ionogram construction in the new system is achieved by cascading the 'peak-detected' impulse responses. Consider the series of diagrams shown in Figure 7.2(a) to Figure 7.2(o); these represent a series of impulse responses at 50 kHz intervals from a Chirpsounder transmitter in Norway. The significant peaks in the impulse response are noted and their positions, with respect to the start of the window, recorded. This information, when concatenated, produces the ionogram data. False peak information is rejected by feeding the impulse response data through an averaging filter, and also utilising knowledge of the ionosphere to interpret the ionogram.

These plots highlight the variability of the ionosphere, thus indicating the complexity necessary any frequency management system attempting to choose a modulation scheme that will minimise the effects of inter-symbol interference and frequency-selective fading caused by modal interactions.

7.1.3 Example Ionograms

The example ionograms shown in Figure 7.3 and Figure 7.4 are taken respectively from a computer screen and the processed output derived from the set of impulse responses seen in Figure 7.2. Both of these ionograms have been generated using soft-decision threshold variables. In this case, the matched filter returns are closely examined to identify the average and peak noise return. This information is then used to identify the peaks that have the highest probability of being valid returns in the impulse response. This algorithm is used to

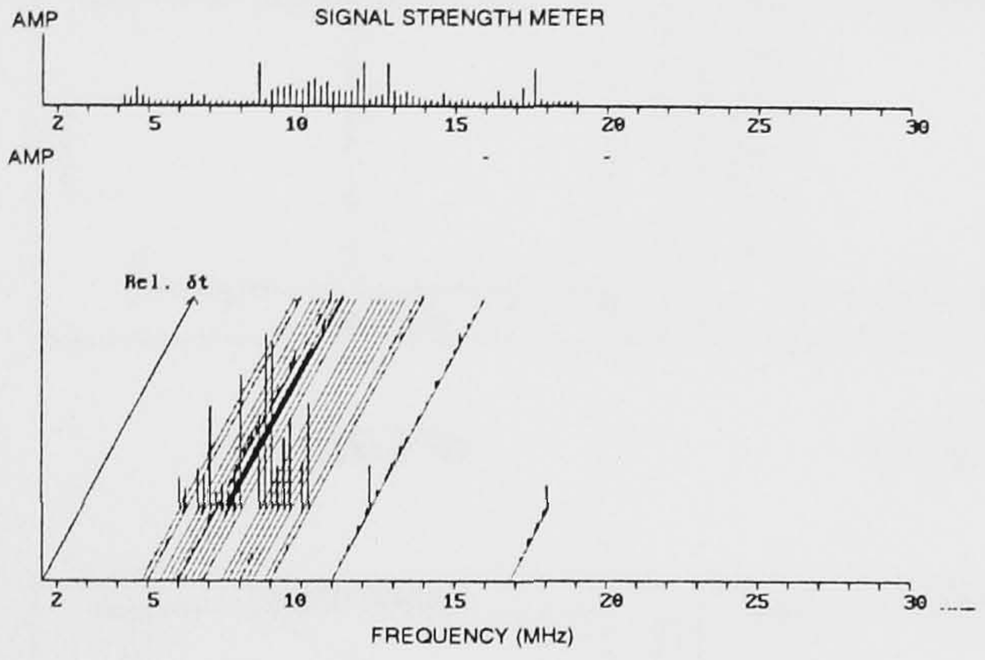

(a) Milltown - Blandford, March 1990

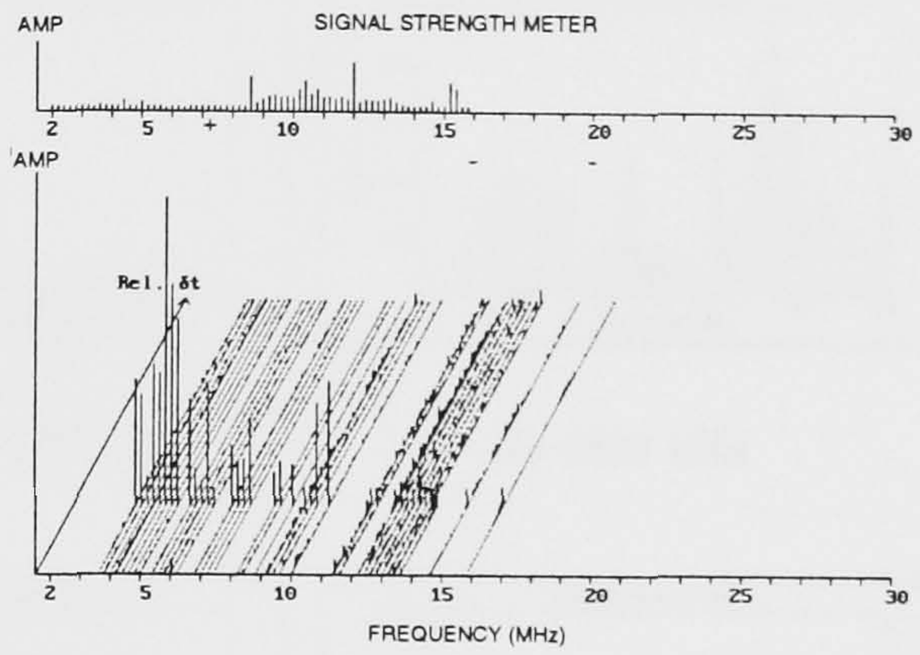

(b) Chelveston - Blandford, March 1990

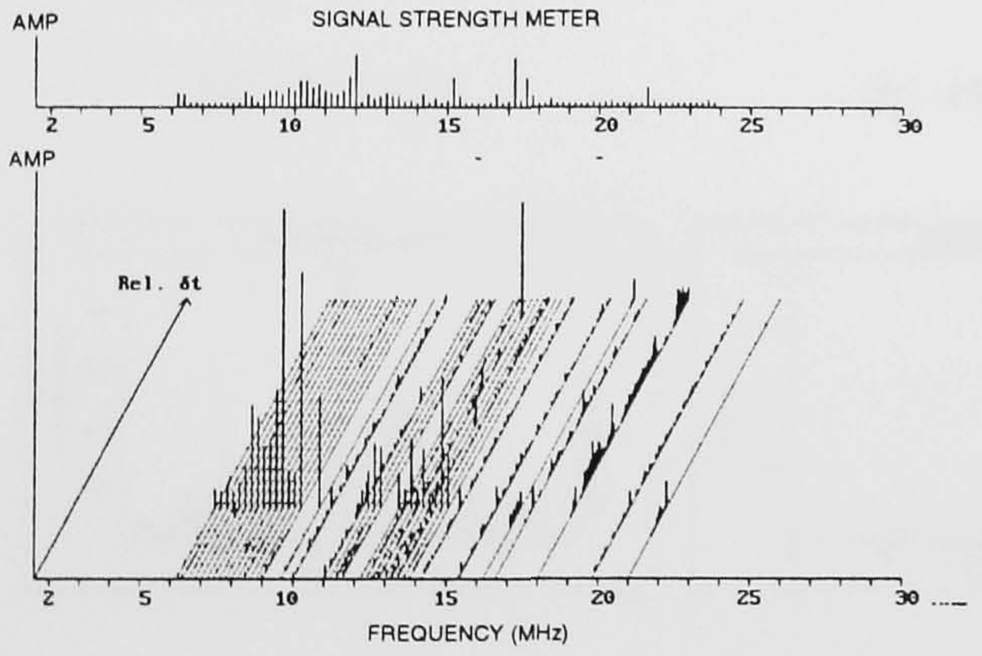

(c) Norway - Blandford, March 1990

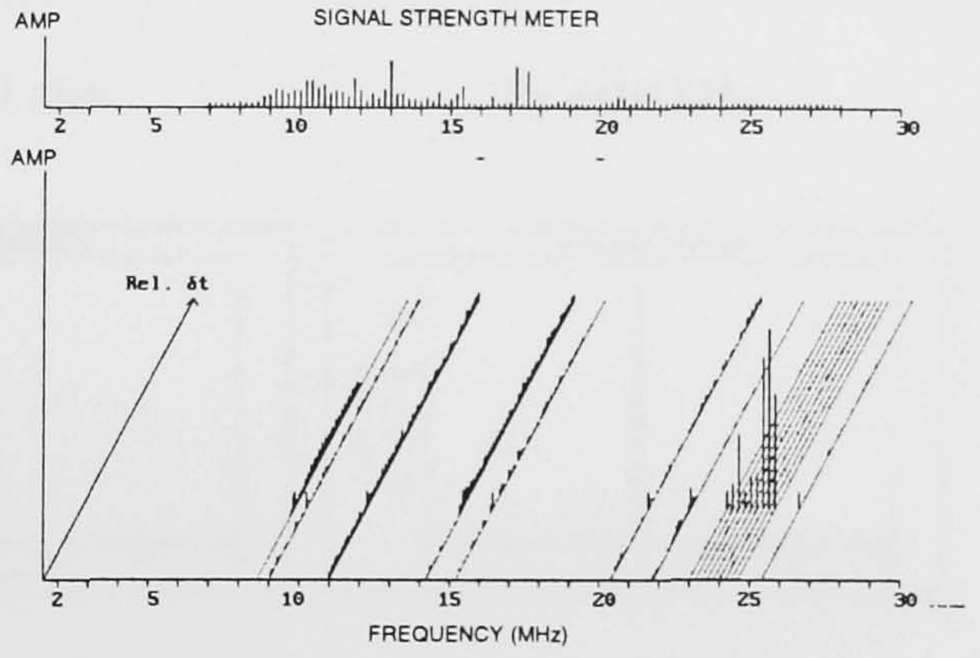

(d) Gibraltar - Blandford, March 1990

Figure 7.1: Initial Plots taken on Various Paths
School of Signals, Blandford, Dorset, March 1990

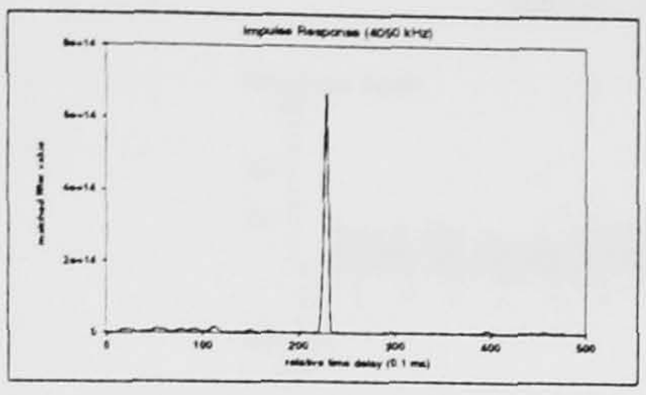

(a) 4050 kHz

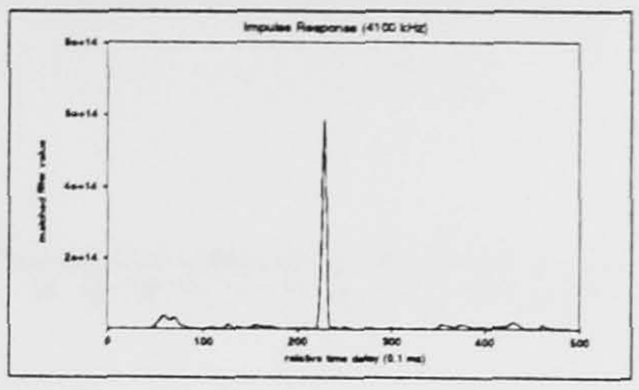

(b) 4100 kHz

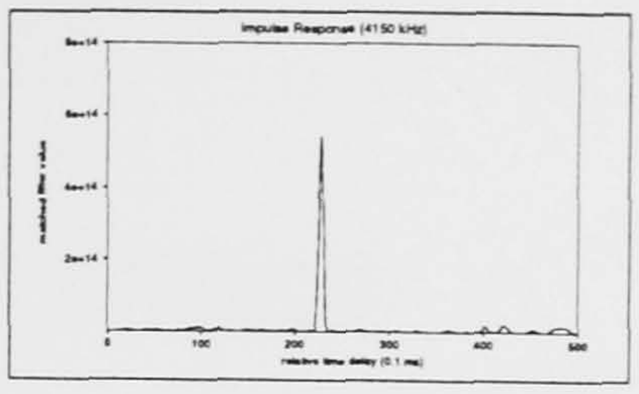

(c) 4150 kHz

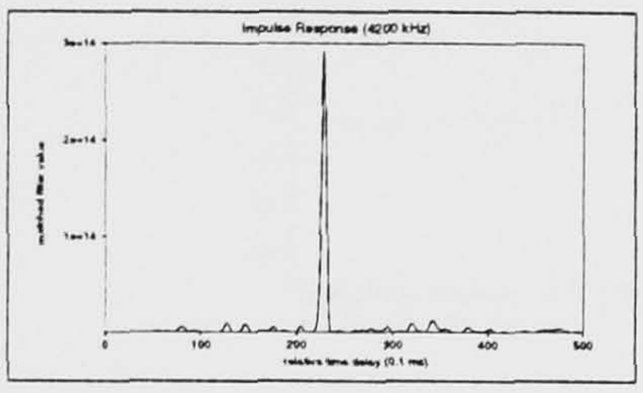

(d) 4200 kHz

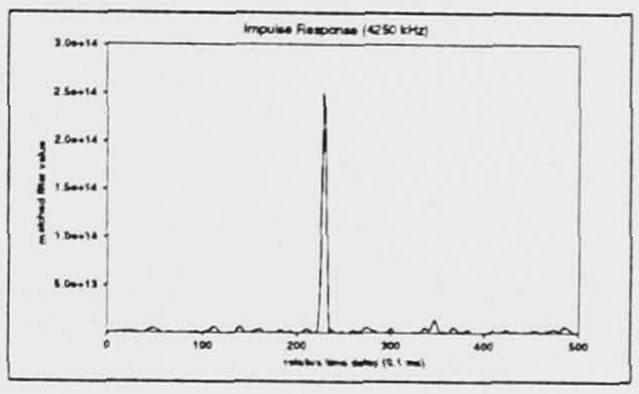

(e) 4250 kHz

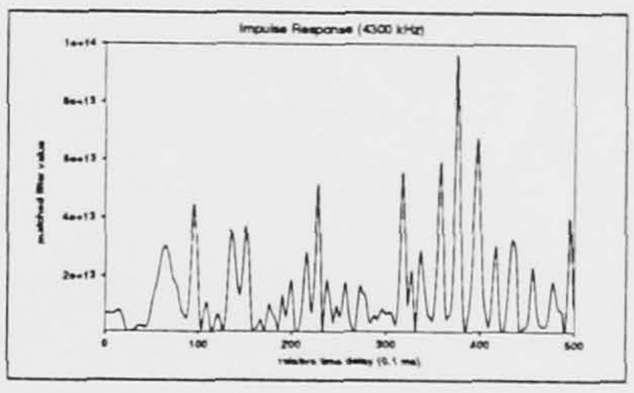

(f) 4300 kHz

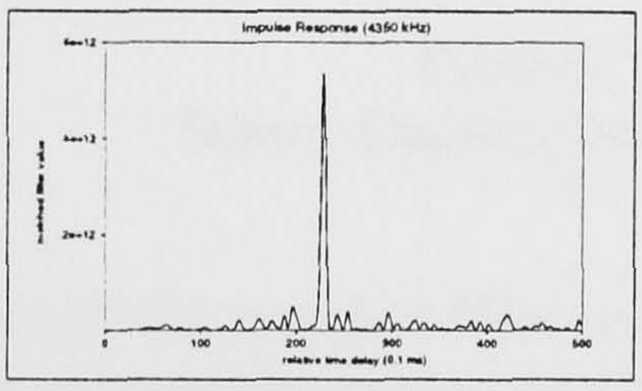

(g) 4350 kHz

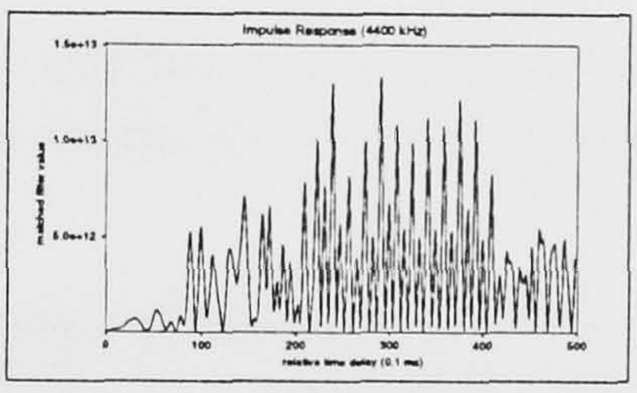

(h) 4400 kHz

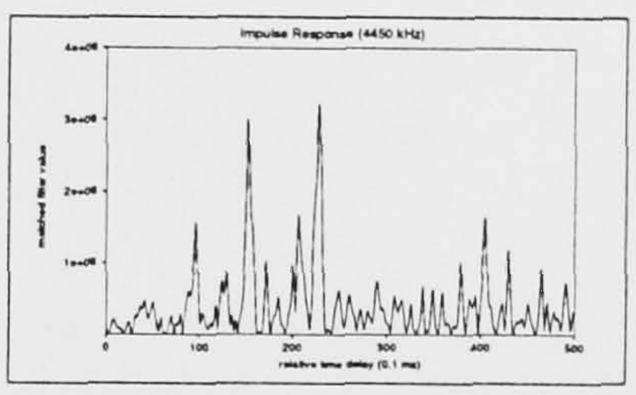

(i) 4450 kHz

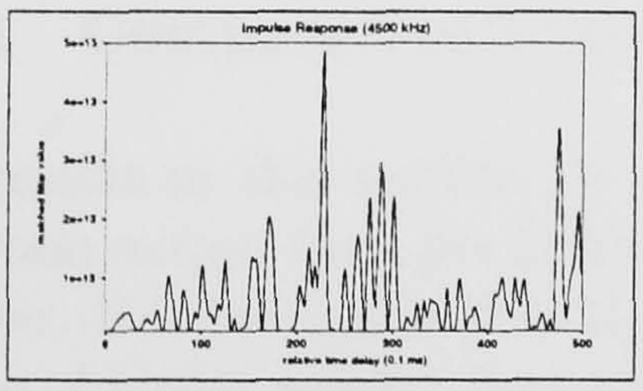

(j) 4500 kHz

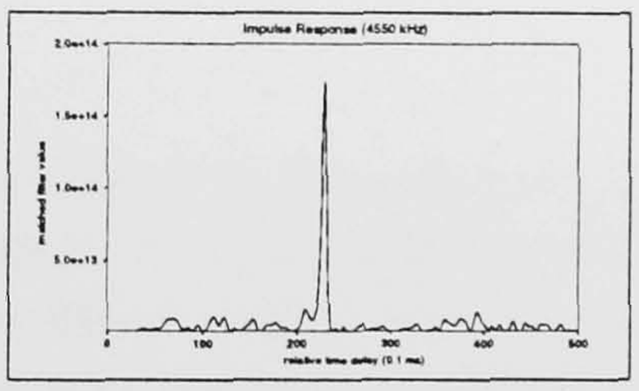

(k) 4550 kHz

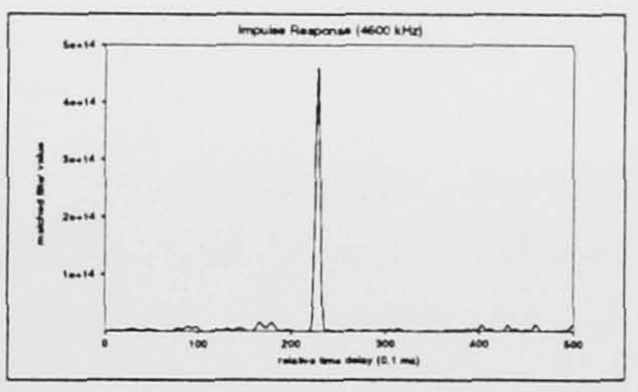

(l) 4600 kHz

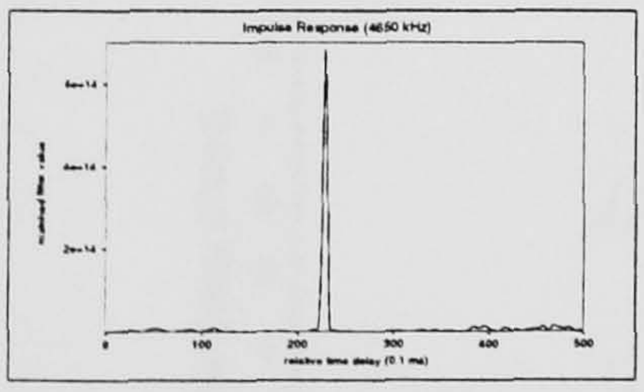

(m) 4650 kHz

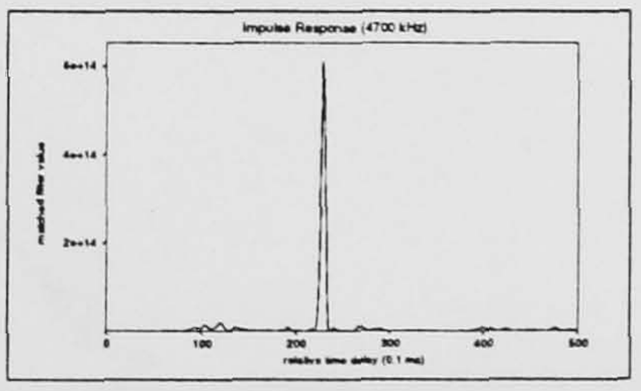

(n) 4700 kHz

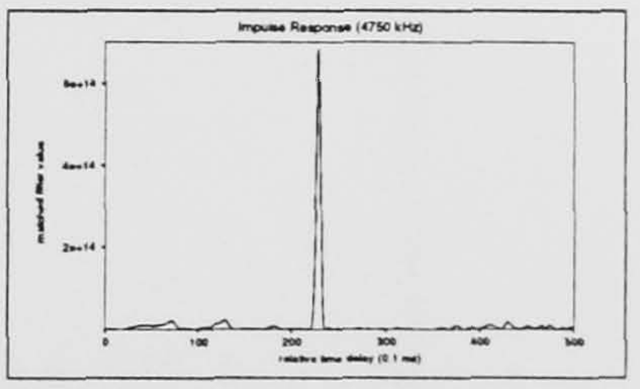

(o) 4750 kHz

Figure 7.2: Series of Impulse Responses
Oslo 10:41:54 8/8/90

Each plot details amplitude versus time delay in 0.1 ms intervals

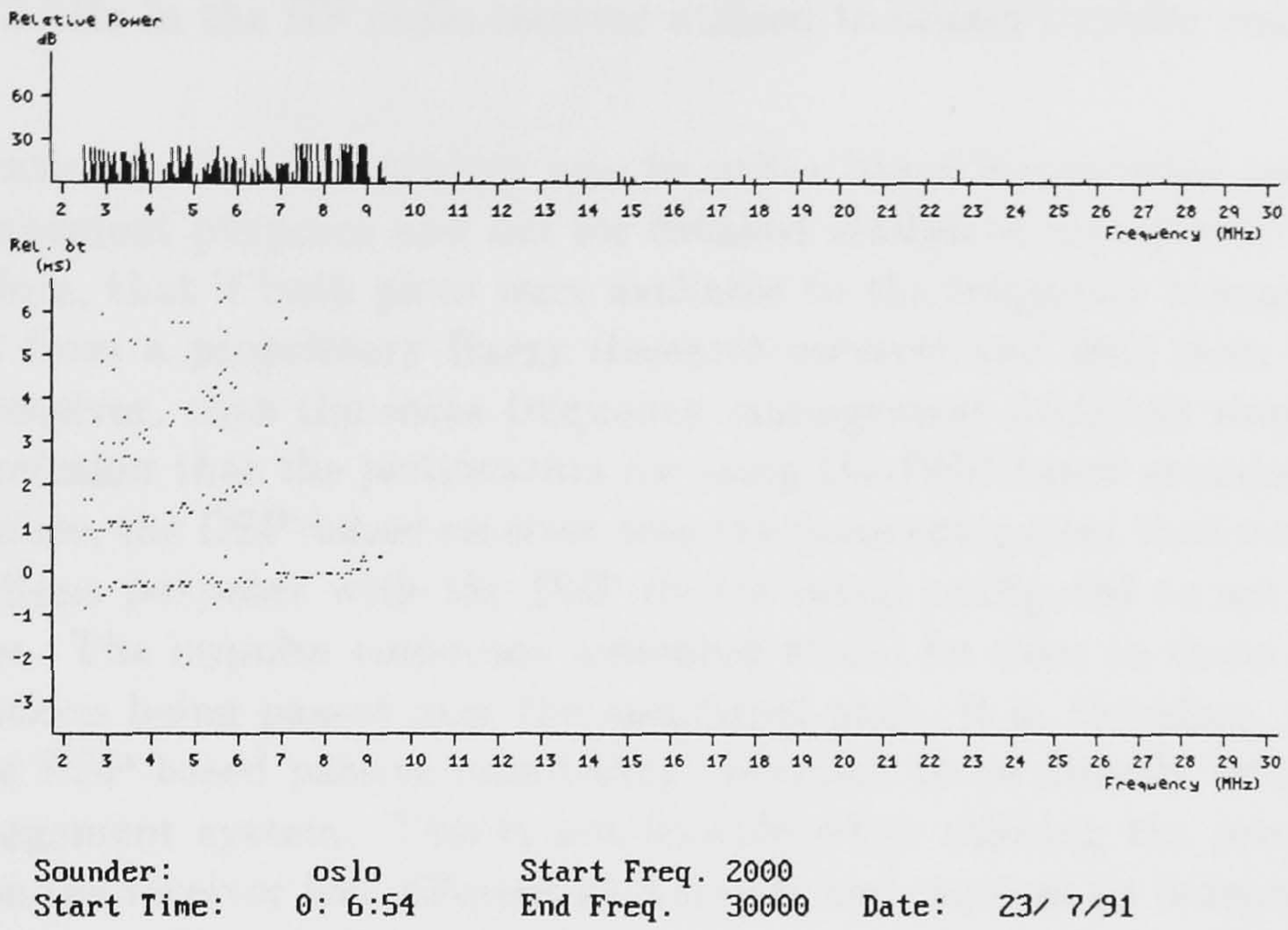

Figure 7.3: Chirpmonitor Output: Oslo - Hull
Screen Capture from Computer Running Chirpmonitor Software

"clean up" the matched filter returns before they are displayed as an ionogram. It is intended in any subsequent project to combine this data extraction process with more conventional image processing routines to further enhance the output from the Chirpmonitor.

7.1.4 Comparative Trials

The results in this section are provided to demonstrate the close correlation between the ionogram output from the DSP-based Chirpmonitor and that of a proprietary Chirpsounder receiver. It is inevitable that the overall output from the proprietary Chirpsounder receiver will be of higher quality than that produced by the DSP-based system; this is due primarily

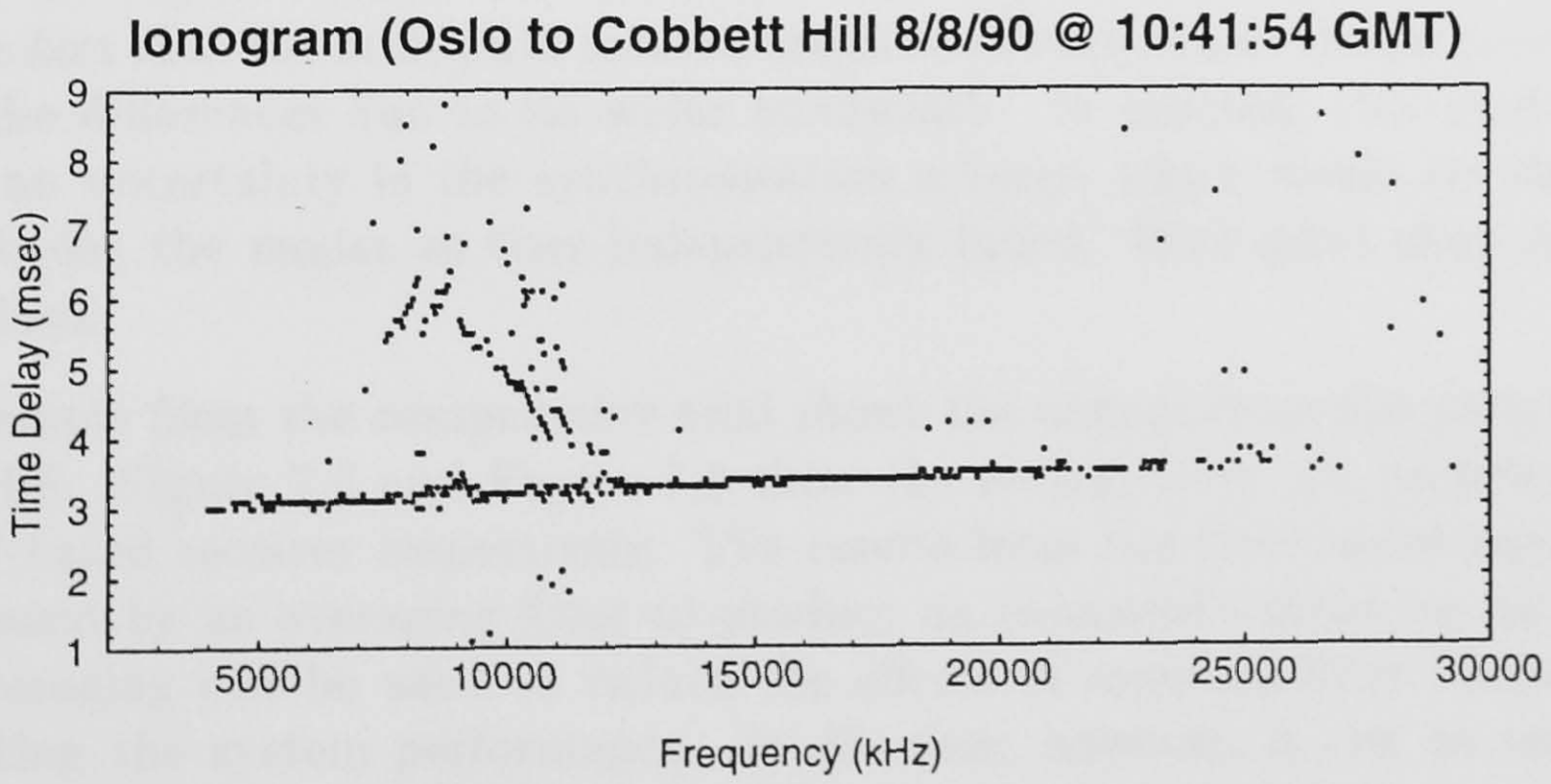

Figure 7.4: Chirpmonitor Output: Oslo - Cobbett Hill

to the baseband bandwidth of 100 kHz in the proprietary Chirpsounder, as opposed to approximately 3 kHz in the HF radio receiver utilised to obtain impulse responses with the Chirpmonitor.

However, the rationale for this project was to utilise the Chirpsounder transmissions for frequency management purposes and not for detailed studies of ionospheric structure. It is believed, therefore, that if both plots were available to the frequency management system, i.e. the output from a proprietary Barry Research receiver and that from the DSP-based Chirpsounder receiver, then the same frequency management decisions would be made. It is from this conclusion that the justification for using the DSP-based sounder receiver is derived: Furthermore, the DSP-based receiver uses the same equipment that would be required for communications purposes with the DSP device being configured to act as a dedicated sounder receiver. The impulse responses measured would be close to those experienced by the communications being passed over the monitored path. It is, therefore, possible for the results from the DSP-based passive monitoring operation to be directly integrated into the frequency management system. This is not feasible when utilising the proprietary Chirpsounder because the receiver has different parameters and requires an independent antenna. Using the proprietary Chirpsounder also implies much greater cost than for the DSP-based Chirpmonitor.

The proprietary ionogram has a time resolution (delay accuracy) of 0.01 ms; this compares with an accuracy of 0.3 ms for the DSP-based receiving system. Furthermore, the frequency resolution is 100 kHz for the proprietary receiver, as compared to the 50 kHz steps of the DSP-based system.

The plots in Figures 7.5 to 7.9 are two examples from a 48 hour trial carried out in August 1990. Many more plots are available, but these are representative outputs from both the Barry receiver (Type 5) and version 1.00 of the DSP-based receiving system. The slight rise of the traces, when using the DSP-based receiver, is due to the crystal-based flywheel timer drifting. This problem has subsequently been corrected.

Figure 7.5 is the proprietary output that corresponds to Figures 7.6 and 7.4, which are respectively the outputs from a screen capture with the system in operation and a post-processed output derived from the DSP matched filter data. Similar features exist on both plots; it can be seen that both traces exhibit the sporadic E component and comparable structures in the region around 8 MHz, where the chirpmonitor loses resolution. This is caused by the fact that the multipath returns are close to each other; the proprietary system can resolve the differences due to its wider bandwidth. In practise, this modal structure would cause an uncertainty in the synchronisation scheme, which would be observed as a switching between the modes as they independently faded. Both plots show similar LUF and MUF values.

A further example from the comparative trial shows the output from the path Hong Kong to Cobbett Hill. Figure 7.7 and Figure 7.8 show the output from the proprietary system and the DSP-based receiver respectively. The results from the DSP-based receiver can be further processed by an averaging filter to produce an enhanced output, as seen in Figure 7.9. This averaging can be used to reduce the effects of matched-filter "noise" which is a factor limiting the system performance. In all cases, however, it can be seen that the DSP-based system output correlates closely with that of the proprietary system. It should also be noted that the proprietary system has a VDU that is only 4 inches across, whereas

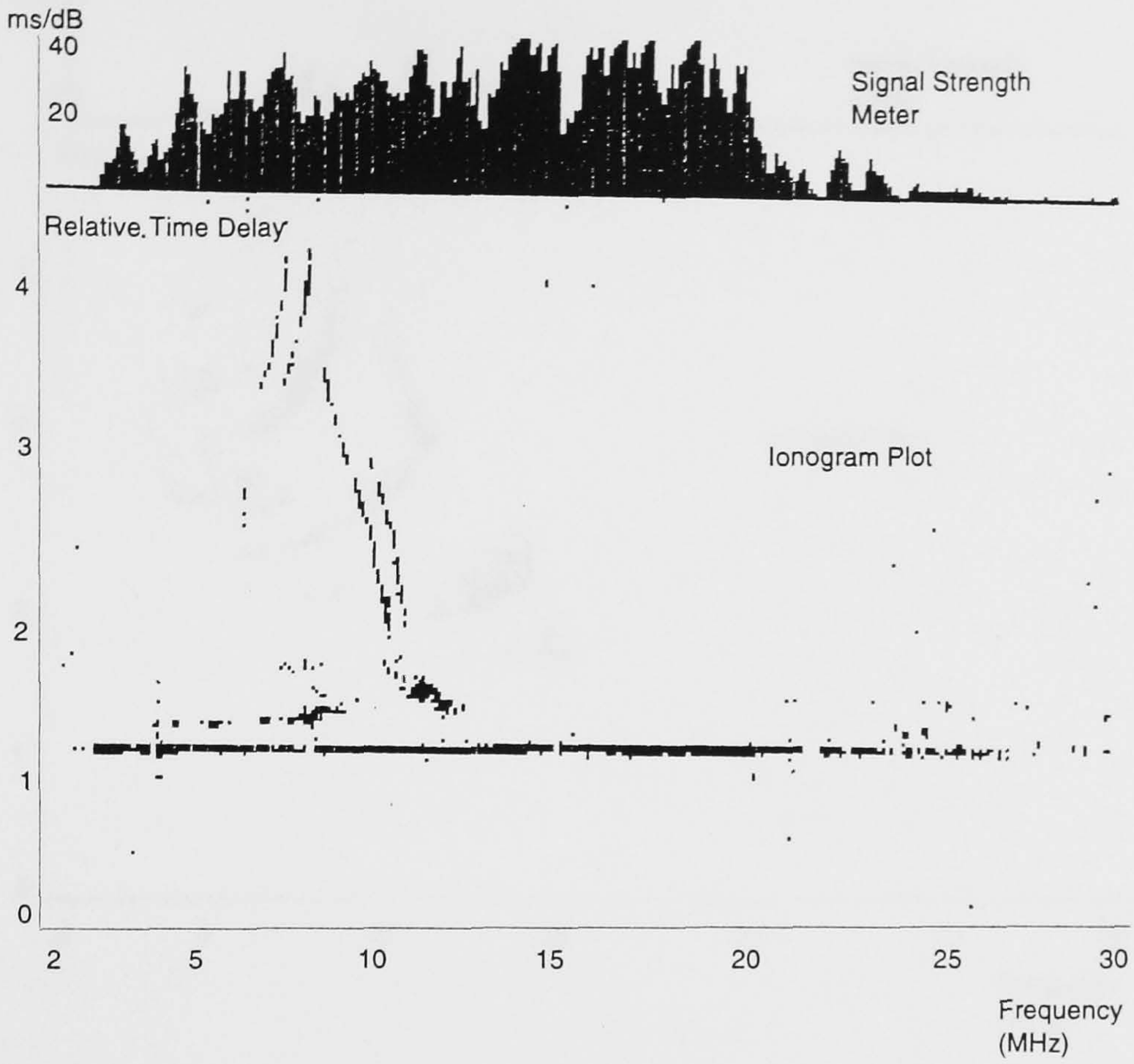

Figure 7.5: Proprietary Chirpsounder Output: Oslo - Cobbett Hill 10:41:51 GMT 8/8/90

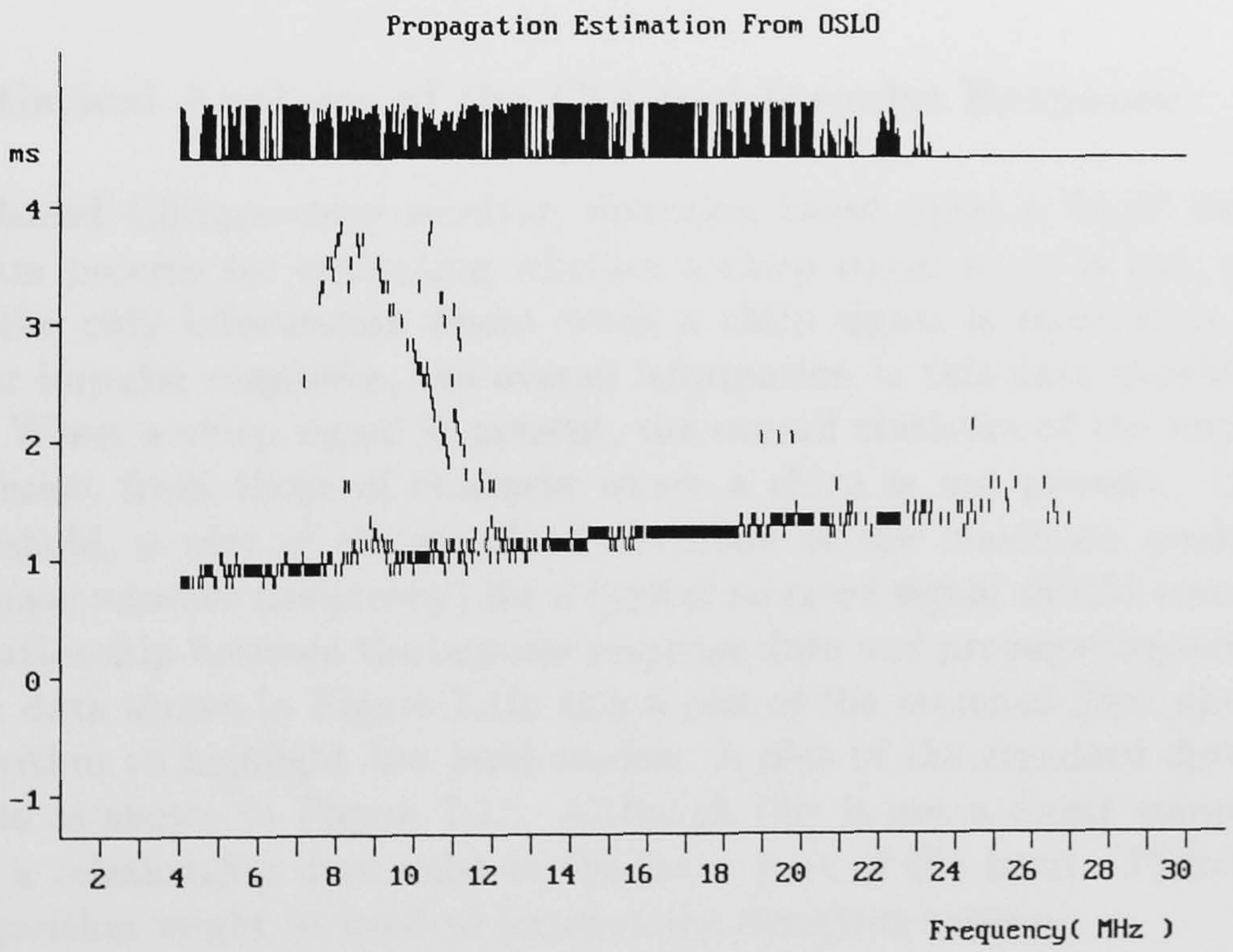

Figure 7.6: Chirpmonitor Output: Oslo - Cobbett Hill

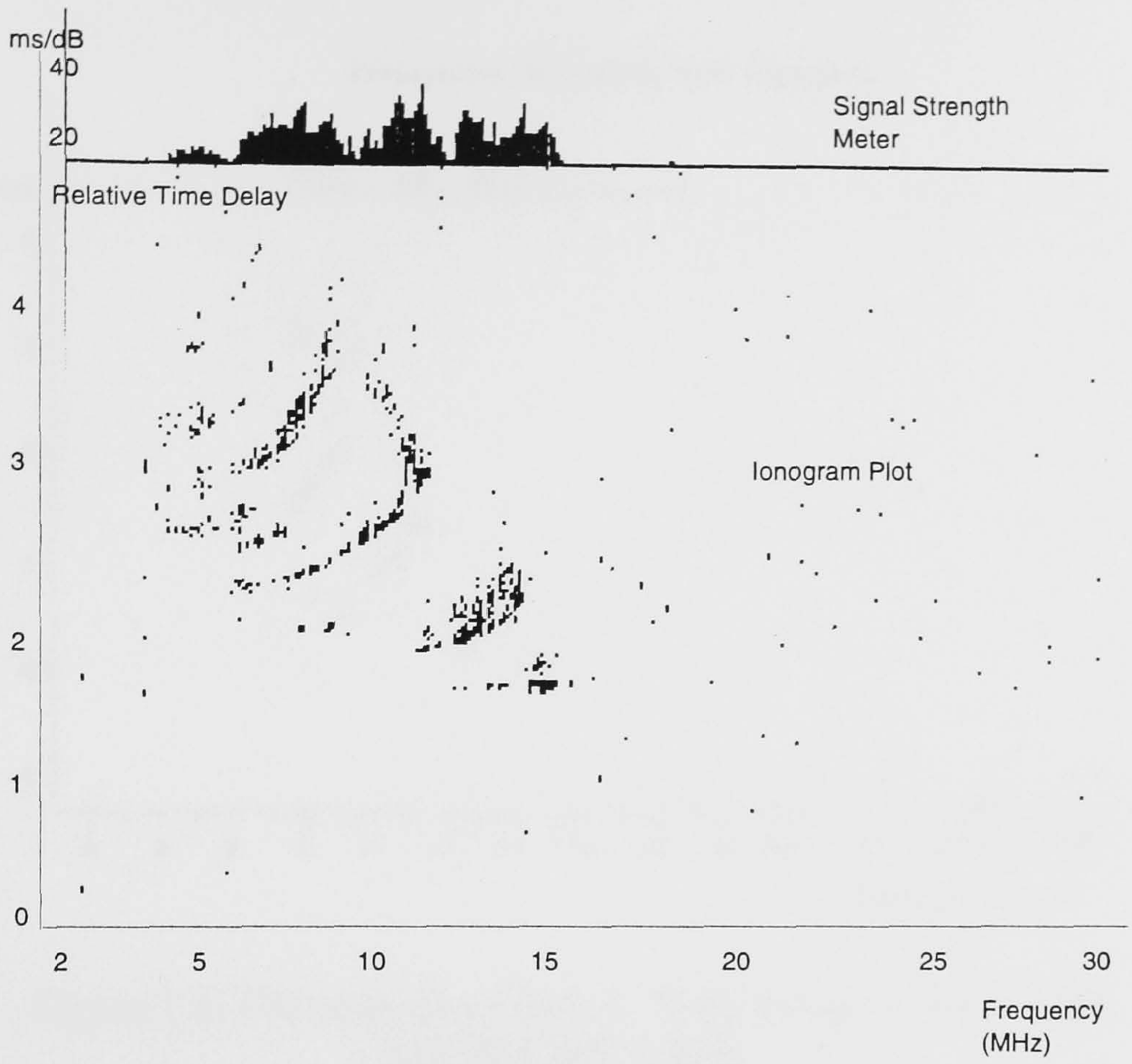

Figure 7.7: Proprietary Chirpsounder Output: Hong Kong - Cobbett Hill 5:57:20 GMT 8/8/90

the DSP-based chirpmonitor employs a normal computer screen.

7.1.5 Statistical Analysis of the Channel Impulse Response

In the DSP-based Chirpsounder receiver, detection based upon a 'hard' decision is only a sub-optimum process for evaluating whether a chirp signal is, or is not, present in the channel. If the only information about when a chirp signal is received is a plot of the matched filter impulse responses, the overall information in this data should be evaluated statistically. When a chirp signal is present, the overall statistics of the impulse response data are different from those of channels where a chirp is not present. Using a 'hard' decision threshold, a plot of the standard deviation of the maximum peak value versus impulse response number (frequency) for a typical received signal should reveal if there is a statistical relationship between the impulse response data and propagating modes. Consider the ionogram data shown in Figure 7.10: this a plot of the matched filter data using a soft decision algorithm to highlight low level modes. A plot of the standard deviation using a hard threshold is shown in Figure 7.11. Although this is not a direct comparison, it can be seen that a relationship does exist in the lower part of the band. Therefore, a simple statistical algorithm might be used to improve the detection process.

Consequently, if a simple statistical routine can be used to indicate if a chirp signal is present then there must be a difference in the probability density functions associated with those

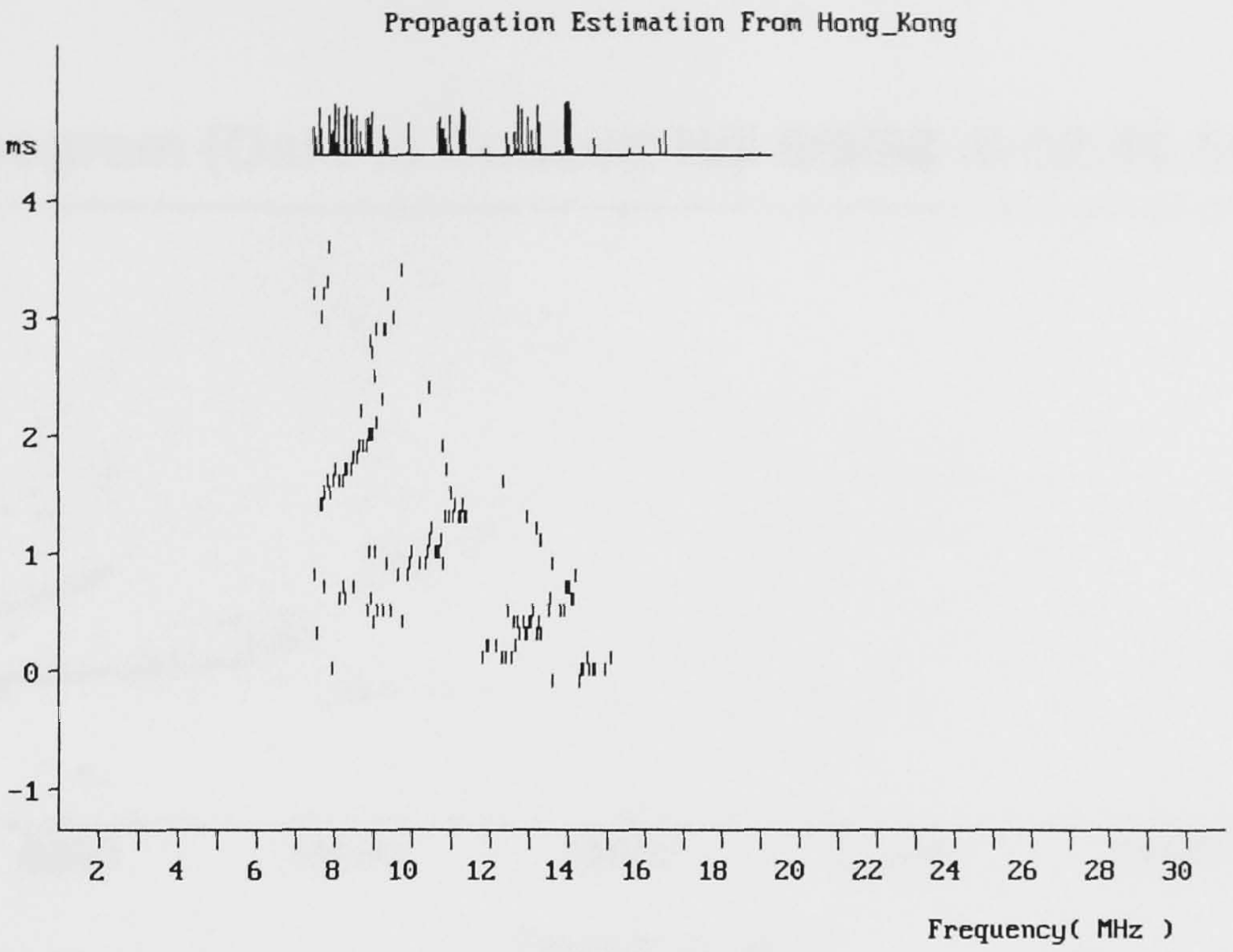

Figure 7.8: Chirpmonitor Output: Hong Kong - Cobbett Hill 5:57:20 GMT 8/8/90

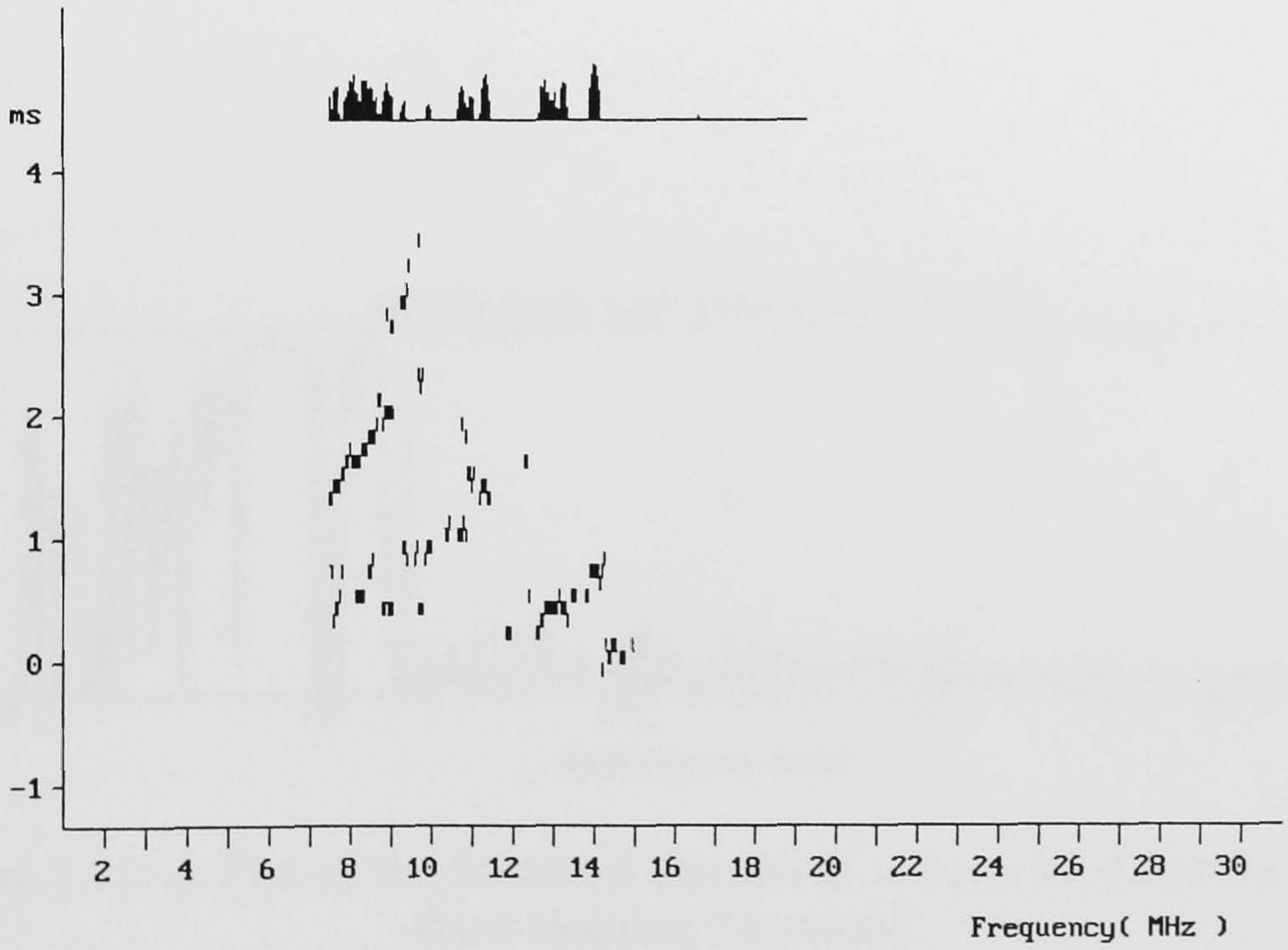

Figure 7.9: Averaged Chirpmonitor Output: Hong Kong - Cobbett Hill 5:57:20 GMT 8/8/90

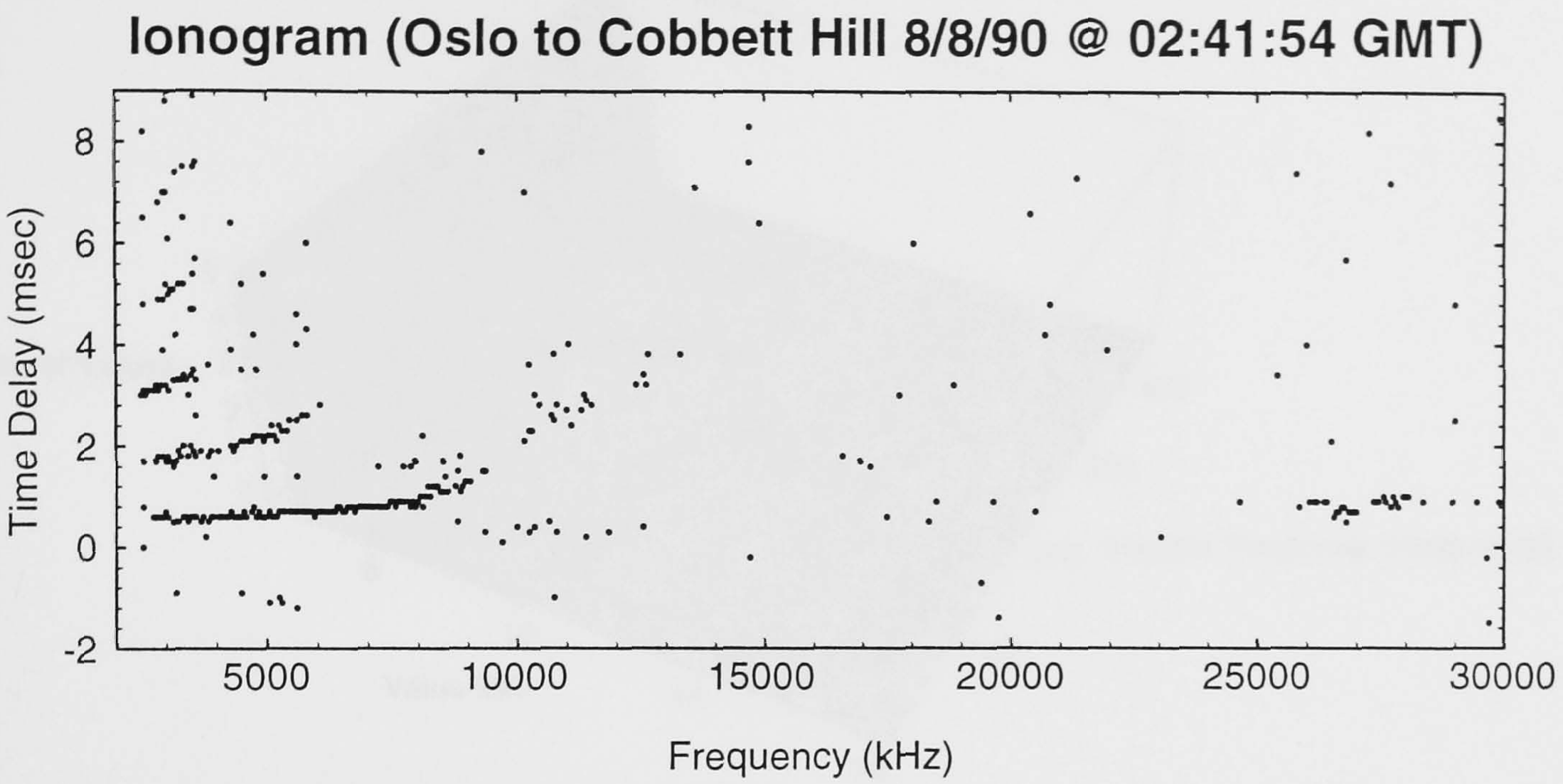

Figure 7.10: An Ionogram showing Propagation Modes:
Soft-Decision Detection Scheme
Oslo to Cobbett Hill 8/8/90 02:41:54 GMT

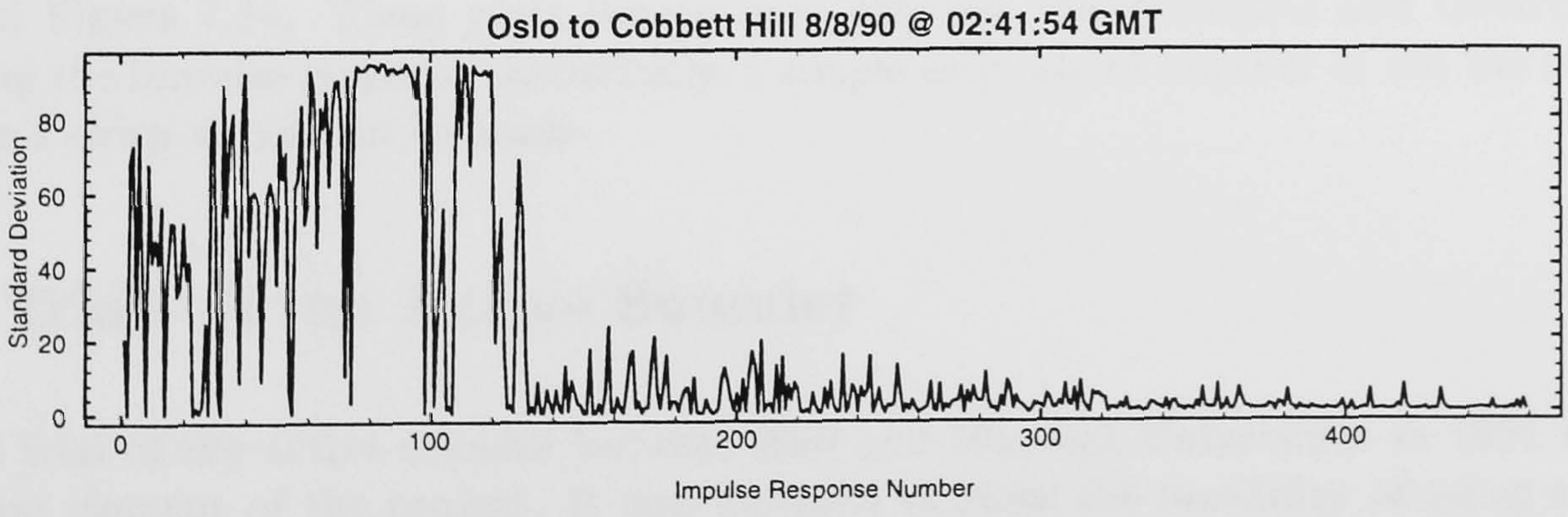

Figure 7.11: A Plot of the Standard Deviations of Impulse Response Data:
Hard-Decision Threshold
Oslo to Cobbett Hill 8/8/90 02:41:54 GMT

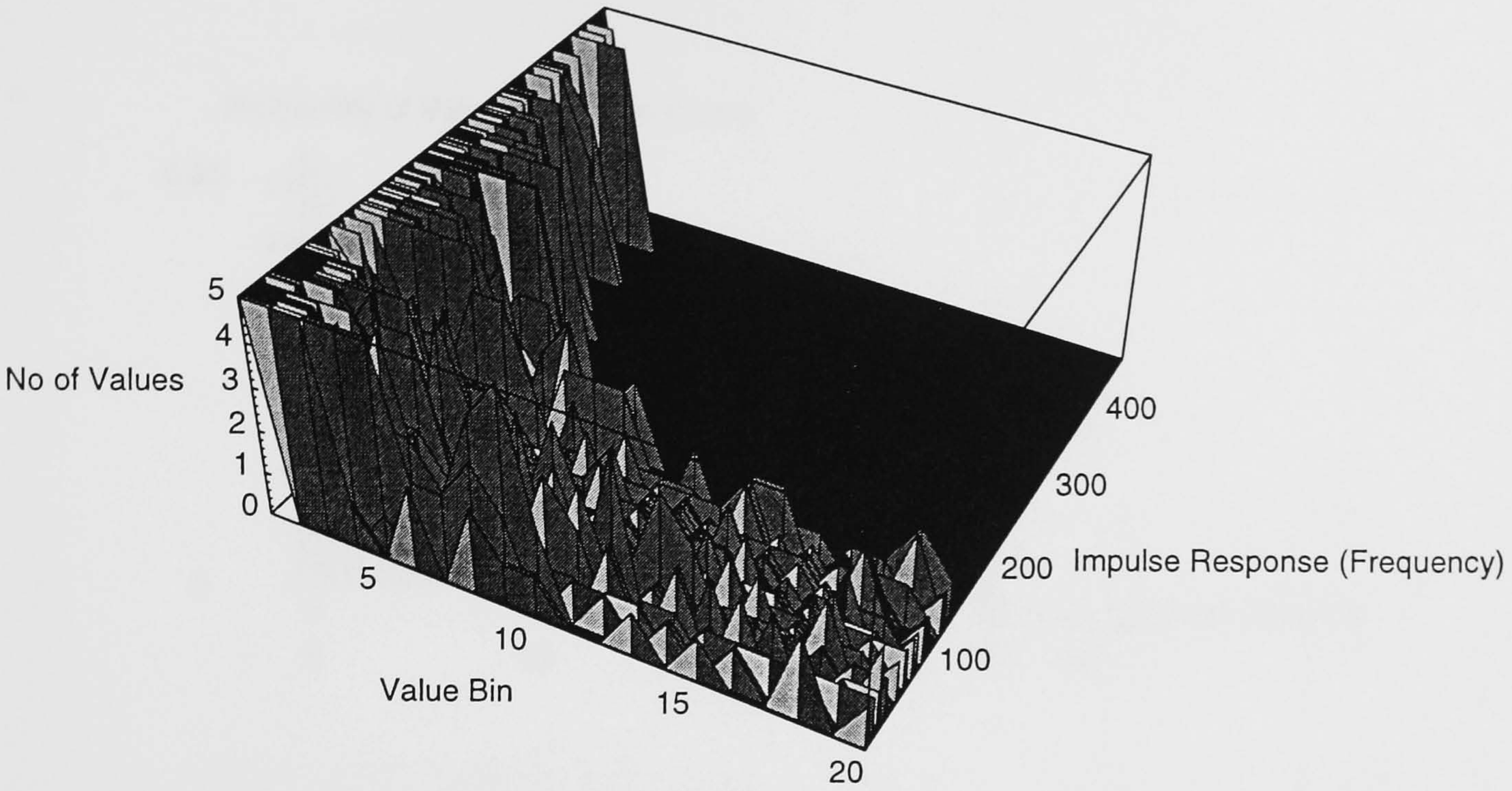

Figure 7.12: Histogram of Impulse Responses
Hard-Decision Threshold
Oslo to Cobbett Hill 8/8/90 02:41:54 GMT

plots that do and do not have chirp signals present. In addition, there could also be a difference in the PDFs of the plots dependent upon the number of modes in their impulse response functions. To estimate the PDF, a plot of the histogram of the different levels within the measured response is constructed; such plots are shown in Figure 7.12, Figure 7.13 and Figure 7.14. These plots clearly have different characteristics and therefore, by analysing the impulse response statistically, a simple estimate of whether or not the channel contains a chirp signal can be made.

7.2 Trials of the Active Sounder

A short trial of the active sounder between Hull and Warwick Universities in 1991 was an important element of the project. It was designed to show the feasibility of using a DSP-based sounding system as a functional element in an adaptive system. The trial took place over a period of 24 hours; ionograms were successfully generated in the latter part of the trial. Problems with synchronisation were due to equipment incompatibilities and these have now been resolved by using a more stable clock reference.

Although several ionograms were generated, the trial should ideally now be repeated since enhancements in software, higher specification crystals on the DSP board, as well as an improved understanding of the nature of the problems is now available. The use of the

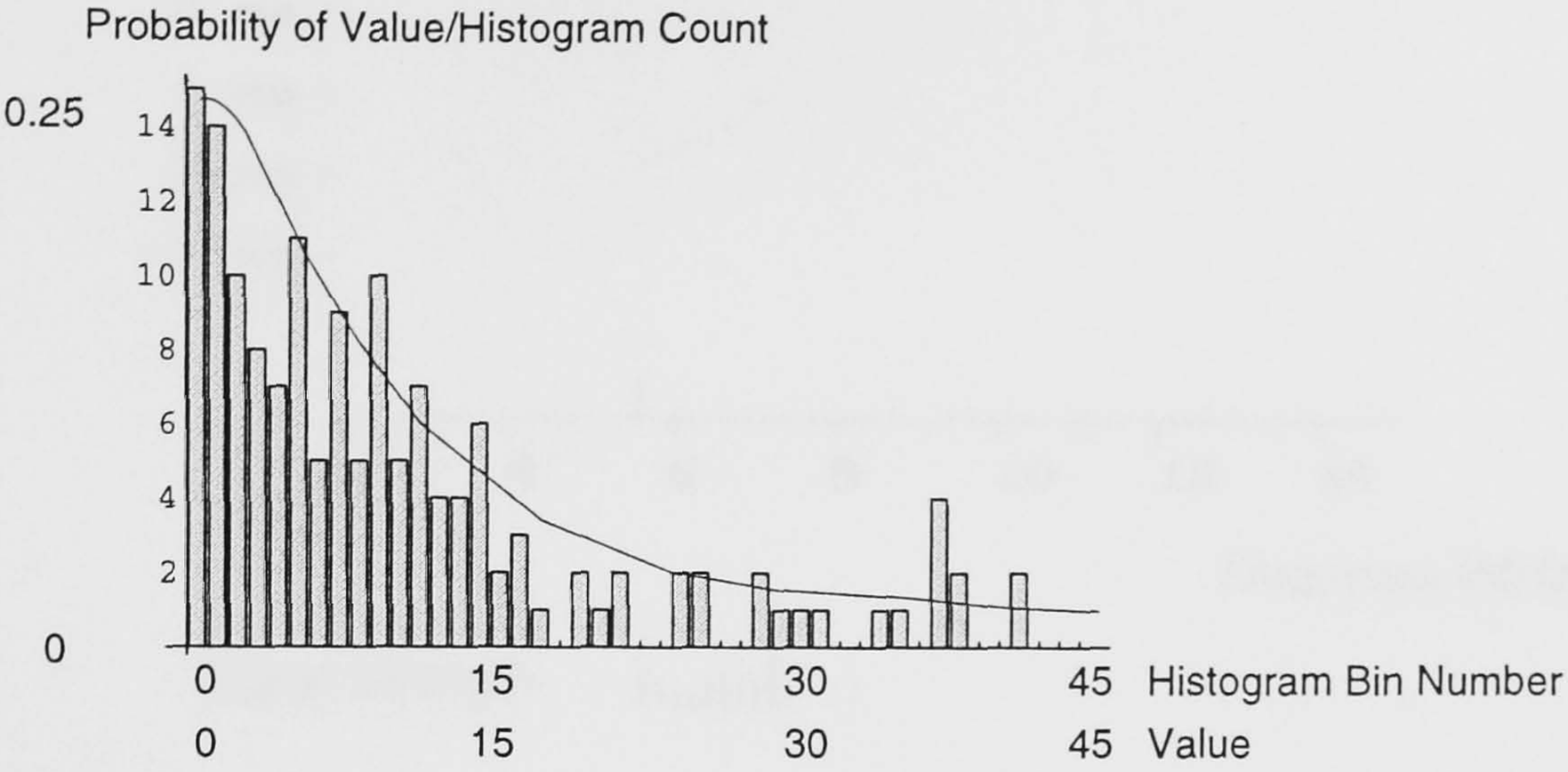

Figure 7.13: Histogram of an Impulse Response when a Chirp Signal *is* Present

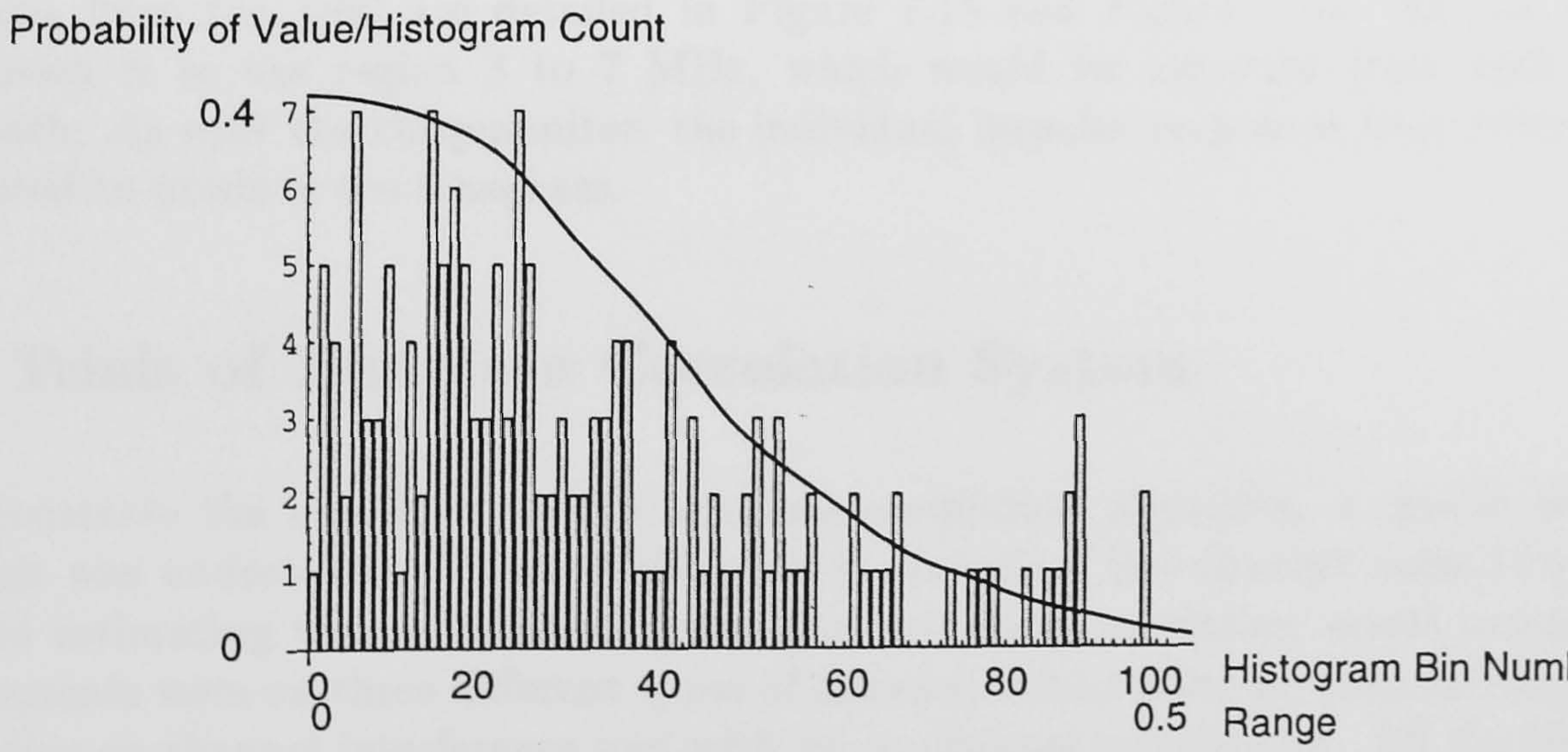

Figure 7.14: Histogram of an Impulse Response when a Chirp Signal is *not* Present

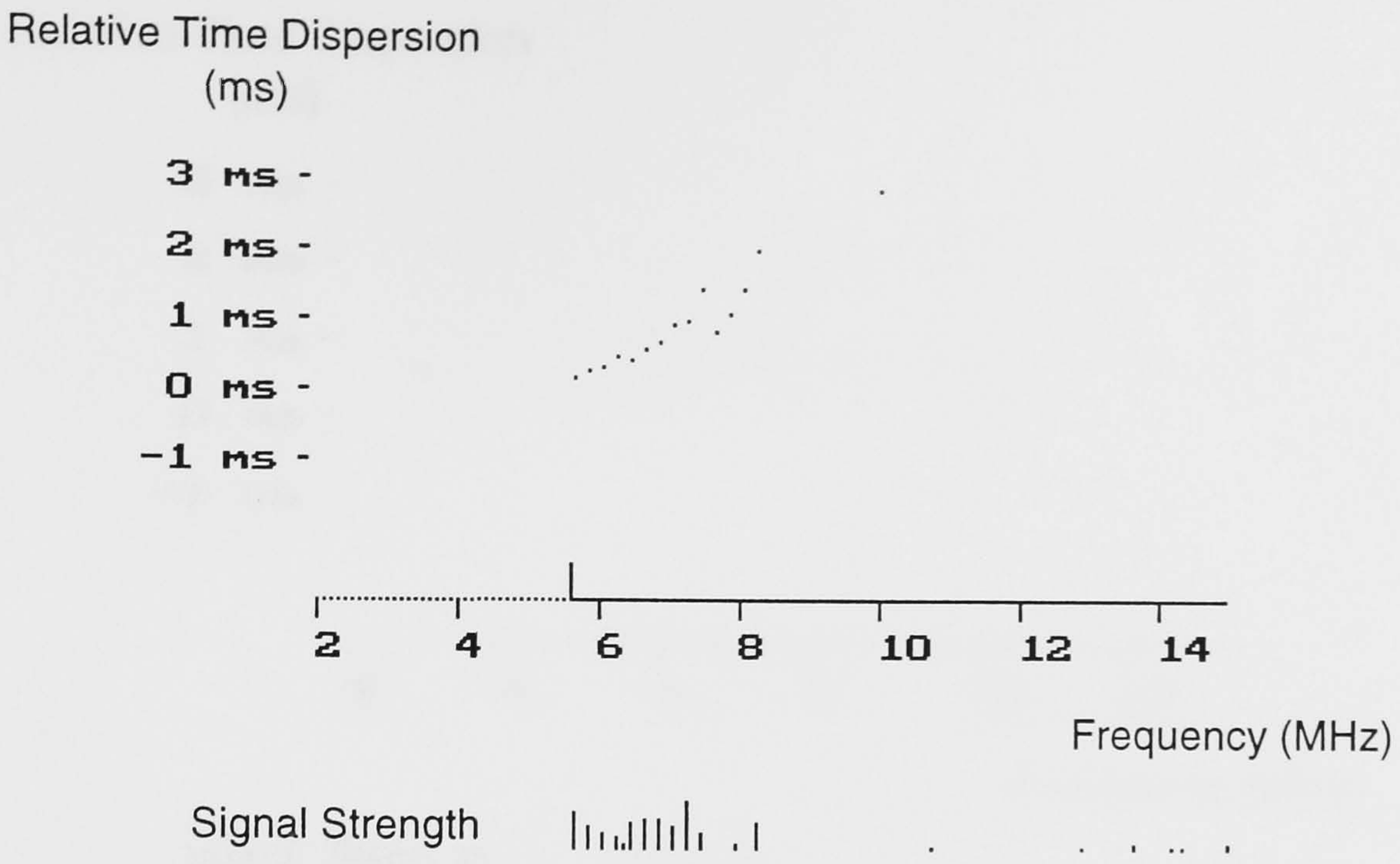

Figure 7.15: First Example Ionogram Generated by DSP Sounder:
Relative Time (ms) Versus Frequency (MHz)
Path Hull-Warwick, 16:16pm, 17 July 1991

segmented swept frequency modulation (SSFM) sounding scheme is one of the areas of novel contribution to engineering knowledge. However, the trial produced a number of formats that could be used for future sounding schemes based upon SSFM. Specifically, a future project should investigate the practical advantages of using segmented sounding schemes, e.g. a lower level of spectral occupancy as compared with the proprietary Chirpsounder system.

Ionograms from the trial are detailed in Figure 7.15 and Figure 7.16. As can be seen, propagation is in the region 3 to 7 MHz, which would be expected from such a short range path. As with the chirpmonitor, the individual impulse responses were recorded and interpreted to produce the ionogram.

7.3 Trials of Template Correlation System

To demonstrate the usefulness of the template correlation algorithm, a simple set of off-line trials was undertaken. These trials involved recording real channel noise/interference data and estimating the performance gains that template correlation would provide. The measurements were on three different types of channel: with steady co-channel interference, with fading co-channel interference and with no co-channel interference. All the interferers were recorded from the maritime mobile bands ($\approx$ 8 MHz and $\approx$ 16 MHz) since these tend to provide repeatable, long-term occupancy structures.

The steady co-channel interferer was the simplest to observe. However, identifying a clear channel and one with a fading interferer was more difficult. However, once recorded, these

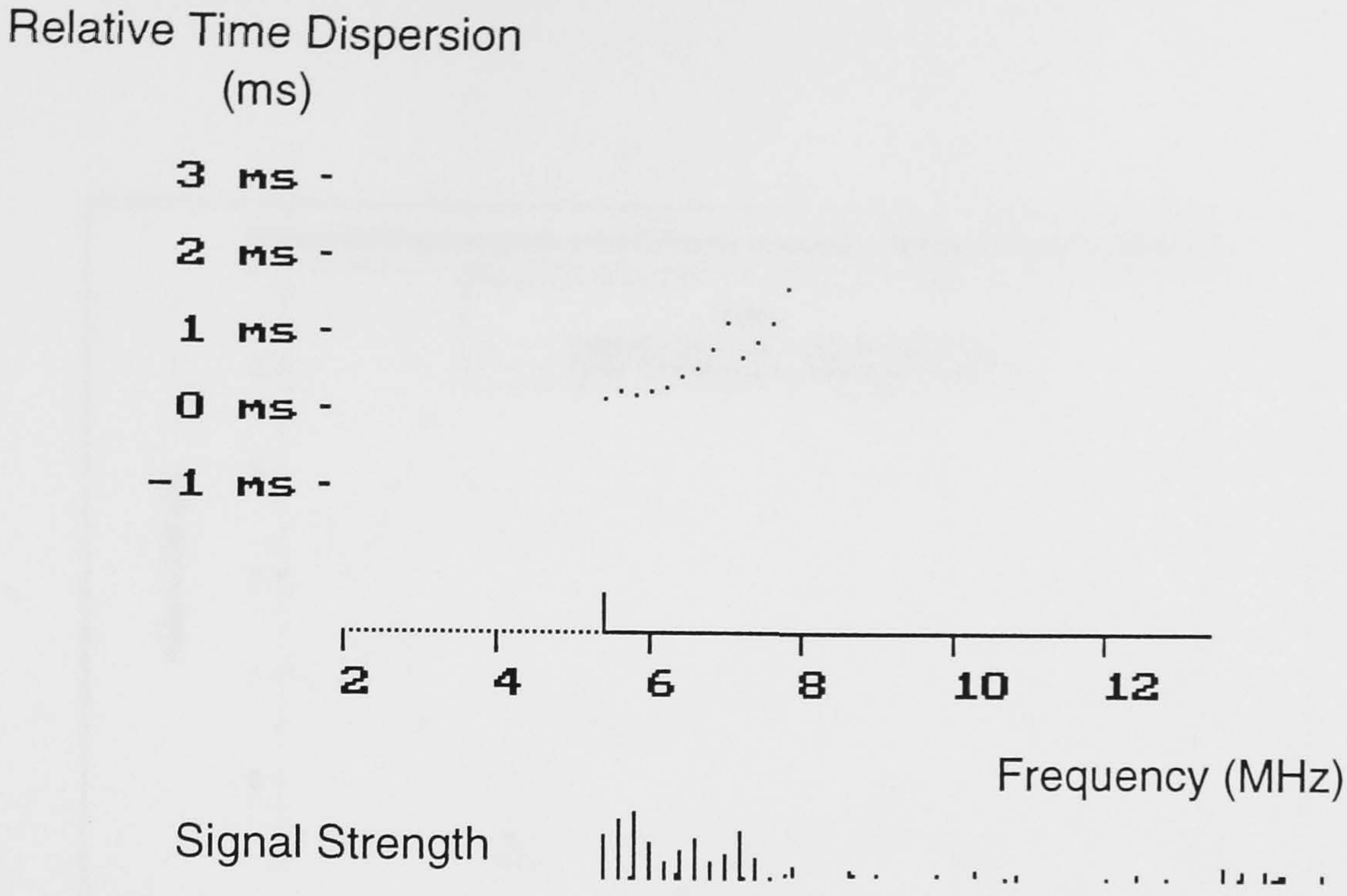

Figure 7.16: Second Example Ionogram Generated by DSP Sounder:
Relative Time (ms) Versus Frequency (MHz)
Path Hull-Warwick, 16:51pm, 17 July 1991

channels provided the most significant results. The results from two steady co-channel interference trials, together with a plot of the interference structures, are shown respectively in Figure 7.17, Figure 7.18 and Figure 7.19. The modem chosen for testing was the FEK modem utilised by HDRS; this has 4 raster tone positions: 975, 1275, 1725 and 2250 Hz; the template correlation routine picked the best two of these, with the other two being left as tones that could be picked at random. The template correlation background FFT data was averaged over a 10, 20 or 40 second period before being recorded in a data file. After undertaking the FFT, the template correlation algorithm was executed. The average FFT and FDCCF were employed to provide threshold values for tone selection.

The steady co-channel interference results show that, on average, a 6dB gain per tone pair can be expected from application of the template correlation process as compared with random selection of tone pairs. This would result in a significant reduction in error probability for most modem types. The results also show that, after a period of time, the performance improvements from the template correlation procedures start to reduce. This means that the algorithm should be re-applied when useful BER improvements are no longer being obtained.

The results from a fading channel were the most interesting. The time variability was initially identified as fading due to propagation effects alone! However, after analysis of the results Figures 7.20 and 7.21, it became evident that this was incorrect; the variation was due to a combination of both message structures and propagation effects. The energy follows a 5 minute fade cycle that infers that the co-channel interference is relatively stable for a significant part of this period. These results confirm the observations of (Gott *et al.*, 1983) who suggested that the co-channel interference structures tend to remain stable for a few

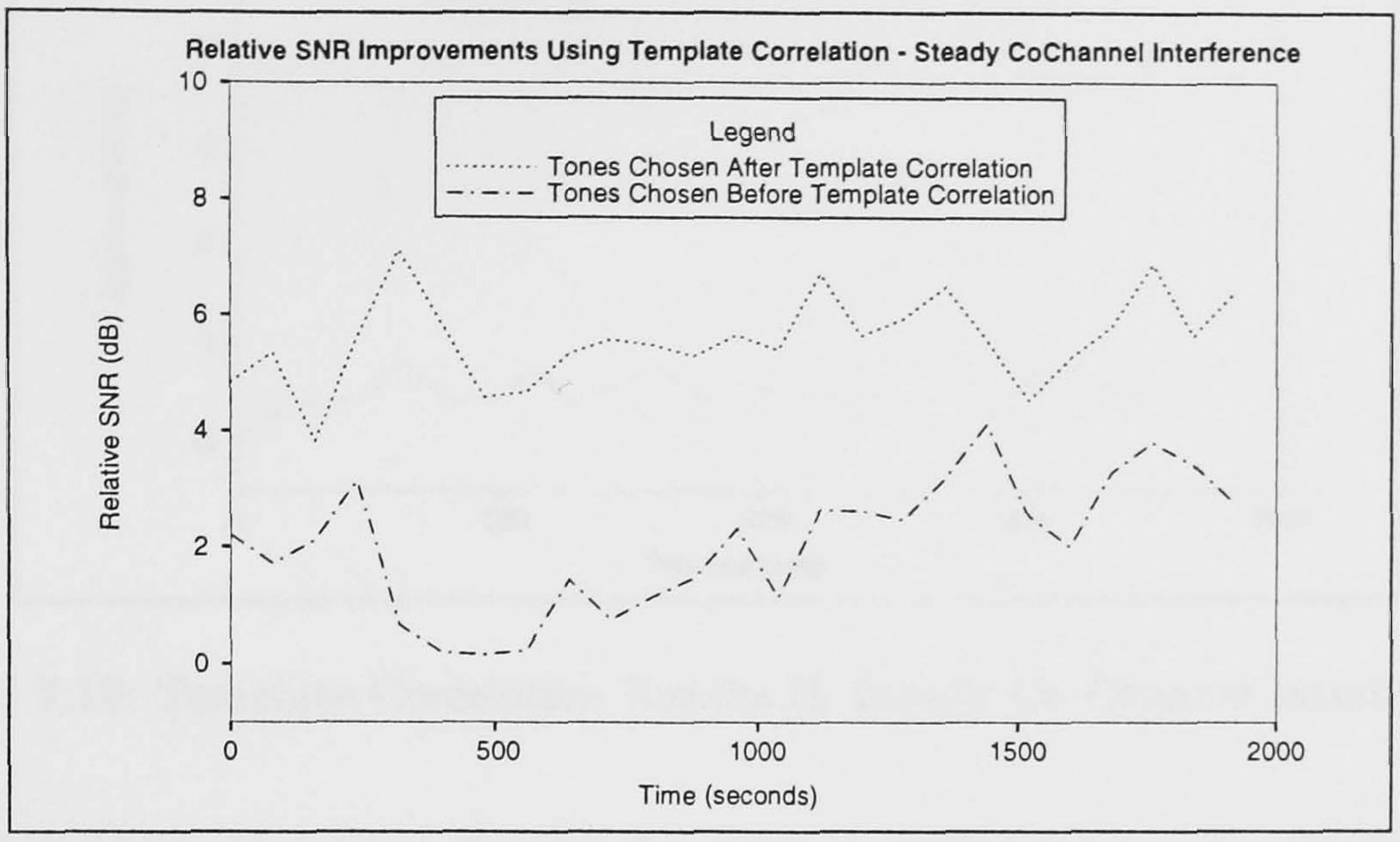

Figure 7.17: Template Correlation Results I: Steady Co-Channel Interference

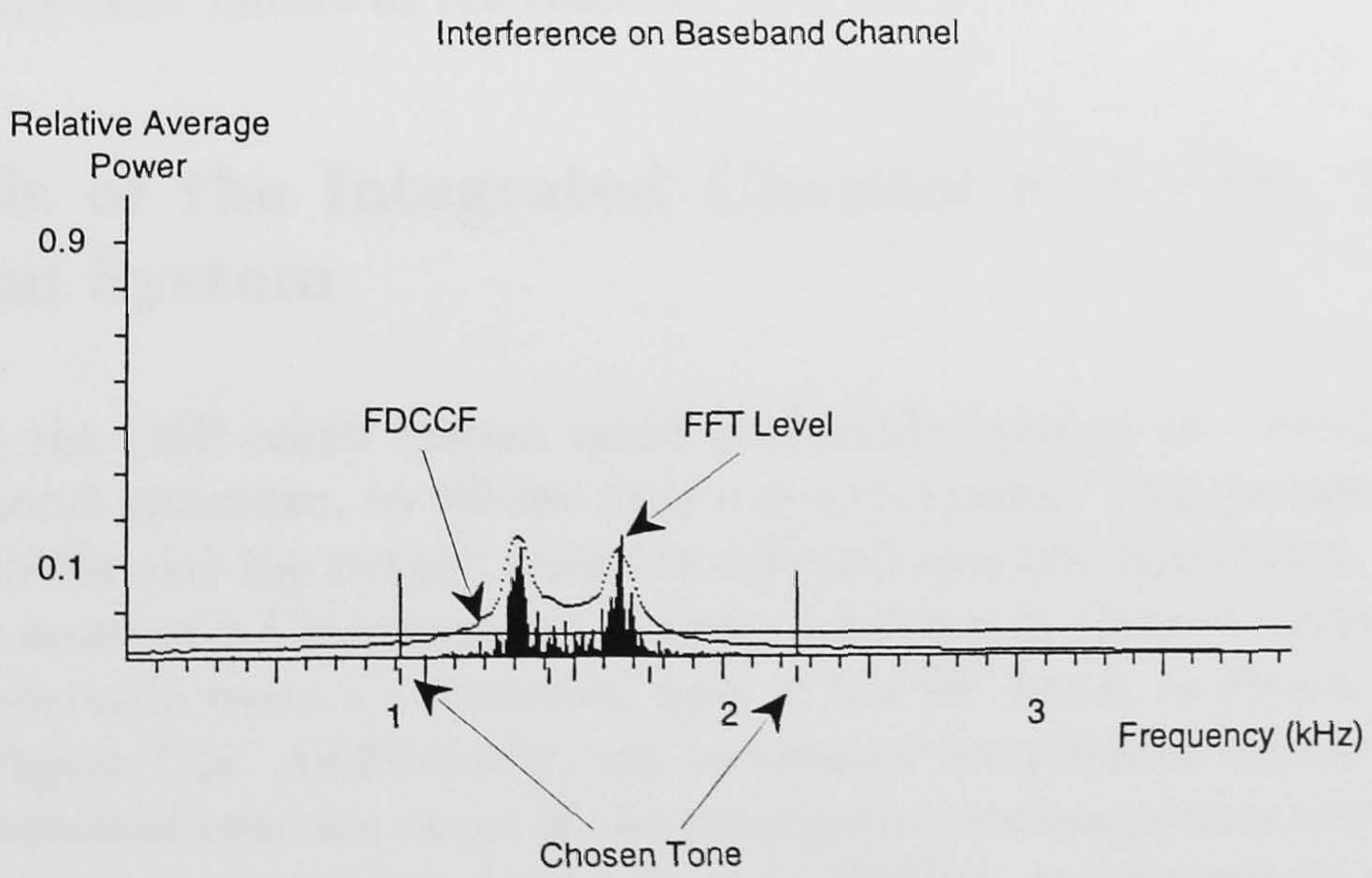

Figure 7.18: Interference Spectrum: Steady Co-Channel Interference

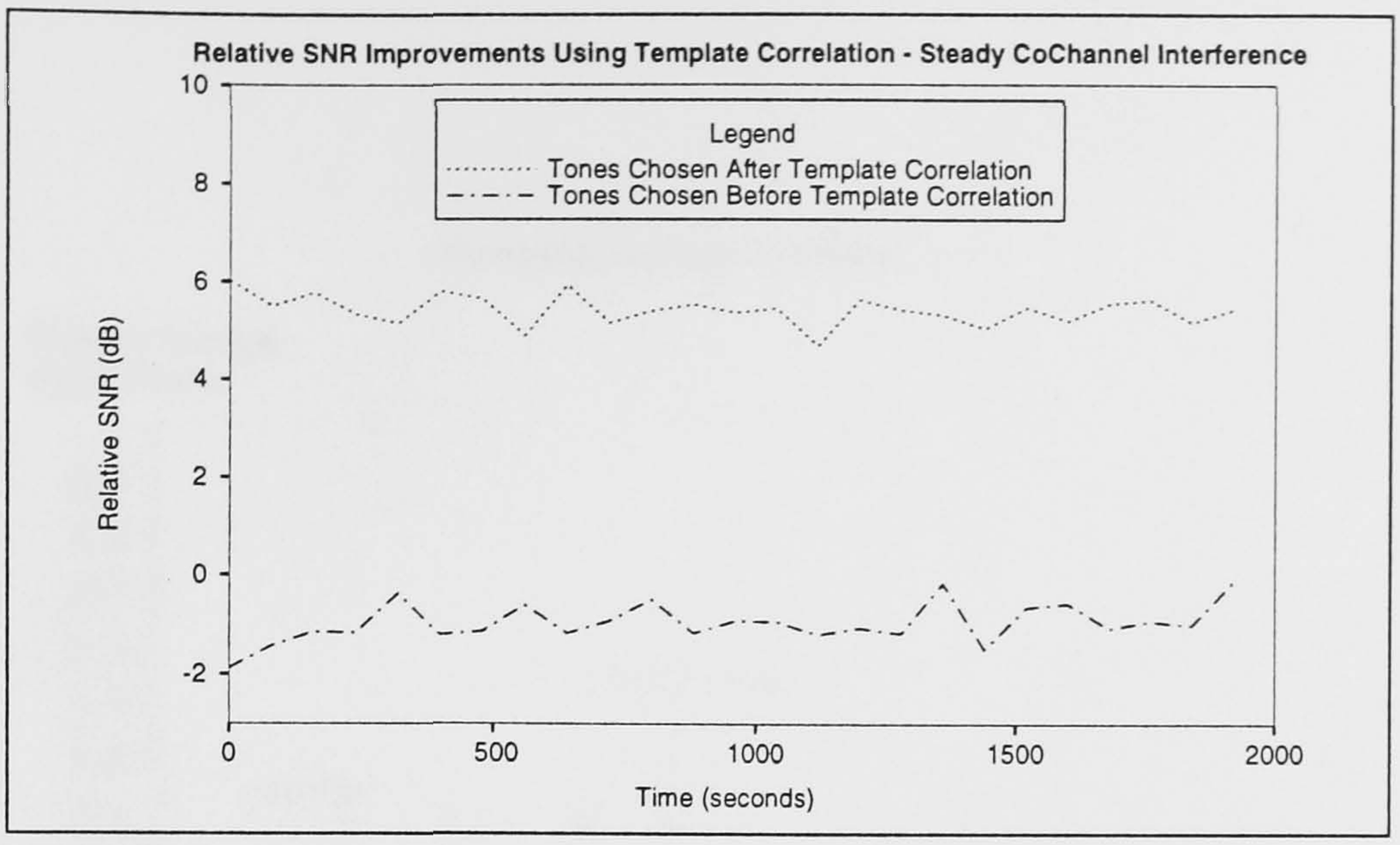

Figure 7.19: Template Correlation Results II: Steady Co-Channel Interference

minutes. It is evident, that when the signal is present similar gains as for steady co-channel interference can be achieved; however, when the signal fades then no performance gains are possible. It can be seen that the spectrum of the observed channel has the co-channel interference in distinct positions and there is minimal interaction between this interference and the transmitted FEK data.

When no co-channel interference was present, as shown in Figure 7.22, no significant gain was produced by the application of the template correlation algorithm. This is an obvious result as the tone selection algorithm needs an interfering signal to avoid if gain is to occur. The results from this trial, Figure 7.23, show that this is in fact the case. In such a situation, the DSP subsystem could be better employed in increasing the rate of the modem to take advantage of the clear nature of the channel.

7.4 Trials of the Integrated Channel Selection and Optimisation System

To verify that the DSP-based system could potentially operate as a combined channel selector and channel optimiser, an off-line trial was undertaken. This procedure combined the chirpmonitor plots and the output from the spectral analysis procedures. The chirpmonitor was set to monitor a Chirpsounder, in this case Akrotiri Cyprus, since the propagation range would normally cover a substantial part of the HF band, as shown by the measured ionogram in Figure 7.24. Additionally, any co-channel interference measured would be statistically uncorrelated over the range of the propagation measurements corresponding to the processed ionogram; propagation would be over 3000km, as opposed to ranges up to 500 km over which interference is typically strongly correlated (Gott *et al.*, 1983). This would allow the propagation and interference to be considered separately. The channels, selected at random (see Table 7.1) were initially sorted according to a single mode propagation selection criterion. This was followed by a further sort using the average interference levels. This research repeats the trials of 1975 (Darnell, 1975b), but the process was undertaken

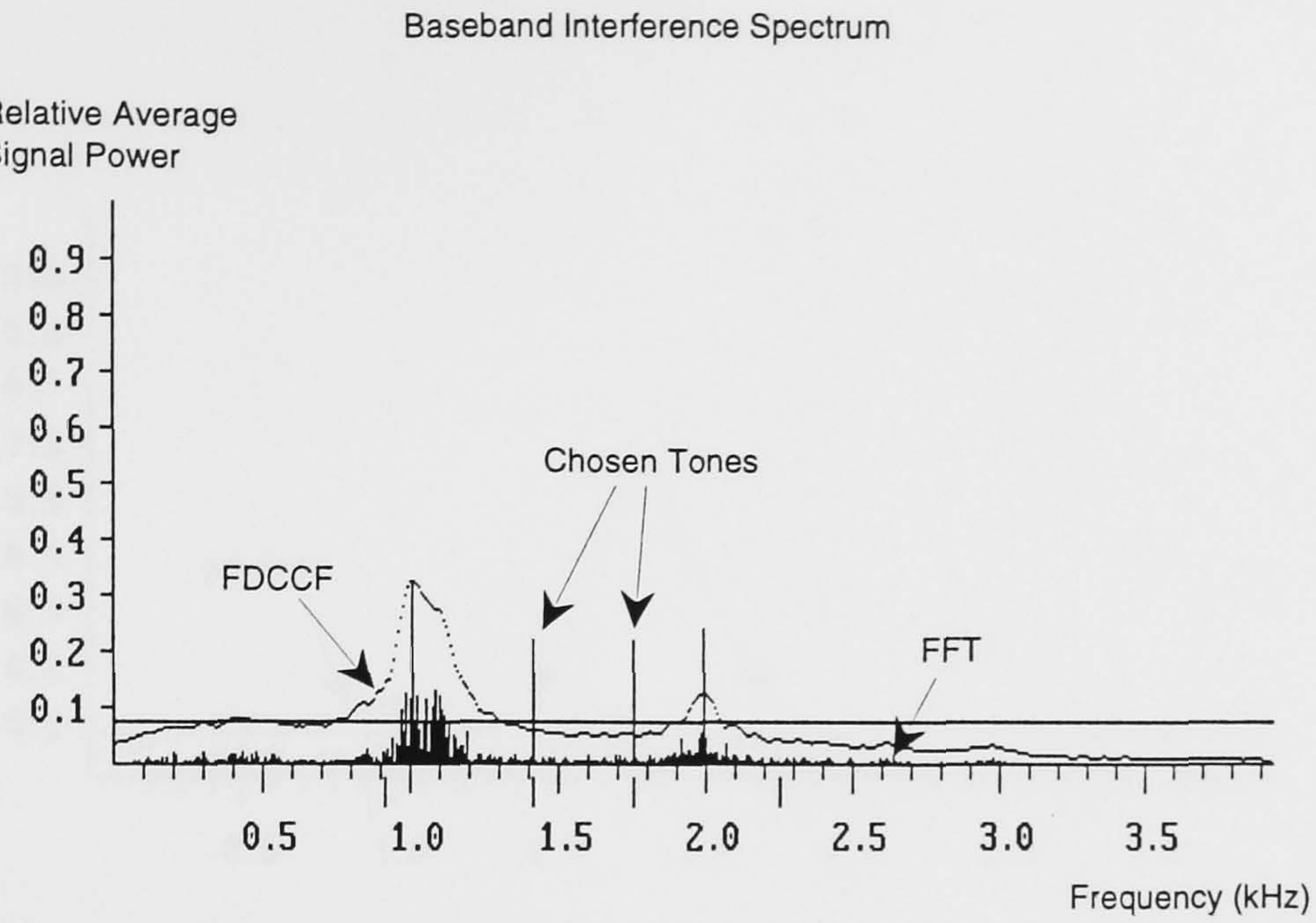

Figure 7.20: Interference Spectrum: Fading Co-Channel Interference

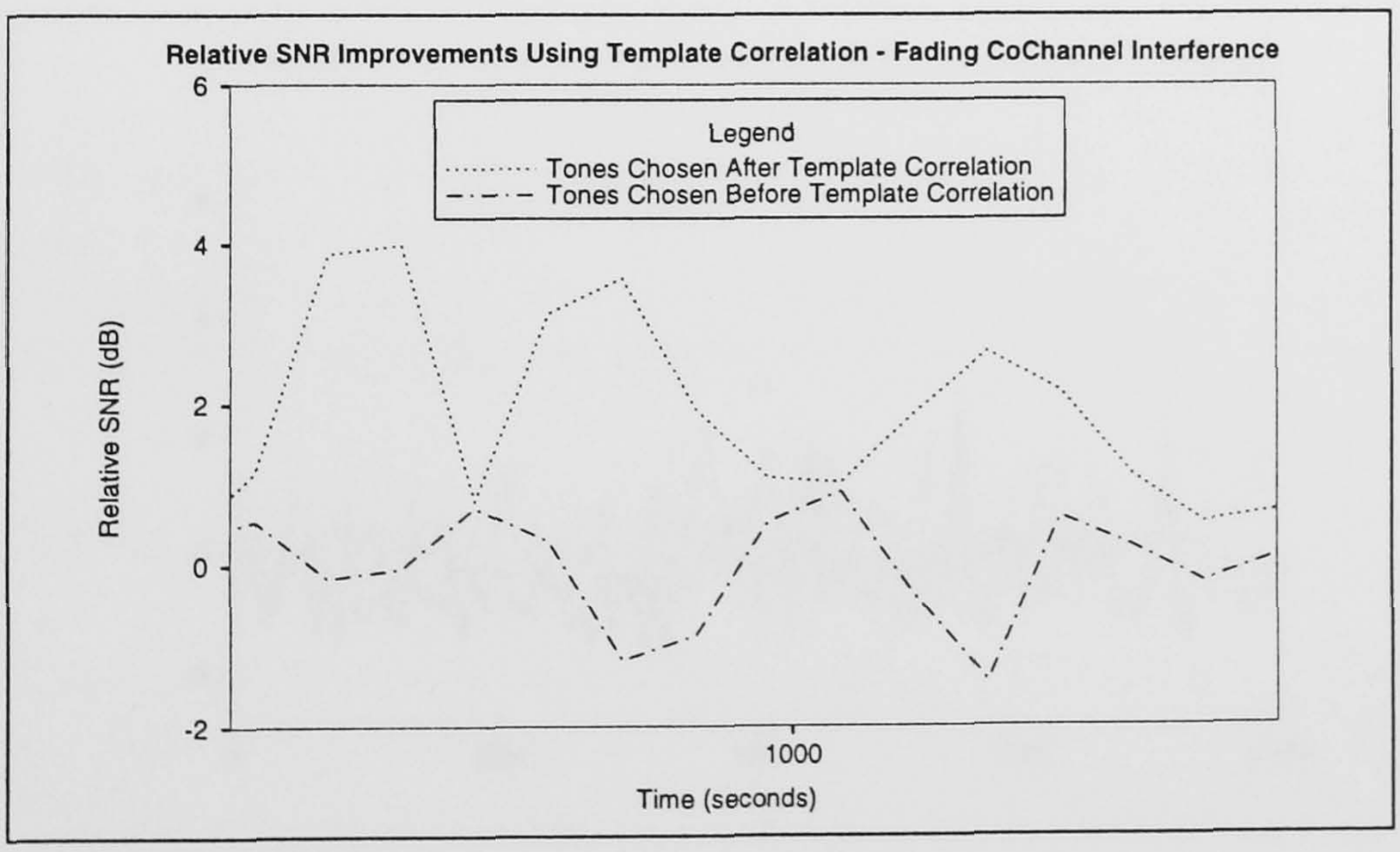

Figure 7.21: Template Correlation: Fading Co-Channel Interference

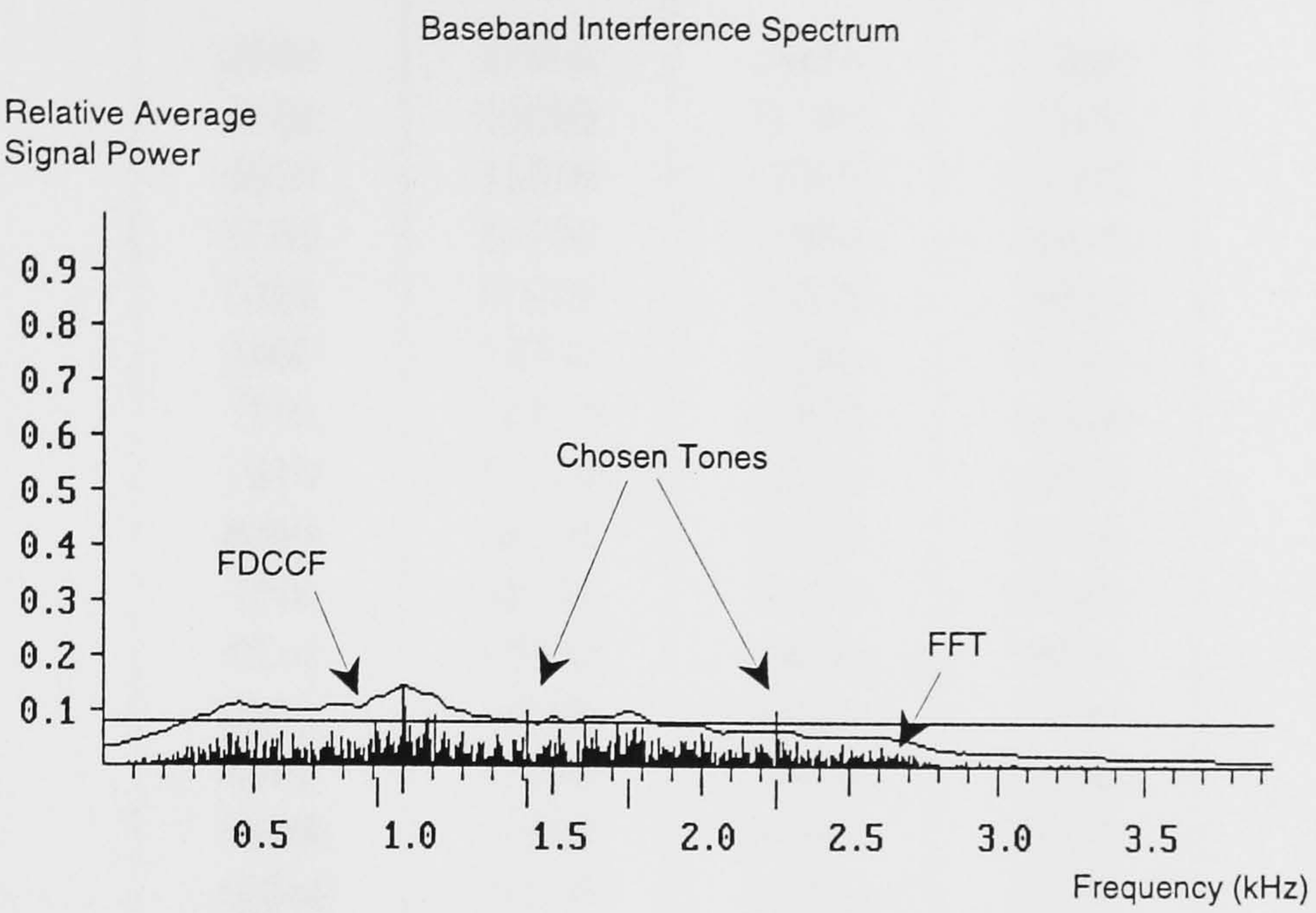

Figure 7.22: Interference Spectrum: No Co-Channel Interference

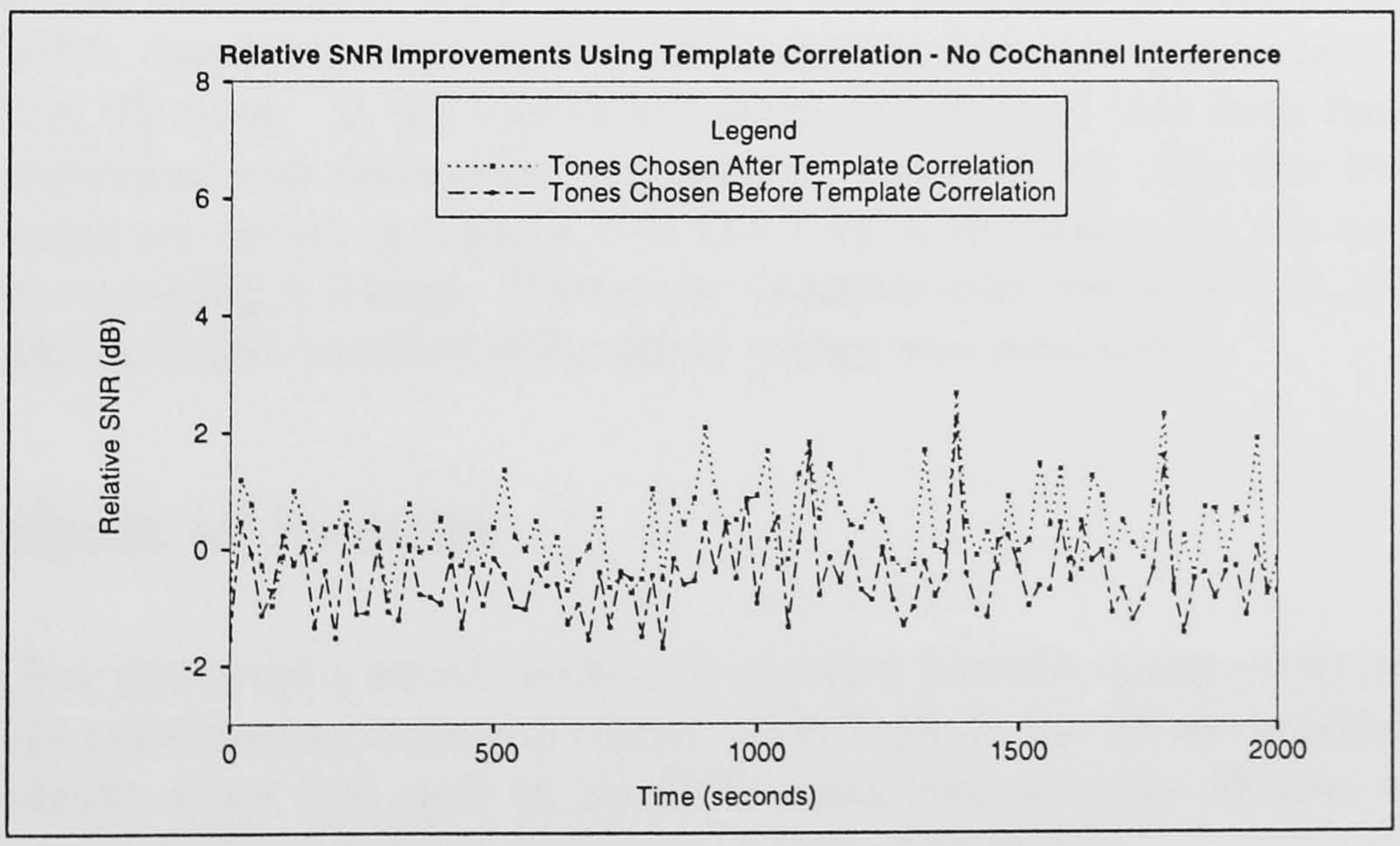

Figure 7.23: Template Correlation: No Co-Channel Interference

Channel Frequency (kHz)	Channel Frequency (kHz)	Channel Frequency (kHz)	Channel Frequency (kHz)
2500	10900	16450	22500
3000	11000	17150	23000
4050	11500	17600	23300
5150	11750	17850	23900
6250	12000	18000	24000
6400	12250	18200	24800
7500	12700	18400	24900
7650	13100	18550	25000
8000	13350	18900	25550
8300	13750	19100	26200
8750	13900	19650	26950
9000	14000	19900	27000
9800	14200	20000	27800
10000	14300	20400	28250
10050	14750	20950	28750
10200	15150	21400	29000
10550	15900	21700	29250
10850	16350	22000	29500

Table 7.1: The example frequencies for the Channel Selection and Optimisation Trial

entirely using DSP devices and a standard HF radio receiver. The results of the two sorts are shown in Table 7.2 and Table 7.3.

It can be seen that the initial sort provides the ten best propagating frequencies between 13 MHz and 20 MHz. The initial random frequency selection provided frequencies that spanned the whole of the HF band. At the second sort stage, the channel with both the best overall interference structure, and favourable propagation, was selected. The two best channel's impulse responses are shown in Figures 7.25 and 7.26 to illustrate that the mode selection algorithm was operating correctly. These two channels also correspond to the frequency range where the strongest received chirp signal energy was measured.

7.5 Analysis of Results

This chapter has presented a set of results, all of which provide strong evidence that DSP-based frequency management tools can operate effectively in the HF environment. Furthermore, these results show that each of the DSP-based tools provide efficient and effective digital alternatives to the currently available analogue techniques.

The results also demonstrate the performance of the two basic elements of a classical frequency management architecture, i.e. channel selection and channel optimisation. In the digital channel selection system, appropriate processing of the impulse response data provided by the active sounder and passive Chirpmonitor provides a set of candidate channels.

Channel Number	Channel Frequency (kHz)	Average FFT Level (mW)
0	19650	89.65
1	18400	90.41
2	16450	111.37
3	15900	111.19
4	14750	117.04
5	18900	69.51
6	13100	99.80
7	18850	96.37
8	19900	98.00
9	20400	89.83

Table 7.2: Channels sorted according to single mode propagation

Channel Number	Channel Frequency (kHz)	Average FFT Level (mW)
5	18900	69.51
0	19650	89.65
9	20400	89.83
1	18400	90.41
7	18850	96.37
8	19900	98.00
6	13100	99.80
3	15900	111.19
2	16450	111.37
4	14750	117.04

Table 7.3: Channels resorted according to average interference level

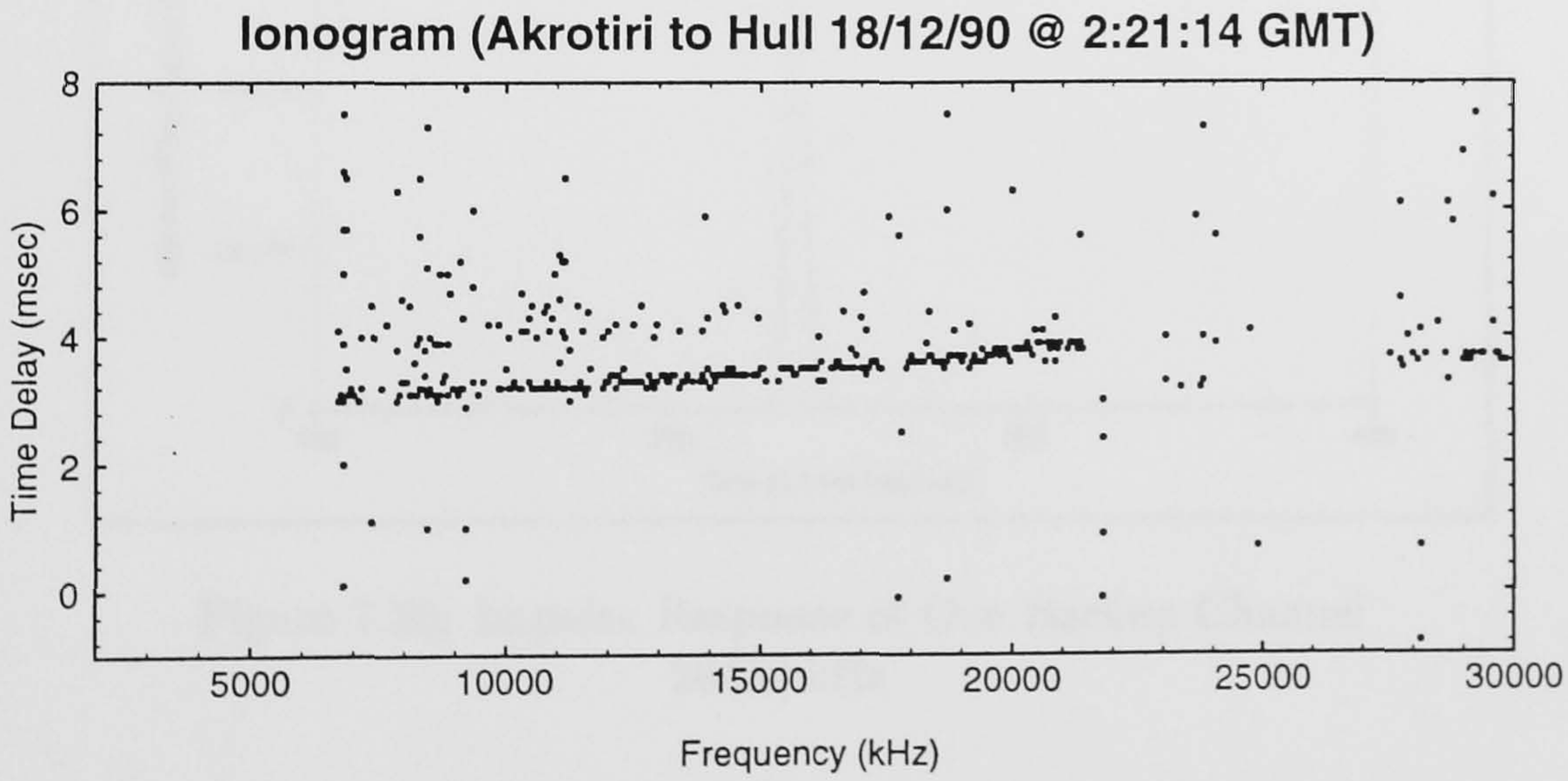

Figure 7.24: Chirpmonitor Output: Akrotiri - Cobbett Hill

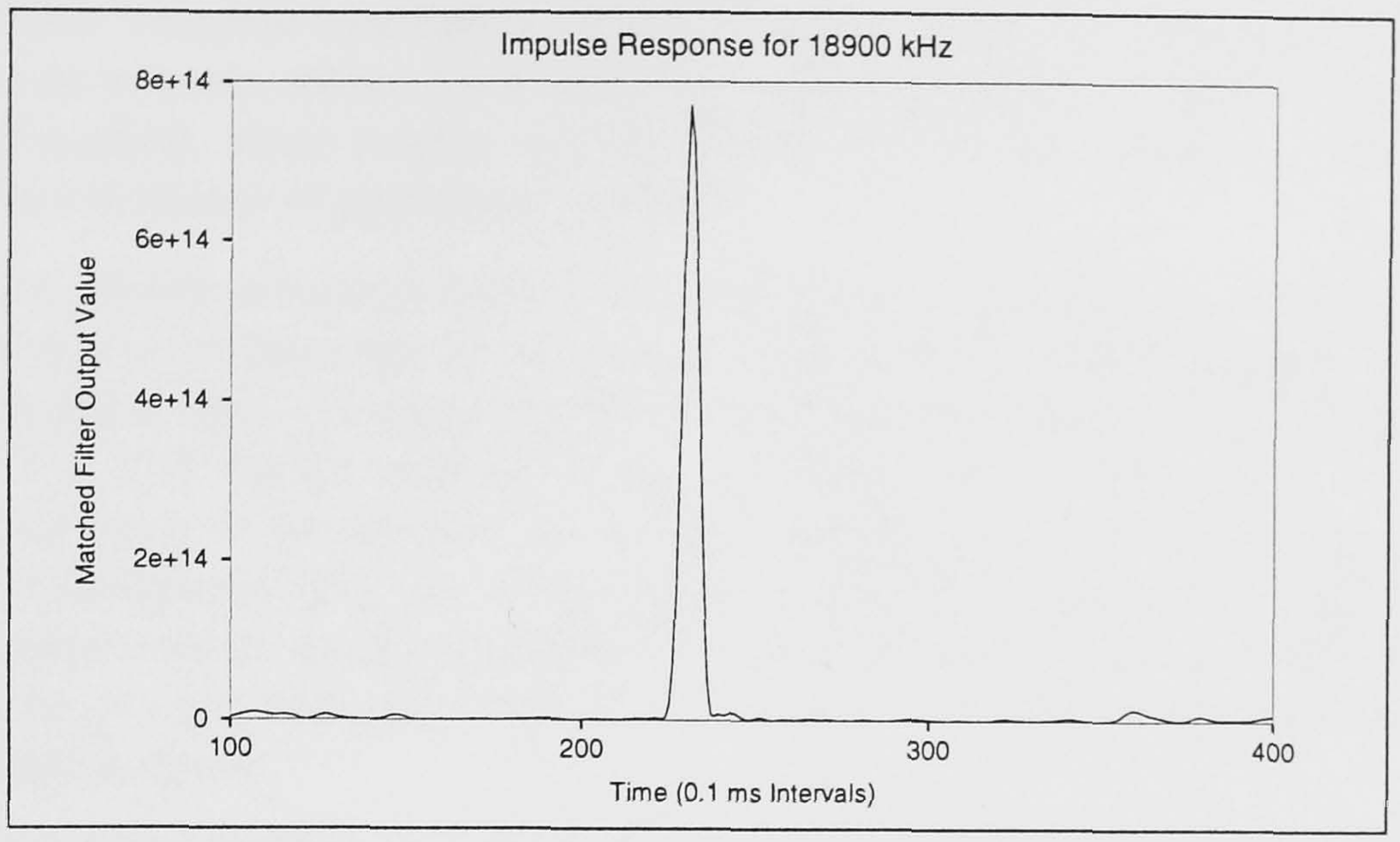

Figure 7.25: Impulse Response of the Best Channel
18900 kHz

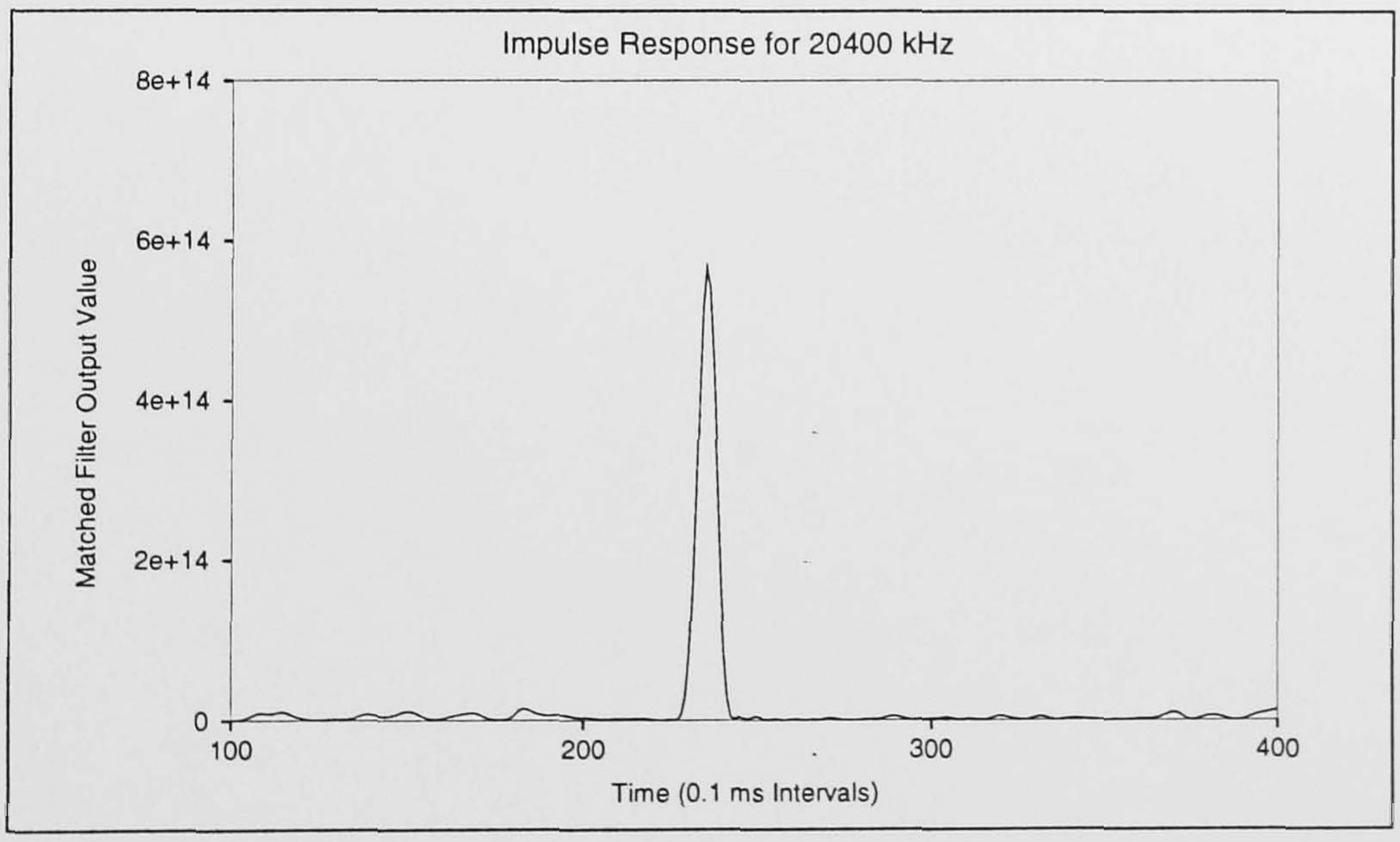

Figure 7.26: Impulse Response of One Backup Channel
20400 kHz

It should be noted that the active sounder would only be utilised when passive propagation estimates are not adequate for the path of interest. Channel optimisation should be undertaken after examination of the interference spectrum. This process would be an enhancement of the template correlation procedure presented here; the templates would be for a range of modem types, rather than the FEK modem utilised by HDRS alone. However, for a simple terminal, these results confirm that a channel can be selected and optimised according to a simple set of predefined criteria.

Comparing the results obtained against the performance specification outlined in Section 4.5, it can be seen that the research programme addressed most of the issues and produced results that suggest that it is possible to use DSP-based frequency management tools in the context of a DSP-based terminal of the type described in this thesis. However, the trials conducted need to be extended to address modem types other than the simple FEK modem. An investigation into the use of MFSK within the terminal has been started and is being complemented by an investigation into the 'figure-of-merit'. However, further trials are necessary to prove conclusively that the techniques developed can be applied to a wider set of transmission types.

The use of the chirp monitor tool has been extremely successful and illustrates the great benefit of the Chirpsounder network in setting up and managing HF links. Since the Chirpsounder network is outside the control of the project, further development the active sounder will be important in order to assess links where access to a proprietary Chirpsounder is not available.

The final chapter concludes the thesis and outlines areas where future work could be usefully undertaken.

Chapter 8

Recommendations for Future Work and Concluding Remarks

This final chapter presents the conclusions from the research programme and details briefly areas where additional research could be usefully undertaken.

8.1 Recommendations for Future Work

This section detailing briefly the future work that could be usefully undertaken as a result of this research programme.

8.1.1 Improvements to the Channel Selection System

The channel selection system developed does not use an accurate timing source when generating the timebase for the ionograms. Therefore, the image tends to drift on the screen and sometimes synchronisation is lost. To mitigate these effects, an accurate timing source should be incorporated. Suitable sources are Rugby MSF, HF timing signals, an accurate crystal and the Global Positioning System (GPS).

The active sounder investigation should be extended; the use of a more accurate timing reference would also be beneficial for this purpose. The active sounding system should investigate the maximum allowable frequency spacing of the sounding channels. This is important in reducing the spectral occupancy of the chirp signal, consequently improving the EMC (electromagnetic compatibility) of the system in terms of unwanted spectral pollution. Similarly, channel spectral occupancy should be investigated via an exhaustive search of the window types used to optimise peak-sidelobe performance.

Finally, a useful combined frequency management tool could be developed by integrating the chirp monitoring system with a propagation prediction system, e.g. CCIR 894 model. This would allow the measured and predicted propagation to be compared directly, and on-line modifications to model parameters made in light of measured channel states.

8.1.2 Improvements to the Channel Optimisation System

The current system uses a simple averaged FFT to gather statistics on the co-channel noise/interference. This approach takes only limited account of the time-varying nature of the noise/interference. Therefore, the investigation should be extended to include time-frequency plots of the noise/interference. This approach would allow the results to be displayed in a more precise format structure and consequently to be processed in a way that might yield further improvements.

The channel optimisation system has concentrated on improving the operation of (M-ary) FSK. This should be extended to other modulation types, for example a serial-tone modem.

8.1.3 System Integration

Although the individual systems od 8.1.1 and 8.1.2 have been combined into a prototype DSP-based terminal, this integration is relatively crude and unsophisticated. Any future project should address this problem more comprehensively. At this stage, the performance characteristics of the integrated terminal could usefully be measured and compared and contrasted against other available frequency management systems.

8.2 Novel Work

This thesis has described a research project that has resulted in the following novel contributions to engineering knowledge and practice:

(i) The propagation monitoring system to enable accurate real-time channel selection, proposed and prototyped in a previous project, has been extended to a stage where complete ionograms can be displayed. These ionograms have been validated against those obtained from standard proprietary equipment. The equipment developed has been termed the "Chirpmonitor".

(ii) DSP-based sounding techniques have been developed to a stage where an 'in-band' sounding system based upon SSFM has been constructed and tested. This sounding system uses digitally generated sounding profiles that can potentially be adapted to changes in the operational environment or user requirements. The system uses the same baseband and RF equipment as is employed for communication purposes;

(iii) Construction of a real-time demonstrator of the channel optimisation system based on the use of the template correlation algorithm has been demonstrated. This demonstrator can generate optimised in-band frequency selections for any fixed-raster modem, or suggest a suitable split raster for an adaptive software DSP-based modem.

(iv) A combined channel selection and optimisation process, termed the 'figure of merit' has been investigated. This empirical algorithm offers the possibility of enhanced frequency management processes based on passively and/or actively

generated channel and propagation statistics, coupled with knowledge of available transmission formats. It is anticipated that this type of algorithm will be one of the requirements for the next stage of development of adaptive and automatic HF radio systems.

(v) A generic architecture for HF radio system terminals has been proposed. This architecture is the host for the software-tools above; each of the software-tools can operate on the same hardware platform. This system departs from the philosophy and implementational techniques inherent in traditional HF system designs and operational requirements.

8.3 Concluding Remarks

The general conclusions that can be drawn from this research programme are that the frequency management process can be specified in a way that makes computer-based automation possible. Furthermore, the use of digital signal processing can provide substantial benefits when applied to HF systems. The introduction of such signal processing enables complex environmental analysis to be undertaken in real-time; the data can then be made available to a frequency management system.

The following sections outline the conclusions specific to each of the key areas addressed by this thesis.

8.3.1 Channel Selection Systems

The linear FM (chirp) DSP-based receiving system can compile reasonable quality ionograms from analysis of the segmented signals received. These have been compared with those from a proprietary system (Barry Research) and similar results were obtained when the same antenna was used. The advantage of this system over the Barry receiver is that the data produced is in a format which can be used directly by the frequency management system since the propagation monitoring tool is an integral part of the system.

Similarly, the active sounding system can be used to generate accurate propagation estimates over a given communication path. The reduced spectral occupancy does not seriously degrade system performance in comparison with the Barry Chirpsounder. The system has an appropriate accuracy for measuring the impulse responses of allocated channels in order to assess the impact of frequency selective fading and inter-symbol interference.

Furthermore, in both the passive receiver and the active sounder the channel selections are made using the same radio equipment and antennas as used for communication purposes. This increases the applicability of the measurements in comparison with the situation where a separate RTCE system is employed.

8.3.2 Channel Optimisation System

The template correlation system has been demonstrated to provide a substantial performance gain when used by a fixed format modem in the presence of co-channel interfer-

ence. The template correlation system has been designed primarily to be interfaced with a frequency-agile modem. The system developed here provides a list of the tone positions that can be used by splitting the tone raster and directing the energy towards regions of low noise/interference in the measured spectrum. This procedure has been shown to be efficient in simulation trials.

8.3.3 Figure of Merit (FOM)

The investigation into the figure of merit (FOM) showed that the fundamental factors affecting system performance can be related directly to the channel scatter function. This scatter function is a mathematical model of the dispersion effects on a channel. A set of simplifications to the process of analysing and using the scatter function has been presented and simulated. The FOM concept needs to be investigated further in any future project to increase the precision of the model data.

8.3.4 System Implications

As already detailed, the use of digital signal processing techniques can benefit HF systems in many ways. In order, to exploit such benefits, a new system architecture has been proposed and demonstrated. The system architecture allows the system to be reconfigured to meet different specifications. Furthermore, the system architecture partitions the embedded computational processes into those suited to signal processing and those more suited to implementation on a general purpose computer.

8.3.5 Specifications

Most of the specifications outlined in Chapter 3 have been met. In those cases where the programme deviated from the specification other aspects have been developed. It is believed that all the tools resulting from this project are in a state where development of a system meeting all the specifications and providing a means of adaptive HF communication is now possible.

8.4 Final Remarks and Acknowledgements

Finally, a goal of the project set initially by Roke Manor Research Ltd., was that of demonstrating the frequency management sub-system technology to interested parties, both within the Siemens organisation and potential customers; this has a been achieved. Both template correlation and chirpmonitor tools have been demonstrated to interested UK companies and Governmental organisations over the period of the project. This has resulted in the chirpmonitor being used as a benchmark for a comparing the frequency management decisions taken by a proposed proprietary HF system. In addition, two new research projects further developing the work described in this thesis have been started. The first of these projects will build an HF terminal incorporating all of the tools described in this project; the other will develop an ionogram labelling system integrated with the chirpmonitor tool.

I wish like to use the final paragraph to reiterate my thanks to SERC, Roke Manor Research, Siemens Plessey Systems, DRA, the University of Hull and all those people that have contributed to making this research possible. I acknowledge the contribution of my supervisor, Professor Mike Darnell for his support and direction, and other members of the communications research group for their encouragement in making the programme both rewarding and enjoyable.

References

Aarons, J., & Grossi, M. D. 1986. Measurements of HF propagation parameters for real-time channel evaluation (RTCE) systems. *In: AGARD LS-145 on 'Propagation impact on modern HF communication system design'.*

Altes, Richard A. 1967. Doppler and acceleration tolerances of high gain wideband linear FM correlation sonars. *Proc. IEEE*, **55**, 627–636.

Altes, Richard A. 1990. Radar/sonar acceleration estimation with linear-period modulated waveforms. *IEEE Trans. Aerospace & Electronic Systems*, **AES 26**(6), 914–923.

Arthur, P. C., Dickson, A. H., & Cannon, P. S. 1991. ROSE–A high resolution, amplitude-coded, high frequency oblique ionosonde. *AGARD Conf. on 'Remote Sensing of the Propagation Environment'*, **CP-502**(October), 10.1–10.7. Çeşme, Turkey.

ATT. 1988. *WE DSP32C Digital Signal Processor.*

Barry, G., & Fenwick, R. B. 1975. Techniques for real-time HF channel measurements and optimum data transmission. *AGARD Conf. on 'Radio systems and the ionosphere'*, **CP 173**, 15.1–15.10. Athens, Greece.

Barry, G.H. 1966. Oblique chirp sounding. *AGARD Conf. on 'Ionospheric oblique radio wave propagation at frequencies near the lowest usable frequency'*. Leicester, UK.

Bayley, D., & Ralphs, J. D. 1972. PICCOLO 32-tone telegraph system in diplomatic communications. *Proc. IEE*, 1229–1236.

Beamish, W. L. 1994. Trends and designs considerations in automated high speed HF data systems. 6^{th} *IEE Int. Conference on 'HF radio systems and techniques'*, **CP-392**.

Bello, P. A. 1963. Characterisation of randomly time-variant linear channels. *IEEE Trans. on Communication Syst.*, **CS-11**(December), 360–393.

Bello, P. A. 1965. Some techniques for the instantaneous real-time measurement of multipath and Doppler spread. *IEEE Trans. on Communication Tech.*, **13**(3), 285–292.

Brookner, E. 1969. The performance of FSK permutation modulations in fading channels and their comparison based on a general method for the comparison of M-ary modulations. *IEEE Trans. on Communication Technology*, **COM-17**(6), 616–639.

Cadzow, J. A. 1982. Spectral estimation: an overdetermined rational model equation. *Proc. IEEE*, **70**(September), 907–938.

CCIR. 1970. *CCIR Report No. 252.* ITU, Geneva.

CCIR. 1982. *CCIR Report No 571.* ITU, Geneva.

CCIR. 1986a. *CCIR Report No 894: An empirical HF prediction model.* ITU. Geneva.

CCIR. 1986b. *Real-time channel evaluation of ionospheric radio circuits.* Tech. rept. ITU, Geneva. CCIR Report No. 889.

Chesmore, E. D. 1991. Artificial Intelligence techniques in HF system design. 5^{th} *IEE Int. Conf. on 'HF radio: systems and techniques'*, **CP-339**(July).

Cook, C. E., & Bernfeld, M. 1967. *Radar signals—an introduction to theory and application.* New York: Academic Press.

Cooley, J.W., Lewis, P., & Welch, P.D. 1967. Historical notes on the Fast Fourier Transform. *IEEE Trans. Audio and Electroacoustics*, **AU-15**(June), 79–79.

Crepeau, P. J. 1992. Uncoded and coded performance of MFSK and DPSK in Nakagami fading channels. *IEEE Trans. Communications*, **COM-40**(3), 487–494.

Daehler, M. 1984. A FOT prediction procedure for HF communications frequency management. *Proceedings of 1984 IEEE Conf on 'Military Communications'—MILCOM '84*, 8.1.1–8.1.5.

Darnell, M. 1975a. Adaptive signal selection and its practical implications in communications system design. *AGARD Conf. on 'Radio systems and the Ionosphere'*, **CP-173**. Athens.

Darnell, M. 1975b. Channel estimation techniques for HF communications. *AGARD Conf. on 'Radio systems and the ionosphere'*, **CP-173**. Athens.

Darnell, M. 1978. Channel evaluation techniques for dispersive communication paths. *In:* Skwirynski, J. K. (ed), *Communication systems and random process theory.* The Netherlands: Sijthoff and Noordhoff.

Darnell, M. 1981. The characteristics of HF propagation and their implication in digital system design. *Proceedings of the 2nd IEE International Conf. on 'Antennas and Propagation' (ICAP 81)*, **CP-195**.

Darnell, M. 1982. An HF data modem with in-band frequency agility. *Proc. II Int. Conf on "Recent advances in HF communications systems and techniques"*, **CP 206**.

Darnell, M. 1983. Real-time channel evaluation. *In: AGARD LS-127 on 'Modern HF communications'.*

Darnell, M. 1986a. The design of static and mobile HF communication systems. *In: AGARD LS-145 on 'Propagation impact on modern HF communication system design'.*

Darnell, M. 1986b. Embedded real-time channel evaluation techniques. *In: AGARD LS-145 on 'Propagation impact on modern HF communication system design'.*

Darnell, M., & Honary, B. 1991. Real-time channel evaluation techniques. *Proc. of 1st Int. Symposium on 'Communications: Theory and Techniques'*, September. Published by HWC Ltd.

Darnell, M., Honary, B., Clark, P. D. J., Maundrell, M., & Vongas. G. 1992. Adaptive DSP-based MFSK modems for HF aeromobile channels. *Proc. IEEE Conf. 'Military Communications' MILCOM*, October, 46.4.1–46.4.5.

Davies, K. 1990. *Ionospheric radio.* IEE Electromagnetic Wave Series 31. Peter Peregrinus.

Dickson, A. H., Arthur, P. A., & Cannon, P. S. 1991. ROSE—A DSP enhancement to the Barry ionospheric sounder. 5^{th} *IEE Int. Conf. on 'HF radio: systems and techniques'*, **CP-339**(July).

El-Shennawy, K., Alim, O. A., & Ezz-El-Arab, M. A. 1987. Linear FM chirp filters in pulse compression radars. *IEEE Trans. Ins & Measurement*, **IM-36**(3), 783–788.

Elvy, S. J. 1985. A design for an automatic HF radio system. *Radio Science*, **20**(3), 261–268.

Fowle, Evert N. 1964. The design of FM pulse compression signals. *IEEE Trans. Info. Theory*, January, 61–67.

Gallagher, M., & Darnell, M. 1990. Performance of a template correlation system for in-band spectrum management. 5^{th} *IEE Int. Conf. on 'Radio receivers and associated systems'*, **CP-325**(July), 212–217.

Gallagher, M., & Darnell, M. 1991. Propagation and interference measurements for use in real-time frequency management. 7^{th} *IEE Int. Conf. on 'Antennas and propagation' (ICAP)*, **CP-333**(April), 2.794–2.799.

Gallagher, M., Bennett, S. A. W., Darnell, M., & Honary, B. 1994. Architectures for advanced radio systems incorporating network and frequency management. 6^{th} *IEE Int. Conf. on 'HF Radio: Systems and Techniques'.*

Goldberg, B. 1966. 300-30 MHz MF/HF. *IEEE Trans. Communication Technology*, **COM-11**(6), 767–784.

Goldman, S. 1953. *Information Theory.* New-York: Prentice-Hall International.

Goodman, J. M. 1992. *HF communications: science and technology.* Van Nostrand Reinhold.

Goodman, J.M., & Daehler, M. 1988. The use of oblique-incidence sounders in HF frequency management. *Proc.* 4^{th} *IEE Int. Conf. on 'HF radio: systems and techniques'*, **CP-284**.

Gott, G. F., & Staniforth, M. J. D. 1978. Characteristics of interfering signals in aeronautical HF voice channels. *Proceedings of the IEE*, **125**(11).

Gott, G. F., Dutta, S., & Doany, P. 1983. Analysis of HF interference with application to digital communications. *IEE Proceedings-Pt. F*, **130**(5), 452–458.

Gott, G. F., Poole, C. R., Laycock, P. J., & Ray, A. R. 1991. Spectral occupancy — measurement and mathematical models. *Proc. 5th IEE Int. Conf. on "HF radio: systems and techniques"*, **CP-339**.

Gott, G. F., Chan, S. K., Pantjiaros, C., Brown, J., Laycock, P. J., Broms, M., & Boberg, S. 1994. Recent work on the measurement and analysis of spectral occupancy at HF. 6^{th} *IEE Int. Conference on 'HF Radio Systems and Techniques'*, **CP-392**.

Hall, M.P.M., & Barclay, L.W. 1990. *Radiowave Propagation.* London: Peter Perigrinus.

Hargreaves, J. K. 1979. *The upper atmosphere and solar-terrestrial relations.* New York: Van Nostrand Reinhold.

Harris, F. J. 1978. On the use of windows for harmonic analysis with the discrete Fourier transform. *Proc. IEEE*, **66**(1), 51–83.

Hlawatsch, F., & Boudreaux-Bartels, G.F. 1992. Linear and quadratic time-frequency signal representations. *IEEE Signal Processing Magazine*, April.

Hunsucker, R. D. 1990. *Radio techniques for probing the terrestrial ionosphere.* New-York: Springer-Verlag.

Hunsucker, R. D., & Bates, H. F. 1969. Survey of polar and auroral region effects on HF propagation. *Radio Science*, 4, 347–365.

IPS. 1991. *ASAPS: Advanced Stand-Alone Prediction System.* Ionospheric prediction service, radio and space services, P.O. Box 1548, Chatswood, NSW 2057, Australia. (Brochure).

Jenkins, G. M., & Watts, D. G. 1968. *Spectral Analysis and Its applications.* San Francisco: Holden-Day.

Jourdain, G., & Tziritas. 1984. Communication over fading, dispersive channels, optimal receivers and signals. *Signal Proc.*, 3–25. North-Holland.

Jowett, A. P. 1989. *Embedded Frequency Management for HF Systems.* Ph.D. thesis, Dept. Electronic Engineering, University of Hull, Hull, HU6 7RX.

Jowett, A. P., & Darnell, M. 1987. Automatic channel selection using template correlation. *Elec. Letts.*, **23**(22), 1209–1211.

Jowett, A.P. 1987. Artificial Intelligence in HF communication systems. *AGARD Conf. on 'Effects of electromagnetic noise and interference on performance of military radio communication systems'*, **CP-420**, 14.1–14.25. Lisbon, Portugal.

Jowett, A.P., Darnell, M., & Riley, N. G. 1989. Passive monitoring of chirpsounder transmissions as an aid to HF frequency management. *Proc of IEE Colloquium on 'Adaptive HF Management'*, **1989/33**(March), 1.1–1.5. London, UK.

Kay, S. M. 1980. A new ARMA spectral estimator. *IEEE. Trans. Acoustics, Speech and Signal Processing*, **ASSP-28**, 585–588.

Kay, S. M., & Marple, S. L. Jr. 1981. Spectrum analysis: a modern perspective. *Proc. IEEE*, November, 1380–1419.

Kennedy, R. S. 1969. *Fading, Dispersive Communication Channels.* New York: Wiley.

Kramer, S. A. 1967. Doppler and acceleration intolerances of high-gain wideband linear FM correlation sonars. *Proc. IEEE*, **55**(June), 1535–1536.

Kroszczyński, Jan J. 1969. Pulse compression by means of Linear-Period Modulation. *Proc. IEEE*, **57**(7), 1260–1266.

Laycock, P. J., Morrell, M., Gott, G. F., & Ray, A. R. 1988. A model for HF spectral occupancy. *Proc. 4th IEE Int. Conf. on "HF radio: systems and techniques"*, **CP-284**.

Masrani, K. D., & Riley, N. G. 1990. Passive monitoring techniques for HF radio signals in determining multi-path. *IEE Colloquium Digest on 'Methods of combatting multi-path'*, January.

Masrani, K. D., & Riley, N. G. 1991. Use of passive monitoring techniques in HF radio systems. 5^{th} *IEE Int. Conf. on 'HF radio: systems and techniques'*, **CP-339**(July).

Massaro, M. J. 1975. Error Performance of M-ary Noncoherent FSK in the Presence of CW Tone Interference. *IEEE Trans. Communication Technology*, November, 1367–1369.

Matshushita, S. 1959. A study of the morphology of ionospheric storms. *J. Geophys. Res.*, **64**, 305.

McCue, J.J.G. 1979. A note on the Hamming weighting of Linear-FM pulses. *Proc. IEEE*, **67**(11), 1575–1577.

McLarnon, B. D. 1982. Real-time channel evaluation in an automatic HF radio telephone system. 2^{nd} *IEE Int. Conf.on 'HF radio: systems and techniques'.*

Milsom, J. D. 1987. Outstanding problems in Short-Term Ionospheric Forecasting. *IEE Int. Conf on 'Antennas and Propagation' (ICAP 87)*, **CP 274**, 316–319.

Nakagami, M. 1960. the m-distribution–A general formula of intensity of intensity distribution of fading. *In:* Hoffman, W. C. (ed), *Statistical methods in radio wave propagation.* New York: Pergamon.

NATO. 1982. *STANAG 4285 High Speed Serial Tone Modulation.* Tech. rept. SHAPE Technical Centre.

Nii, H. P. 1986. Blackboard Systems. *AI Magazine*, 7(3 & 4).

North, D. O. 1943. An analysis of the factors which determine signal-to-noise discrimination in pulsed carrier systems. *RCA Lab Rpt. PTR-6C.*

Noyes, R. W. 1982. *The Sun.* Cambridge, MA, USA: Harvard University Press.

Peres, M., & Finkelberg, L. 1981. Evaluation of the absorption prediction methods of the CCIR. *CCIR Report*, **XI**. Geneva.

Petrie, L. E. 1986. Adaptive systems in operation. *In: AGARD LS-145 on 'Propagation impact on modern HF communication system design'.*

Proakis, J. G., & Manolakis, D. G. 1992. *Digital Signal Processing: Principles, algorithms and applications.* Maxwell-Macmillan International.

Ralphs, J. D. 1985. *Principles and Practices of Multi-Frequency Telegraphy.* Peter Perigrinus.

Reed, A. P. C., & Hopkinson, J. N. 1988. Adaptive data link protocols: design and performance over automated HF skywave links. 4^{th} *IEE Int. Conf. on 'HF radio: systems and techniques'*, **CP-284**(April), 6–11.

Rhoads, R. L., & Elastrom, M. P. 1968. Removal of intervening system distortion by deconvolution. *IEEE Trans. on Instrumentation and Measurement*, **IM-17**(4), 333–337.

Rihaczek, A. W. 1969. *Principles of high resolution radar.* Mc-Graw Hill.

Rioul, O., & Vetterli, M. 1992. Time-scale energy distributions: a general class extending wavelet transforms. *IEEE Trans. Sig. Proc*, July.

Sailors, D. B., Sprague, R. A., & Rix, W. H. 1986. *MINIMUF-85: An improved HF MUF prediction model.* Tech. Report NOSC-TR1121. Naval Ocean Systems Centre, San Diego, CA.

Salz, J. 1970. Communication efficiency of certain digital modulation systems. *IEEE Trans. on Communication Tech.*, **COM-18**(2), 97–102.

Scholz, J. B. 1988. A real-time knowledge-based system for frequency management in communications. *Proc. Aust. Joint AI Conf. (AI88).*

Schwartz, M. 1981. *Information, Transmission, Modulation, and Noise.* Mc-Graw Hill.

Sell, P. S. 1985. *Expert systems – a Practical Introduction.* London: McMillan.

Silberstein, R. 1959. The origin of the current nomenclature of the ionospheric layers. *Journ. Atmos. Terr. Phys.*, **13**, 382.

Singleton, R. C. 1967. An method for computing the mixed radix fast Fourier transform with auxiliary memory and limited high speed storage. *IEEE Trans. Audio and Electroacoustics*, **AU-15**(June).

Soliman, S. S., & Scholtz, R. A. 1988. Synchronisation over fading dispersive channels. *IEE Trans. Communications*, **COM-36**(4), 499–505.

Speight, T. J. 1991. Nonorthogonal reception of orthogonally transmitted signal sets. *Proc 3rd Bangor Symposium on Communications*, May, 97–100.

Speight, T. J. 1992. *Improved design of distributed HF communication systems involving mobile terminals.* Ph.D. thesis, University of Hull.

Stevens, E. E. 1968. The CHEC sounding systems. *Pages 359–369 of: Ionospheric Radio Communication.* New York: Plenum.

Stremler, F. G. 1992. *Introduction to communication systems.* Addison-Wesley.

Teters, L.R., Lloyd, J. L., Haydon, G. W., & Lucas, D. L. 1983. *Estimating the performance of telecommunications systems using the ionosphere transmission channel.* Report 83-127. National Telecommunication and Information Administration, US Dept. of Commerce, Boulder, CO 80303.

Thrane, E. V. 1986a. Propagation I: State of the art of modelling and prediction in HF prediction. *In: AGARD LS-145 on 'Propagation impact on modern HF communication system design'.*

Thrane, E. V. 1986b. Propagation II: Problems in HF propagation. *In: AGARD LS-145 on 'Propagation impact on modern HF communication system design'.*

Trees, H. L. 1971. *Detection, Estimation and Modulation Theory, Part III.* Wiley.

Tsai, S. 1969. Markov characterization of the HF channel. *IEEE Trans. Communication Tech.*, **COM-17**(1), 24–32.

Turin, G. L. 1960. An introduction to matched filters. *IRE Trans. Info. Theory*, IT-6, 311–329.

Wainstein, L. A., & Zubakov, D. A. 1962. *Extraction of signals from noise.* Prentice-Hall International.

Watterson, C. C., Juroshek, J. R., & Bensema, W. D. 1970. Experimental confirmation of an HF channel model. *IEEE Trans. on Communication Tech.*, **COM-18**(6), 792–803.

Weiner, N. 1949. *Extrapolation, interpolation and smoothing of stationary time series with engineering applications.* New York: Wiley.

Wilkinson, R. G. 1982. A statistical analysis of HF radio interference and its application in communication systems. *Proc. IEE. Int. Conf. on "HF communication systems and techniques"*, **CP-206**, 101–105.

Williams, D. J. S, & Clarke, E. T. 1988. Practical real-time frequency management for automated HF networks. *Proc. 4th IEE Int. Conf. on 'HF radio: systems and techniques'*, **CP-284**.

Wong, N. F., Gott, G. F., & Barclay, L.W. 1985. HF spectral occupancy and frequency planning. *Proc. IEE Pt.-F*, **132**(7), 548–557.

Woodward, P. M. 1953. *Probability and information theory with applications to radar.* McGraw Hill.

Appendix A

Overview of HF Propagation

This appendix is intended to support the discussion in Chapter 2

A.1 Ionospheric Propagation Effects

Ionisation is caused by the sun's energy affecting the uppermost parts of the earth's atmosphere. The ionising radiation strips electrons from the rarefied gases. The ionised plasma that is continuously recreated after the individual electrons and positive ions recombine. The ionised plasma is affected by the terrestrial and solar magnetic fields and gravity forming it into distinct layers of differing ionisation density. These layers were first described in detail by Appleton who gave them the nomenclature E and F (Davies, 1990). However, as more layers have been discovered, the nomenclature has been refined to introduce the F_1 and F_2 layers and the D and C layers (Silberstein, 1959).

The solar-terrestrial interaction is important since solar activity is the predominant source of energy for creating the ionosphere. In particular, it has been discovered that, in addition to the diurnal cycle of effects, an underlying eleven-year cycle, dependent upon the index of solar activity (sun-spot number) is also present (Hargreaves, 1979). A sun spot is a cooler part of the sun's surface that causes an intense amount of hard radiation to be emitted (Noyes, 1982). Solar flares and other solar events in solar storms can also cause the ionosphere to become less stable than usual. This can cause skywave communication to become difficult.

The properties of each ionospheric layer and their approximate height above the earth's surface are well documented (Davies, 1990; Hargreaves, 1979); a schematic of the ionospheric profile is given in Figure A.2. The following list is a precis of the information:

D Layer: this is an absorbing layer that lies in the range 50-80 km above the earth's surface. This layer is only usually apparent in the daytime when greater radiation levels cause it to be formed. It acts as a signal attenuator at HF.

E Layer: This is a refracting (reflecting) layer in the region 90-140 km above the earth's surface produced mainly by soft, solar X-rays. It is at this layer height that sporadic E, E_s, exists.

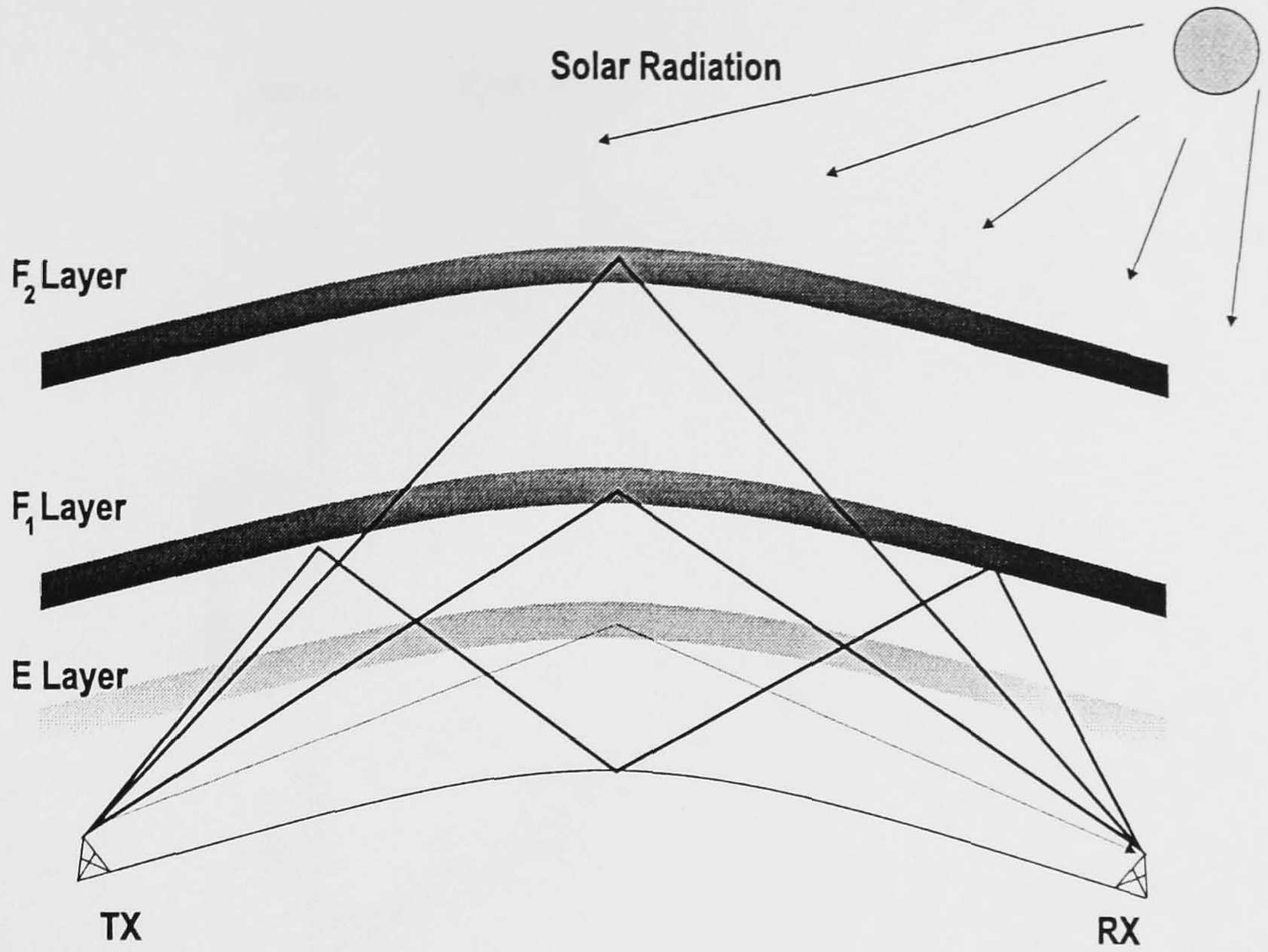

Figure A.1: Ionospheric Skywave Propagation

F Layer: It is in this layer that the peak electron densities occur and the main refractive (reflective) processes exist. This layer is divided into the F_1 and F_2 layers, although the these layers combine at night when ionisation from the sun is reduced. The F layer exists at altitudes above 140 km.

A diagram illustrating the effects that these layers can cause to transmitted signals is given in Figure A.3. It can be seen that a pulse of sufficient energy will be refracted by several of these layers; hence, multipath dispersion is a common phenomenon.

The *D layer* which tends only to exist in the daytime is an important layer for MF broadcasters as they tend to rely on its presence to attenuate skywave interference which will cause the signal to fade at the receiver. This layer is relatively transparent to HF signals (apart from some limiting absorption) and can only be detected with specialised equipment (Davies, 1990). At night, however, the absence of the D layer can cause long distance signals to increase local interference and hence raise the level of the background noise.

The *E layer* is more highly ionised than the D layer and can give rise to refractive processes in the daytime. At night, however, the E layer tends to be much more of an absorber (Hargreaves, 1979). In addition to the normal E layer ionisation, there are patches of higher ionisation density caused by solar effects, termed Sporadic E. These patches of dense ionisation can enable communication links to be established at frequencies far above the normal maximum usable frequency (MUF). However, the presence of Sporadic E can also cause interference on those links not engineered to exploit such a propagation mode. The E region can usually support single hop transmission to a distance of about 2000 km.

The *F layer* which is divided into the F_1 and F_2 layers provides the dominant skywave transmission mode. The F_1 layer exists in daytime at a height of about 200 km, whereas the F_2 layer exists at about 250–450 km. The F_1 layer is not normally significant for

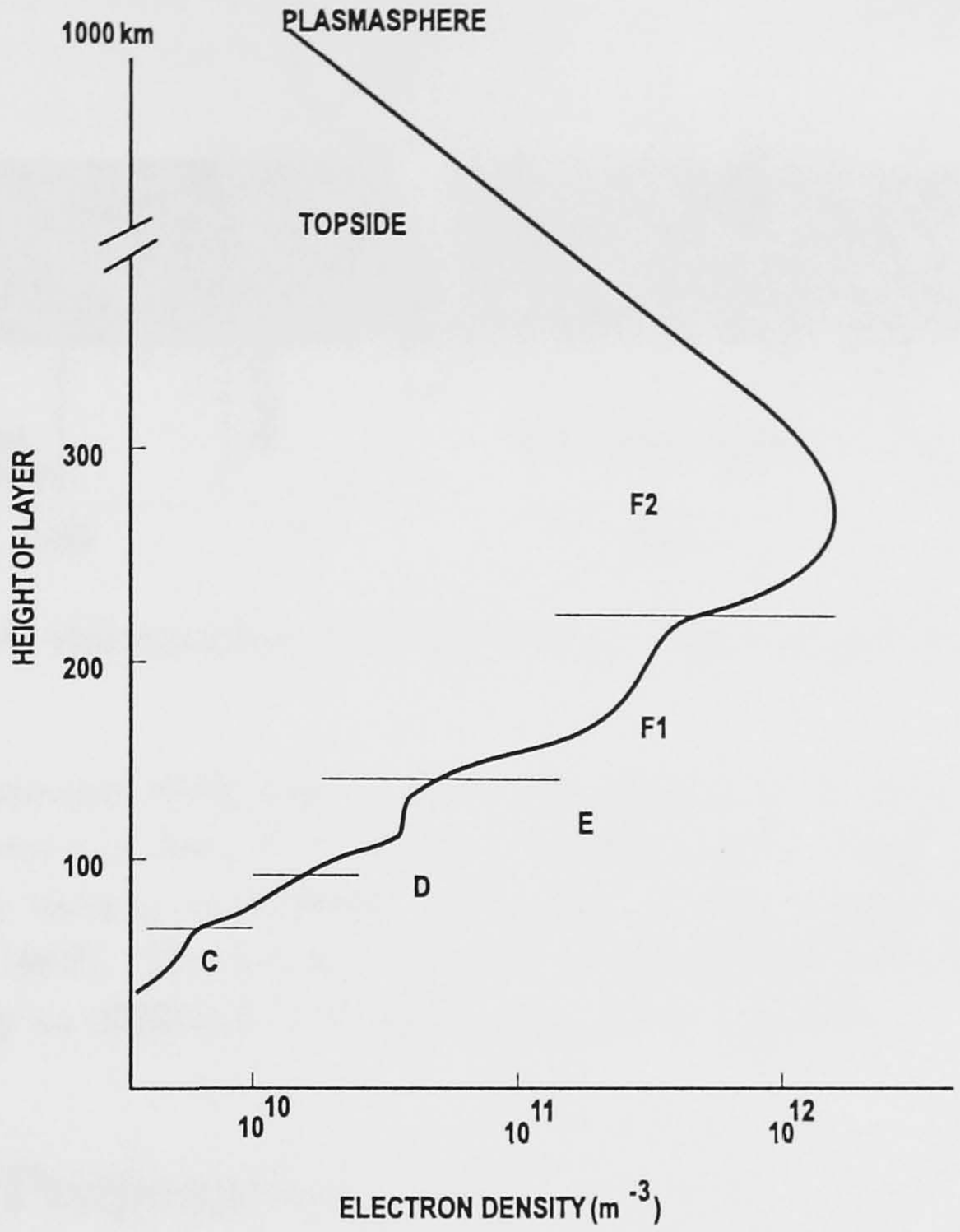

Figure A.2: Ionospheric Structure: Summer's day, Mid-Latitude

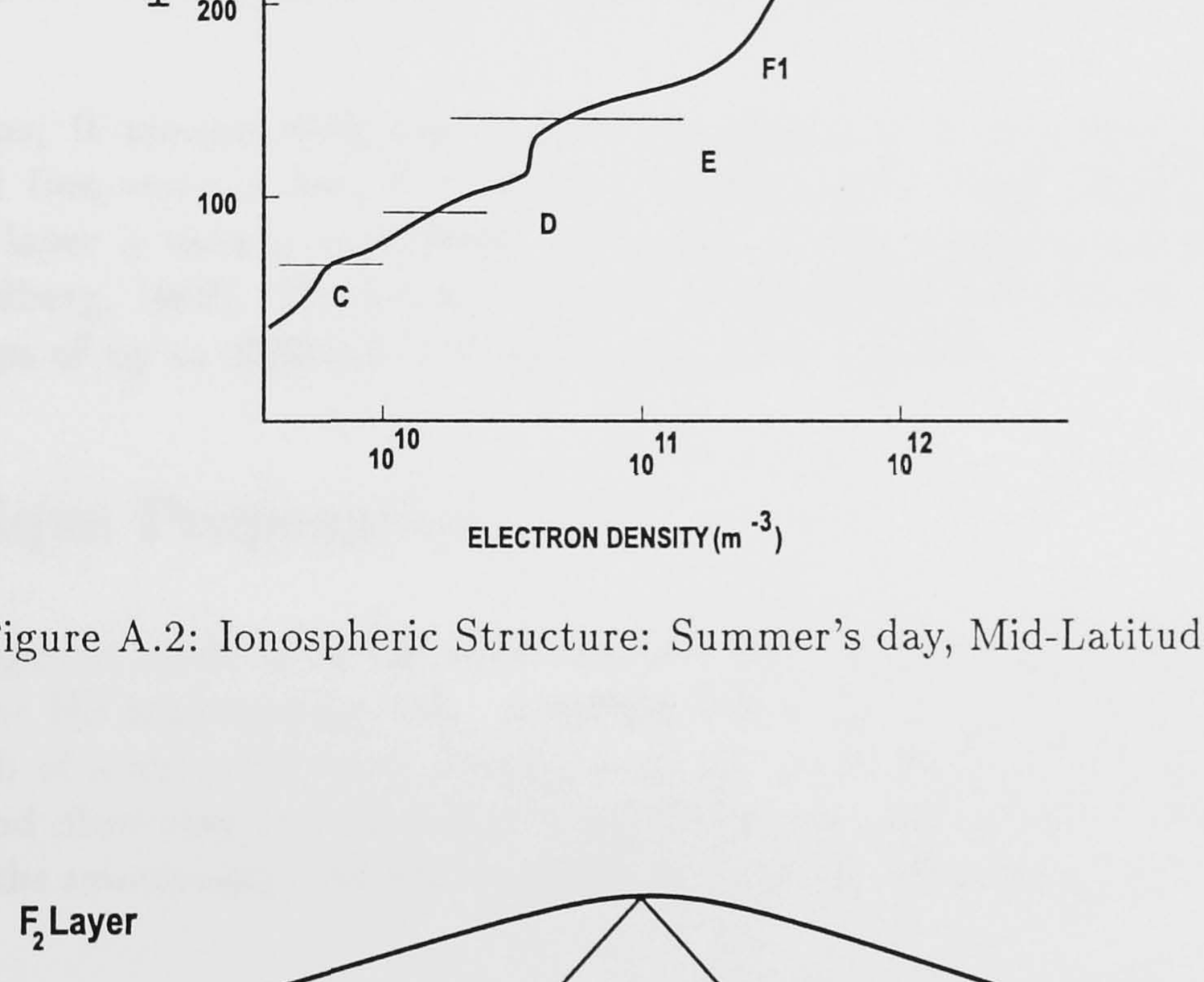

Figure A.3: Plot of the effects of layers in the Ionosphere

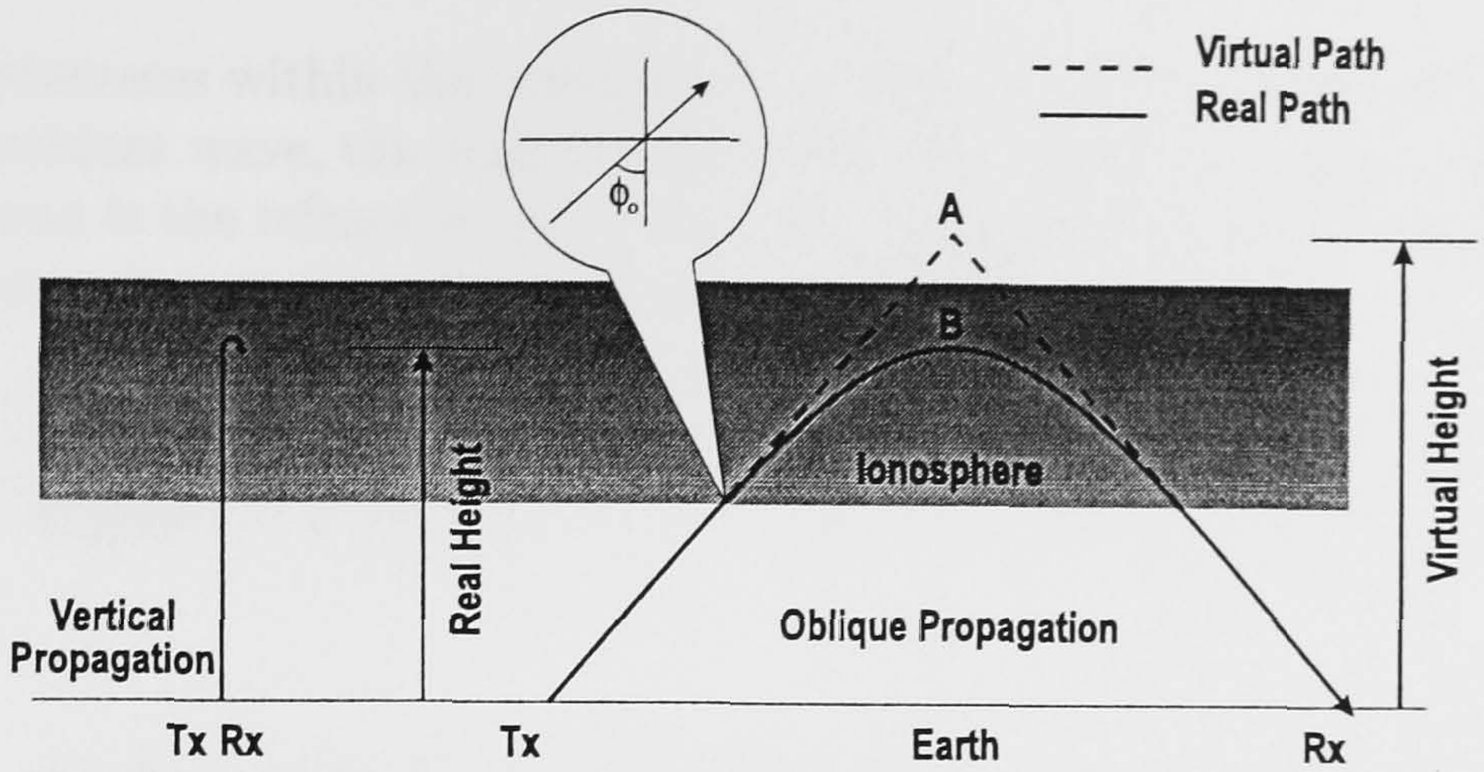

Figure A.4: Relationship between Oblique and Vertical Propagation

communications; it merges with the F_2 layer at night and is only clearly defined when the F_2 critical frequency is low, for example during a solar cycle minimum (Goodman, 1992). The F layer is usually considered as a single entity for communication engineering purposes (Goldberg, 1966). The dense ionisation in the F layer can support communication with single hops of up to 4000 km and frequencies up to 50 MHz.

A.2 Oblique Propagation

Oblique propagation tends to be the normal mechanism for supporting communication over a point-to-point HF transmission link. A stylised link is shown in figure A.4. This diagram shows the path of a refracted wave through a planar ionosphere of constant height. Using Snell's Law, and observing the difference between the real height and the 'virtual' height, it can seen that the relationship between vertical frequency f_v and oblique incidence frequency f_o is:

$$f_o = f_v \sec \phi_o \tag{A.1}$$

where

f_o = oblique incidence frequency;
ϕ_o = incident angle;
f_v = vertical frequency needed to reach virtual height.

This model assumes an ionosphere of constant height and with ionisation that varies with height, but is horizontally uniform. It is clearly incomplete and does not take into account the true nature of the ionosphere. Other models based upon parabolic layers of increasing ionisation are much more accurate. These models are discussed fully in a common set of reference texts (Davies, 1990; Hargreaves, 1979; Thrane, 1986a). These models are used by ionospheric physicists to compare propagation measurements against theoretical predictions.

The refractive processes within the ionosphere are related to the transmitted energy, the frequency of the incident wave, the magnetic field, the electron density and angle of incidence. The key parameter is the refractive index, and the relationship between the refractive index, u, and other parameters is given by the following simplified equation

$$u = \sqrt{1 - \frac{4\pi N e^2}{E_o m \omega^2}} \tag{A.2}$$

where

u = refractive index of the ionospheric medium;
N = electron density;
e, m = charge and mass of electron;
E_o = permittivity of free space;
ω = radian frequency.

The above equation, does not provide the effects induced by the magnetic field component. The full equation is given in (Davies, 1990).

The wavefront will reach a maximum height before being returned to earth at a point where N takes a value which causes:

$$u = \sin\phi \tag{A.3}$$

where ϕ is the angle of incidence of the wavefront with the ionosphere. When a vertical incidence wave is used, $\phi = 0$, $\sin\phi = 0$ and $u = 0$. Such a wave will reach a height determined only by the value N, and then will be returned towards the earth. Rearranging equation A.2 and substituting gives:

$$N = \left(\frac{E_o m}{4\pi e^2}\right)\omega^2 = 1.24 \times 10^4 f^2 \tag{A.4}$$

where f is the frequency of the wave in MHz. The critical frequency, f_o, is the maximum frequency which will be successfully refracted from the ionosphere at vertical incidence,and is obviously dependent upon the value of N, the electron density. Hence, for a given electron density, all frequencies above f_o will not be refracted. For vertical incidence waves the value of f_o can be obtained from:

$$f_o = \sqrt{\frac{N}{1.24 \times 10^4}} = 9 \times 10^{-3}\sqrt{N} \tag{A.5}$$

As the critical frequency is dependent on peak electron density, a plot of the critical frequency versus diurnal and seasonal variations can illustrate the wide variations possible when using the ionosphere for communication. The plot is shown in Figure A.5 and assumes a stylised ionosphere (Davies, 1990; Goldberg, 1966; Hargreaves, 1979). It is also obvious that latitude and solar cycle will also modify the shape of the plot.

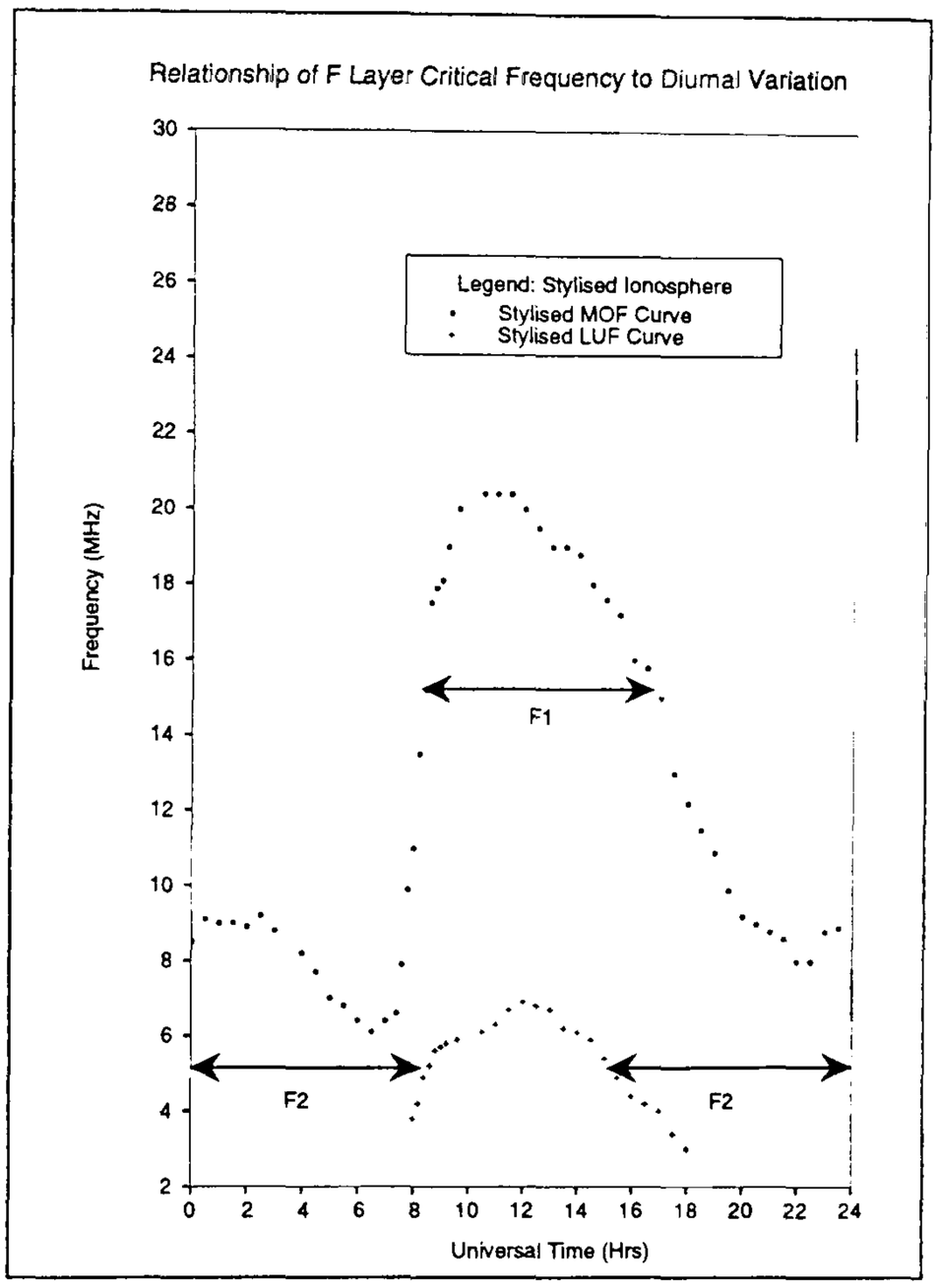

Figure A.5: Plot of F layer critical frequency for diurnal variation:
Stylised Ionosphere—Winter in Mid-Latitudes, Sunspot Number = 29,
Path Length = 1000km, Predictions From SUP252
User Transmission Frequencies F1 and F2 Identified

A.3 Oblique Propagation Parameters

Oblique propagation has a normal maximum single-hop range of about 4000km. This is achieved with a very low launch angle (about 2°) and needs specialised antennas to provide a focused beam. A typical field antenna (dipole) can support single hop communication to a distance of about 2500km (Petrie, 1986; Darnell, 1986a). Single hop propagation is one of the most important modes of communication as the multipath dispersion is minimised and the system has to tolerate only two D-layer crossings. Distances of greater than 4000km can be achieved via multihop communication. In this mode of propagation, the signal is reflected from the terrestrial surface back into the ionosphere. This means that the signal is attenuated strongly by the D-layer and the received SNR may be comparatively poor. Another long distance communication mechanism involves the signal being reflected internally within the ionosphere; this termed a 'chiral mode'. It produces a very dispersed signal, but with a better received SNR than with multihop communication. Round-the-world echoes have been documented (Barry, 1966), but transmission capacity may be very low due to the high levels of multipath dispersion and attenuation.

The link orientation has a significant impact on the coverage of the HF signal. If a low elevation angle is used, an area known as the *skip-zone* will exist. The skip zone is the area where no signal is received because it lies outside the normal groundwave propagation range and inside the range where a skywave signal can be received. If coverage in this area is desired, then the antenna orientation , beam pattern and operating frequency should be changed.

As indicated previously, the 'skip-zone' is the region between groundwave coverage and the start of the skywave zone. The skip-zone can be reduced by increasing the elevation angle of the antenna. In regions of the earth where groundwave signals are strongly attenuated due to poor surface conductivity this form of communication is very important. It is termed near-vertical incident skywave (NVIS). NVIS is the typical propagation mechanism in areas such as deserts and mountainous regions. NVIS systems used to counter the skip-zone problems have a coverage which is very limited.

A.4 Noise and Interference

A plot of the typical noise levels as a function of frequency is shown in Figure A.6 (Davies, 1990; Hargreaves, 1979). This plot clearly shows the frequency dependencies of the various noise sources. It can be seen that in the lower part of the band the dominant sources of noise are due to man-made noise, galactic noise, and atmospheric noise. These factors are much reduced in the upper part of the band where internal noise generated in the radio receiver begins to dominate.

A.5 Appendix Review

This appendix has provided extra information on accepted concepts of HF propagation, noise and interference. It extends the work in the main body of the thesis and provides extra references.

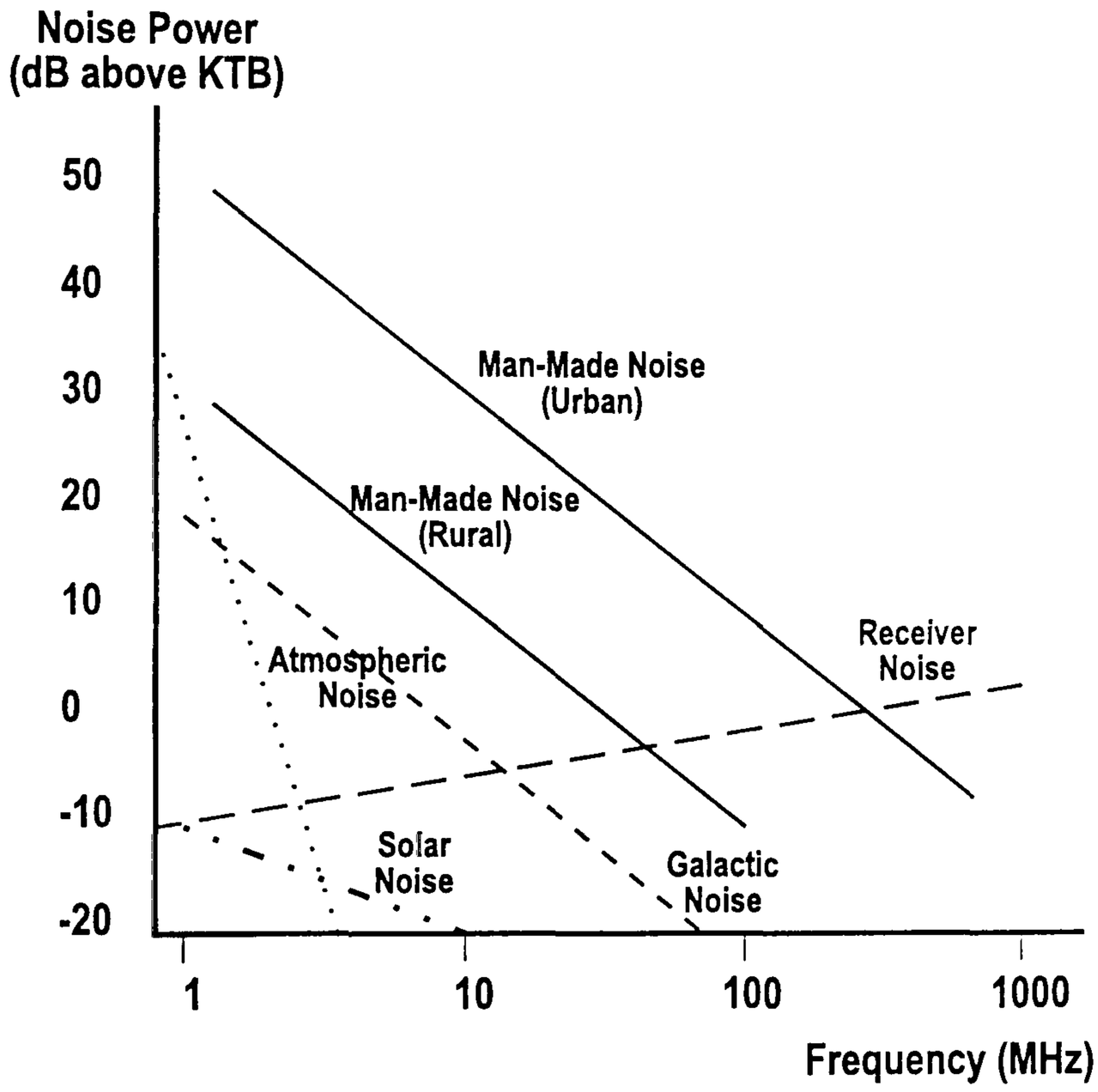

Figure A.6: Noise Levels as a function of Frequency from Various Sources

Appendix B

Chirp Detection Ambiguity Functions

This appendix outlines the concept of "ambiguity" when matched filtering a signal. The ambiguity function is particularly important when utilising a linear FM as such signals have a dispersive ambiguity function; a time shift is observed in the matched filter as a frequency shift, and a frequency shift is observed as a time shift.

B.1 Linear FM

As described in Chapter 5, the 'chirp' waveform is a linear FM signal. The envelope is described by equation B.1.

$$\mu(t) = a(t)e^{j\pi kt^2} \tag{B.1}$$

where

$$|k| = \frac{T}{B} \tag{B.2}$$

and

T = time duration of the signal,

B = bandwidth of the signal.

In a more convenient form, equation B.1, i.e. a linear FM signal with a rectangular envelope, becomes

$$\mu(t) = \frac{1}{\sqrt{T}} \text{rect}\left(\frac{t}{T}\right) e^{j\pi kt^2} \tag{B.3}$$

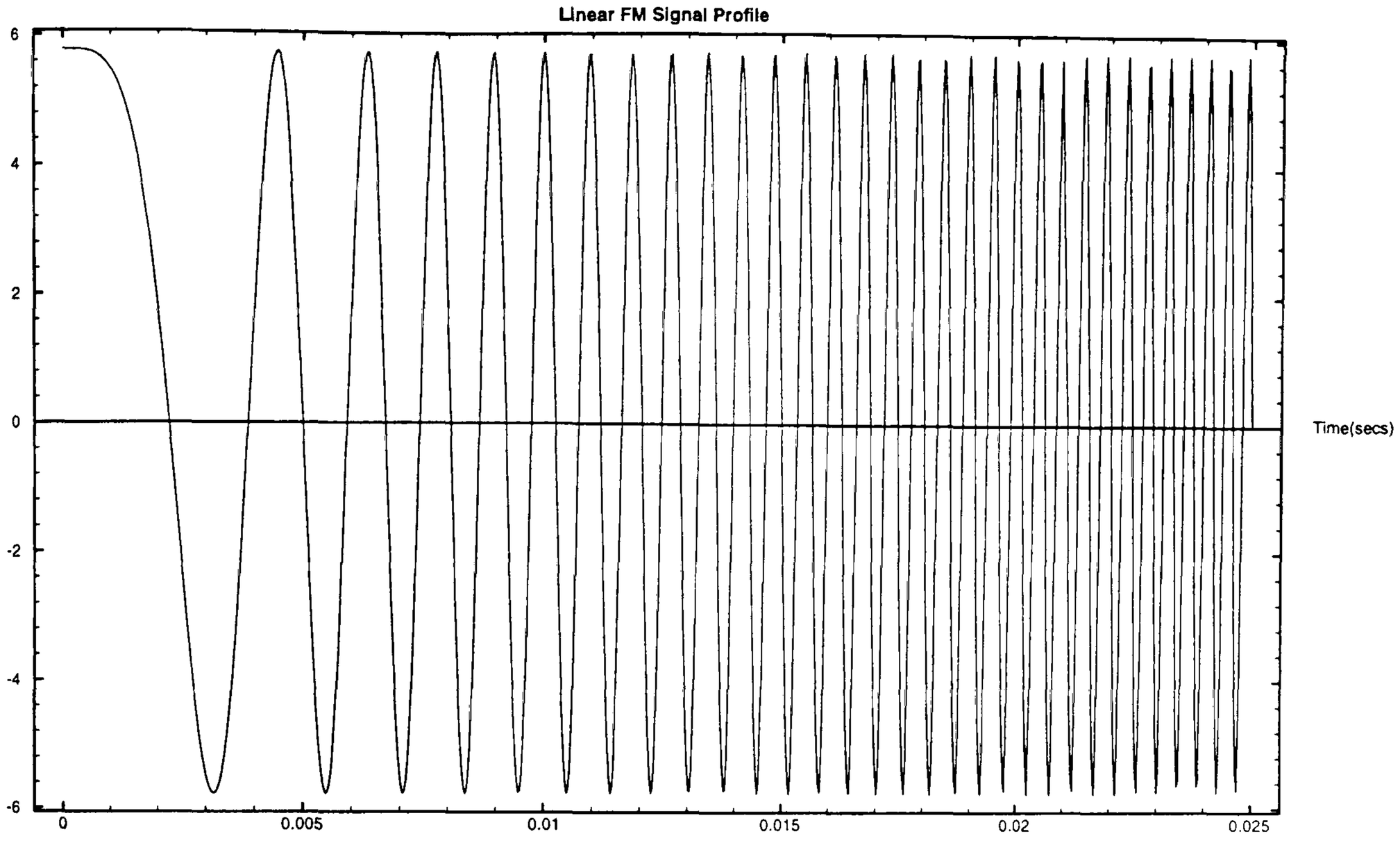

Figure B.1: Complex Envelope of Simple Linear FM

This complex envelope can be seen in figure B.1. In addition, the instantaneous frequency of the complex signal is

$$f_i = \frac{1}{2\pi}\frac{d\phi(t)}{dt} = kt \tag{B.4}$$

where k determines the rate of change of the FM; with k positive, the linear FM has a constant increase in frequency and when k is negative, the signal has constant decrease in frequency.

B.2 Matched Filter Detection

The matched filter can be shown to be the optimum receiver for a known signal immersed in noise and other interference from a channel that exhibits some memory. The matched filter is a unique compromise between theoretical performance and ease of implementation. The design of the matched filter attempts to maximise the signal-to-noise ratio (SNR) at the receiver output (North, 1943; Turin, 1960).

Consider a passive linear filter when the noise is additive and Gaussian, with a constant power spectral density of $N_0/2$. In this case the power spectrum extends over the entire frequency range; thus, the spectral band, W, contains the a total noise energy of $N = WN_0$. If the noise is passed through a filter with transfer function $H(f)$, the noise power density at the filter's output can be shown to be $(N_0/2)\,|H(f)|^2$, and the average noise output is

(Schwartz, 1981; Wainstein & Zubakov, 1962)

$$N = \frac{N_0}{2} \int_{-\infty}^{\infty} |H(f)|^2 \, df = \frac{N_0}{2} \int_{0}^{\infty} |Z(f)|^2 \, df \tag{B.5}$$

The SNR is defined as the ratio of peak received signal (wanted signal + noise) to average noise power given by equation B.6.

$$d = \frac{\left| \int_0^{\infty} \Psi(f) Z(f) e^{j2\pi f \tau} \right|^2}{N_0 \int_0^{\infty} |Z(f)|^2 \, df} \tag{B.6}$$

where

$\Psi(f)$ = The frequency domain representation of the signal.

Using the Schwartz inequality (Schwartz, 1981) (equation B.7) to find the maximum of d:

$$\left| \int_a^b u(x) v(x) dx \right|^2 \leq \int_a^b |u(x)|^2 \, dx \int_a^b |v(x)|^2 \, dx \tag{B.7}$$

This equality is only true for

$$u(x) = k v^*(x) \tag{B.8}$$

where k is an arbitary constant. Application of this inequality to the numerator of equation B.6 gives

$$\left| \int_0^{\infty} \Psi(f) Z(f) e^{j2\pi f \tau} df \right|^2 \leq \int_0^{\infty} |Psi(f)|^2 \, df \int_0^{\infty} |Z(f) e^{j2\pi f \tau}|^2 \, df \tag{B.9}$$

The integral

$$\int_0^{\infty} |\Psi(f)|^2 \, df$$

is equal to twice the signal energy. Substituting equation B.9 into equation B.6, and cancelling the two like terms, the resultant is

$$d \leq d_{\max} = \frac{2E}{N_0} \tag{B.10}$$

Therefore, the overall energy can be seen to depend on the input signal's energy and the noise power density.

The filter that maximises the SNR is specified by (B.8) which is the condition for obtaining $d = d_{\max}$. Identifying $u(x)$ with $Z(f)$, and $v(x)$ with $\Psi(f)e^{j2\pi f\tau}$, the filter transform $Z(f) = ke^{-j2\pi f\tau}\Psi^*(f)$ is obtained.

The term τ is used to specify the point in time where the maximum filter response appears or, alternatively, it can be viewed as representing the signal delay in the filter. Since this value is a constant, the notation τ_d is more convenient and the filter's transfer function is represented by

$$Z(f) = ke^{j2\pi f\tau_d}\Psi^*(f) \tag{B.11}$$

The impulse response of the filter is the Fourier transform of (B.11),

$$\zeta(t) = k\psi^*(\tau_d - t) \tag{B.12}$$

or, in real notation

$$h(t) = ks(\tau_d - t) \tag{B.13}$$

This filter, which maximises the SNR, is called the *matched filter* because it is a copy of the input signal with a reversed time axis (i.e. the signal is reversed).

B.3 The ambiguity function of Linear FM Signals

The *ambiguity function* of a matched filter is a measure of the correlation efficiency of the matched filter scheme with respect to the waveform being detected. Hence, a non-favourable ambiguity function indicates that the output from the matched filter has a significant amount of the detection energy located in the filter side-lobes or the detection threshold must take account of the poor resolution of the filter, i.e. there exists a large amount of dispersion. This detection threshold is also particularly important when multiple returns may be received by the matched filter (multipath structures) since all significant paths should be correctly detected and matched filter side-lobe noise rejected.

B.3.1 Rectangular Window

The ambiguity function, $\chi(\tau, \nu)$, is defined as (Woodward, 1953)

$$\chi(\tau, \nu) = \int_{-\infty}^{\infty} \mu(t)\mu^*(t - \tau)e^{2j\nu\tau}\, dt \tag{B.14}$$

Therefore, using equation B.1 and substituting this into equation B.14 and using the equality B.15 to account for large time-bandwidth products, the following equality is generated:

$$\nu' = \nu + \tau\frac{B}{T} \tag{B.15}$$

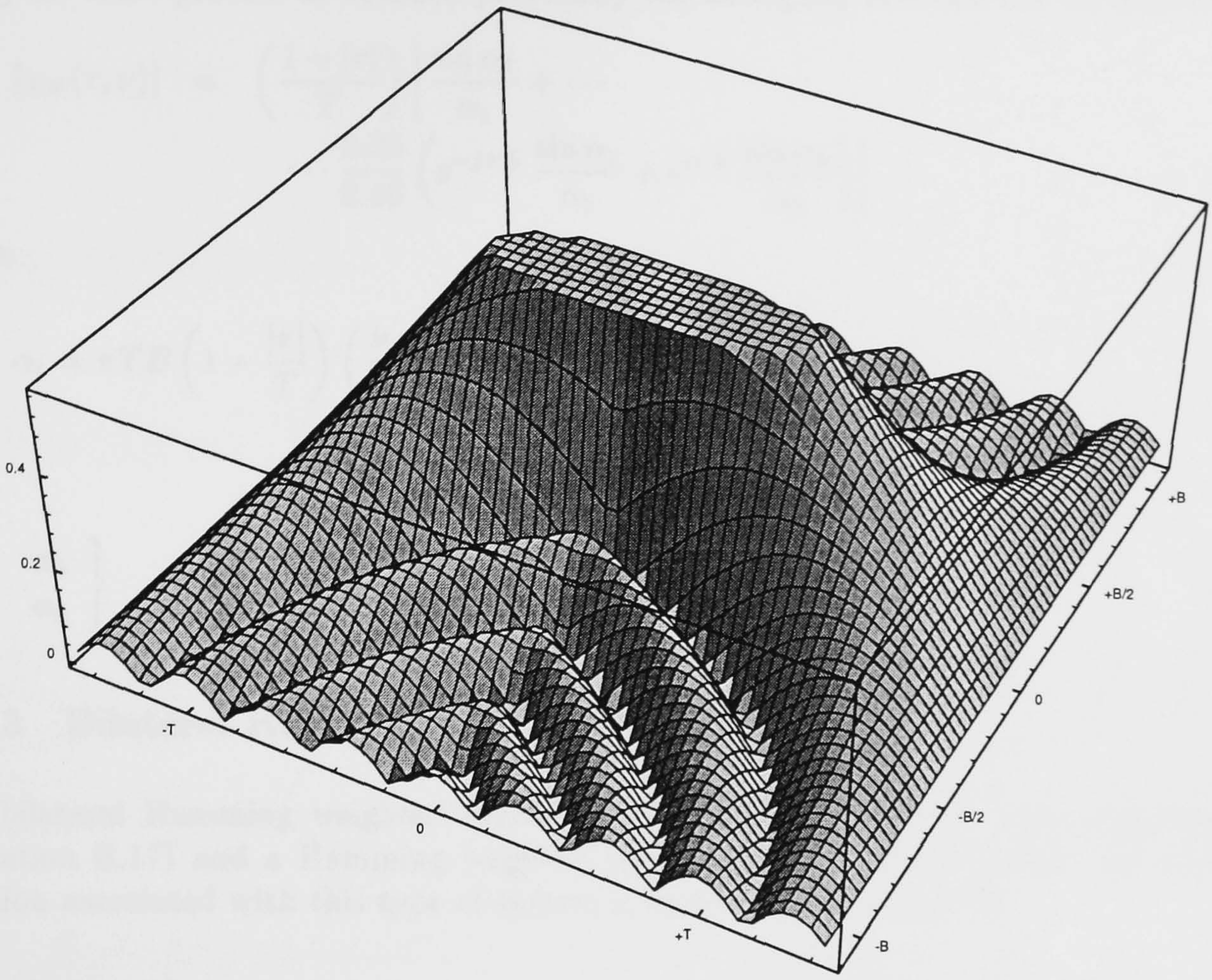

Figure B.2: Surface Plot of Linear FM Ambiguity Function

The resultant is the ambiguity function (Rihaczek, 1969), where a rectangular window over the transmitted chirp and matched-filter taps is assumed:

$$\chi(\tau,\nu) = \left(\frac{1-|\tau|}{T}\right)\left[\frac{\sin\left\{\pi T\nu'\left(1-\frac{|\tau|}{T}\right)\right\}}{\pi T\nu'\left(1-\frac{|\tau|}{T}\right)}\right] \tag{B.16}$$

where

$$|\tau| \leq T$$

The surface plot of this ambiguity function is shown in figure B.2

B.3.2 Unilateral Hamming Window

For a Hamming windowed chirp signal the normalised complex envelope is described by

$$\mu_H(t) = \frac{1}{\sqrt{T}}\,\text{rect}\left(\frac{t}{T}\right)\left(1+\frac{0.46}{0.54}\cos\left[\frac{2\pi t}{T}\right]\right)e^{j\pi kt^2} \tag{B.17}$$

Using the same process as outlined previously the ambiguity function can be derived as:

$$\begin{aligned} |\chi_H(\tau,\nu)| &= \left(\frac{1-|\tau|}{T}\right)\left|\frac{\sin\alpha_1}{\alpha_1}+\cdots\right. \\ &\left.\cdots\frac{0.23}{0.46}\left(e^{-j\pi\frac{\tau}{T}}\frac{\sin\alpha_2}{\alpha_2}+e^{j\pi\frac{\tau}{T}}\frac{\sin\alpha_3}{\alpha_3}\right)\right| \end{aligned} \tag{B.18}$$

where

$$\alpha_1 = \pi TB\left(1-\frac{|\tau|}{T}\right)\left(\frac{\nu}{B}+\frac{\tau}{T}\right) \tag{B.19}$$

and

$$\left.\begin{matrix}\alpha_2\\ \alpha_3\end{matrix}\right\} \quad \alpha_1 \pm \left[\pi\left(1-\frac{|\tau|}{T}\right)\right] \tag{B.20}$$

B.3.3 Bilateral Hamming Window

If a bilateral Hamming weighted system is used, i.e. a Hamming chirp is transmitted (Equation B.17) and a Hamming weighted matched filter is utilised, then the ambiguity function associated with this type of system is shown in Equation B.21.

$$\begin{aligned} |\chi_{HH}(\tau,\nu)| &= 0.734\left(\frac{1-|\tau|}{T}\right) \\ &\left|\left[1+\frac{1}{2}\left(\frac{0.46}{0.54}\right)^2\cos\left(\frac{2\pi\tau}{T}\right)\right]\frac{\sin\alpha_1}{\alpha_1}+\cdots\right. \\ &\cdots\frac{0.46}{0.54}\left(\cos\left[\frac{\pi\tau}{T}\right]\right)\left(\frac{\sin\alpha_2}{\alpha_2}+\frac{\sin\alpha_3}{\alpha_3}\right)+\cdots \\ &\left.\cdots\left(\frac{0.23}{0.54}\right)^2\left(\frac{\sin\alpha_4}{\alpha_4}+\frac{\sin\alpha_5}{\alpha_5}\right)\right| \end{aligned} \tag{B.21}$$

where

$$\alpha_1 = \pi TB\left(1-\frac{|\tau|}{T}\right)\left(\frac{\nu}{B}+\frac{\tau}{T}\right) \tag{B.22}$$

and

$$\left.\begin{matrix}\alpha_2\\ \alpha_3\end{matrix}\right\} \quad \alpha_1 \pm \pi\left(1-\frac{|\tau|}{T}\right) \tag{B.23}$$

$$\left.\begin{matrix}\alpha_4\\ \alpha_5\end{matrix}\right\} \quad \alpha_2 \pm 2\pi\left(1-\frac{|\tau|}{T}\right) \tag{B.24}$$

Appendix C

Spectral Estimation Methods

This appendix focuses on supporting theory for the estimation of the frequency-domain spectrum of a set of input signals. It has particular significance for the channel optimisation procedures, since, the template correlation algorithm uses the a Fourier transform to obtain its noise/interference spectrum estimate. This appendix provides detailed theory and discussion in support of these concepts.

C.1 Spectral Analysis of In-Band Signals

The following sections will describe several of the methods investigated in the research programme.

C.1.1 Fourier Analysis Techniques

Fourier analysis is one of the most important signal processing tools. It is by using Fourier analysis that the magnitudes and phase relationships of spectral components can be identified. The Fourier transform is given by equations C.1 and C.2. Equation C.1 is commonly known as the "synthesis equation", or inverse transform. Conversely, equation C.2 is known as the "analysis equation" or direct transform.

$$x(t) = \int_{-\infty}^{\infty} X(f) e^{j2\pi ft} df \tag{C.1}$$

$$X(f) = \int_{-\infty}^{\infty} x(t) e^{-j2\pi ft} dt \tag{C.2}$$

This latter equation can be further reduced by using the fact that angular frequency variable, ω, is related to the frequency, F, by $\omega = 2\pi f$. Therefore equation C.2 becomes:

$$X(\omega) = \int_{-\infty}^{\infty} x(t) e^{-j\omega t} dt \tag{C.3}$$

and equation C.1 becomes

$$x(t) = \frac{1}{2\pi} \int_{-\infty}^{\infty} X(\omega) e^{j\omega t} d\omega \tag{C.4}$$

Fourier analysis of sampled data signal is achieved by using the discrete time Fourier transform (DTFT) and the discrete Fourier transform (DFT). The discrete time Fourier transform is the continuous spectrum formed by analysis of discrete time data. The DFT is the sampled form of the DFT. It is the DFT that is most widely used in signal processing systems.

C.1.1.1 Discrete Fourier Transform

The DFT is a method for converting sampled time domain data into a discrete spectrum. The DFT is an approximation to the full Fourier transform, but can suffer from realisation complexity in that it needs N^2 computations, where N is the number of time domain samples. This makes the algorithm inconvenient for real-time operation. Other short-comings of the DFT include energy leakage into other frequency bins due to the effects of convolving a rectangular sample window with the incoming sample stream. These problems are well recognised and can be offset by pre-windowing the input signal to mitigate the generation of this leakage. However, the DFT remains one of the most important tools available for use by signal processors since the advantage of computing a discrete spectrum can outweigh the computational disadvantages.

Considering the DFT as a set of N samples $\{X(k)\}$ of the Fourier transform $X(\omega)$ for the finite duration time domain sequence $\{x(n)\}$ of length $L \leq N$. The sampling of $X(\omega)$ occurs at the N equally spaced frequencies $\omega_k = 2\pi k/N, k = 0, 1, 2, \ldots, N-1$. The DFT and its inverse function (or IDFT) for an N-point sequence $\{x(n)\}$ are described by the following equations:

$$DFT: \quad X(k) = \sum_{n=0}^{N-1} x(n) W_N^{kn}, \qquad k = 0, 1, \ldots, N-1 \tag{C.5}$$

$$IDFT: \quad x(n) = \frac{1}{N} \sum_{k=0}^{N-1} X(k) W_N^{-kn}, \qquad n = 0, 1, \ldots, N-1 \tag{C.6}$$

where

$$W_N = e^{-j2\pi/N} \tag{C.7}$$

The DFT and IDFT are transforms that have special properties such as linearity, circular symmetry and periodicity. These are standard processes which are well described in many signal processing texts e.g. (Proakis & Manolakis, 1992). The notation for a N-point DFT pair $x(n)$ and $X(k)$ is:

$$x(n) \overset{DFT}{\underset{N}{\longleftrightarrow}} X(k) \tag{C.8}$$

Implementations of the DFT do not take into account some of the simplifications possible to reduce computation, in particular the symmetry in the format of W_N. It is this symmetry that the fast Fourier transform (FFT) exploits.

C.1.1.2 Fast Fourier Transform

The fast Fourier transform (FFT) exploits the following properties in the evaluation of W_N:

$$Symmetry: \quad W_N^{k+N/2} = -W_N^k \tag{C.9}$$

$$Periodicity: \quad W_N^{k+N} = W_N^k \tag{C.10}$$

The FFT uses these two well-defined properties to reduce the number of computations from N^2 to $(N/2)\log_2 N$. This makes the FFT 200 times more efficient when computing the spectrum of a 1024-point data set than the direct DFT approach, with no loss in resolution. The inverse FFT (IFFT) has a similar advantage over the inverse DFT (IDFT). The FFT is one of the most popular methods for estimating a spectrum of a signal and it is particularly suited for implementation on a DSP device, especially when used in its *decimation in frequency* configuration. The FFT is a well developed algorithm and is described in many reference texts e.g. (Cooley *et al.*, 1967; Singleton, 1967).

C.1.2 Linear Prediction Techniques

Power spectrum estimation and characterisation using averages is important when the signals are transient, subject to fluctuations and have additive noise. Statistical characteristics can be modelled after nonparametric estimation and averaging; this can be viewed as using the raw FFT and averaging a number of the spectral estimates. Parametric estimation using a linear predictor, for example the *autoregresssive-moving average* (ARMA) predictor, can often give similar results with reduced computational overhead. This is because the energy distribution is estimated initially in the time domain prior to a single Fourier transform providing the spectral estimate of the signal. The linear prediction technique essentially preconditions the signal using a characteristic filter which allows statistical correlation of the true power spectrum (Kay & Marple, 1981).

C.1.2.1 Common Theory

The linear prediction technique for power spectral estimation is based upon the following well-developed rationale: consider a sequence $x(n)$ which is a sample stream derived from an analogue signal, $x_a(t)$, sampled at a constant rate, F_s. Only a finite duration of the data set of $x(n)$ is available. If $x_a(t)$ is a finite energy signal, then its energy, E, is given by:

$$E = \int_{-\infty}^{\infty} |x_x(t)|^2 dt < \infty \tag{C.11}$$

The Fourier transform must also exist, and is given by

$$X_a(F) = \int_{-\infty}^{\infty} x_a(t) e^{-j2\pi Ft} dt \tag{C.12}$$

Using Parseval's theorem (Stremler, 1992)

$$E = \int_{-\infty}^{\infty} |x_a(t)|^2 dt = \int_{-\infty}^{\infty} |X_a(F)|^2 dF \tag{C.13}$$

$|X_a(F)|^2$ represents the signal energy distribution as a function of frequency and is termed the energy density spectrum of the signal, i.e.

$$S_{xx} = |X_a(F)|^2 \tag{C.14}$$

The total energy of the signal is the integral of $S_{xx}(F)$ with respect to F or, more simply, the area under $S_{xx}(F)$. Using standard signal processing theory, $S_{xx}(F)$ may also be calculated using the autocorrelation function, $R_{xx}(\tau)$, of $x_a(t)$. This is defined as

$$R_{xx}(\tau) = \int_{-\infty}^{\infty} x_a^*(t) x_a(t+\tau) dt \tag{C.15}$$

where the asterisk indicates a complex conjugate. It therefore follows that

$$\int_{-\infty}^{\infty} R_{xx}(\tau) e^{-j2\pi F\tau} d\tau = S_{xx}(F) = |X_a(F)|^2 \tag{C.16}$$

so that $R_{xx}(\tau)$ and $S_{xx}(F)$ form a Fourier transform pair. When the signals have been sampled, the discrete process of generating the autocorrelation function is defined by

$$r_{xx}(k) = \sum_{n=-\infty}^{\infty} x^*(n) x(n+k) \tag{C.17}$$

The Fourier transform of this signal is

$$S_{xx}(f) = \sum_{k=-\infty}^{\infty} r_{xx}(k) e^{-j2\pi kf} \tag{C.18}$$

This is an indirect method of estimating the power spectrum. The direct method is

$$S_{xx}(f) = |X(f)|^2 \tag{C.19}$$

$$= \left| \sum_{n=-\infty}^{\infty} x(n) e^{-j2\pi fn} \right|^2 \tag{C.20}$$

where k and f represent the discrete (sampled) time domain and discrete spectrum domain.

The above equations are for systems where the transform of $x_a(t)$ corresponds to a finite energy spectrum. If the system does not have a finite-energy spectrum, then it may not have a finite Fourier transform. Such systems have a finite average power and hence are characterised by a power density spectrum. If $x(t)$ is a stationary random process then its ACF is

$$\gamma_{xx}(\tau) = E[x_*(t)x(t+\tau)] \tag{C.21}$$

where $E[\cdot]$ denotes the statistical average. Using the Wiener-Khintchine theorem, the power density spectrum of the stationary random process is the Fourier transform of the ACF (Weiner, 1949). That is

$$\Gamma_{xx}(F) = \int_{-\infty}^{\infty} \gamma_{xx}(\tau)e^{-j2\pi F\tau}dt \tag{C.22}$$

If only a part of the total series that describes the complete function is available, then only an estimate of $\gamma_{xx}(\tau)$ can be derived. Consequently, the Fourier transform to $\Gamma_{xx}(F)$ cannot be made. However, a time-average ACF can be formed from a single measurement

$$R_{xx}(\tau) = \frac{1}{2T_0}\int_{-T_0}^{T_0} x^*(t)x(t+\tau)dt \tag{C.23}$$

where $2T_0$ is the observation interval. If the stationary random process is *ergodic* then

$$\gamma_{xx}(\tau) = \lim_{T_0\to\infty} R_{xx}(\tau) \tag{C.24}$$

$$= \lim_{T_0\to\infty} \frac{1}{2T_0}\int_{-T_0}^{T_0} x^*(t)x(t+\tau)dt \tag{C.25}$$

In this case the power spectrum estimate, $P_{xx}(F)$, can be described by

$$P_{xx}(F) = \int_{-T_0}^{T_0} R_{xx}(\tau)e^{-j2\pi F\tau}d\tau \tag{C.26}$$

$$= \frac{1}{2T_0}\int_{-T_0}^{T_0}\left[\int_{-T_0}^{T_0} x^*(t)x(t+\tau)dt\right]e^{-j2\pi F\tau}d\tau \tag{C.27}$$

$$= \frac{1}{2T_0}\left|\int_{-T_0}^{T_0} x(t)e^{-j2\pi Ft}dt\right|^2 \tag{C.28}$$

The actual power density spectrum is the expected value of $P_{xx}(F)$ in the limit as $T_0 \to \infty$, or

$$\Gamma_{xx}(F) = \lim_{T_0\to\infty} E[P_{xx}(F)] \tag{C.29}$$

$$= \lim_{T_0\to\infty} E\left[\frac{1}{2T_0}\left|\int_{-T_0}^{T_0} x(t)e^{-j2\pi Ft}dt\right|^2\right] \tag{C.30}$$

Considering the realisation of this algorithm using discrete time samples of $x_a(t)$, where $x(n)$ is the range $0 \leq n \leq N-1$. The discrete time-average ACF is

$$r'_{xx}(m) = \frac{1}{N-m} \sum_{n=0}^{N-|m|-1} x^*(n)x(n+m), \quad m = 0, 1, \ldots, N-1 \tag{C.31}$$

$$r'_{xx}(m) = \frac{1}{N-|m|} \sum_{n=|m|}^{N-1} x^*(n)x(n+m), \quad m = -1, -2, \ldots, 1-N \tag{C.32}$$

The power density spectrum is defined by

$$P'_{xx}(f) = \sum_{m=-N+1}^{N-1} r'_{xx}(m)e^{-j2\pi fm} \tag{C.33}$$

The normalisation factor $(N-|m|)$ in equation C.32 results in in an estimate with mean value

$$E[r'_{xx}(m)] = \frac{1}{N-|m|} \sum_{n=0}^{N-|m|-1} E[x^*(n)x(n+m)] \tag{C.34}$$

$$= \gamma_{xx}(m) \tag{C.35}$$

where $\gamma_{xx}(m)$ is the statistical autocorrelation sequence of $x(n)$. Hence, $r'_{xx}(m)$ is an unbiased estimate of such a correlation function. The variance of the estimate $r'_{xx}(m)$ is approximately (Jenkins & Watts, 1968)

$$\text{var}[r'_{xx}(m)] \approx \frac{N}{[N-|m|]^2} \sum_{n=-\infty}^{\infty} [|\gamma_{xx}(n)|^2 + \gamma^*_{xx}(n-m)\gamma_{xx}(n+m)] \tag{C.36}$$

Clearly,

$$\lim_{N\to\infty} \text{var}[r'_{xx}(m)] = 0 \tag{C.37}$$

provided that

$$\sum_{n=-\infty}^{\infty} |\gamma_{xx}(n)|^2 < \infty \tag{C.38}$$

If $r'_{xx}(m)$ converges to r_{xx} as $N \to \infty$ then, from equation C.33

$$P_{xx}(f) = \sum_{m=-N+1}^{N-1} r_{xx}(m)e^{-j2\pi fm} \tag{C.39}$$

Using the premise that for large lags there are fewer data points entering the estimate, $r_{xx}(m)$ may be modified from equation C.32

$$r_{xx}(m) = \frac{1}{N} \sum_{n=0}^{N-|m|-1} x^*(n)x(n+m), \quad m = 0, 1, \ldots, N-1 \tag{C.40}$$

$$r_{xx}(m) = \frac{1}{N} \sum_{n=|m|}^{N-1} x^*(n)x(n+m), \quad m = -1, -2, \ldots, 1-N \tag{C.41}$$

The power estimate may be rewritten as

$$P_{xx}(f) = \frac{1}{N}\left|\sum_{n=0}^{N-1} x(n)e^{-j2\pi fn}\right|^2 = \frac{1}{N}|X(f)|^2 \tag{C.42}$$

where $X(f)$ is the Fourier transform of the sample sequence $x(n)$. This power spectrum estimate is commonly termed a *periodogram.*

It is upon this theory that all non-direct power spectrum estimation is based. The main disadvantage of using such a scheme is that phase information is not preserved.

C.1.2.2 Parametric Power Spectrum Estimation

Parametric spectrum estimation assumes that the sequence to be analysed is generated by a system model, whereas the non- parametric methods, such as the Fourier transform, make no assumptions about the generation or state of the data. It the generation of the system model that makes the parametric models so useful in spectral estimation. Non-parametric estimation needs large data sets and the conversion techniques used, such as the DFT, need to be prewindowed to reduce the spectral leakages which can mask weak spectral components. Parametric models need no prewindowing and can be used to resolve the spectrum of weaker signals. The main limitation on non-parametric schemes is that the autocorrelation function $r_{xx}(m)$ is zero for all $m \geq N$, as implied by equation C.39. This is the limitation on frequency resolution and, hence, on the quality of the generated spectral estimate.

Parametric models exploit functions that do not use such assumptions. These methods extrapolate the values of the autocorrelation for lags $m \geq N$. Such extrapolation is only possible if *a priori* information on the how the data was generated is available. When an appropriate model to provide this information is generated, reasonable extrapolations are possible. It is this modelling approach that eliminates the need for windowing the signal and overcomes the limitation that the autocorrelation sequence is zero for all $|m| \geq N$.

The model is based upon characterising the sequence $x(n)$ as an output from a linear system having the sampled data (z transform) function given by

$$H(z) = \frac{B(z)}{A(z)} = \frac{\sum_{k=0}^{q} b_k z^{-k}}{1 + \sum_{k=1}^{p} a_k z^{-k}} \tag{C.43}$$

As in a difference equation, this becomes

$$x(n) = -\sum_{k=1}^{p} a_k(n-k) + \sum_{k=0}^{q} b_k w(n-k) \tag{C.44}$$

where $w(n)$ is the input sequence to the system and $x(n)$ is the observed data. In a power spectrum estimate, the input sequence is not observable but, if the output is a random

stationary process, then the input must be of the same form. Therefore, the power density spectrum can be characterised by

$$\Gamma_{xx}(f) = |H(f)|^2 \Gamma_{ww}(f) \tag{C.45}$$

where $\Gamma_{ww}(f)$ is the power density spectrum of the input and $H(f)$ is the transfer function of the system. The input is assumed to be white noise, with zero mean, that possesses an autocorrelation

$$\gamma_{ww}(m) = \sigma_w^2 \delta(m) \tag{C.46}$$

where σ_w^2 is the variance or $\sigma_w^2 = E[|w(n)|^2]$. This means that the power density spectrum of the observed data is simply

$$\Gamma_{xx}(f) = \sigma_w^2 |H(f)|^2 = \sigma_w^2 \frac{|B(f)|^2}{|A(f)|^2} \tag{C.47}$$

In this parametric, model-based approach the spectrum estimation is undertaken in two steps. Given the sequence $x(n), 0 \leq n \leq N-1$, the parameters $\{a_k\}$ and $\{b_k\}$ are estimated; using these estimates the power spectrum estimate is then computed. The pole-zero model approach (of equation C.43) is termed an *autoregressive moving average process* (ARMA) of order (p, q). If $H(z) = 1/A(z)$, then the resultant is known an an autoregressive (AR) estimator. Conversely, if $H(z) = B(z)$, then the estimator is known as a moving average process. AR models are the most popular.

For an ARMA model, the autocorrelation sequence γ_{xx} is defined by

$$\gamma_{xx}(m) = \begin{cases} -\sum_{k=1}^{p} a_k \gamma_{xx}(m-k), & m > q \\ -\sum_{k=1}^{p} a_k \gamma_{xx}(m-k) + \sigma_w^2 \sum_{k=0}^{q-m} h(k) b_{k+m'}, & 0 \leq m \leq q \\ \gamma_{xx}^*(-m), & m < 0 \end{cases} \tag{C.48}$$

This can be used to determine $\{a_k\}$ by restricting it to the case when $m > q$. The linear equations

$$\begin{bmatrix} \gamma_{xx}(q) & \gamma_{xx}(q-1) & \cdots & \gamma_{xx}(q-p+1) \\ \gamma_{xx}(q+1) & \gamma_{xx}(q) & \cdots & \gamma_{xx}(q-p+2) \\ \vdots & \vdots & & \\ \gamma_{xx}(q+p-1) & \gamma_{xx}(q+p-2) & \cdots & \gamma_{xx}(q) \end{bmatrix} \begin{bmatrix} a_1 \\ a_2 \\ \vdots \\ a_p \end{bmatrix} = \begin{bmatrix} \gamma_{xx}(q+1) \\ \gamma_{xx}(q+2) \\ \vdots \\ \gamma_{xx}(q+p) \end{bmatrix} \tag{C.49}$$

may be used to solve for the parameters $\{a_k\}$ when $m \geq q$. The values of $\{b_k\}$ are determined using the knowledge of $\{a_k\}$ and the non-linear equation

$$\sigma_w^2 \sum_{k=0}^{q-m} h(k) b_{k+m} = \gamma_{xx}(m) + \sum_{k=1}^{p} a_k \gamma_{xx}(m-k) \tag{C.50}$$

This transformation is termed the *least-squares modified Yule-Walker method.* A further weighting factor may be applied to reduce the effects of the least reliable high-lag estimates. The parameters for the AR have now been estimated and the system can be described by

$$\hat{A}(z) = 1 + \sum_{k=1}^{p} \hat{a}_k z^{-k} \tag{C.57}$$

The sequence $x(n)$ is filtered by the FIR filter $\hat{A}$ to yield the following sequence

$$v(n) = x(n) + \sum_{k=1}^{p} \hat{a}_k x(n-k), \qquad m = 0, 1, \ldots, N-1 \tag{C.58}$$

The sequence $v(n)$ is used to form the estimated correlation sequence $r_{vv}(m)$ and from this the MA spectrum is obtained

$$\hat{P}_{xx}^{MA}(f) = \sum_{m=-q}^{q} r_{vv}(m) e^{-j2\pi fm} \tag{C.59}$$

Note that the parameters b_k are not needed to estimate the power spectrum, and that $r_{vv}(m)$ is an estimate of the ACF used in an MA model. This estimate is used to de-emphasize correlation estimates for large lags. The final ARMA power spectrum is given by

$$\hat{P}_{xx}^{\text{ARMA}}(f) = \frac{\hat{P}_{xx}^{MA}(f)}{\left|1 + \sum_{k=1}^{p} \hat{a}_k e^{-j2\pi fk}\right|^2} \tag{C.60}$$

It can be shown that the convergence of this ARMA algorithm can be used to provide excellent power spectrum estimates (Kay, 1980). The notation used in the algorithm, i.e. ARMA(p, q), is used to denote the p^{th} order in the AR combined with the q^{th} order in the MA algorithm.

C.1.3 Wavelet Transform

The current spectral estimation algorithms only operate in a single dimension. It is reasonable to extend the algorithms in order to evaluate their performance when operating in two dimensions, frequency and time. When such a plot is made of the data in these dimensions, distinct patterns will exist for transient signals and steady co-channel interferers. With this extra information available, an additional application for the in-band monitoring and template correlation algorithm becomes apparent, i.e. to precondition the signal before passing it to a demodulation stage. For example, the time-frequency template for a multi-tone FSK modem can be generated for each valid codeword. This pattern could be applied to the input signal deriving extra synchronisation information and possible demodulation weightings. In addition, co-channel interference could be adaptively filtered out, even if the interference is closely aligned with one of the tones. This cannot be accomplished by any simple analogue system and would improve the performance of the system. In addition, maximum

although the output depends upon knowledge of the sampled impulse response, $h(n)$. The simplicity of this equation indicates why the AR model is very popular; with $q = 0$, the initial autocorrelation sequence simplifies to

$$\gamma_{xx}(m) = \begin{cases} -\sum_{k=1}^{p} a_k \gamma_{xx}(m-k), & m > 0 \\ -\sum_{k=1}^{p} a_k \gamma_{xx}(m-k) + \sigma_{w'}^2, & m = 0 \\ \gamma_{xx}^*(-m), & m < 0 \end{cases} \tag{C.51}$$

C.1.2.3 ARMA Model for Power Spectrum Estimation

The ARMA (autoregressive moving average) model for power spectrum estimation is particularly suitable for systems where the signals have been corrupted by noise. This is typical of the HF channel where noise processes include thermal, co-channel interference and burst noise. In an ARMA system it is assumed that the data $x(n)$ has been generated by an AR system and the output is corrupted by white noise. The z-transform of the ACF of the resultant output is

$$\Gamma_x x(z) = \frac{\sigma_w^2}{A(z)A(z^{-1})} + \sigma_n^2 \tag{C.52}$$

$$= \frac{\sigma_w^2 + \sigma_n^2 A(z)A(z^{-1})}{A(z)A(z^{-1})} \tag{C.53}$$

where σ_n^2 is the variance of the additive noise. Therefore, the process x(n) is ARMA(p, p), where p is the order of the autocorrelation process. For lags $|m| > q$, the equation only involves the AR parameters $\{a_k\}$. With estimates substituted for $\gamma_{xx}(m)$, the solution of p equations to obtain a_k is possible. However, for high-order models, this approach is likely to yield poor estimates of the ACF due to large lags.

With an overdetermined set of linear equations for $m > q$, the use of the method of least-squares on those equations (Cadzow, 1982) is more reliable. To determine the autocorrelation sequence up to lag M, where $M > p + q$, the following sequence of linear equations may be employed:

$$\begin{bmatrix} r_{xx}(q) & r_{xx}(q-1) & \cdots & r_{xx}(q-p+1) \\ r_{xx}(q+1) & r_{xx}(q) & \cdots & r_{xx}(q-p+2) \\ \vdots & \vdots & & \\ r_{xx}(M-1) & r_{xx}(M-2) & \cdots & r_{xx}(M-p) \end{bmatrix} \begin{bmatrix} a_1 \\ a_2 \\ \vdots \\ a_p \end{bmatrix} = \begin{bmatrix} r_{xx}(q+1) \\ r_{xx}(q+2) \\ \vdots \\ r_{xx}(M) \end{bmatrix} \tag{C.54}$$

or equivalently

$$\mathrm{R}_{xx}\mathrm{a} = -\mathrm{r}_{xx} \tag{C.55}$$

Since R_{xx} is of dimension $(M-q) \times p$, and $(M-q) > p$, the application of least squares can solve for the parameter vector $\hat{a}$. This results in

$$\hat{\mathrm{a}} = -(\mathrm{R}'_{xx}\mathrm{R}_{xx})^{-1}\mathrm{R}'_{xx}\mathrm{r}_{xx} \tag{C.56}$$

likelihood demodulation based on techniques other than a simple matched filter become possible. These techniques include time and frequency averaging to enhance tone output, although it must be emphasised that a fine frequency resolution FFT has performance that is analogous to that of a matched filter.

A time-frequency plot of the signal can be obtained in several ways. The most popular is the frame-sampled FFT; this is termed a *spectrogram*. The latest technique which reduces the frequency smearing inherent in FFT processing is termed the wavelet transform. This uses a non-causal, prewindowing technique, based upon complex-pole prefilters, prior to a Fourier transform to obtain the frequency domain information. This research area is relatively new. The prewindow is termed the 'kernel'. Kernels based upon the use of wavelets, or short fractal operators, are most promising for producing high resolution and time resolved time-frequency plots. The wavelet transform uses an analysing wavelet, or complex bandpass function, centered around f_0 as its operator, and from this the plot can be made.

The sliding frame Fourier transform, or spectrogram $\mathrm{FT}_x^{(\gamma)}(t,f)$, can be described by

$$\mathrm{FT}_x^{(\gamma)}(t,f) = \int_{t'} x(t')\gamma^*(t'-t)e^{-j2\pi ft'}dt' = e^{-j2\pi tf}\int_{f'} X(f')\Gamma^*(f'-f)e^{j2\pi tf'}df' \quad \text{(C.61)}$$

Conversely, the wavelet transform, $\mathrm{WT}_x^{(\gamma)}$ is described by

$$\mathrm{WT}_x^{(\gamma)} = \int_{t'} x(t')\sqrt{\left|\frac{f}{f_0}\right|}\gamma^*\left(\frac{f}{f_0}(t'-t)\right)dt' \quad \text{(C.62)}$$

$$= \int_{f'} X(f')\sqrt{\left|\frac{f}{f_0}\right|}\Gamma^*\left(\frac{f}{f_0}(f')\right)df' \quad \text{(C.63)}$$

The above two equations are linear and possess well defined qualities (Rioul & Vetterli, 1992). However, if Parseval's theorem is to be observed, and the instantaneous energy used to form an energy density spectrum, a sub-class of the general transforms, termed quadratic time-frequency transformations, must be used. The most popular and most frequently used, due to its excellent frequency and time-resolution properties, is the Smoothed Pseudo-Wigner Distribution (SPWD) transform. The Wigner distribution (WD), $W_x(t,f)$, is based upon the following analysis system

$$\mathrm{W}_x(t,f) = \int_{\tau} x\left(t+\frac{\tau}{2}+\right)x^*\left(t-\frac{\tau}{2}-\alpha\right)e^{-j2\pi f\tau}d\tau \quad \text{(C.64)}$$

$$= \int_{\nu} X\left(f+\frac{\nu}{2}\right)X^*\left(f-\frac{\nu}{2}\right)e^{-j2\pi t\nu}d\nu \quad \text{(C.65)}$$

The SPWD is based upon preweighting the output and integrating over the period of the window. This has the effect of reducing the spectral estimates that cross between windows. The SPWD, $\mathrm{SW}_x^{(g,\eta)}$, is defined by

$$\mathrm{SW}_x^{g,\eta}(t,f) = \int_{\tau}\left[\int_{t'} g(t-t')x\left(t'+\frac{\tau}{2}\right)x^*\left(t'-\frac{\tau}{2}\right)dt'\right]\eta\left(\frac{\tau}{2}\right)\eta^*\left(-\frac{\tau}{2}\right)e^{-j2\pi f\tau}d\tau \quad \text{(C.66)}$$

$$= \int_{t'}\int_{f'} g(t-t')H(f-f')W_x(t,f')dt'df' \quad \text{(C.67)}$$

where

$$H(f) = \int_{\tau} \eta\left(\frac{\tau}{2}\right) \eta^*\left(-\frac{\tau}{2}\right) e^{-j2\pi f\tau} d\tau \tag{C.68}$$

The terms $g(t)$ and $H(f)$ represent two windows whose effective lengths independently determine the time smoothing spread, Δt, and frequency smoothing spread, Δf, respectively. This is an advantage since the time and frequency smoothing are effectively decoupled, thus simplifying computation.

C.2 Appendix Review

This appendix provides relevant theory for channel spectral estimation. It has also considered time-frequency analysis which may offer extra information on the state of the channel. The time-frequency analysis means that the time-averaged frequency components, usually concealed in a normal spectrum, may be observable.

Appendix D

Maximum Likelihood Detection of Signals in the Time-Frequency Domain

D.1 Introduction

Most frequency management systems use an engineering order wire (EOW) to pass essential control information between terminals. For efficient operation, this link needs to have extremely robust coding and modulation. It is this important consideration that necessitates more detailed examination of the demodulation process when the signal is immersed in non-Gaussian noise.

The matched filter is the optimum demodulator for any signal in Gaussian white noise. Even in coloured noise, a matched filter remains almost optimal. It is only in non-Gaussian conditions, where interferers exist, that matched filter performance degrades. In this case, the interference must be partially or wholly excised to improve performance. This is not always possible because the interfering signal can be non-stationary. Time-frequency domain processing offers the possibility of achieving this pre-filtering and thus again making the matched filtering process near-maximum-likelihood.

Time-frequency processing makes it possible to examine the signal over a complete codeword, as well as over individual symbol intervals. Patterns may be detected using maximum-likelihood detectors in the time and/or frequency domain. The spectrum is then weighted to reduce unwanted signal components. This weighting could form a metric for any subsequent soft-decision decoding process. The weights are then related to time-specified and shaped "notch" filters that are applied to the signal data, which is then passed to the matched filter and subsequent decoder. Clearly, this procedure may involve a substantial pre-processing delay.

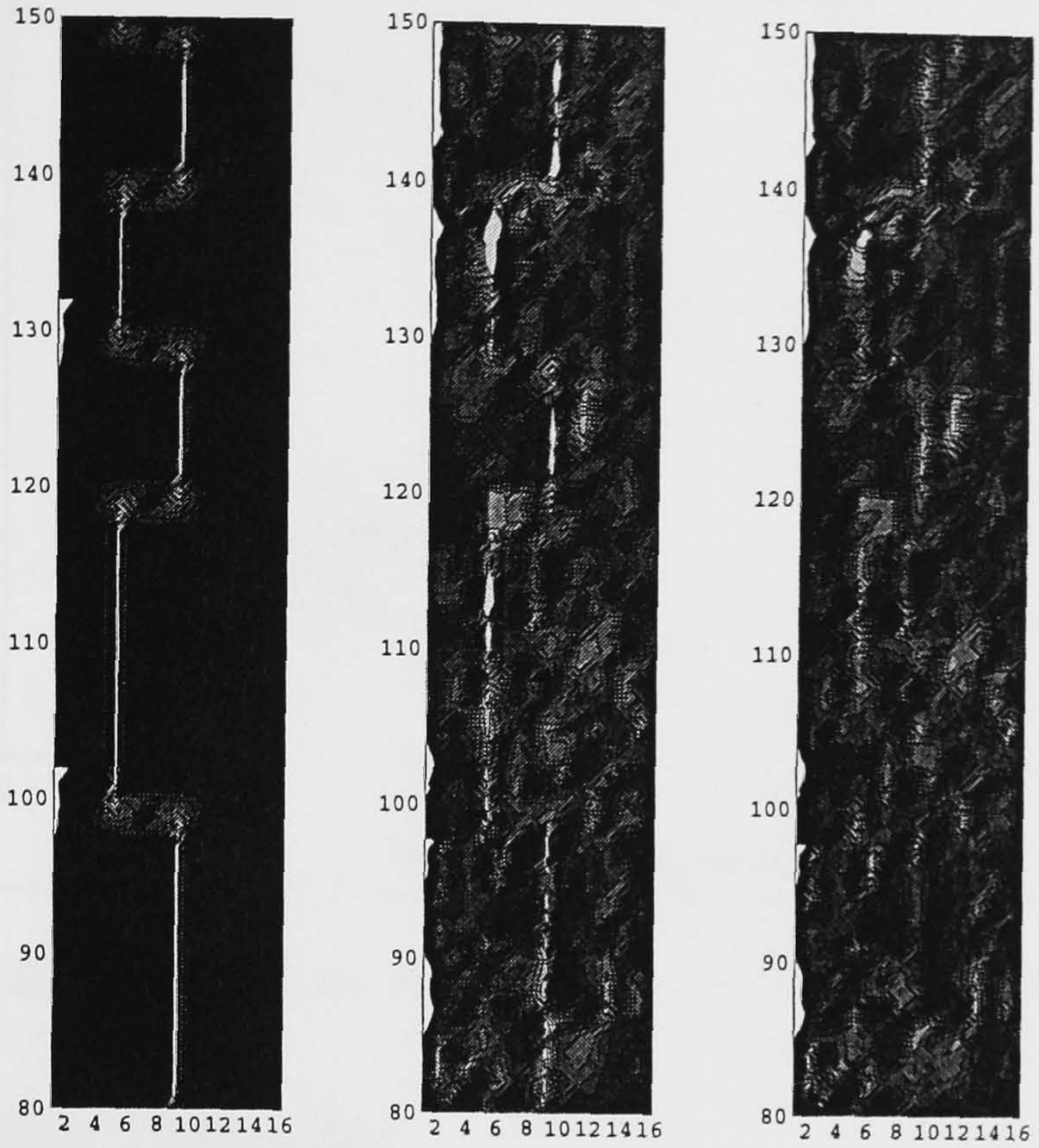

(a) High SNR (b) Med. SNR (c) Low SNR

Figure D.1: Contour Plots of FSK Signal
Time (Vertical Axis - ms) versus Frequency Bin(Horizontal Axis - 128 Hz resolution)

D.2 Algorithm Details and Results

The first stage in examination of this novel process was to undertake a short feasibility study. The investigation attempted to show that symbol feature extraction and enhanced demodulation were possible using the time-frequency domain plot. The plots shown in figures D.1(a), D.1(b) and D.1c are contour plots of the time-frequency information for an FSK signal under degrading Gaussian channel conditions. The contour plots were derived using a 32-point FFT. A maximum-likelihood detector based upon signal energy estimation with respect to frequency was constructed. The results from this are shown in Figure D.2.

These results show that signals can be identified from a time-frequency plot. Hence, unwanted signal artifacts can be identified and reduced. Burst noise would appear as time-dependent lines in the time-frequency plot; impulsive noise would appear as a wideband, short duration signals. Conversely single tone interferers would appear as constant frequency lines. A maximum-likelihood detector can be biased when estimating in the presence of these artifacts and hence reduce their effects.

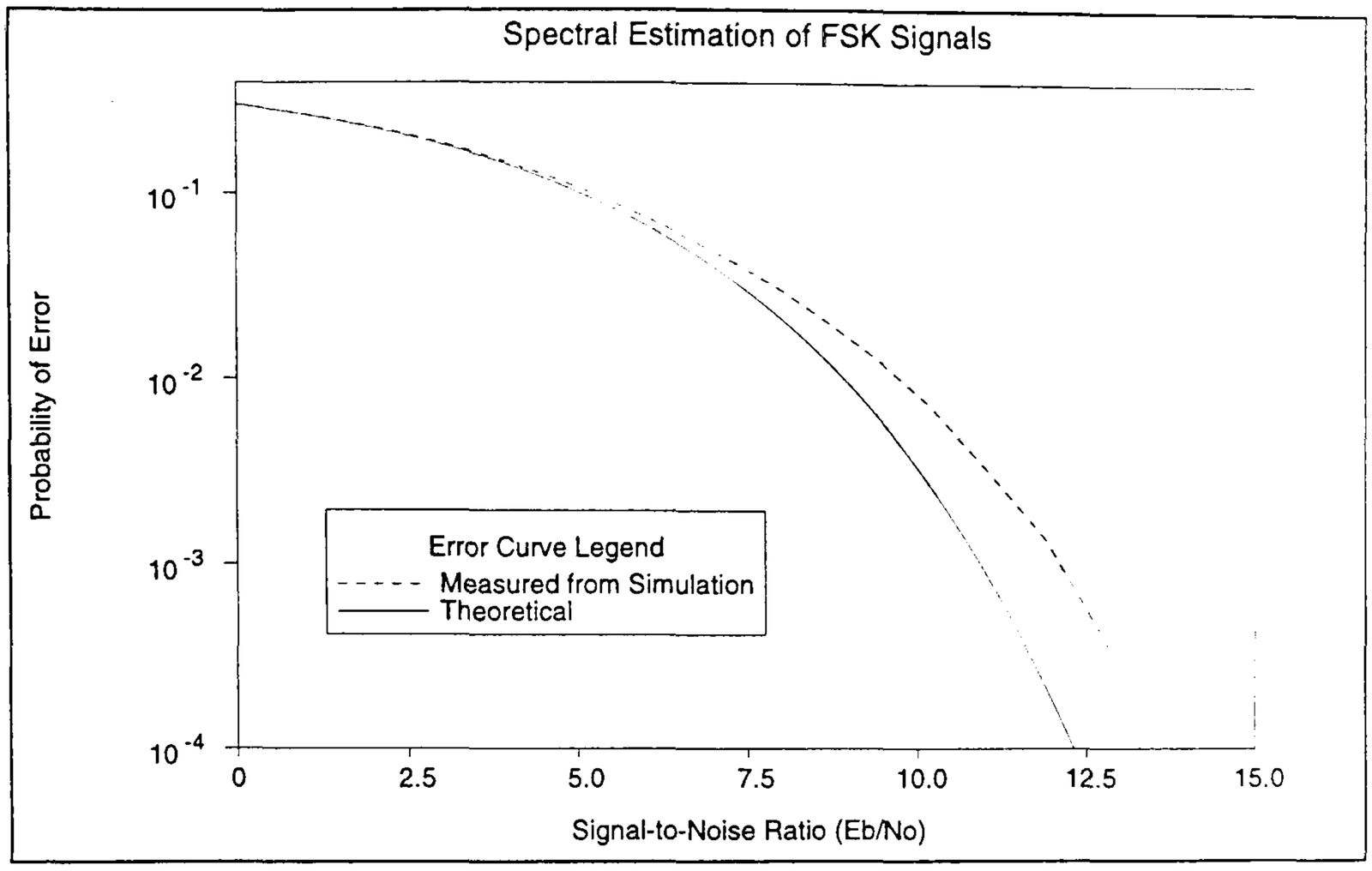

Figure D.2: Error-Curve Results from FFT-based demodulator

D.3 Concluding Remarks

It can be seen from these preliminary results that significant performance gains can potentially be made via pre-analysis of the time-frequency domain signal representation before passing it to the matched filter. The investigation, although limited, has highlighted possible areas for further research. The time-frequency generation would be better suited to DSP implementation of the smoothed pseudo Wigner distribution (SPWD) described earlier. This would reduce the smearing that occurs at transitions between tones. In addition, the robust nature of any channel decoder employing these techniques would be suitable for systems where data recovery at low SNR was vital; hence, its particular suitability for EOW applications.

Appendix E

Analytical Description of the Template Correlation Algorithm

It can be shown that for the maximum information rate in a noisy communication channel, the power spectrum of the desired signal should be adjusted so that the sum of the signal and the noise power spectral density is frequency-independent (Goldman, 1953) wherever possible in the channel bandwidth.

The analytical basis of template correlation is detailed below. Let

$$\int_{f_1}^{f_2} S(f)\, df = P \tag{E.1}$$

$$\int_{f_1}^{f_2} N(f)\, df = N \tag{E.2}$$

where

$S(f)$ = power spectral density of the *desired* signal,
$N(f)$ = power spectral density of the noise/interference,
P = total signal power in the range f_1 to f_2,
N = total noise power in the range f_1 to f_2.

Assuming that the noise is Gaussian in nature, there is no inter-symbol interference in the frequency domain and the signal also possesses Gaussian properties: considering the frequency band between f_1 and f_2 to be divided into a set of small equal width bands so that the noise power spectral density, $N(f)$, is approximately constant in each sub-band. Using the equality that the entropy of any given distribution, H, can be given by

$$H = -\int p(x) \log_e \{p(x)\}\, dx \tag{E.3}$$

The probability density function (pdf) of a signal, $p(x)$, is given by

$$p(x) = \frac{e^{\frac{-x^2}{2\sigma^2}}}{\sqrt{2\pi\sigma^2}} \tag{E.4}$$

where

σ = standard deviation of a Gaussian signal.

Simplifying equation E.3 using equation E.4 gives

$$H = \log_e \sqrt{2\pi e\sigma^2} \tag{E.5}$$

Therefore, for a Gaussian source that has n sample points, the entropy of each point, H_k is given by

$$H_k = \log_e \sqrt{2\pi e\sigma_1^2} \tag{E.6}$$

where σ_1 is the r.m.s. of x about the mean at that particular sample point (NB the mean square of x corresponds to the variance σ^2). For this particular noise source let $N = \sigma_1^2$, i.e. let the mean square noise power in a 1Ω load be the variance of the distribution (as per the definition of variance).

Thus the entropy of each sample point is

$$h = \log_e \sqrt{(2\pi eN)} \tag{E.7}$$

This is the entropy per degree of freedom per sample. If Nyquist sampling as assumed and the degrees of freedom are limited to one, as sampling is carried out in either frequency or time, then the total entropy is given by

$$H = T.W.\log_e(2\pi eN) \tag{E.8}$$

where T and W are equal to the time and bandwidth of the signal respectively. Hence the entropy of the combined signal and noise in a narrow bandwidth Δf is

$$H(s+n) = T.\Delta f.\log_e(2\pi e(S(f).\Delta f + N(f).\Delta f)) \tag{E.9}$$

The entropy of the noise alone in the bandwidth Δf is

$$H(n) = T.\Delta f.\log_e(2\pi e(N(f).\Delta f)) \tag{E.10}$$

The information rate, R, is then given by

$$R = \frac{H(s+n) - H(n)}{T} \tag{E.11}$$

as $T \to \infty$. Thus the information rate in the bandwidth Δf is

$$R(\Delta f) = \Delta f . \log_e \left(\frac{S(f) + N(f)}{N(f)} \right) \tag{E.12}$$

Integrating this over the bandwidth, f_1 to f_2 gives an indication of the information rate in that bandwidth.

$$R(W) = \int_{f_1}^{f_2} \log_e \left(\frac{S(f) + N(f)}{N(f)} \right) df \tag{E.13}$$

The rate should be maximised given the following constraint

$$P = \int_{f_1}^{f_2} s(f) df \tag{E.14}$$

Using calculus of variations the result is

$$\frac{\partial}{\partial S(f)} \log_e \left(1 + \frac{S(f)}{N(f)} \right) + \lambda = 0 \tag{E.15}$$

where λ is a constant. Therefore

$$\frac{N(f)}{S(f)} + N(f) \times \frac{1}{N(f)} = -\lambda \tag{E.16}$$

which results in

$$S(f) + N(f) = -\frac{1}{\lambda} \tag{E.17}$$

This means that for maximum information rate the sum of the noise and signal power spectral densities should be frequency-independent wherever possible in the channel bandwidth.

Appendix F

Publications

As a consequence of the research undertaken, the following papers have been published:

1. Gallagher, M. and Darnell, M. "Performance of a template correlation system for in-band spectrum management" 5^{th} IEE Int. Conf. on 'Radio Receivers and Associated Systems', CP-325, July, 1990.

2. Gallagher, M. and Darnell, M. "Propagation and interference measurements for use in real-time frequency management" 7^{th} IEE Int. Conf. on 'Antennas and Propagation' (ICAP 91), CP-333, April 1991.

3. Gallagher, M. and Darnell, M. "Adaptive architecure for radio communication systems" 3^{rd} Symposium on 'Communications', UCNW, Bangor, May 1991.

4. Gallagher, M. and Darnell, M. "An economic ionospheric sounding system using standard HF system elements" 5^{th} IEE Int. Conf. on 'HF radio: systems and techniques', CP-339, July 1991.

5. Gallagher, M., Riley, N. G. and Darnell, M. "Channel Sounding Techniques", Proc. ARMMS, Bath, September 1991.

6. Gallagher, M., Darnell, M. and Clark, P. D. J. "Architectural considerations for adaptive digital signal processing within long-range radio communication system terminals", 6^{th} IEE Int. Conf. on 'Digital signal processing of signals in communications', CP-340, September 1991.

7. Gallagher, M. and Darnell, M. "Architectural considerations for long-range radio systems", 1^{st} Int. Symposium on 'Communications: theory and techniques', September 1991.

8. Gallagher, M. and Darnell, M. "Adaptive remote sensing of the ionosphere to minimise spectral intrusion", AGARD Conf. on 'Remote sensing of the Propagation Environment', AGARD CP-502, pp 13.1-13.15, Çeşme, Turkey, October 1991.

9. Gallagher, M. and Darnell, M. "A multi-functional radio system terminal", IEE Colloquium on 'Implementations of Novel Harware for Radio Systems', Publication No. 1992/126, May 1992.

10. Gallagher, M. and Darnell, M. "Radio system terminal architecture incorporating DSP elements", 1^{st} Int. Symposium on 'DSP techniques for Communications', September 1992.

11. Darnell, M. and Gallagher, M. "Embedded Ionospheric Sounding Systems", 8^{th} IEE Conf. on 'Antennas and Propagation' (ICAP 93), March 1993.

12. Gallagher, M., Darnell, M, Ripley, M. R. and Bartlett, A. "Channel state quantification", 2^{nd} Int. Symposium on 'Communications: theory and techniques', Ambleside, 1993.

13. Gallagher, M., Bennett, S. A. W., Darnell, M. and Honary, B., "Architectures for advanced radio systems incorporating network and frequency management", 6^{th}IEE Int. Conf. on 'HF Radio: Systems and Techniques' ,1994.